January 2010

Functional Genomic Examinations Of Interactions Between Common Members Of The Human Gut Microbiota

Michael Mahowald
Washington University in St. Louis

WASHINGTON UNIVERSITY

Division of Biology and Biomedical Sciences

Molecular Microbiology and Microbial Pathogenesis

Dissertation Examination Committee:
Jeffrey I. Gordon, Chair
Douglas E. Berg
Michael G. Caparon
Daniel E. Goldberg
Elaine R. Mardis
Clay F. Semenkovich

FUNCTIONAL GENOMIC EXAMINATIONS OF INTERACTIONS BETWEEN COMMON MEMBERS OF THE HUMAN GUT MICROBIOTA

by

Michael Anthony Mahowald

A dissertation presented to the
Graduate School of Arts and Sciences
of Washington University in
partial fulfillment of the
requirements for the degree
of Doctor of Philosophy

May 2010

Saint Louis, Missouri

Dedication

To my parents, Anthony P. and Mary Briody Mahowald

ABSTRACT OF THE DISSERTATION

Functional genomic examinations of interactions between

common members of the human gut microbiota

by

Michael Anthony Mahowald

Doctor of Philosophy in Biology and Biomedical Sciences
(Molecular Microbiology and Microbial Pathogenesis)

Washington University in St. Louis, 2010

Professor Jeffrey I. Gordon, Chairperson

The adult human gut microbiota consists of hundreds to thousands of bacterial species, the majority belonging to the Bacteroidetes and the Firmicutes. Differences in the balance between these phyla has been linked to obesity in mice and humans. However, little is known about their interactions *in vivo*. I have used comparative and functional genomics, proteomics and biochemical assays to identify the ways they marshal their genomic resources to adapt to life together in the distal gut.

I first annotated the complete genome sequences of two human gut Bacteroidetes (*Bacteroides vulgatus* and *Parabacteroides distasonis)* and two Firmicutes *(Eubacterium rectale* and *E. eligens)*. By comparing the genomes of all sequenced gut Bacteroidetes and Firmicutes, I found that gut Bacteroidetes' genomes contain large groups of genes responsible for (i) sensing, binding, and metabolizing the varied polysaccharides that they encounter in the distal intestine; and (ii) constructing their polysaccharide capsules. These portions of their genomes have been shaped by lateral gene transfer, including phage and conjugative transposons, as well as by gene duplication. By colonizing germ-free mice with *B. thetaiotaomicron,* or *B. vulgatus,* or both species together, I documented that *B. vulgatus* upregulates its unique glycan-degrading enzymes to adapt to the presence of *B.*

thetaiotaomicron.

In contrast to the Bacteroidetes, the Firmicutes have smaller genomes, a significantly smaller proportion of glycan-degrading genes, and are suited to degrade a more specialized assortment of dietary carbohydrates. By colonizing germ-free mice with *E. rectale* and/or *B. thetaiotaomicron*, I showed that *B. thetaiotaomicron*, like *B. vulgatus,* upregulates its unique glycoside hydrolase activities to adapt to the presence of *E. rectale,* increasing its degradation of host-derived glycans that *E. rectale* cannot use. In contrast, *E. rectale* downregulates its polysaccharide degradation genes and upregulates nutrient transporters, likely allowing it to access sugars released by *B. thetaiotaomicron's* glycoside hydrolases. These models of the human gut microbiota illustrate niche specialization and functional redundancy within the Bacteroidetes, the adaptable niche specialization that likely underlies the success of Firmicutes in this habitat, and the importance of host glycans as a nutrient foundation that ensures ecosystem stability.

Acknowledgements

Jeffrey Gordon's lab has been an amazing place to do research. His constant encouragement and indomitable enthusiasm are incredible to behold, and have been an enormous boost at the times when I've felt things ought to be going better. I am enormously thankful for the trust and patience he has shown me as I've learned my way over the years. The amount of freedom I've had to explore scientifically has been wonderful and is clearly quite unique. His attitude makes his lab a fun place to be a student.

Without a doubt the best aspect of the lab has been the outstanding group of people he has brought together and continues to renew. I count myself enormously privileged to have had the chance to interact with and learn from everyone who has been a part of his dynamic group. I could not have accomplished any of this work without more help, expertise, enthusiasm, advice, support, and care from the whole group than I can possibly recount. Nonetheless, a few deserve special mention.

Jill Manchester, in addition to her fabulous abilities as a biochemist (without whom virtually none of the biochemical assays reported here would have been done), has been a great lab mom, extremely caring and supportive throughout, in spite of all the forgotten messes I've left around the lab (sorry!). Sabrina Wagoner, Dave O'Donnell and Maria Karlsson are all incredibly talented and patient and made all the mouse work, among many other things, possible. It's hard to imagine how the Gordon lab could function without them.

Dr. Janaki Guruge and my classmate Lara Crock started work in the lab on *E. rectale,* and I am very thankful to them for the groundwork that made my way forward much, much easier. Janaki has been a great friend and source of microbiological advice and laughs.

I started my work in the lab with J. F. Rawls, who was as good a mentor, and as kind a person, as I have encountered. Aside from his outstanding science, his ability to plan and

see the big picture outlook for his work were and are an inspiring example and served as a perfect introduction to the lab.

Federico Rey and Henning Seedorf have been of particular help with the second half of this work; they have both taught me an enormous amount about bacterial metabolism and been a true joy to work with. Their help, enthusiasm and generosity has made this work far better than it could have been otherwise. Eric Martens holds an encyclopedic knowledge of microbiology in general and the *B. theta* genome in particular, and has been a model example of technical and scientific rigor and focus – not to mention a fun and kind individual and master brewer. I counted on Buck Samuel as a constant source of technical and grad-student-life advice and generous and careful feedback. The lab would have been a substantially more difficult place to be a student without him. Dan Peterson and Peter Crawford have both been fountains of career advice and encouragement, as well as extremely valuable constructive criticism and perspective, whom I'll miss a great deal. Swaine Chen has helped deepen my understanding of biostatistics and has also been a great source of critical feedback. Priya Sudarsanam has made a great bay-mate over the last year and helped me keep my lab work in proper perspective even as she's challenged me to think more deeply about it. Justin Sonnenburg was a valuable glycobiology resource. Ruth Ley offered much of her always creative critique and insight to all matters to do with microbial ecology. Doug Leip taught me much about software design and scripting, and has been a supportive friend.

Marios Giannakis and I entered Wash. U. as classmates, and his friendship has been a great blessing over the last six years since we joined the Gordon lab; I hope it will be so for years to come. He was (and remains) the one person I know I can ask for instantaneous recall of anything I might have once known in medical school or college; combining an incredible memory with intellect, enthusiasm, and kindness to match made his influence on me, and I venture to suppose, the lab in general, one that will be missed. He brings the same

enthusiasm to everything from major league eating to studying chronic atrophic gastritis (although in some ways those two aren't so unrelated).

Pete Turnbaugh entered the lab soon after I did, and his critiques probably have an even larger part of the work shown here than I realize – and that, by the way, is saying quite a lot. His scientific opinion, as well as his taste in movies, has been an inspiration over the years, and hopefully will continue to be.

Many other friends within the medical school, especially Vinod Rao, Tina Ling, Chung Lee, Bill Hucker, Bryson Katona, Ram Akilesh and Bill McCoy, have been supportive of all my efforts. Many a good time spent over a pitcher, a few rounds of darts, or a good dinner will be fondly remembered. Also, of course, the MSTP staff, Brian Sullivan, Andrew Richards, Christy Durbin and Liz Bayer, have been a huge help with keeping everything going behind the scenes, and more importantly, in setting up, together with the directors, Dan Goldberg and Wayne Yokoyama, such a well-oiled machine of a program. Their work over the years has saved me much trouble (and excessive class time) and made for a much nicer experience. My thesis committee, particularly my chair, Doug Berg, has offered great advice and much of their time to this project, and I thank them for their help. Laura Kyro, Stephanie Amen and Debbie Peterson are the three highly able assistants in the C.G.S., without whom countless tasks, not least of them piecing together this thesis, would be much more difficult.

Finally, and most importantly, I want to thank my family. My father introduced me to science before I can remember. His curiosity and enthusiasm for inquiry have been infectious and taught me the most important things I've had to have to enjoy the journey to this point. If I'd followed more of his advice along way, I'd be even better off, but without him I'd never have reached this point. My parents' unconditional love, support and encouragement mean more to me than I know how to express or deserve. My two sisters have always told me that I had it easy, because they were older and had to learn all the hard les-

sons, so that I could learn from. Frankly, they're right, and not just in growing up: Maureen went to grad school first and offered all manner of advice on how to pick a lab. But both of them are always encouraging to me, and are always quick to help me set my priorities straight and remember that the most important things are, in fact, not in lab. Lastly but far from least, my thanks to my enormously talented and exceedingly generous wife, Grace, whose love and support of me seem to know no bounds, and without whom I think I've pretty nearly forgotten how to survive.

Table of Contents

Chapter 1

Introduction

Chapter 2

Evolution of symbiotic bacteria in the distal human intestine

Chapter 3

Characterizing a model human gut microbiota composed of members of its two dominant phyla

Chapter 4

Future Directions

Appendices

List of Figures

Chapter 1

Introduction

Chapter 2

Evolution of symbiotic bacteria in the distal human intestine

Chapter 3

Characterizing a model human gut microbiota composed of members of its two dominant phyla

Chapter 4

Future Directions

List of Tables

Chapter 2

Evolution of symbiotic bacteria in the distal human intestine

Chapter 3

Characterizing a model human gut microbiota composed of members of its two dominant phyla

Chapter 4

Future Directions

Curriculum Vitae

Name: Michael Anthony Mahowald

Date of Birth: August 23, 1976

Address: 4355 Maryland Ave., #427
St. Louis, MO 63108

Telephone: (314) 533-2584

Business address: Center for Genome Sciences, Box 8510
Washington University in St. Louis
4444 Forest Park Blvd.
St. Louis, MO 63108
Telephone: (314) 362-3963
Fax: (314) 362-2156

E-mail: mahowald@wustl.edu

Education:

2002-present **Medical Scientist Training Program (MSTP)**
Ph.D. in Molecular Microbiology and Microbial Pathogenesis
MD/Ph.D. candidate
Washington University in St. Louis School of Medicine
Ph.D. advisor: Jeffrey I. Gordon

1995-1999 **Bachelor of Arts**
Swarthmore College, Swarthmore, PA
Major in Biology

Research Experience:

2004-present **Ph.D. student**
Laboratory of Jeffrey I. Gordon
Title of thesis: Functional and comparative genomic examinations of interactions between common members of the human gut microbiota

2003 **MSTP research rotation**
Laboratory of Virginia Miller
Dept. of Molecular Microbiology
Washington University in St. Louis School of Medicine.
Conducted a screen for virulence factors in a murine inhalation model of *Klebsiella pneumoniae* pneumonia.

2002 **MSTP research rotation**
Laboratory of Michael Caparon
Dept. of Molecular Microbiology

	Washington University in St. Louis School of Medicine Screened *Streptococcus pyogenes* transposon library for novel secreted proteins.
2001-2002	**Research Assistant** **Laboratory of Thomas Gajewski** University of Chicago, IL Conducting clinical trials and surveillance of cancer immunotherapies.
2000-2001	**Research Assistant** **Laboratory of Bruce Lahn** University of Chicago, IL Studied the molecular evolution of the primate nervous system
1997, 1998	**Summer Research Assistant** **Laboratory of Steven L. Reiner** University of Chicago, IL Studying the immune response to*Leishmania* infection and the development of murine helper T cells.
1996	**Summer Research Assistant** **Laboratory of Michael Wade** University of Chicago, IL Studying speciation of *Tribolium* flour beetles.
1994	**Summer Research Intern** **Laboratory of R. Michael Garavito** University of Chicago, IL Developing purification scheme for F_1F_0 ATPase.

Teaching Experience:

2004	**Teaching Assistant** **Cell and Organ Systems Biology: Physiology** (1st year) Washington University in St. Louis School of Medicine. Coursemaster: Robert Wilkinson
1999-2000	**High School Teacher** Cristo Rey Jesuit High School Capuchin Franciscan Volunteer Corps and Americorps Chicago, IL Teaching 10th grade Biology, 12th grade Human Anatomy and 11th grade Algebra classes.
1998	**Teaching Assistant** **Computer Science 10: UNIX and C** Swarthmore College, Swarthmore, PA. Professor: James Marshall

Honors and Fellowships:

2006-8	**Infectious Diseases Training Grant (NIH)** Washington University in St. Louis School of Medicine
1998	**Sigma Xi Scientific Research Society, Student Member**
1998	**Gwen Knapp Summer Research Fellow** Knapp Center for Lupus and Immunology Research University of Chicago, IL

Manuscripts in preparation:

Mahowald GK, Moon C, Khor B, **Mahowald MA**, Sleckman BP. Intron-dependent nonsense-mediated decay of TCR-ß locus transcripts in developing thymocytes. In preparation.

Publications:

Mahowald GK, Baron JM, **Mahowald MA**, Kulkarni S, Bredemeyer AL, Bassing CH, Sleckman BP. Aberrantly resolved Rag-mediated DNA breaks in Atm-deficient lymphocytes target chromosomal breakpoints in cis. Proc Natl Acad Sci U S A., 2009 Oct 27;106(43):18339-44.

Mahowald MA,* Rey FE,* Seedorf H, Turnbaugh PJ, Fulton RS, Wollam A, Shah N, Wang C, Magrini V, Wilson RK, Cantarel BL, Coutinho PM, Henrissat B, Crock LW, Russell A, Verberkmoes NC, Hettich RL, Gordon JI. Characterizing a model human gut microbiota composed of members of its two dominant bacterial phyla. Proc Natl Acad Sci U S A. 2009 Apr 7;106(14):5859-64.

Xu, X.*, **M.A. Mahowald***, R.E. Ley, C.A. Lozupone, M. Hamady, E.C. Martens, B. Henrissat, P.M. Coutinho, P. Minx, P. Latreille, H. Cordum, A. Van Brunt, K. Kim, R. Fulton, S.W. Clifton, R.K. Wilson, R.D. Knight, and J.I. Gordon. Evolution of symbiotic bacteria in the distal human intestine. *PLoS Biology,* 2007 June 19; **5**(7): e156.

Rawls J.F., **M.A. Mahowald**, A.L. Goodman, C.M. Trent, and J.I. Gordon (2007). In vivo imaging and genetic analysis link bacterial motility and symbiosis in the zebrafish gut. *Proc Natl Acad Sci U S A.* **104**(18): 7622-7.

Turnbaugh, P.J., R.E. Ley, **M.A. Mahowald,** V. Magrini, E.R. Mardis and J.I. Gordon. An obesity-associated gut microbiome with increased capacity for energy harvest. *Nature,* 2006 December 21; **444**(7122): 1027-31.

Rawls, J.F., **M.A. Mahowald**, R.E. Ley, and J.I. Gordon (2006). Reciprocal gut microbiota transplants from zebrafish and mice to germ-free recipients reveal host habitat selection. *Cell* **127**(2): 423-33.

Aklilu, M., W.M. Stadler, M. Markiewicz, N.J. Vogelzang, **M. Mahowald,** M. Johnson and T.F. Gajewski (2004). Depletion of normal B cells with rituximab as an adjunct to IL-2 therapy for renal cell carcinoma and melanoma. *Ann Oncol* **15**(7): 1109-14.

Dorus, S., E.J. Vallender, P.D. Evans, J.R. Anderson, S.L. Gilbert, **M. Mahowald,** G.J. Wyckoff, C.M. Malcom and B.T. Lahn (2004). Accelerated evolution of nervous system genes in the origin of Homo sapiens. *Cell* **119**(7): 1027-40.

Harlin, H., A.S. Artz, **M. Mahowald**, B.I. Rini, T. Zimmerman, N.J. Vogelzang and T.F. Gajewski (2004). Clinical responses following nonmyeloablative allogeneic stem cell transplantation for renal cell carcinoma are associated with expansion of CD8+ IFN-gamma-producing T cells. *Bone Marrow Transplant* **33**(5): 491-7.

Bird, J.J., D.R. Brown, A.C. Mullen, N.H. Moskowitz, **M.A. Mahowald,** J.R. Sider, T.F. Gajewski, C.R. Wang and S.L. Reiner (1998). Helper T cell differentiation is controlled by the cell cycle. *Immunity* **9**(2): 229-37.

* Contributed equally

Chapter 1

Introduction

Introduction

Studies of germ-free animals have revealed that the mammalian gut microbial community ('microbiota') is essential to normal host development, nutrition and health. It stimulates normal gut and immune system development, and synthesizes essential vitamins and ferments otherwise indigestible dietary polysaccharides ("fiber") to short chain fatty acids (SCFA), principally acetate, propionate, and butyrate, which are absorbed by the gut epithelium and used for energy [1]. This process accounts for up to 10% of our daily calories [2].

Diversity of the gut microbiota

In humans, the gut microbial community contains an estimated 10^{14} organisms; most of these reside in our distal gut, and most belong to the domain Bacteria, although the other two domains of life (Archaea and Eukarya) are also represented. The total number of microbial cells inhabiting our gut is estimated to be ~10-fold more than the total number of human cells in our adult body [3].

Among the Bacteria, hundreds to thousands of species-level phylogenetic types (phylotypes) are present in the distal gut microbiota [4, 5]. The community is dominated, however, by just two Bacterial phyla: the Bacteroidetes and the Firmicutes [4-6]. Results obtained from the small number of individuals and demographic groups sampled thus far have led to the conclusion that there are no microbial species-level phylotypes associated with all adult human guts [4]. Detailed, culture-independent surveys have revealed that the dominant phylotypes within this community can vary greatly between individuals, and even in the same individual over time [4, 7]. However, the current view, based on these culture-independent surveys, is that the overall microbiota membership in an individual adult remains relatively constant despite variation between dominant types.

Analyses of humans as well as animal models suggest that the stability of overall membership extends beyond a single generation. Analyses of twin pairs and their mothers indicate that gut communities cluster by families, suggesting that the microbiota is vertically transmitted [4, 8]. Mouse and other mammalian studies support this notion. For instance, 16S rRNA sequence-based analyses of the gut microbiotas of female mice and their offspring (separated at weaning and individually housed) have demonstrated that two mothers who are sisters produce offspring whose gut microbiota is more similar to one another, and to their mothers, than to the offspring of an unrelated mother of the same inbred strain [7]. Furthermore, a survey of the gut microbiotas of 59 non-human mammalian species (including 17 non-human primate lineages) showed that individuals belonging to a given mammalian species ('conspecifics') harbor closely related gut communities independent of their provenance (i.e., whether animals are in one of two different zoos, or are in the wild or domesticated), suggesting that vertical transmission of the microbiota is a general characteristic of mammals [9].

This global mammalian gut survey indicated that diet, host phylogeny and digestive physiology/gut structure (i.e., foregut vs. midgut and hindgut fermenters) contribute to microbiota structure (**Figure 1**). Most extant mammals are herbivores, although ancestral mammals are thought to have been carnivorous. The microbial solution to herbivory has been similar among mammals: in other words, there are shared features of gut microbial community structure among herbivores, and these encompass animals that occupy quite distinctive positions in the mammalian tree. Increased plant consumption is also associated with the increased diversity in the gut microbiota (herbivory > omnivory > carnivory) [9]. This richness likely reflects the vast chemical complexity of glycosidic linkages present in plant polysaccharides and the relatively paltry number of glycoside hydrolases and polysaccharide lyases present in mammalian genomes. As noted above, microbial fermentation of these polysaccharides allows for harvest of energy from the diet that would otherwise be lost.

Gut microbial affects on adiposity

Given its importance in health, it is not surprising that changes in the gut microbial community have been observed in various pathological states. Members of our lab found that inoculation of adult germ-free mice with a distal gut microbial community harvested from conventionally raised animals (a process known as "conventionalization") induces a rapid and sustained increase in body fat (within 10 days) despite a decrease in food consumption. This occurs in multiple mouse strains, in male and female animals, and does not require mature T- or B-lymphocytes or Ppar-α [10]. Conventionalization increases fermentation of polysaccharides to SCFA, which are then absorbed from the gut and metabolized by the body, stimulating *de novo* lipogenesis in the liver [10]. Colonization also represses expression of fasting induced adipose factor (Fiaf) in the gut epithelium. Fiaf is a secreted protein that inhibits lipoprotein lipase (LPL), a key enzyme involved in uptake of lipids into adipocytes and other tissues. Suppression of intestinal Fiaf expression produces a significant increase in LPL activity in adipocytes and a concomitant increase in adiposity [10]. Studies of gnotobiotic *Fiaf*$^{-/-}$ and wild type littermates have established the important contribution of Fiaf to the microbiota-induced increase in adiposity [10]. However, the microbial factors that lead to these shifts in *Fiaf* expression remain uncertain. Studies of germ-free and conventionalized wild type and knockout mice have identified other genes whose expression in the gut epithelium is essential for this microbiota-dependent increase in adiposity [11]. Thus, the microbiota regulates both sides of the energy balance equation: the efficiency with which energy is harvested from the diet as well as host signaling pathways that are important for modulating how absorbed energy is processed and deposited in adipocytes.

Additional experiments suggest that the microbiota and its genes (microbiome) should be considered as possible risk factors for development of obesity. Both genetically obese *(ob/ob)* mice, as well as obese humans, possess a significantly higher proportion of Firmicutes and reduced proportion of Bacteroidetes than their lean counterparts [7, 12].

The difference in relative proportions of the Firmcutes and the Bacteroidetes is not due to any specific clades within either phylum, and studies of runted *ob*/*ob* mice suggest that it is not due to increased food consumption per se. Transfer of the distal gut microbial community from *ob*/*ob* mice to wild type (+/+) germ-free recipients produces a larger gain in adiposity than does transfer of the microbiota from lean +/+ donors to +/+ germ-free recipients, after 2 weeks [13]. This was correlated with increased SCFA production and decreased energy content in feces, suggesting increased energy extraction by the obese microbial community. Consistent with these results, metagenomic sequencing of the gut microbiomes of ob/ob and +/+ littermates revealed an increased representation of microbial genes involved in processing of dietary polysaccharides in the former compared to the latter.

As obese humans lose weight, the proportion of Bacteroidetes in their guts rises progressively, with the magnitude of the increase correlating significantly with their weight loss. Intriguingly, this change in the proportion of Bacteroidetes to Firmicutes occurred both in individuals placed on both a low fat and on a low carbohydrate diet [7]. These findings in humans indicate that gut microbial ecology is dynamically linked to obesity. The studies in mice, particularly the microbiota transplant experiments and comparative metagenomic analyses, suggest that the microbiota is a mediator of increased adiposity and that the phenotype is transmissible.

More recently, members of the lab have examined the effects of obesity induced by consumption of a prototypic Western diet, enriched in fats and simple sugars, on the distal gut microbiota and microbiome [14]. Similar to *ob*/*ob* mice, there was a phylum wide suppression of Bacteroidetes in animals with diet-induced obesity (DIO) compared to lean controls who had consumed a standard, polysaccharide rich, low fat diet. Unlike the *ob*/*ob* microbiota, the proportional increase in the Firmicutes in this model was attributable to a bloom in a single clade within the Mollicutes class of Firmicutes. This bloom did not require a functional adaptive or innate immune system since it occurred in both *Rag1*$^{-/-}$ and

Myd88$^{-/-}$ hosts, and was reversible when adiposity was stabilized or reduced by switching animals to a reduced calorie low fat or low carbohydrate diet [14]. Comparative metagenomic analyses of the microbiome revealed an enrichment in genes involved in import and processing of dietary sugars associated with DIO. Microbiota transplant experiments showed that the adiposity phenotype could be transmitted to germ-free recipients [14]. Together, these findings further emphasize the dynamic interrelationship between gut microbial community structure, diet, and energy balance.

Large scale, phylum-wide changes in the gut microbiota make dissection of the contributions of individual members of this community to energy/nutrient harvest very challenging. Therefore, the goal of my thesis has been to conduct comparative genomic, functional genomic and biochemical analyses of the ways in which human gut-derived Bacteroidetes and Firmicutes interact *in vivo*. I have done so by constructing a simplified model of the human gut microbial community in gnotobiotic mice, using sequenced members of our distal intestinal microbiota.

Meet the gut microbiota: Bacteroidetes

The Bacteroidetes are Gram-negative obligate anaerobic bacilli (for a 16S rRNA based phylogenetic tree see **Figure 2**). Human gut Bacteroidetes have long been studied as opportunistic pathogens; in particular, *Bacteroides fragilis* is the most commonly isolated organism from abdominal abscesses, vastly overrepresented among such isolates compared to its proportion within the gut microbial community [15]. In healthy individuals, though, Bacteroidetes are commensal, or perhaps mutualistic, members of the community. A number of studies over the last decade have significantly improved our understanding of the metabolism and properties of a model *Bacteroides* species, *B. thetaiotaomicron,* on a genomic level.

Completion of the first *Bacteroides* genome sequence revealed a bacterium with an unprecedented genomic structure. *B. thetaiotaomicron's* 6.2 Mbp genome possesses

240 glycoside hydrolases and polysaccharide lyases; in comparison, the 500-fold larger human genome possesses only 99. These enzymes are organized into gene clusters, termed polysaccharide utilization loci (PULs), that contain various combinations of glycosidic enzymes. There are 88 individual PULs in the *B. thetaiotaomicron* genome [16], and other gut and non-gut Bacteroidetes also possess PULs [17-20]. All PULs identified to date possess two linked genes encoding homologs of two outer membrane proteins, SusC and SusD, that are components of the first identified PUL - the starch utilization system (Sus) [21]. SusC is predicted to be a TonB-dependent, β-barrel-type outer membrane transporter and is essential for importing α1,4-linked glucose polymers into the periplasm. SusD is an outer membrane α-helical starch binding lipoprotein needed for growth on starch molecules containing ≥6 glucose units [22]. The conserved genomic organization of the PULs [17], together with the frequent presence of linked genes encoding sensor/regulator functions (*e.g.*, ECF-σ/anti-σ factor pairs, 'hybrid' two component phosphorelay systems, plus others) have given rise to the notion that individual PULs encode the functions needed to act as carbohydrate substrate-specific sensing and acquisition systems [16].

GeneChip analyses of *B. thetaiotaomicron* gene expression in the distal guts of gnotobiotic mice colonized with this organism alone indicate that *B. thetaiotaomicron* is capable of harvesting dietary plant glycans as well as host mucosal glycans [16, 23, 24]. Specifically, comparison of the transcriptional profiles of *B. thetaiotaomicron* in the ceca of adult gnotobiotic mice fed a standard, plant polysaccharide-rich chow versus (i) a diet rich in simple sugars but devoid of plant polysaccharides [16, 24] and (ii) suckling mice (diet rich in oligosaccharides; [23]) revealed that in both polysaccharide-poor conditions, *B. thetaiotaomicron* downregulates a variety of PULs targeting plant-derived glycans, and upregulates other PULs predicted to access and process host-derived mucin glycans. Many of the same loci are also induced in log-phase growth in minimal medium supplemented with porcine gastric mucin as the sole carbon source, compared to minimal medium plus glucose [16]. The capacity to turn to host glycans as a nutrient source when dietary poly-

saccharides are not available may be very advantageous: this type of opportunitistic, or flexible foraging for glycans could help *B. thetaiotaomicron* to (i) maintain its foothold in the very competitive distal gut microbiota; (ii) be transmitted from mothers to her offspring; (iii) provide the products of polysaccharide fermentation to other members of the community (i.e., promotion of syntrophic relationships), and (iv) contribute to ecosystem robustness [16].

Meet the gut microbiota: Firmicutes

Firmicutes are diverse group of low-GC Gram-positive Bacteria (for a 16S rRNA-based tree, see **Figure 2**). The global mammalian gut microbiota survey described earlier revealed that the Firmicutes are inevitably present in mammalian GI tracts and are the dominant phylum [9]. Abundant human gut-associated Firmicutes are less well studied than Bacteroidetes. However, they have several properties that are important to mammalian physiology. One is the capacity to produce butyrate. Butyrate is one of the principal fermentation products of the gut microbial community, and is generated by phylotypes scattered throughout the Firmicutes phylogenetic tree (e.g., see lineages marked with an asterisk in **Figure 2**). Compared to other SCFAs, butyrate is preferentially absorbed and utilized by the gut epithelium [25, 26]. Since it is longer than the other commonly generated SFCAs, it yields more energy upon oxidation.

Butyrate has profound effects on the growth of colonic cell lines *in vitro,* a fact that has led to many investigations concerning its role in mediating the long-studied link between diet and colorectal carcinoma. Butyrate can inhibit inflammation, and induces apoptosis as well as differentiation in adenocarcinoma-derived gut epithelial cell lineages [27]. The majority of animal studies have shown that increasing butyrate concentrations (e.g., by feeding slowly fermented fiber, or by colonization with butyrate-producing organisms), correlates with reduced epithelial proliferation, and decreased incidence of precancerous lesions [28-31]. However, other studies show opposing effects [32-34]. These results may

conflict because the consumption of fiber or bacteria, as in all these *in vivo* studies, produces poorly defined shifts in the microbial community structure and metabolic activity.

Other metabolic activities associated with members of the Firmicutes include the 7-α dehydroxylation of bile acids to yield the secondary bile acids deoxycholate and lithocholate, which have been implicated in promoting colon cancer [35, 36]; production of conjugated linoleic acids, which have been implicated in decreasing both adiposity and cancer risk [37]; and acetogenesis, a process by which acetate is produced by reductive fixation of carbon dioxide via the Wood-Ljungdahl pathway [38].

At the start of this thesis project, very few genome structures of common human gut Firmicutes were defined, and many branches of the tree were completely unrepresented by genomic sequence. Similarly, their niche space remained poorly defined, and potentially vast.

Overview of the dissertation

The goal of this thesis was to better characterize the genomic and metabolic properties of the two dominant phyla of mammalian gut bacteria, the Bacteroidetes and the Firmicutes, and use a more simplified model microbial community to explore the way in which they adapt themselves to life in the gut and to one another.

Chapter 2 describes the insights gained from the complete genomic sequencing of two common members of the Bacteroidetes, *B. vulgatus* and *P. distasonis*. I compared the genome content of these two Bacteroidetes with the five available completed Bacteroidetes genomes, including three gut Bacteroidetes (two strains of *B. fragilis* as well as *B. thetaiotaomicron),* and two non-gut Bacteroidetes *(Cytophaga hutchinsonii* and *Porphyromonas gingivalis)*. I assigned all the proteins from these seven genomes to functional categories, and compared the proportion of genes in each category in each genome. I found that gut Bacteroidetes in general could be differentiated from their non-gut relatives by the

large proportion of genes devoted to environmental sensing, carbohydrate metabolism, and membrane transport; these genes are typically arranged in PULs, like those present in *B. thetaiotaomicron*. I then showed that although all the gut Bacteroidetes share large numbers of genes in these functional categories, the individual genes in each represented category have diverged substantially, suggesting some niche differentiation among Bacteroidetes. The genomes of *B. vulgatus* and *P. distasonis* possess a significantly smaller proportion of glycoside hydrolases and other carbohydrate-active enzymes than *B. thetaiotaomicron*. *P. distasonis* possesses a larger proportion of predicted proteases, while *B. vulgatus* has a larger proportion of genes involved in degrading pectins, as well as genes involved in processing xylans, which *B. thetaiotaomicron* is unable to utilize.

We then used a phylogenetic approach to identify genes within these species that were acquired due to lateral gene transfer (LGT) from outside the Bacteroidetes phylum. The results indicated that an average of 5.5% of the genes in each genome were acquired via this mechanism. We observed predicted conjugative transposons and prophage elements within some of these loci, suggesting that these transmissible elements are at least partially responsible for the large number of laterally transferred genes within these loci.

In Chapter 3, I built on these observations by comparing the genomes of gut Firmicutes to those of Bacteroidetes, and assessing the ways in which model members of each phylum adapt themselves to coexistence with each other in the distal gut habitats of gnotobiotic mice. First, I annotated the first two finished genomes from human gut Clostridium Cluster XIVa, one of the most common gut Firmicute clades. By comparing these genome sequences with the genome sequences of 16 other gut Firmicutes and those of human gut Bacteroidetes, I was able to show that gut Firmicutes possess smaller genomes, a significantly smaller proportion of glycan-degrading genes, and a more specialized or restricted ability to acquire and process carbohydrates compared to the Bacteroidetes. Four gut Firmicutes also possess flagellar genes, suggesting that motility helps them adopt a more

specialized lifestyle in which they are able to move to areas where their preferred nutrient source is abundant.

To test whether these predicted differences in the ability to process exogenous carbohydrates reflect niches that are important in the gut, I identified differences in the ability of three sequenced human gut symbionts to grow on different carbon sources *in* vitro. This demonstrates that, as predicted, *B. thetaiotaomicron* and *B. vulgatus* grow on many more simple and complex sugars than does *E. rectale*. However, *B. vulgatus* does successfully degrade pectin and xylan substrates that *B. thetaiotaomicron* cannot, while *E. rectale* grows on at least one substrate that neither *Bacteroides* is able to utilize, namely cellobiose, the disaccharide building block of plant cell walls.

To determine whether their differences in polysaccharide utilization were important to the metabolism of these microbes in the guts of mice, I colonized germ-free mice with *B. thetaiotaomicron* or *E. rectale* alone (monoassociation), or together (co-colonization), and similarly, with either *B. thetaiotaomicron* or *B. vulgatus,* or both together. I found that *B. vulgatus* almost exclusively upregulated operons of genes involved in xylan and pectin degradation in co-colonization compared to monoassociation – i.e., the same classes of glycan-degrading genes that were predicted to encode its unique activities. *B. thetaiotaomicron's* response to the presence of *E. rectale* was similar: it upregulated PULs invoved in the degradation of host-derived mucin glycans such as α-mannans, which *E. rectale* cannot utilize. These responses are similar to those seen when *B. thetaiotaomicron* interacts with other bacterial lineages [39].

On the other hand, *E. rectale's* response to *B. thetaiotaomicron* was quite distinct. Carbohydrate metabolic genes, particularly glycoside hydrolases, were proportionally overrepresented among the downregulated genes when comparing the transcriptome expressed *in vivo* in co-colonization versus monoassociation. Instead, *E. rectale* became more selective in the glycans it utilized, upregulating four predicted sugar transport genes,

while downregulating 14. It also induced a variety of amino acid and peptide transporters. *E. rectale* broadly upregulated expression of translational and biosynthetic genes, as well as central metabolic regulators, similar to what I observed during log-phase growth *in vitro*, suggesting that it had sufficient or even improved access to nutrients in the presence of *B. thetaiotaomicron in vivo*. *In vitro* studies confirmed that *E. rectale* is able to harvest simple sugars released by the enzymes expressed by *B. thetaiotaomicron*.

Together, these comparative genomic, functional genomic and biochemical studies, conducted using gnotobiotic models of the human gut microbiota, illustrate niche specialization and functional redundancy within the Bacteroidetes. Furthermore, they demonstrate the adaptable niche specialization that likely underlies the success of Firmicutes in this habitat. Finally, these studies underscore the importance of host glycans as a nutrient foundation that ensures ecosystem stability.

References

1. Hooper, L.V., T. Midtvedt, and J.I. Gordon, 2002. How host-microbial interactions shape the nutrient environment of the mammalian intestine. *Annu Rev Nutr*, **22** p. 283-307.

2. Roberfroid, M.B., 1999. Caloric Value of Inulin and Oligofructose. *J. Nutrition*, **129** (7 (Supplement)), p. 1436S-1437S.

3. Luckey, T.D., 1972. Introduction to intestinal microecology. *Am J Clin Nutr*, **25** (12), p. 1292-4.

4. Turnbaugh, P.J., M. Hamady, T. Yatsunenko, B.L. Cantarel, A. Duncan, R.E. Ley, M.L. Sogin, W.J. Jones, B.A. Roe, J.P. Affourtit, B. Henrissat, A.C. Heath, R. Knight, and J.I. Gordon, 2008. Inheritance of a core gut microbiome in obese and lean monozygotic twin pairs. *submitted*.

5. Eckburg, P.B., E.M. Bik, C.N. Bernstein, E. Purdom, L. Dethlefsen, M. Sargent, S.R. Gill, K.E. Nelson, and D.A. Relman, 2005. Diversity of the human intestinal microbial flora. *Science*, **308** (5728), p. 1635-8.

6. Ley, R.E., R. Knight, and J.I. Gordon, 2007. The human microbiome: eliminating the biomedical/environmental dichotomy in microbial ecology. *Environ Microbiol*, **9** (1), p. 3-4.

7. Ley, R.E., P.J. Turnbaugh, S. Klein, and J.I. Gordon, 2006. Microbial ecology: human gut microbes associated with obesity. *Nature*, **444** (7122), p. 1022-3.

8. Zoetendal, E.G., A.D. Akkermans, and W.M. De Vos, 1998. Temperature gradient gel electrophoresis analysis of 16S rRNA from human fecal samples reveals stable and host-specific communities of active bacteria. *Appl Environ Microbiol*, **64** (10), p. 3854-9.

9. Ley, R.E., M. Hamady, C. Lozupone, P.J. Turnbaugh, R.R. Ramey, J.S. Bircher, M.L. Schlegel, T.A. Tucker, M.D. Schrenzel, R. Knight, and J.I. Gordon, 2008. Evolution of mammals and their gut microbes. *Science*, **320** (5883), p. 1647-51.

10. Backhed, F., H. Ding, T. Wang, L.V. Hooper, G.Y. Koh, A. Nagy, C.F. Semenkovich, and J.I. Gordon, 2004. The gut microbiota as an environmental factor that regulates fat storage. *Proc Natl Acad Sci U S A*, **101** (44), p. 15718-23.

11. Samuel, B.S., A. Shaito, T. Motoike, F.E. Rey, F. Backhed, J.K. Manchester, R.E. Hammer, S.C. Williams, J. Crowley, M. Yanagisawa, and J.I. Gordon, 2008. Effects of the gut microbiota on host adiposity are modulated by the short chain fatty acid binding G protein-coupled receptor, Gpr41. *Proc Natl Acad Sci U S A*, **submitted**.

12. Ley, R.E., F. Backhed, P. Turnbaugh, C.A. Lozupone, R.D. Knight, and J.I. Gordon, 2005. Obesity alters gut microbial ecology. *Proc Natl Acad Sci U S A*, **102** (31), p. 11070-5.

13. Turnbaugh, P.J., R.E. Ley, M.A. Mahowald, V. Magrini, E.R. Mardis, and J.I. Gordon, 2006. An obesity-associated gut microbiome with increased capacity for energy harvest. *Nature*, **444** (7122), p. 1027-31.

14. Turnbaugh, P.J., F. Backhed, L. Fulton, and J.I. Gordon, 2008. Diet-induced obesity is linked to marked but reversible alterations in the mouse distal gut microbiome. *Cell Host Microbe*, **3** (4), p. 213-23.

15. Polk, B.F. and D.L. Kasper, 1977. Bacteroides fragilis subspecies in clinical isolates. *Ann Intern Med*, **86** (5), p. 569-71.

16. Martens, E.C., H.C. Chiang, and J.I. Gordon, 2008. Mucosal Glycan Foraging Enhances the Fitness and Transmission of a Saccharolytic Human Gut Symbiont. *submitted*.

17. Xu, J., M.A. Mahowald, R.E. Ley, C.A. Lozupone, M. Hamady, E.C. Martens, B.

Henrissat, P.M. Coutinho, P. Minx, P. Latreille, H. Cordum, A. Van Brunt, K. Kim, R.S. Fulton, L.A. Fulton, S.W. Clifton, R.K. Wilson, R.D. Knight, and J.I. Gordon, 2007. Evolution of Symbiotic Bacteria in the Distal Human Intestine. *PLoS Biol*, **5** (7), p. e156.

18. Xie, G., D.C. Bruce, J.F. Challacombe, O. Chertkov, J.C. Detter, P. Gilna, C.S. Han, S. Lucas, M. Misra, G.L. Myers, P. Richardson, R. Tapia, N. Thayer, L.S. Thompson, T.S. Brettin, B. Henrissat, D.B. Wilson, and M.J. McBride, 2007. Genome sequence of the cellulolytic gliding bacterium Cytophaga hutchinsonii. *Appl Environ Microbiol*, **73** (11), p. 3536-46.

19. Bauer, M., M. Kube, H. Teeling, M. Richter, T. Lombardot, E. Allers, C.A. Wurdemann, C. Quast, H. Kuhl, F. Knaust, D. Woebken, K. Bischof, M. Mussmann, J.V. Choudhuri, F. Meyer, R. Reinhardt, R.I. Amann, and F.O. Glockner, 2006. Whole genome analysis of the marine Bacteroidetes 'Gramella forsetii' reveals adaptations to degradation of polymeric organic matter. *Environ Microbiol*, **8** (12), p. 2201-13.

20. Pinhassi, J., J.P. Bowman, O.I. Nedashkovskaya, I. Lekunberri, L. Gomez-Consarnau, and C. Pedros-Alio, 2006. Leeuwenhoekiella blandensis sp. nov., a genome-sequenced marine member of the family Flavobacteriaceae. *Int J Syst Evol Microbiol*, **56** (Pt 7), p. 1489-93.

21. Reeves, A.R., G.R. Wang, and A.A. Salyers, 1997. Characterization of four outer membrane proteins that play a role in utilization of starch by Bacteroides thetaiotaomicron. *J Bacteriol*, **179** (3), p. 643-9.

22. Koropatkin, N.M., E.C. Martens, J.I. Gordon, and T.J. Smith, 2008. Starch catabolism by a prominent human gut symbiont is directed by the recognition of amylose helices. *Structure*, **16** (7), p. 1105-15.

23. Bjursell, M.K., E.C. Martens, and J.I. Gordon, 2006. Functional genomic and metabolic studies of the adaptations of a prominent adult human gut symbiont, Bacteroides thetaiotaomicron, to the suckling period. *J Biol Chem*, **281** (47), p. 36269-79.

24. Sonnenburg, J.L., J. Xu, D.D. Leip, C.H. Chen, B.P. Westover, J. Weatherford, J.D. Buhler, and J.I. Gordon, 2005. Glycan foraging in vivo by an intestine-adapted bacterial symbiont. *Science*, **307** (5717), p. 1955-9.

25. Bergman, E.N., 1990. Energy contributions of volatile fatty acids from the gastrointestinal tract in various species. *Physiol Rev*, **70** (2), p. 567-90.

26. Ritzhaupt, A., I.S. Wood, A. Ellis, K.B. Hosie, and S.P. Shirazi-Beechey, 1998. Identification and characterization of a monocarboxylate transporter (MCT1) in pig and human colon: its potential to transport L-lactate as well as butyrate. *J Physiol*, **513 (Pt 3)** p. 719-32.

27. Medina, V., B. Edmonds, G.P. Young, R. James, S. Appleton, and P.D. Zalewski, 1997. Induction of caspase-3 protease activity and apoptosis by butyrate and trichostatin A (inhibitors of histone deacetylase): dependence on protein synthesis and synergy with a mitochondrial/cytochrome c-dependent pathway. *Cancer Res*, **57** (17), p. 3697-707.

28. Ohkawara, S., H. Furuya, K. Nagashima, N. Asanuma, and T. Hino, 2005. Oral administration of butyrivibrio fibrisolvens, a butyrate-producing bacterium, decreases the formation of aberrant crypt foci in the colon and rectum of mice. *J Nutr*, **135** (12), p. 2878-83.

29. Nakanishi, S., K. Kataoka, T. Kuwahara, and Y. Ohnishi, 2003. Effects of high amylose maize starch and Clostridium butyricum on metabolism in colonic microbiota and formation of azoxymethane-induced aberrant crypt foci in the rat colon. *Microbiol Immunol*, **47** (12), p. 951-8.

30. Cassidy, A., S.A. Bingham, and J.H. Cummings, 1994. Starch intake and colorectal cancer risk: an international comparison. *Br J Cancer*, **69** (5), p. 937-42.

31. McIntyre, A., P.R. Gibson, and G.P. Young, 1993. Butyrate production from dietary fibre and protection against large bowel cancer in a rat model. *Gut*, **34** (3), p. 386-91.

32. Folino, M., A. McIntyre, and G.P. Young, 1995. Dietary fibers differ in their effects on large bowel epithelial proliferation and fecal fermentation-dependent events in rats. *J Nutr*, **125** (6), p. 1521-8.

33. Zoran, D.L., N.D. Turner, S.S. Taddeo, R.S. Chapkin, and J.R. Lupton, 1997. Wheat bran diet reduces tumor incidence in a rat model of colon cancer independent of effects on distal luminal butyrate concentrations. *J Nutr*, **127** (11), p. 2217-25.

34. Lupton, J.R. and P.P. Kurtz, 1993. Relationship of colonic luminal short-chain fatty acids and pH to in vivo cell proliferation in rats. *J Nutr*, **123** (9), p. 1522-30.

35. Ridlon, J.M., D.J. Kang, and P.B. Hylemon, 2006. Bile salt biotransformations by human intestinal bacteria. *J Lipid Res*, **47** (2), p. 241-59.

36. Bernstein, H., C. Bernstein, C.M. Payne, K. Dvorakova, and H. Garewal, 2005. Bile acids as carcinogens in human gastrointestinal cancers. *Mutat Res*, **589** (1), p. 47-65.

37. Devillard, E., F.M. McIntosh, S.H. Duncan, and R.J. Wallace, 2007. Metabolism of linoleic acid by human gut bacteria: different routes for biosynthesis of conjugated linoleic acid. *J Bacteriol*, **189** (6), p. 2566-70.

38. Drake, H.L., K. Küsel, and C. Matthies, *Acetogenic Prokaryotes*, in *Prokaryotes*, M. Dowrkin, S. Falkow, E. Rosenberg, K.H. Schleifer, and E. Stackebrandt, Editors. 2006, Springer: New York. p. 354-420.

39. Sonnenburg, J.L., C.T. Chen, and J.I. Gordon, 2006. Genomic and metabolic studies of the impact of probiotics on a model gut symbiont and host. *PLoS Biol*, **4** (12), p. e413.

40. Lozupone, C., M. Hamady, and R. Knight, 2006. UniFrac--an online tool for comparing microbial community diversity in a phylogenetic context. *BMC Bioinformatics*, **7** p. 371.

41. DeSantis, T.Z., Jr., P. Hugenholtz, K. Keller, E.L. Brodie, N. Larsen, Y.M. Piceno, R. Phan, and G.L. Andersen, 2006. NAST: a multiple sequence alignment server for comparative analysis of 16S rRNA genes. *Nucleic Acids Res*, **34** (Web Server issue), p. W394-9.

42. Ludwig, W., O. Strunk, R. Westram, L. Richter, H. Meier, Yadhukumar, A. Buchner, T. Lai, S. Steppi, G. Jobb, W. Forster, I. Brettske, S. Gerber, A.W. Ginhart, O. Gross, S. Grumann, S. Hermann, R. Jost, A. Konig, T. Liss, R. Lussmann, M. May, B. Nonhoff, B. Reichel, R. Strehlow, A. Stamatakis, N. Stuckmann, A. Vilbig, M. Lenke, T. Ludwig, A. Bode, and K.H. Schleifer, 2004. ARB: a software environment for sequence data. *Nucleic Acids Res*, **32** (4), p. 1363-71.

Figure Legends

Figure 1. Unweighted pair group method with arithmetic mean (UPGMA) clustering of bacterial communities for each host based on pair-wise differences determined using the UniFrac metric. The tree shows clustering based on species, diet and gut type (foregut fermenter, hindgut fermenter). UniFrac is based on the premise that related communities share an evolutionary history that can be estimated as the fraction of shared branch length in a common phylogenetic tree [40]. The tree was constructed by computing the UniFrac metric based on a neighbor-joining tree of the 21,619 16S rRNA gene sequences in the mammalian gut survey [9]. Labels are colored according to diet (carnivores, red; herbivores, green; omnivores, blue). Vertical bars located to the left of animal names indicate coclustering of conspecific hosts. Non-clustering conspecifics are indicated with same-color stars. Details concerning the human samples are provided in parentheses and include sample ID, descriptors used in the original studies and PubMed ID for each study where available (e.g., T0 and T4 refer to the initial and one-year time point samples for lean control subjects 13 and 14 in PubMed ID 17183309). The circles and squares at internal nodes in the tree indicate jackknife support of ≥50% for 100 iterations; the key at the upper right corner of the figure shows the minimum number of sequences retained per sample for each jackknife analysis. Figure taken from [9].

Figure 2. Phylogenic relationships of select human gut-associated Firmicutes and Bacteroidetes. A phylogeny, based on 16S rRNA gene sequences, showing the relationships between representatives from the two dominant bacterial phyla in the gut microbiota. Green, genomes generated by the Human Gut Microbiome Initiative (www.genome.gov/Pages/Research/Sequencing/SeqProposals/HGMISeq.pdf). Black, other available related genomes. Red, organisms sequenced as part of this work. Asterisks denote those organisms known to produce butyrate. The phylogenetic tree was created by aligning 16S rRNA gene sequences from each genome using the NAST aligner [41], importing the alignment into Arb [42], and then adding them to an existing database of 16S rRNA sequences derived from enumerations of the human gut [5, 7].

Figures

Figure 1.

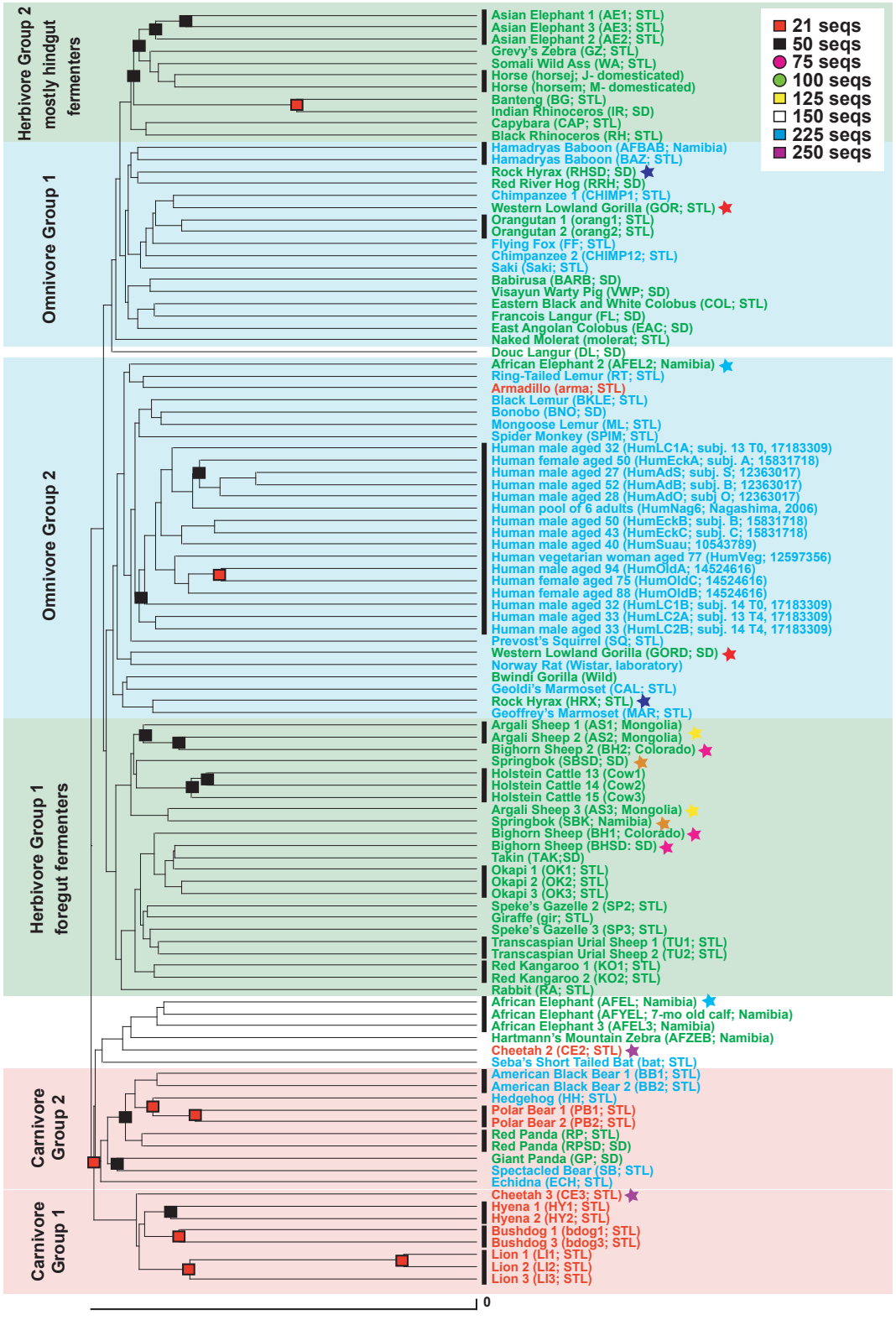

Figure 2.

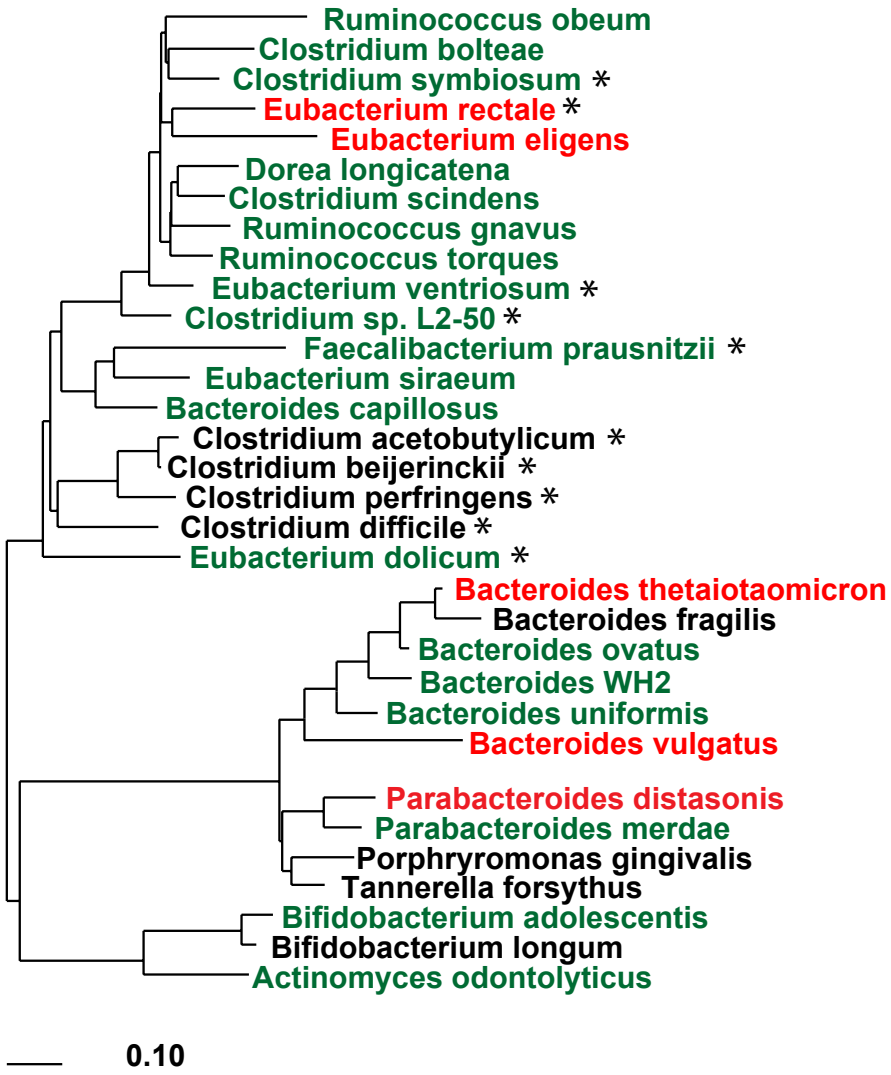
Ruminococcus obeum
Clostridium bolteae
Clostridium symbiosum *
Eubacterium rectale *
Eubacterium eligens
Dorea longicatena
Clostridium scindens
Ruminococcus gnavus
Ruminococcus torques
Eubacterium ventriosum *
Clostridium sp. L2-50 *
Faecalibacterium prausnitzii *
Eubacterium siraeum
Bacteroides capillosus
Clostridium acetobutylicum *
Clostridium beijerinckii *
Clostridium perfringens *
Clostridium difficile *
Eubacterium dolicum *
Bacteroides thetaiotaomicron
Bacteroides fragilis
Bacteroides ovatus
Bacteroides WH2
Bacteroides uniformis
Bacteroides vulgatus
Parabacteroides distasonis
Parabacteroides merdae
Porphryromonas gingivalis
Tannerella forsythus
Bifidobacterium adolescentis
Bifidobacterium longum
Actinomyces odontolyticus
0.10

Chapter 2

Evolution of symbiotic bacteria in the distal human intestine

Chapter 2

Jian Xu[1,2*], Michael A. Mahowald[1*], Ruth E. Ley[1], Catherine A. Lozupone[3], Micah Hamady[4], Eric C. Martens[1], Bernard Henrissat[5], Pedro M. Coutinho[5], Patrick Minx[2], Philippe Latreille[2], Holland Cordum[2], Andrew Van Brunt[2], Kyung Kim[2], Robert S. Fulton[2], Lucinda A. Fulton[2], Sandra W. Clifton[2], Richard K. Wilson[1,2], Robin D. Knight[6], and Jeffrey I. Gordon[1]

[1]Center for Genome Sciences and [2]Genome Sequencing Center, Washington University School of Medicine, St. Louis, MO 63108, [3]Department of Molecular, Cellular and Developmental Biology and [4]Department of Computer Science, University of Colorado, Boulder, CO 80309, [5]CNRS-UMR6098, Universités Aix-Marseille I & II, Marseille, France, and [6]Department of Chemistry and Biochemistry, University of Colorado, Boulder, CO 80309

*Contributed equally

Correspondence to: jgordon@wustl.edu; Ph 314:362-7243; Fax 314:362-7047

Running title: Evolution of human gut Bacteroidetes

Abstract

The adult human intestine contains trillions of bacteria, representing hundreds of species and thousands of subspecies. Little is known about the selective pressures that have shaped and are shaping this community's component species, which are dominated by members of the Bacteroidetes and Firmicutes divisions. To examine how the intestinal environment affects microbial genome evolution, we have sequenced the genomes of two members of the normal distal human gut microbiota, *Bacteroides vulgatus* and *Bacteroides distasonis*, and by comparison with the few other sequenced gut and non-gut Bacteroidetes, analyzed their niche and habitat adaptations. The results show that lateral gene transfer, mobile elements, and gene amplification have played important roles in affecting the ability of gut-dwelling Bacteroidetes to vary their cell surface, sense their environment, and harvest nutrient resources present in the distal intestine. Our findings show that these processes have been a driving force in the adaptation of Bacteroidetes to the distal gut environment, and emphasize the importance of considering the evolution of humans from an additional perspective, namely the evolution of our microbiomes.

Introduction

Our distal gut is one of the most densely populated and most thoroughly surveyed bacterial ecosystems in nature. This microbiota contains more bacterial cells than all of our body's other microbial communities combined. The gut microbial community and its collective genome (microbiome) endow us with physiological attributes that we have not had to evolve on our own, including the ability to break down otherwise indigestible polysaccharides [1,2]. The most complete 16S rRNA gene sequence-based enumerations available indicate that >90% of phylogenetic types (phylotypes) belong to just two of the 70 known divisions of Bacteria, the Bacteroidetes and the Firmicutes, with the remaining phylotypes distributed among eight other divisions [3]. With an estimated 500-1,000 species, and over 7,000 strains [4], the evolutionary tree of our distal intestinal microbiota can be visualized as a grove of ten palm trees (divisions), each topped by fronds representing divergent lineages, and with each frond composed of many leaves representing closely related bacteria [1]. In contrast, soil, Earth's terrestrial 'gut' for degrading organic matter, can be viewed as a bush, composed of many more intermediate and deeply diverging lineages [5].

It is unclear how selective pressures, microbial community dynamics, and the environments in which we live shape the genomes and functions of members of our gut microbiota, and hence our 'micro-evolution.' Ecological principles predict that functional redundancy encoded in genomes from divergent bacterial lineages insures against disruption of food webs. These principles also predict that host-driven, "top-down" selection for such redundancy should produce a community composed of distantly related members, whose genomes convergently evolve functionally *similar* suites of genes [4]. Lateral gene transfer (LGT), which allows for rapid transfer of genes under strong selection, such as those encoding antibiotic resistance [6], represents one way that members of the microbiota could share metabolic and other capabilities. In contrast, competition between members of a microbiota should exert a "bottom-up" selective pressure that produces specialized genomes with functionally *distinct* suites of genes. These distinct suites define ecological

niches (professions), and, once established, could be maintained by barriers to homologous recombination [4].

To explore whether and how these principles apply to the gut microbiota and its microbiome, we have determined the complete genome sequences of two Bacteroidetes with highly divergent 16S rRNA phylotypes that are prominently represented in the distal gut of healthy humans - *Bacteroides vulgatus* and *Bacteroides distasonis* (now also known as *Parabacteroides distasonis*; [7]). *B. distasonis* is basal to the *Bacteroides* clade, and diverged from the common ancestor of the other *Bacteroides* prior to their differentiation. The results of comparisons with other sequenced gut- and non-gut-associated Bacteroidetes, described below, provide insights about the evolution of niche specialization in this highly competitive ecosystem, including the role of lateral gene transfer (LGT).

Results

Functional categorization of genomic adaptations to the distal human gut habitat

The 5,163,189 bp genome of the human gut-derived *B. vulgatus* type strain ATCC 8482 encodes a predicted 4,088-member proteome, while the 4,811,369 bp genome of *B. distasonis* type strain ATCC 8503 possesses 3,867 predicted protein-coding genes (**Table S1** and **Figure S1**). These genomes were initially compared to the genomes of two other Bacteroidetes that live in the distal human gut: *B. thetaiotaomicron* (type stain ATCC 29148; [2] and *B. fragilis* (strains YCH 46 and NCTC 9343; [8,9]. We identified 1,416 sets of orthologous protein-coding genes shared among these gut Bacteroidetes; 1,129 (79.7%) of these conserved gene sets were assigned to COGs (Clusters of Orthologous Groups: **see Figure S2** and **Table S2** for a COG-based categorization). The two most prominently represented COG categories in each of the gut-associated Bacteroidetes proteomes are G (carbohydrate transport and metabolism) and M (cell wall/membrane/envelope biogenesis). The two most prominent COG categories in their shared proteome are E (amino acid

transport and metabolism) and J (translation, ribosomal structure and biogenesis) (**Figure S2**).

The average pairwise amino acid sequence identity among the shared orthologs was 82.0% for *B. thetaiotaomicron-B. fragilis*, 72.1% for *B. thetaiotaomicron-B. vulgatus*, 62.1% for *B. thetaiotaomicron-B. distasonis*, and 61.7% for *B. vulgatus-B. distasonis*. These values are consistent with the 16S rRNA phylogenetic tree for Bacteroidetes (**Figure 1**). Although the evolution of these gut Bacteroidetes is characterized by comprehensive deterioration of global synteny (**Figure S3)**, a total of 257 "patches" of local synteny were identified, composed of adjacent orthologous genes encompassing 765 of the 1,416 shared orthologs (54%; average of 3.0 orthologs per cluster).

The distal gut microbiota is exposed to several prominent nutrient sources: (i) dietary plant polysaccharides that are not digested in the small intestine by the host because our human proteome lacks the requisite glycoside hydrolases and polysaccharide lyases (see the Carbohydrate Active Enyzmes database (CAZy) at http://afmb.cnrs-mrs.fr/CAZY/ for a comprehensive annotation of the human 'glycobiome'), (ii) undigested plant proteins [10], and (iii) host glycans associated with the continuously renewing epithelium that lines the gut and with the even more rapidly replenished mucus layer which overlies this epithelium.

To identify genomic features related to adaptation to life within this distal human gut habitat, we compared shared orthologs among all five completely sequenced gut Bacteroidetes genomes to the subset that is shared with the two Bacteroidetes that occupy non-gut habitats. These non-gut Bacteriodetes are *Porphyromonas gingivalis* W83, a member of the human oral microbiota [11], and *Cytophaga hutchinsonii* ATCC 33406, which is found in soil (http://www.ncbi.nlm.nih.gov/entrez/query.fcgi?db=genomeprj&cmd=Retrieve&dopt=Overview&list_uids=54). Each proteome was searched for conserved domains. These domains were used to assign a functional identifier (InterPro ID) that was then mapped

onto GO (Gene Ontology) terms [12] using InterProScan [13]. The results were compiled and statistical comparisons made between the number of genes assigned to each GO term in different genomes. The complete list of GO assignments for all seven Bacteroidetes genomes is available at http://gordonlab.wustl.edu/BvBd.html.

The subset of orthologs *shared* with non-gut Bacteroidetes is enriched for core metabolic activities, suggesting that all Bacteroidetes have inherited a core metabolome from their common ancestor (**Figure 2A,** compare data in column 7w versus data in 5w). The subset of orthologs *unique* to the gut Bacteroidetes is enriched for genes related to amino acid biosynthesis, membrane transport, carbon-oxygen lyases, and environment sensing/ regulation (see GO terms highlighted in red/pink in the column labeled 5wU in **Figure 2A**). Furthermore, while a comparison of each gut-dwelling Bacteroidetes proteome to the proteomes of its non-gut relatives **(Figure 2B)** revealed that the four gut species are all enriched for genes that belong to GO categories related to three general functions: (i) polysaccharide metabolism, (ii) environmental sensing and gene regulation, and (iii) membrane transport, most of these GO categories are depleted among the subset of orthologs that are unique to the gut-associated Bacteroidetes (**Figure 2A,** 5w vs. Bt-G). Thus, while all four sequenced gut Bacteroidetes species have increased numbers of genes in categories (i)-(iii), this analysis suggests that each one has evolved a divergent array of sensing, regulatory and polysaccharide degradation genes that augment the core metabolome they share with other members of their division.

Niche specialization of Bacteroidetes

To further define the niches occupied by the gut Bacteroidetes, we compared each one to *B. thetaiotaomicron*. *B. thetaiotaomicron* was selected as the reference species because there is a wealth of information about its functional attributes. Scanning electron microscopy, whole genome transcriptional profiling, and mass spectrometry-based metabolomic studies performed in gnotobiotic mice colonized with this prominent human

gut symbiont have shown that it is a remarkably flexible forager for polysaccharides that opportunistically deploys different subsets of its 209 paralogs of SusC and SusD (two outer membrane proteins involved in the binding and import of starch and maltooligosaccharides [14,15]), and 226 predicted glycoside hydrolases and 15 polysaccharide lyases, so that it can feast on dietary or host mucus glycans depending upon the polysaccharide content of the host's diet [16] (**Table S1**).

Compared to the other Bacteroidetes, the *B. thetaiotaomicron* proteome has the most glycoside hydrolases known or predicted to degrade plant glycans (e.g., 64 arabinosidases; our human proteome has none), and the most enzymes for harvesting host glycans (e.g., sulfuric ester hydrolases, hexosaminidases and fucosidases) (**Figure 2B** and **Table S3**). It is also the only sequenced gut Bacteroidetes that possesses candidate polysaccharide lyases for degrading animal tissue glycans (e.g., heparin, chondroitin, hyaluronan; **Table S3**). *B. thetaiotaomicron's* ability to opportunistically use many glycan sources likely makes it an important generalist among intestinal Bacteroidetes.

Compared to *B. thetaiotaomicron*, *B. distasonis* is a specialist. It has the smallest genome among the sequenced human gut-associated Bacteroidetes, the smallest repertoire of genes that are members of the environmental sensing and gene regulation GO categories, and the smallest number of genes associated with carbon source degradation (**Figure 2B** and **Table S1**). *B. distasonis* lacks many accessory hemicellulases (arabinosidases, α-glucuronidases), pectinases, and other polysaccharidases that target non-plant carbohydrates, such as chitinases. Moreover, the number of genes present in each CAZy enzyme class represented in its proteome is markedly reduced compared to the other intestinal Bacteroidetes (e.g., *B. distasonis* has only one candidate α-fucosidase while the other gut-associated species have 9 or 10) (**Table S3**).

B. distasonis has two classes of carbohydrate-processing enzymes that are more abundant in its proteome in than the proteomes of other gut Bacteroidetes: CAZy glycoside

hydrolase family 13 (α-amylase-related proteins), and family 73 (N-acetylhexosaminidases which can target host glycans as well as bacterial cell walls). Its proteome also contains more polysaccharide deacetylases (7 versus 4 in *B. thetaiotamicron* and 1-2 in the *B. fragilis* strains, as characterized by InterPro ID IPR002509; see http://gordonlab.wustl.edu/BvBd.html for a complete list of InterPro ID assignments). Host epithelial glycans contain O-acetylated sugars, including sialic acids, that protect them from direct cleavage by microbial glycoside hydrolases. Thus, *B. distasonis* has the capacity to make the deacetylated products available for itself and other components of the microbiota. Finally, *B. distasonis* devotes a greater proportion of its genome to protein degradation than does *B. thetaiotaomicron* (GO:0006508, 'proteolysis'; P<0.0003 by binomial test; **Figure 2B)**.

The *B. vulgatus* glycobiome has features consistent with *ex vivo* studies indicating that its substrate range for polysaccharides is intermediate between that of *B. distasonis* and *B. thetaiotaomicron* [17]. *B. vulgatus* has the largest and most complete complement of enzymes that target pectin, a common fruit-associated class of glycans (includes pectin methylesterases, pectin acetylesterases, polygalacturonases, and accessory δ-4,5 unsaturated glucuronyl hydrolases). According to the CAZy classification scheme, *B. vulgatus* is the only sequenced gut Bacteroidetes with a gene encoding a xylanase (Bv0041c). Together, these findings reveal overlapping but distinct niches among these gut Bacteroidetes. We next examined the role of lateral gene transfer in shaping their genomes.

Lateral gene transfer

Determining whether a gene is laterally transferred is widely acknowledged to be a difficult problem (e.g. [18-21] and **Supporting Information**). We chose a phylogenetic approach (see **Materials and Methods**) to identify genes that appeared to have been laterally acquired and probably selected for after the divergence of individual gut species. Our approach could potentially identify two types of genes: genes that were laterally transferred only into one lineage, and genes that were lost in all lineages except one. We confirmed

that LGT was the more likely scenario for these genes by demonstrating that they differed in composition from the rest of the genome. This approach allowed us to investigate the adaptations of individual lineages to their specific niche. For simplicity, we refer to these genes as 'laterally transferred' in the remainder of this study, although a minority of them may actually represent differential gene loss, which would still likely indicate species-specific selection [22].

Our approach was to use sensitive, iterated profile searches to retrieve homologs of each protein-coding gene in the genomes of interest from publicly available databases. We then built phylogenetic trees of the related sequences, used the NCBI taxonomy database to assign taxonomy information to each sequence, and employed the Fitch parsimony algorithm [23] to assign the most likely bacterial taxon to each internal node. This analysis allowed us to differentiate four classes of genes: (i) those whose closest relatives are outside the gut Bacteroidetes, suggesting a lateral transfer event and/or differential gene loss; (ii) those whose closest relative is within the gut Bacteroidetes, indicating likely vertical inheritance; (iii) those without any homologs in the database (i.e., 'novel'); and (iv) those whose pattern of inheritance, whether lateral or vertical, could not be determined (i.e., 'unresolved'). Parsimony was used to assign a likely direction ('in' or 'out') to each lateral transfer event where possible (see **Table S4** and **Materials and Methods**).

We did not attempt to resolve lateral transfer events within the gut Bacteroidetes in this study, primarily because the lack of sufficient taxonomic sampling within the Bacteroidetes made it impossible to distinguish transfer from biased sampling. Previous studies have observed that a number of novel genes in other bacterial genomes seem to be laterally acquired [24]. However, for the purposes of our functional analyses, these novel genes were excluded because little functional information is available about them. Because we wished to analyze adaptation to the gut, we also excluded genes that appeared to have been transferred out of the Bacteroidetes.

Our method identified an average of 5.5% of the genes in each genome as being laterally transferred from outside the gut Bacteroidetes (312 for *B. distasonis*, 184 for *B. vulgatus*, 277 for *B. thetaiotaomicron*, 199 for *B. fragilis* NCTC 9343, 214 for *B. fragilis* YCH 46, and 103 for *P. gingivalis)*. We verified that the genes we identified as 'laterally transferred' differed from those classified as 'not transferred' both in terms of GC content ($p<0.0001$ for each genome by two-tailed t-test using Welch's correction for unequal variances) and codon bias ($p<0.0001$ for each genome by chi-squared test). These results, together with the functions represented by this class of genes (see below), confirm that LGT is the most likely scenario accounting for these genes, although we cannot rule out ancient paralogs from the data available because of different rates and patterns of evolution in different lineages, and other confounding factors.

A complete classification of laterally transferred protein-coding genes in the gut Bacteroidetes, and *P. gingivalis,* is provided in **Table S4**. Genes involved in core cellular processes, such as translation (e.g., ribosomal proteins) are less susceptible to LGT than other genes [25]. Primary metabolism (GO:0044238) and protein biosynthesis (GO:0006412) are among the GO terms most enriched in the set of genes *not* subject to LGT **(Figure 3A).** These results suggest that our criteria exclude many genes that would be expected not to undergo LGT. In contrast, genes that are known to be subject to LGT, such as restriction-modification systems [26-28], were enriched in the set of laterally transferred genes we detected **(Figure 3B).**

B. distasonis has a significantly larger proportion of laterally transferred genes than the other gut Bacteroidetes **(Figure 3C).** This excess of LGT does not correlate with a larger number of identifiable mobile elements: *B. distasonis* has fewer of the integrases and transposases that can catalyze the insertion of foreign DNA than do the other Bacteroidetes, and similar numbers of phage (five versus two to five for the other species; see **Table S1**). The excess of LGT genes in *B. distasonis* is also not simply attributable to its more distant phylogenetic relationship to the other gut Bacteroidetes, because *P. gingivalis* does not share

this feature **(Figure 3C**). Instead, *B. distasonis* has a striking elevation in the proportion of DNA methylation proteins classified as laterally transferred. Seventy percent of genes classified as "DNA methylation" (GO:0006306; e.g., restriction-modification systems) are predicted to be laterally transferred, even though *B. distasonis* has fewer DNA methylation genes overall (10 versus an average of 11.5 for other gut Bacteroidetes; **Figure 3C).** The combination of a smaller number of restriction-modification systems, together with their acquisition from unrelated bacteria, would be expected to reduce the barriers to LGT by allowing *B. distasonis* to acquire genes from those bacteria. These laterally acquired genes may contribute to the success of *B. distasonis* within the gut habitat. For example, among the set of transferred genes is a ten-gene hydrogenase complex (**Figure 3D),** which would allow *B. distasonis* to use hydrogen as a terminal electron acceptor.

The role of lateral gene transfer in the evolution of capsular polysaccharide biosynthesis (*CPS*) loci

Capsular polysaccharide biosynthesis (*CPS*) locus expression and the functional importance of capsular structural variation have been best characterized in *B. fragilis*. For example, studies in gnotobiotic mice indicate that the zwitterionic capsular polysaccharide from one *B. fragilis CPS* locus (*PSA*) is presented by intestinal dendritic cells, resulting in expansion of CD4+ T-cells, induction of IFNγ production by the T-helper 1 subtype (Th1), and reversal of the T-helper 2 (Th2) bias found in the absence of colonization. The result is a balanced Th1/Th2 cytokine profile that should help promote co-existence with a microbiota, and perhaps tolerance to a variety of environmental antigens, including those found in food [29].

B. vulgatus has 9 *CPS* loci, while *B. distasonis* has 13. Like *B. thetaiotaomicron* (8 *CPS* loci) and *B. fragilis* (9 each in strains NCTC 9343 and YCH 46), each *CPS* cluster is composed of a pair of linked upstream UpcY and UpcZ homologs that act as a 'regulatory

cassette', and downstream genes encoding glycosyltransferases, carbohydrate transporters, and other proteins that form a 'structural cassette' (**Table S5**).

Among gut-associated Bacteroidetes, we found that glycosyltransferases and genes in *CPS* loci are enriched for laterally transferred genes (**Figure 3B**). *P. gingivalis,* in contrast, does not show a biased representation of lateral transfer within its set of glycosyltransferases, suggesting that laterally acquired genes serve an important function in providing new genetic material for the rapid divergence of these loci in gut Bacteroidetes.

CPS loci are among the most polymorphic sites in the four gut-associated Bacteroidetes species [30,31]. A comparison of the two sequenced *B. fragilis* genomes [8,9] revealed that the genome-wide synteny evident in the two closely related *B. fragilis* strains is disrupted in 8 of their 9 *CPS* loci (**Figure S4**, **Table S6**).

Conjugative transposons, phage and other mechanisms involved in promoting *CPS* diversity

Conjugative transposons

We observed that conjugative transposons (CTns) are associated with the duplication of *CPS* loci within a genome. In *B. vulgatus*, Bv0624-Bv0699 (75,747 bp) is a copy of another region (Bv1479c-Bv1560, 75,277 bp) (**Figure 4A** and **Table S5**). Each copy contains a CTn followed by a complete *CPS* locus. The average amino acid sequence identity of the 64 homologous gene pairs comprising the repeated regions is 90%. Two exact 28,411 bp copies harbor a major portion of the structural cassettes of these duplicated *CPS* loci, plus part of a CTn (**Figure 4A**). The strict nucleotide-level sequence conservation in coding and non-coding sequences suggests a recent homologous recombination event at the structural cassettes of the *CPS* loci. There is also evidence that the function of *CPS* loci can be disrupted by CTns, as in *CPS* locus 8 of *B. fragilis* YCH 46 where an α-1,2-fucosyltransferase gene is interrupted by a 127Kb, 132-gene CTn (**Table S5**).

Phages

Phages also appear to modulate *CPS* locus function. In *B. distasonis*, *CPS* locus 5 contains a block of five genes inserted between its regulatory cassette and genes encoding carbohydrate biosynthetic enzymes. This inserted segment, oriented in the opposite direction to the upstream regulatory UpxY (and UpxZ) genes and downstream carbohydrate biosynthetic genes, consists of a homolog of phage T7 lysozyme (N-acetylmuramoyl-L-alanine amidase) followed by four genes encoding hypothetical proteins. Three more *B. distasonis CPS* loci each harbor a block of these genes (two to five genes per block; each block with a similar orientation; only the T7 lysozyme is conserved among all copies of the putative phages; **Figure 4B** and **Table S5**).

B. distasonis is the only sequenced type strain where a phage disrupts *CPS* loci between their regulatory cassettes and structural cassettes. *B. vulgatus* has five copies of this phage, all associated with *CPS* loci. *B. thetaiotaomicron* has ten copies, only two of which are associated with *CPS* loci, while the *B. fragilis* strains each have one (**Table S5**).

Phase variation

LGT, CTn-mediated duplication and translocation of *CPS* loci, and disruption of *CPS* loci by phage appear to operate in combination with at least two other mechanisms to promote the rich diversity of surface glycan structures in Bacteroidetes. In *B. fragilis*, a serine site-specific recombinase (Mpi) regulates expression of 7 of its 8 *CPS* loci through phase variation (DNA inversion) at *CPS* promoters [32]. *B. vulgatus*, *B. distasonis*, and *B. thetaiotaomicron* have Mpi orthologs (one, three and one, respectively). In addition, five of the nine *CPS* loci in *B. vulgatus*, 11 of the 13 *CPS* loci in *B. distasonis*, 4 of the 8 *CPS* loci in *B. thetaiotaomicron,* and only one of the 10 *CPS* loci in *B. fragilis* NCTC 9343 have an gene encoding a tyrosine type site-specific recombinase immediately upstream of a *upxY* homolog. This juxtaposition suggests that inversions of some *CPS* loci may be subjected to local as well as global regulation. Such sequence inversions were observed in the assem-

blies of the *B. vulgatus* and *B. distasonis* genomes (data not shown).

Fkp and fucose utilization

B. fragilis can also alter *CPS* glycan composition by means of Fkp, a protein whose N-terminus is homologous to mammalian L-fucose-1-P-guanyltransferase and whose C-terminus is similar to L-fucose kinases. Fkp generates GDP-L-fucose from exogenous L-fucose; fucose from GDP-L-fucose can be incorporated into *CPS* glycan structures, thereby linking L-fucose availability in the organism's intestinal habitat to *CPS* capsular structure [33]. Although Fkp is highly conserved in *B. distasonis, B. vulgatus, B. thetaiotaomicron* and *B. fragilis*, their L-fucose acquisition and utilization capacities are not. *B. distasonis, B. vulgatus, B. thetaiotaomicron,* and *B. fragilis* all possess α-fucosidases for harvesting L-fucose, which is a common component of host mucus and epithelial cell glycans. In *B. thetaiotaomicron* and *B. fragilis*, a complete fucose utilization system is incorporated into a gene cluster (*fucRIAKXP*). In *B. vulgatus*, this gene cluster (Bv1339c-Bv1341c) contains an ortholog of *B. thetaiotaomicron's* L-fucose-inhibited repressor (R), fucose isomerase (I) and fucose permease (P), but not L-fuculose-1-phosphate aldolase (A) or L-fuculose kinase (K). *B. distasonis* lacks all elements of this gene cluster.

The role of gene duplication in diversification of gut Bacteroidetes: a case study of SusC/SusD paralogs

As noted above, the gut Bacteroidetes genomes contain large numbers of paralogs involved in environmental sensing and nutrient acquisition. We used one of the largest families, the SusC/SusD paralogs (**Table S1**), as a model for investigating relationships among members. SusC paralogs are predicted to be TonB-dependent, β-barrel-type outer membrane proteins. Thus, in addition to binding nutrients such as polysaccharides, SusC paralogs likely participate in their energy-dependent transport into the periplasmic space [34]. SusD paralogs are predicted to be secreted and to have an N-terminal lipid tail that

would allow them to associate with the outer membrane [14]. Genes encoding SusC and SusD paralogs are typically positioned adjacent to one another in the *B. thetaiotaomicron* genome (102 of 107 loci encoding SusC paralogs), and are often part of multigene clusters that also encode enzymes involved in carbohydrate metabolism (62 of 107 loci) [2]. Eighteen of the 62 clusters that encode SusC/SusD paralogs and glycoside hydrolases, also contain ECF-σ factors and adjacent anti-σ factors. A subset of SusC paralogs contain an extra N-terminal domain with homology to the N-terminal domain of the *Escherichia coli* FecA iron-dicitrate receptor protein [35]. FecA interacts directly with an anti-σ factor (FecR) via this domain, thereby controlling gene expression through modulation of its associated ECF-σ factor (FecI).

These clusters provide case studies of the evolution of gut Bacteroidetes genomes. Their glycoside hydrolase content varies considerably within a given species (**Table S7**). Our studies in *B. thetaiotaomicron* indicate that ECF-σ factors are required for transcription of their adjacent polysaccharide utilization gene clusters, and that chromosomally linked anti-σ factors act as repressors of this transcription. Moreover, several *B. thetaiotaomicron* loci containing ECF-σ and anti-σ factors are differentially regulated during growth on various complex glycans ([16] and E. C. Martens and J.I. Gordon, unpublished observations), suggesting that these systems act as components of carbohydrate sensors responsible for regulating loci appropriate for utilizing available nutrients.

Six of these clusters in *B. distasonis* (2-6 and 16 in **Table S7-A**) include predicted sulfatases, while there are fewer such loci in the other genomes: two clusters in *B. vulgatus* (5 and 11 in **Table S7-B**), four in *B. thetaiotaomicron,* and three in each of the two *B. fragilis* strains. These enzymes could be involved in the desulfation of sulfomucins that contain galactose-3-sulfate, galactose-6-sulfate, and *N*-acetylglucosamine-6-sulfate residues. These or other sulfatases could also be involved in the desulfation of glycosaminoglycans such as chondroitin and heparin.

To explore the role of gene duplication in the diversification of the Bacteroidetes, we generated lists of all paired SusC and SusD paralogs from the four gut- and one non-gut-associated Bacteroidetes species (see **Materials and Methods**). *P. gingivalis* has four such pairs, while the other five intestinal *Bacteroidetes* species have a total of 370 (**Table S1**). A cladogram generated from the multiple sequence alignment shows that many SusC/SusD pairs have close relatives among several Bacteroidetes. However, certain specialized groups are unique to each species, with *B. thetaiotaomicron* containing one particularly large expansion (**Figure 5A**). Gene clusters encoding related SusC/SusD pairs also contain other genes that are closely related to one another. The homology and synteny of these loci suggest that genomic duplication is a mechanism driving their amplification and diversification (e.g., **Figure 5B,C**). An intriguing feature of some of these amplified loci is that they contain clusters of genes with unique functions that are located downstream of the 'core' duplicated genes; this may serve to further diversify the roles of these loci in nutrient acquisition (e.g., **Figure 5B** in which diverse dehydrogenase, sulfatase and glycoside hydrolase functions are included downstream of a syntenic core of amplified genes).

Discussion

The trillions of bacteria that colonize our distal gut largely belong to two bacterial divisions, and can be classified by 16S rRNA gene sequence analysis into hundreds of "species" that share a common ancestry [4,36] but whose genome content may vary considerably. Forces that shape the genome content of bacteria in the gut include the inter-microbial dynamics of competition and cooperation in resource partitioning that shape complex food webs, as well as other community-shaping forces, such as phage attacks, that can result in 'selective sweeps' that remove cells with similar susceptibilities. In a competitive environment where innovation in resource acquisition strategies can breed success, and where resistance to phage can mean surviving a phage selective sweep, bacteria can be expected to differentiate their genome content. For the host to thrive and produce more gut habitats

(by reproducing), the gut microbial ecosystem must be functionally stable over time despite the internal dynamics of the community. The constituent bacteria might therefore be expected to have a high degree of functional redundancy between species, so that the loss of one lineage would not adversely impact ecosystem services to the host. Our investigation of the genomes of human gut Bacteroidetes species shows that the "top-down" forces imposed by selection at the host-level that would result in a homogenized microbiome, and the "bottom-up" forces of inter-microbial dynamics that would result in completely differentiated genomes, are both at work in the distal gut. The genomes of the gut Bacteroidetes species that have been sequenced harbor suites of genes with similar functions, but differ in the number of genes within functional categories and their specific sequence. It appears that the differences between genomes are enough to carve out specific niches within the gut habitat, such that the species are not in direct competition but are sufficiently similar to confer resistance to disturbance to the host through functional redundancy.

Our findings demonstrate a key role for lateral gene transfer in shaping the adaptation of individual Bacteroidetes to distinct niches within the human gut. It is unclear how and when laterally transferred genes were introduced during evolution of distal gut Bacteroidetes. We have performed 16S rRNA gene sequence-based enumeration studies of the fecal microbiota of 59 different mammalian species: the results reveal that none of the four sequenced gut Bacteroidetes species is restricted to the human gut (R. E. Ley and J.I. Gordon, unpublished observations). Nonetheless, the impact of lateral gene transfer is likely profound for these gut symbionts and their human hosts. A large and varied gene pool of glycosyltransferases provides a capacity for diversification of surface polysaccharide structures that could endow symbionts with varied capacities to shape a host immune system so that it can accommodate a microbiota (and perhaps related food and other environmental antigens). Since the environment surrounding each human being varies, this gene flow may promote the generation of host-specific microbiomes. Acquisition of new types of carbohydrate binding proteins, transporters, and degradation enzymes through both LGT and gene

amplification should influence the types of substrates that can be exploited for energy harvest. It may also affect our predisposition to conditions such as obesity where the efficiency of caloric harvest may be influenced by the relationship between an individual's microbial glycoside hydrolase repertoire and the glycan content of his/her diet [37,38].

These considerations emphasize the need to have a more comprehensive view of our genetic landscape as a composite of human and microbial genes, a transcendent view of human evolution as involving our microbial partners, and a commitment to investigating human biology in the larger framework of environmental microbiology. Attention to these issues is timely given the onset of efforts to sequence the human 'microbiome' [39]. These metagenomic studies will allow investigators to address new, but fundamental, questions about humans. Do we share an identifiable core 'microbiome'? If there is such a core, how does the shell of diversity that surrounds the core influence our individual physiologic properties? How is the human microbiome evolving (within and between individuals) over varying time scales as a function of our changing diets, lifestyle, and biosphere? Finally, how should we define members of the microbiome when microbes possess pan-genomes (all genes present in any of the strains of a species) with varying degrees of 'openness' to acquisition of genes from other microbes?

Materials and Methods

Genome sequencing

The *B. vulgatus* and *B. distasonis* genomes were assembled from two types of whole genome shotgun libraries: a plasmid library with an average insert size of 5Kb, and a fosmid library with an average insert size of 40Kb. For each genome, both Phrap (http://www.phrap.org/) and PCAP [40] assemblies were generated and then compared, resulting in a 'hybrid' assembly that takes advantage of the strength of both assemblies. Regions that

contained a gap in one assembly but not in the other were made contiguous in the final assembly for finishing by using Consed [41].

Sequence gaps were filled by primer-walking on spanning clones. Physical gaps were amplified by PCR and closed by sequencing the PCR products. Poor quality regions were detected using Consed, amplified with PCR, and resequenced. The integrity and accuracy of the assembly were verified by clone constraints. Regions of lower coverage, or that contained ambiguous assemblies, were resolved by sequencing spanning individual fosmids. Regions that underwent sequence inversions were identified based on inconsistency of constraints for a fraction of read pairs in those regions. The final assemblies consisted of 12.6X and 13.2X sequence coverage for *B. vulgatus* and *B. distasonis* respectively. For each base, the Phred quality value was at least 40.

rRNA and tRNA genes were identified with BLASTN and tRNA-Scan [42], respectively. Proteins coding genes were identified using GLIMMER v.2.0 [43], ORPHEUS v.2.0 [44] and CRITICA v.0.94h [45]. WUBLAST (http://blast.wustl.edu/) was used to identify all predicted proteins with significant hits to the NR database. Predicted protein coding genes containing <60 codons and without significant homology (e-value threshold of 10^{-6}) to other proteins were eliminated. Gene start site predictions were fine-tuned using MED-Start [46] and BLAST homology. In general, no overlapping genes were allowed. Potential frameshift errors were identified by sequence alignment with known proteins, and confirmed or corrected by re-sequencing. The final set of genes, compiled from the analysis described above, was manually curated. Protein annotation was based on homology searches against public databases and domain analysis with HMMER (http://hmmer.wustl.edu/). Functional classification was based on homology searches against COGs using WU-BLAST and COGnitor [47], followed by manual curation. Metabolic pathways were constructed with reference to KEGG [48]. Phage genes were identified using Prophage finder [49].

Functional comparisons

Orthologs of the five intestinal Bacteroidetes genomes were identified based on (i) mutual BLASTP best hits with an e-value threshold of 10^{-6} and (ii) a requirement that each pair-wise protein alignment covers at least 60% of query length in both search directions. The amino acid sequences of each set of orthologs were aligned using ClustalW [50] and processed with Gblocks [51].

CPS loci in the five intestinal Bacteroidetes genomes were defined with the following criteria. First, an intact *CPS* locus included a UpxY homolog (as annotated) and a number of downstream genes on the same strand. These downstream genes included those that encoded functions related to surface polysaccharide synthesis (such as glycosyltransferases, carbohydrate export proteins, epimerases, glycoside hydrolases, etc), conserved hypothetical proteins, or hypothetical proteins. Second, the 5' boundary of each locus was determined by the UpxY homolog. Third, the 3' end of each locus generally was positioned where switch of coding strand occurred. Alternatively, the 3' end of the locus was positioned where downstream genes on the same strand encoded functions that were defined but unrelated to capsular polysaccharide synthesis (e.g., rRNA/tRNA and two-component signaling systems). However, the 3' end of the locus was extended if the coding strand was disrupted by a single hypothetical protein (to accommodate possible annotation errors), or a mobile element composed of one or multiple genes.

Gene Ontology (GO) categories and InterPro ID were assigned using (InterProScan release 12.1 [13]). The number of genes in each genome assigned to each GO term, or its parents in the hierarchy (according to the ontology description available as of June 6, 2006; [12]), were totaled. All terms assigned to at least 10 genes in a given genome were tested for overrepresentation, and all terms with a total of 10 genes across all tested genomes were tested for under-representation. Significantly over- and under-represented genes were identified using a binomial comparison with the indicated reference set. To control for dif-

ferences in the specificity of gene prediction, genes that could not be assigned to a GO category were excluded from the reference sets. A correction was then applied to each distinct set of tests (e.g., over- or under-representation in a genome) to achieve a false discovery rate of 0.05 for each set [52]. These tests were implemented using the Math::CDF Perl module (E. Callahan, Environmental Statistics, Fountain City, WI; available at http://www.cpan.org/), and scripts written in Perl.

16S rRNA phylogeny

Phylogenetic trees were constructed based on alignment of 16S rRNA fragments using the NAST aligner [53]. The alignment was filtered using a Lane mask, then modeled using ModelTest 3.7 [54]: a maximum likelihood tree was found by an exhaustive search using Paup (v. 4.0b10, http://paup.csit.fsu.edu/) employing parameters estimated by ModelTest.

Laterally transferred genes

Overview of strategy used to identify lateral gene transfer - See **Supporting Information**

Identifying classes of genes that were potentially laterally transferred or otherwise under selection in the gut Bacteroidetes - We identified genes that were laterally acquired and probably selected for after the divergence of gut Bacteroidetes species, and thus potentially involved in niche differentiation. These genes could either have been transferred into an individual species by lateral gene transfer, or retained in that species despite being lost in all other related sequenced species. It is difficult, perhaps impossible, to distinguish these two cases using the tree topology alone. We identified this class of genes by determining whether each gene met one of the following criteria. (i) No homologs were found in an augmented NCBI non-redundant protein database (nr, plus the proteins from the newly sequenced strains). This case indicated that either (a) the gene has been lost in every other se-

quenced organism but retained in this genome, or (b) that the gene was laterally transferred from an organism that is not represented in the database. (ii) The only homologs found were from the same species. This case is the same as case (i), except that either (a) the gene was sequenced multiple times and deposited in the database under separate records, or (b) there are paralogs, i.e., multiple copies of the gene in the genome being analyzed. Both case (i) and (ii) were termed 'novel'. (iii) The only homologs found are either from the same species or from other divisions or non-gut Bacteroidetes. This case indicates that the sequence is in this genome, and also in the genome of distantly related organisms, but not in the closely related gut Bacteroidetes genomes that have been completely sequenced. This case also provides evidence that the gene was either transferred or retained despite loss in related organisms. (iv) The gene is more closely related to genes from other divisions or to non-gut Bacteroidetes than it is to other gut Bacteroidetes that are in the tree, and parsimony analysis indicates that the direction of transfer was into rather than out of the genome. This pattern is most consistent with lateral gene transfer, although differential gene loss cannot in principle be ruled out (however, differences in composition between this class of genes and the rest of the genome provides compelling supporting evidence). Both case (iii) and (iv) above were termed 'laterally transferred' (LGT).

Genomes - We carried out the analysis on six different genomes: *Bacteroides vulgatus* ATCC 8482 and *Bacteroides distasonis* ATCC 8503, *Bacteroides fragilis* NCTC 9343 (NC_0023338), *Bacteroides fragilis* YCH 46 (NC_006347), *Bacteroides thetaiotaomicron* ATCC 29148 (NC_004663), and *Porphyromonas gingivalis* W83 (NC_002950).

Finding homologs - For each gene in each genome, we identified potential homologs using PSI-BLAST against NCBI's non-redundant protein database. In order to use all of the available data for the Bacteroidetes and their relatives, we augmented this database with proteins predicted by Glimmer (v. 2.0) from draft genomes in the Bacteroidetes group that were available at NCBI. These additional genomes included *Prevotella ruminicola* 23 (The Institute for Genomic Research; TIGR; http://www.tigr.org), *Prevotella intermedia* 17

(TIGR), *Pelodictyon phaeoclathratiforme* BU-1 [Dept. of Energy-Joint Genome Institute (DOE-JGI); http://www.jgi.doe.gov], *Pelodictyon luteolum* DSM 273 (DOE-JGI), *Chlorobium phaeobacteroides* DSM 266 (DOE-JGI), *Chlorobium limicola* DSM 245 (DOE-JGI), *Chlorobium chlorochromatii* CaD3 (DOE-JGI), *Bacteroides forsythus* (TIGR), and *Bacteroides fragilis* 638R (Wellcome Trust Sanger Institute; http://www.sanger.ac.uk).

To find the top BLAST hits using the most stringent e-value threshold possible, we used a multi-step PSI-BLAST. In the first PSI-BLAST iteration, we used an e-value threshold of $\leq 10^{-50}$. If fewer than 50 hits were found, we used the hits to make a profile for a subsequent PSI-BLAST that was four orders of magnitude less stringent (i.e., with an e-value of 10^{-46}). We repeated this procedure, increasing the e-value by a factor of 10^{-4} at each iteration, until either 50 hits were found or, after 12 iterations, the maximum allowed e-value of 10^{-6} was reached. To remove from consideration sequences that were significant only because of a conserved domain rather than similarity over the whole gene, we excluded genes that differed from the length of the query sequence by more than 30%. We also omitted hits that contained gaps greater than 50 amino acids in length or that contained gaps at greater than 50% of the positions after performing a multiple sequence alignment with the other sequences in the set.

Making phylogenetic trees **-** We performed multiple sequence alignment using MUSCLE [55], omitting sequences that were poorly aligned to the query sequence as described above. We used this alignment to make a neighbor-joining tree using ClustalW [50]. We used bootstrapping to collapse nodes that were not statistically supported. Specifically, we randomly re-sampled columns from the alignment 100 times and made new neighbor joining trees with ClustalW. We collapsed into polytomies all nodes in the original tree that were recovered in fewer than 70% of the bootstrap replicates.

Assigning taxonomy information to sequences **-** We parsed the NCBI taxonomy database and used it to assign division and genus information for each PSI-BLAST hit in

the phylogenetic tree. Sequences that could not be assigned to any particular division were removed from the tree. We also removed nematode and arthropod genomes, because we found that these often provided close hits to the Bacteroidetes genomes. We expect that these bacteria-to-eukaryote hits actually arise because gut and/or salivary gland bacteria contaminated the DNA preparations used for genomic sequencing. We also used the genus annotations in the taxonomy to determine whether sequences from the Bacteroidetes division were from the gut. We assigned sequences as gut Bacteroidetes if they were in the genera *Prevotella, Porphyromonas, Tannerella, Dysgonomonas*, or *Bacteroides*, and as non-gut Bacteroidetes otherwise.

Finding genes that are laterally transferred or differentially lost (under recent selective pressure) **-** We used the bootstrap neighbor joining trees to identify genes that met any of the four criteria described above. We first marked genes 'novel' if the PSI-BLAST protocol returned only the query gene, indicating that they met criterion (i), or if all of the genes in the tree were from the same species, indicating that they met criterion (ii). We assigned each sequence to a species using the NCBI taxonomy. If genes from other species were present in the tree, we used the following algorithm. (*1*) Start at the query sequence. (*2*) Step back in tree until a bootstrap-supported node containing sequences from a different species is found. If this node has, as descendants, sequences from other gut Bacteroidetes only, mark the gene as not laterally transferred (not selected for). If the node has, as descendants, sequences from both gut Bacteroidetes and other divisions or non-gut Bacteroidetes, mark the gene as unresolved. If the node has, as descendants, sequences from other divisions or non-gut Bacteroidetes only, mark the gene as laterally transferred (selected for) and proceed to the parsimony analysis. (*3*) Use parsimony analysis to determine whether a potential transfer would have been into the Bacteroidetes species (indicating that it is important for the gut), or out of the Bacteriodetes species into another lineage. Assign division information to all internal nodes in the tree using the Fitch parsimony algorithm [23]. These assignments minimize the number of transfers between divisions needed to explain

the distribution of divisions in the modern sequences. If the query sequence is surrounded by many sequences from unrelated divisions, the parsimony analysis will indicate that the most likely event was a transfer into the species. As noted in Supporting Information (*Overview of strategy used to identify lateral gene transfer*)**,** the method we used provides an automated technique for assigning taxon labels to individual gene trees. Specifically, we treat each taxon label (division labels, "gut Bacteroidetes", or "non-gut Bacteroidetes") as a character state, and use the Fitch parsimony algorithm [23] to infer the ancestral state at each node. We are not using this method in the sense of a formal evolutionary model of taxon switching, but as a heuristic that recaptures the intuition that a phylogenetic tree with a clade leading to sequences from one taxon that sprouts from within a clade leading to sequences from a completely different taxon probably represents an lateral gene transfer event, even if the inner clade is represented by more sequences. This type of strategy has been widely applied both manually and computationally to detect lineage-specific transfers (e.g., [56-58]), and is related to a method used in studies of host-parasite co-speciation [59], a problem that is mathematically equivalent to lateral gene transfer detection.

SusC/SusD alignments

Pairs of genes encoding SusC and SusD paralogs were identified in the Bacteroidetes genome sequences by performing individual BLASTP searches against each genome using amino acid sequences of previously annotated SusC and SusD paralogs as queries. The low-scoring hits from each search (e-values between 10^{-4} and

10^{-10}) were themselves used as BLASTP queries to reveal more divergent putative paralogs in each genome. This process repeated until no new paralogs were identified. Lists of putative SusC and SusD paralogs were compared for each species. Paralogs were included in subsequent ClustalW analysis based on the requirement that each had a separately predicted, adjacent partner. This process was instrumental in excluding related TonB-dependent hemin, vitamin B_{12} and iron-siderophore receptors from the list of puta-

tive SusC paralogs. The resulting dataset included 374 paralog pairs: 102 in *B. thetaiotaomicron*, 69 in *B. fragilis* NCTC 9343, 65 in *B. fragilis* YCH 46, 80 in *B. vulgatus*, 54 in *B. distasonis* and four in *P. gingivalis*. Because polysaccharide binding by SusC and SusD has been shown to require both polypeptides [14], and because individual SusC and SusD alignments suggested these paired functions have evolved in parallel (data not shown), each pair was joined into a single sequence prior to alignment. Sequences were aligned using ClustalW [50] (version 1.83), and a neighbor-joining cladogram was created from the alignment using Paup (v. 4.0b10, http://paup.csit.fsu.edu/). Bootstrap values were determined from 100 trees. Branches retained in **Figure 5A** represent groups with ≥ 70% bootstrap values.

Acknowledgements

This work was supported by a grant from the National Science Foundation (EF0333284). C. Lozupone was supported by a NIH pre-doctoral training grant (T32 GM08759), M. Hamady by a gift from the Jane and Charlie Butcher Foundation and W.M. Keck Foundation RNA Bioinformatics Initiative, and E.C. Martens by a NIH post-doctoral training grant (T32 HD07409). The sequence data of *Cytophaga hutchinsonii* ATCC 33406, *Pelodictyon phaeoclathratiforme* BU-1; *Pelodictyon luteolum* DSM 273, *Chlorobium phaeobacteroides* DSM 266, *Chlorobium limicola* DSM 245 and *Chlorobium chlorochromatii* CaD3 were produced by the US Department of Energy Joint Genome Institute (http://www.jgi.doe.gov/). Preliminary sequence data for *Prevotella ruminicola* 23, *Prevotella intermedia* 17, and *Bacteroides forsythus* were obtained from The Institute for Genomic Research through its website at http://www.tigr.org. Sequencing of *Prevotella intermedia* and *Prevotella ruminicola* 23 was accomplished with support from NIH-NIDCR and USDA respectively. The draft sequence of *Bacteroides fragilis* 638R was produced by the Pathogens Sequencing Group at the Sanger Institute and can be obtained from ftp://ftp.sanger.ac.uk/pub/pathogens.

GenBank Accession Numbers

The genome sequences of *B. vulgatus* ATCC 8482 and *B. distasonis* ATCC 8503 have been deposited in GenBank under accession numbers CP000139 and CP000140, respectively.

Abbreviations

LGT – lateral gene transfer; Sus – starch utilization system paralog; CPS – capsular polysaccharide synthesis

References

1. Backhed F, Ley RE, Sonnenburg JL, Peterson DA, Gordon JI (2005) Host-bacterial mutualism in the human intestine. Science 307: 1915-1920.

2. Xu J, Bjursell MK, Himrod J, Deng S, Carmichael LK, *et al*. (2003) A genomic view of the human-Bacteroides thetaiotaomicron symbiosis. Science 299: 2074-2076.

3. Eckburg PB, Bik EM, Bernstein CN, Purdom E, Dethlefsen L, *et al*. (2005) Diversity of the Human Intestinal Microbial Flora. Science.

4. Ley RE, Peterson DA, Gordon JI (2006) Ecological and evolutionary forces shaping microbial diversity in the human intestine. Cell 124: 837-848.

5. Dunbar J, Barns SM, Ticknor LO, Kuske CR (2002) Empirical and theoretical bacterial diversity in four Arizona soils. Appl Environ Microbiol 68: 3035-3045.

6. Salyers AA, Gupta A, Wang Y (2004) Human intestinal bacteria as reservoirs for antibiotic resistance genes. Trends Microbiol 12: 412-416.

7. Sakamoto M, Benno Y (2006) Reclassification of Bacteroides distasonis, Bacteroides goldsteinii and Bacteroides merdae as Parabacteroides distasonis gen. nov., comb. nov., Parabacteroides goldsteinii comb. nov. and Parabacteroides merdae comb. nov. Int J Syst Evol Microbiol 56: 1599-1605.

8. Kuwahara T, Yamashita A, Hirakawa H, Nakayama H, Toh H, *et al*. (2004) Genomic analysis of Bacteroides fragilis reveals extensive DNA inversions regulating cell surface adaptation. Proc Natl Acad Sci U S A 101: 14919-14924.

9. Cerdeno-Tarraga AM, Patrick S, Crossman LC, Blakely G, Abratt V, *et al*. (2005) Extensive DNA inversions in the B. fragilis genome control variable gene expression. Science 307: 1463-1465.

10. Millward DJ (1999) The nutritional value of plant-based diets in relation to human amino acid and protein requirements. Proc Nutr Soc 58: 249-260.

11. Nelson KE, Fleischmann RD, DeBoy RT, Paulsen IT, Fouts DE, *et al*. (2003) Complete genome sequence of the oral pathogenic Bacterium porphyromonas gingivalis strain W83. J Bacteriol 185: 5591-5601.

12. Ashburner M, Ball CA, Blake JA, Botstein D, Butler H, *et al*. (2000) Gene ontology: tool for the unification of biology. The Gene Ontology Consortium. Nat Genet 25: 25-29.

13. Mulder NJ, Apweiler R, Attwood TK, Bairoch A, Bateman A, *et al*. (2005) InterPro, progress and status in 2005. Nucleic Acids Res 33: D201-205.

14. Shipman JA, Berleman JE, Salyers AA (2000) Characterization of four outer membrane proteins involved in binding starch to the cell surface of Bacteroides thetaiotaomicron. J Bacteriol 182: 5365-5372.

15. Cho KH, Salyers AA (2001) Biochemical analysis of interactions between outer membrane proteins that contribute to starch utilization by Bacteroides thetaiotaomicron. J Bacteriol 183: 7224-7230.

16. Sonnenburg JL, Xu J, Leip DD, Chen CH, Westover BP, *et al*. (2005) Glycan foraging in vivo by an intestine-adapted bacterial symbiont. Science 307: 1955-1959.

17. Salyers AA, Vercellotti JR, West SE, Wilkins TD (1977) Fermentation of mucin and plant polysaccharides by strains of Bacteroides from the human colon. Appl Environ Microbiol 33: 319-322.

18. Ragan MA (2001) On surrogate methods for detecting lateral gene transfer. FEMS Microbiol Lett 201: 187-191.

19. Kurland CG, Canback B, Berg OG (2003) Horizontal gene transfer: a critical view. Proc Natl Acad Sci U S A 100: 9658-9662.

20. Lawrence JG, Hendrickson H (2003) Lateral gene transfer: when will adolescence end? Mol Microbiol 50: 739-749.

21. Ragan MA, Harlow TJ, Beiko RG (2006) Do different surrogate methods detect lateral genetic transfer events of different relative ages? Trends Microbiol 14: 4-8.

22. Berg OG, Kurland CG (2002) Evolution of microbial genomes: sequence acquisition and loss. Mol Biol Evol 19: 2265-2276.

23. Fitch WM (1970) Distinguishing homologous from analogous proteins. Syst Zool 20: 406-416.

24. Hansen-Wester I, Stecher B, Hensel M (2002) Analyses of the evolutionary distribution of Salmonella translocated effectors. Infect Immun 70: 1619-1622.

25. Garcia-Vallve S, Romeu A, Palau J (2000) Horizontal gene transfer in bacterial and archaeal complete genomes. Genome Res 10: 1719-1725.

26. Jeltsch A, Pingoud A (1996) Horizontal gene transfer contributes to the wide distribution and evolution of type II restriction-modification systems. J Mol Evol 42: 91-96.

27. Nakayama Y, Kobayashi I (1998) Restriction-modification gene complexes as selfish gene entities: roles of a regulatory system in their establishment, maintenance, and apoptotic mutual exclusion. Proc Natl Acad Sci U S A 95: 6442-6447.

28. Gressmann H, Linz B, Ghai R, Pleissner KP, Schlapbach R, *et al*. (2005) Gain and loss of multiple genes during the evolution of Helicobacter pylori. PLoS Genet 1: e43.

29. Mazmanian SK, Liu CH, Tzianabos AO, Kasper DL (2005) An immunomodulatory molecule of symbiotic bacteria directs maturation of the host immune system. Cell 122: 107-118.

30. Comstock LE, Coyne MJ, Tzianabos AO, Kasper DL (1999) Interstrain variation of the polysaccharide B biosynthesis locus of Bacteroides fragilis: characterization of the region from strain 638R. J Bacteriol 181: 6192-6196.

31. Comstock LE, Pantosti A, Kasper DL (2000) Genetic diversity of the capsular polysaccharide C biosynthesis region of Bacteroides fragilis. Infect Immun 68: 6182-6188.

32. Coyne MJ, Weinacht KG, Krinos CM, Comstock LE (2003) Mpi recombinase globally modulates the surface architecture of a human commensal bacterium. Proc Natl Acad Sci U S A 100: 10446-10451.

33. Coyne MJ, Reinap B, Lee MM, Comstock LE (2005) Human symbionts use a host-like pathway for surface fucosylation. Science 307: 1778-1781.

34. Reeves AR, D'Elia JN, Frias J, Salyers AA (1996) A Bacteroides thetaiotaomicron outer membrane protein that is essential for utilization of maltooligosaccharides and starch. J Bacteriol 178: 823-830.

35. Koebnik R (2005) TonB-dependent trans-envelope signalling: the exception or the rule? Trends Microbiol 13: 343-347.

36. Eckburg PB, Lepp PW, Relman DA (2003) Archaea and their potential role in human disease. Infect Immun 71: 591-596.

37. Ley RE, Turnbaugh PJ, Klein S, Gordon JI (2006) Microbial ecology: human gut microbes associated with obesity. Nature 444: 1022-1023.

38. Turnbaugh PJ, Ley RE, Mahowald MA, Magrini V, Mardis ER, *et al*. (2006) An obesity-associated gut microbiome with increased capacity for energy harvest. Nature 444: 1027-1031.

39. Gill SR, Pop M, Deboy RT, Eckburg PB, Turnbaugh PJ, *et al*. (2006) Metagenomic analysis of the human distal gut microbiome. Science 312: 1355-1359.

40. Huang X, Wang J, Aluru S, Yang SP, Hillier L (2003) PCAP: a whole-genome assembly program. Genome Res 13: 2164-2170.

41. Gordon D, Abajian C, Green P (1998) Consed: a graphical tool for sequence finishing. Genome Res 8: 195-202.

42. Lowe TM, Eddy SR (1997) tRNAscan-SE: a program for improved detection of transfer RNA genes in genomic sequence. Nucleic Acids Res 25: 955-964.

43. Delcher AL, Harmon D, Kasif S, White O, Salzberg SL (1999) Improved microbial gene identification with GLIMMER. Nucleic Acids Res 27: 4636-4641.

44. Frishman D, Mironov A, Mewes HW, Gelfand M (1998) Combining diverse evidence for gene recognition in completely sequenced bacterial genomes. Nucleic Acids Res 26: 2941-2947.

45. Badger JH, Olsen GJ (1999) CRITICA: coding region identification tool invoking comparative analysis. Mol Biol Evol 16: 512-524.

46. Zhu HQ, Hu GQ, Ouyang ZQ, Wang J, She ZS (2004) Accuracy improvement for identifying translation initiation sites in microbial genomes. Bioinformatics 20: 3308-3317.

47. Tatusov RL, Fedorova ND, Jackson JD, Jacobs AR, Kiryutin B, *et al*. (2003) The COG database: an updated version includes eukaryotes. BMC Bioinformatics 4: 41.

48. Kanehisa M, Goto S, Kawashima S, Okuno Y, Hattori M (2004) The KEGG resource for deciphering the genome. Nucleic Acids Res 32: D277-280.

49. Bose M, Barber RD (2006) Prophage Finder: a prophage loci prediction tool for prokaryotic genome sequences. In Silico Biology 6: 0020.

50. Chenna R, Sugawara H, Koike T, Lopez R, Gibson TJ, *et al*. (2003) Multiple sequence alignment with the Clustal series of programs. Nucleic Acids Res 31: 3497-3500.

51. Castresana J (2000) Selection of conserved blocks from multiple alignments for their use in phylogenetic analysis. Mol Biol Evol 17: 540-552.

52. Benjamini Y, Hochberg Y (1995) Controlling the false discovery rate: A practical and powerful approach to multiple testing. Journal of the Royal Statistical Society B 57: 289-300.

53. DeSantis TZ, Jr., Hugenholtz P, Keller K, Brodie EL, Larsen N, *et al*. (2006) NAST: a multiple sequence alignment server for comparative analysis of 16S rRNA genes. Nucleic Acids Res 34: W394-399.

54. Posada D, Crandall KA (1998) MODELTEST: testing the model of DNA substitution. Bioinformatics 14: 817-818.

55. Edgar RC (2004) MUSCLE: multiple sequence alignment with high accuracy and high throughput. Nucleic Acids Res 32: 1792-1797.

56. Hooper SD, Berg OG (2003) Duplication is more common among laterally transferred genes than among indigenous genes. Genome Biol 4: R48.

57. Kunin V, Ouzounis CA (2003) GeneTRACE-reconstruction of gene content of ancestral species. Bioinformatics 19: 1412-1416.

58. Daubin V, Ochman H (2004) Bacterial genomes as new gene homes: the genealogy of ORFans in E. coli. Genome Res 14: 1036-1042.

59. Brooks DR (1981) Hennig's parasitological method: a proposed solution. Syst Zool 30: 229-249.

60. DeSantis TZ, Dubosarskiy I, Murray SR, Andersen GL (2003) Comprehensive aligned sequence construction for automated design of effective probes (CASCADE-P) using 16S rDNA. Bioinformatics 19: 1461-1468.

Figure Legends

Figure 1. Phylogenetic relationships of fully sequenced Bacteroidetes. **(A)** 16S rRNA sequences were taken from a previously published alignment created using the NAST aligner [60]. A maximum likelihood tree was generated using parameters estimated with ModelTest 3. 7 and Paup (version 4.0b11). Terminal branch lengths are not drawn to scale. **(B)** The average percent amino acid sequence identities were calculated using ClustalW alignments for the 530 sets of 7-way orthologs that include the five intestinal Bacteroidetes genomes, *P. gingivalis* and *C. hutchinsonii*. *B. thetaiotaomicron* was used as a reference.

Figure 2. Sensing, regulatory and carbohydrate metabolism genes are enriched among all gut-associated Bacteroidetes. The number of genes assigned to each GO term from each genome is shown. Significant enrichment is denoted by pink ($p<0.05$) or red ($p<0.001$) while depletion is indicated by light blue ($p<0.05$) or dark blue ($p<0.001$), as calculated by a binomial comparison followed by Benjamini-Hochberg false-discovery rate correction (see **Materials and Methods**). (**A**) Genes assigned to GO terms related to core metabolic functions are enriched in the subset of common gut-associated Bacteroidetes orthologs shared with non-gut Bacteroidetes (seven-way comparison; abbreviated 7w), compared to the reference set of 1,416 orthologs common to the five sequenced gut Bacteroidetes genomes (5w), suggesting that all Bacteroidetes have inherited a core metabolome from their common ancestor. The set of orthologs that is not shared with non-gut-associated Bacteroidetes (5-way unique; 5wU) is enriched, relative to all orthologs (5w), for genes in three classes: amino acid biosynthesis; membrane transport; and two-component signal transduction systems, suggesting that these genes were important in the process of adaptation to the gut and/or other habitats by the common ancestor of gut Bacteroidetes. (**B**) Various GO terms related to environmental sensing, gene regulation and carbohydrate degradation are enriched in gut Bacteroidetes relative to *C. hutchinsonii*. A similar pattern is observed relative to *P. gingivalis* (data not shown). Note that these same classes of genes are depleted in the subset of shared gut Bacteroidetes orthologs (**Figure 2A,** 5w) relative to the full *B.*

thetaiotaomicron (Bt) Genome (**Figure 2A,** Bt-G). Thus, these classes of genes, though enriched in all gut Bacteroidetes, are widely divergent between them. Others classes of genes vary between species: *B. distasonis* and *B. vulgatus* show an expanded repertoire of proteases, while *B. thetaiotaomicron* lacks genes involved in synthesis of cobalamin. Other abbreviations**:** *B. distasonis* (Bd), *B. vulgatus* (Bv), *B. fragilis* NCTC 9343 (BfN), *B. fragilis* YCH 46 (BfY), *P. gingivalis* (Pg), *C. hutchinsonii* (Ch), orthologs shared by the five sequenced gut Bacteroidetes genomes (Bt, Bv, Bd, plus two Bf strains), and Pg (6w),

Figure 3. Analyses of lateral gene transfer events in Bacteroidetes lineages reveal its contribution to niche specialization. (**A**) Genes involved in core metabolic processes are enriched among non-laterally transferred genes identified by a phylogenetic approach (see **Materials and Methods**). The proportion of genes identified as not laterally transferred in each genome (light blue), as well as assigned to the GO terms 'Primary metabolism' (yellow) and 'Protein biosynthesis' (red), are shown. Significant increases (enrichment) relative to each whole genome are shown by an upward pointing arrowhead, and decreases (depletion) by a downward pointing arrowhead, while the corresponding probability, determined by a binomial test, is denoted by asterisks: *, P<0.05, **; P<0.01, ***; P<0.001. (**B**) Laterally transferred genes are enriched among genes assigned to the GO term 'DNA methylation' (e.g., restriction-modification systems) (red), relative to each complete genome (light blue). Glycosyltransferases (yellow) and genes located within *CPS* loci (green) are also enriched within the set of transferred genes. Significance was determined and denoted as in panel A. (**C**) *B. distasonis* (light blue) possesses a significantly larger proportion of laterally transferred genes than the other Bacteroidetes, as shown by significant increases in the proportion of genes in each category of our analysis ('LGT in', laterally transferred into the genome; 'Novel', no homologs identified from other species, 'LGT direction unresolved', laterally transferred but direction unknown; 'LGT out', laterally transferred out of the genome; 'Unresolved,' lateral transfer uncertain; see **Materials and Methods** for detailed explanations of categories and http://gordonlab.wustl.edu/BvBd.html for a complete

list of genes in each category). Significant changes, denoted as in panel A, were determined by a binomial test, using the average proportion within all other genomes used in the analysis as the reference. Other strains are *B. vulgatus* (red), *B. thetaiotaomicron* (yellow), *B. fragilis* NCTC 9343 (green), *B. fragilis* YCH 46 (purple) and *P. gingivalis* (orange). (**D**) A prominent laterally transferred locus within *B. distasonis* contains a 10-gene hydrogenase complex, likely allowing *B. distasonis* to use hydrogen as a terminal electron acceptor in anaerobic respiration. Genes transferred into *B. distasonis* are colored red, while genes whose phylogeny could not be resolved are yellow. Letters indicate functional components of the hydrogenase complex: M, maturation or accessory factor, S, small subunit, L, large subunit.

Figure 4. Evolutionary mechanisms that impact Bacteroidetes *CPS* loci. **(A)** CTn-mediated duplication of *B. vulgatus CPS* loci. Homologous gene pairs in the two duplicated regions are linked with fine gray lines, underscoring the high level of synteny. Genes constituting *CPS* locus 1 and 2 are highlighted in red, with the first and last genes numbered. Green denotes essential component genes of CTns. Blue brackets indicate two sub-regions that share 100% nucleotide sequence identity. The asterisk indicates three open reading frames encoding two conserved hypothetical proteins and a hypothetical protein, suggesting an insertion that occurred after the duplication event. (**B**) Locations of putative glycosyltransferase xenologs and inserted phage genes in *CPS* loci of the sequenced gut Bacteroidetes**.** Color code: integrases (green), UpxY transcriptional regulator homologs (black), putative xenologs (primarily glycosyltransferases, red), phage genes (blue) and remaining genes (gray). See **Table S5** for functional annotations.

Figure 5. Cladogram comparison of SusC/SusD pairs shows both specialized and shared branches among the Bacteroidetes. **(A)** Cladogram generated from all fully sequenced Bacteroidetes. Branches that are unique to each species are color-coded as indicated. The homologous RagA/RagB proteins from *P. gingivalis* were selected as an arbitrary root (dashed branches). Dashed lines surrounding the tree indicate (i) a clade that is

dominated by *B. thetaiotaomicron* SusC/SusD pairs (39/45 pairs, red dashes) and (ii) a clade that is poorly represented in *B. thetaiotaomicron* (7/34 pairs, black dashes). Colored hash marks surrounding the cladogram represent the linkage of two other protein families, which show syntenic organization within related *B. thetaiotaomicron* SusC/SusD containing loci: NHL-repeat containing proteins (light blue) and a group of conserved hypothetical lipidated proteins (light green). These protein families are not represented in the other sequenced Bacteroidetes, occur only adjacent to SusC/SusD pairs, and have no predicted functions. See http://gordonlab.wustl.edu/BvBd.html for locus tags for each taxon, branch bootstrap values, and lists of SusC/SusD-linked genes. (**B)** An example of a recently amplified polysaccharide utilization locus in which the synteny of three flanking SusC/SusD genes has been maintained. The locations of the four SusC/SusD pairs encoded within these amplified clusters are indicated on the cladogram shown in panel A by asterisks. The locus schematic is arranged so that groups of related proteins (mutual best BLAST hits) are aligned vertically, within the yellow box. The functions of amplified genes are indicated by numbers over each vertical column and, where applicable, are color-coded to correspond to panel A: 1, conserved hypothetical lipidated protein; 2, SusD paralog; 3, SusC paralog, 4, NHL-repeat containing protein; and 5, glutaminase A (note that in three clusters, this gene has been partially deleted). Gray-colored genes downstream of each amplified cluster encode hypothetical proteins or predicted enzymatic activities (e.g., dehydrogenase, sulfatase and glycoside hydrolase) that are unique to each cluster. A xenolog that has been inserted in one gene cluster is indicated in red, other genes are black. Dashed lines connecting gene clusters show linkage only, and do not correspond to actual genomic distance. **(C)** An example of a recently duplicated locus from *B. distasonis* that includes duplicated regulatory genes. Syntenic regions are aligned as in panel B and include a single sulfatase (1, dark green), a SusD paralog (2, light purple), SusC paralog (3, dark purple), an anti-σ factor (4, light orange) and an ECF-σ factor (5, dark orange). Two other downstream sulfatase genes (gray) are also included in one cluster.

Figures

Figure 1.

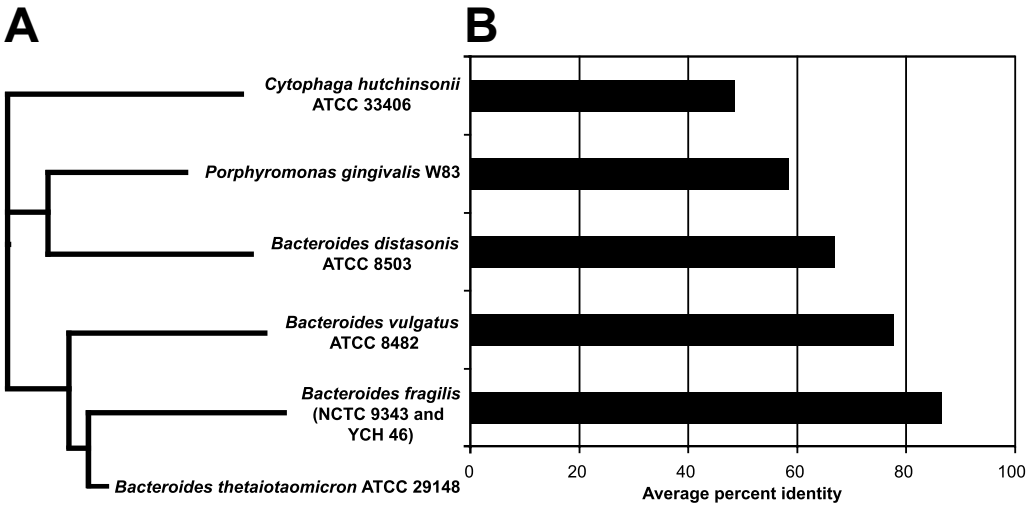

Figure 2.

A

	Category	Description	5w	5wU	6w	7w	*Bt*-G
Core metabolism	GO:0009059	macromolecule biosynthesis	113	8	105	97	163
	GO:0006412	protein biosynthesis	87	4	83	78	97
	GO:0044238	primary metabolism	582	178	404	302	1289
Amino acids	GO:0008652	amino acid biosynthesis	56	37	19	16	71
Membrane transport	GO:0005386	carrier activity	46	31	15	5	68
	GO:0006811	ion transport	55	35	20	5	96
	GO:0016020	membrane	185	108	77	31	564
Environment sensing and regulation	GO:0004871	signal transducer activity	37	29	8	2	246
	GO:0000160	two-component signal transduction system (phosphorelay)	18	15	3	1	91
	GO:0006355	regulation of transcription, DNA-dependent	55	30	25	12	233
	GO:0003700	transcription factor activity	39	21	18	8	189
	GO:0016987	sigma factor activity	9	4	5	2	51
Polysac-charide metabolism	GO:0016835	carbon-oxygen lyase activity	30	21	9	7	39
Total genes assigned to a GO term			**964**	**314**	**648**	**435**	**2559**

B

	Category	Description	Bd	Bv	Bt	BfN	BfY	Pg	Ch
Polysac-charide metabolism	GO:0004553	hydrolase activity, hydrolyzing O-glycosyl compounds	64	111	161	98	99	11	44
	GO:0016798	hydrolase activity, acting on glycosyl bonds	69	115	166	102	103	14	48
	GO:0008484	sulfuric ester hydrolase activity	20	15	31	18	18	3	2
	GO:0006044	N-acetylglucosamine metabolism	10	12	14	8	11	3	2
	GO:0005996	monosaccharide metabolism	45	46	53	38	39	13	23
	GO:0006040	amino sugar metabolism	13	14	16	10	13	5	4
	GO:0009253	peptidoglycan catabolism	11	9	15	7	8	3	3
	GO:0044262	cellular carbohydrate metabolism	126	119	146	110	115	46	81
	GO:0005976	polysaccharide metabolism	45	47	57	42	46	17	24
	GO:0005975	carbohydrate metabolism	206	246	322	222	227	71	144
Environment sensing and regulation	GO:0004871	signal transducer activity	181	173	246	185	187	26	112
	GO:0003700	transcription factor activity	123	142	189	146	140	35	83
	GO:0004872	receptor activity	85	100	127	95	96	14	22
	GO:0003677	DNA binding	293	349	431	308	329	163	194
	GO:0043565	sequence-specific DNA binding	74	90	120	86	89	17	45
	GO:0006352	transcription initiation	36	41	51	45	43	8	19
	GO:0016986	transcription initiation factor activity	36	41	51	45	43	8	19
	GO:0016987	sigma factor activity	36	41	51	45	43	8	19
	GO:0040029	regulation of gene expression, epigenetic	11	10	13	12	15	6	4
	GO:0003676	nucleic acid binding	376	447	534	396	416	236	282
Membrane transport	GO:0005215	transporter activity	303	293	363	321	316	88	171
	GO:0006855	multidrug transport	14	12	12	13	12	6	1
	GO:0009935	nutrient import	16	14	19	17	18	0	2
	GO:0006810	transport	447	412	522	441	436	167	300
	GO:0015297	antiporter activity	27	19	20	23	22	8	10
	GO:0015290	electrochemical potential-driven transporter activity	44	37	39	39	38	13	21
	GO:0015672	monovalent inorganic cation transport	45	46	47	46	46	18	22
	GO:0006814	sodium ion transport	11	11	13	11	11	6	3
Protein degradation	GO:0006508	proteolysis	89	87	78	74	76	51	53
	GO:0008233	peptidase activity	88	86	78	74	76	51	55
	GO:0008236	serine-type peptidase activity	34	33	29	25	26	17	18
	GO:0016806	dipeptidyl-peptidase and tripeptidyl-peptidase activity	10	8	5	4	4	3	0
	GO:0008238	exopeptidase activity	23	22	16	16	16	13	7
Cofactor biosynthesis	GO:0009236	cobalamin biosynthesis	15	16	2	13	12	12	2
Total genes assigned to a GO term			**2157**	**2186**	**2559**	**2194**	**2231**	**1086**	**1803**

Figure 3.

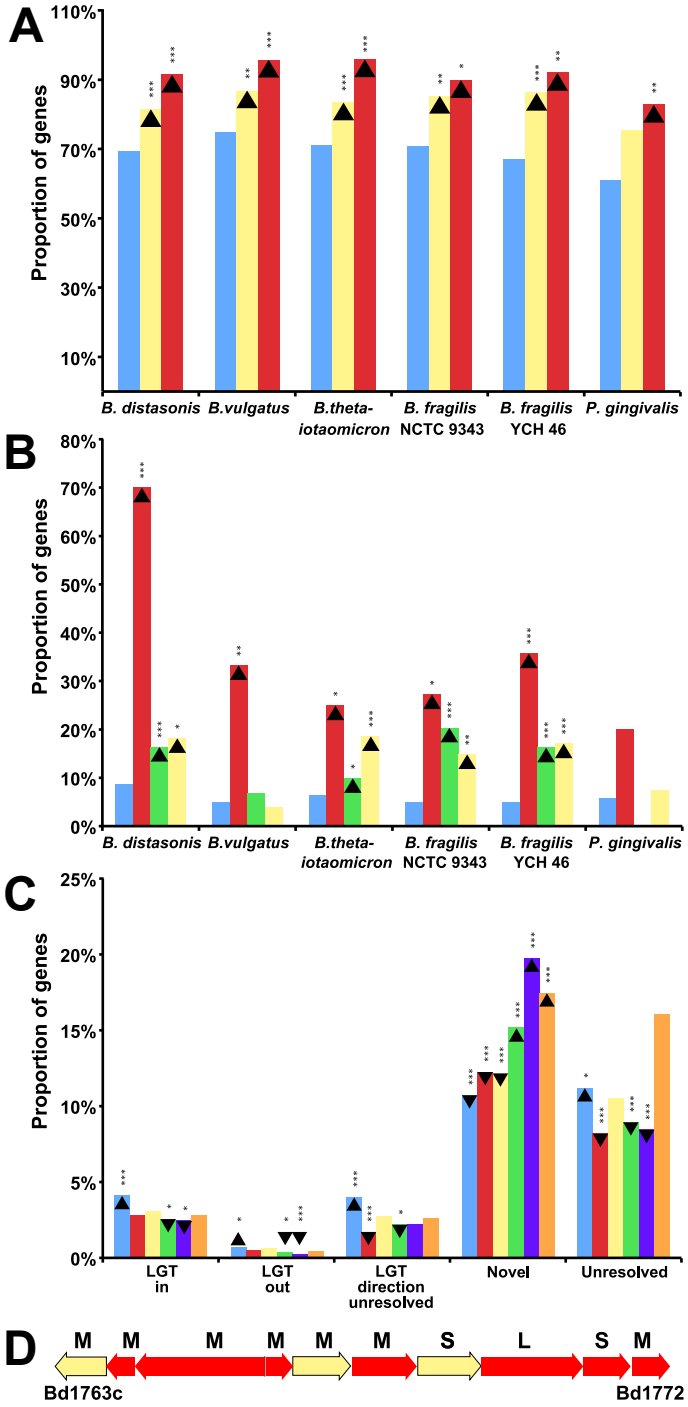
A
Proportion of genes
110%
90%
70%
50%
30%
10%
B. distasonis
B.vulgatus
B.theta-iotaomicron
B. fragilis NCTC 9343
B. fragilis YCH 46
P. gingivalis
B
Proportion of genes
80%
70%
60%
50%
40%
30%
20%
10%
0%
C
Proportion of genes
25%
20%
15%
10%
5%
0%
LGT in
LGT out
LGT direction unresolved
Novel
Unresolved
D
M M M M M M S L S M
Bd1763c
Bd1772

Figure 4.

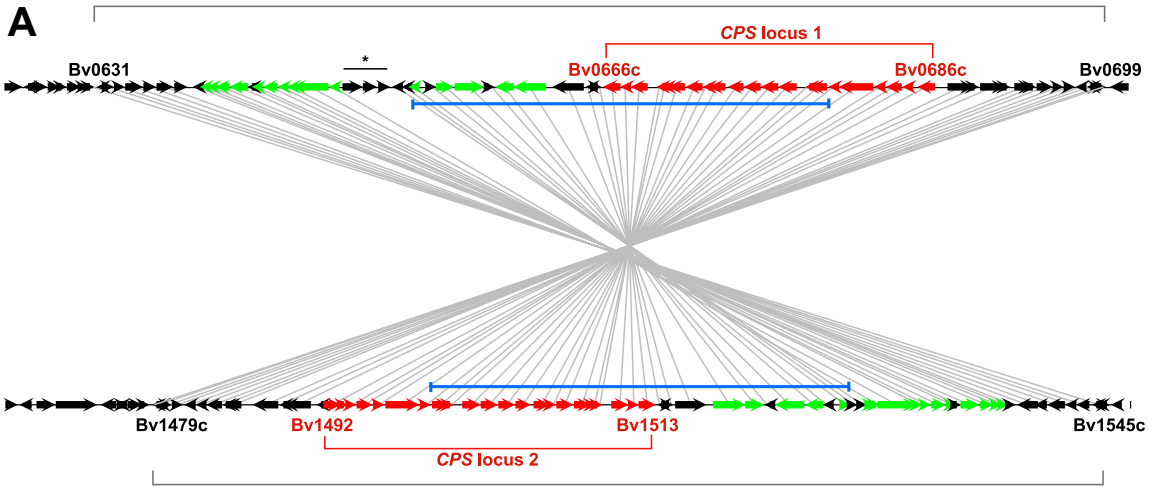
A
CPS locus 1
Bv0631
*
Bv0666c
Bv0686c
Bv0699
Bv1479c
Bv1492
Bv1513
Bv1545c
CPS locus 2

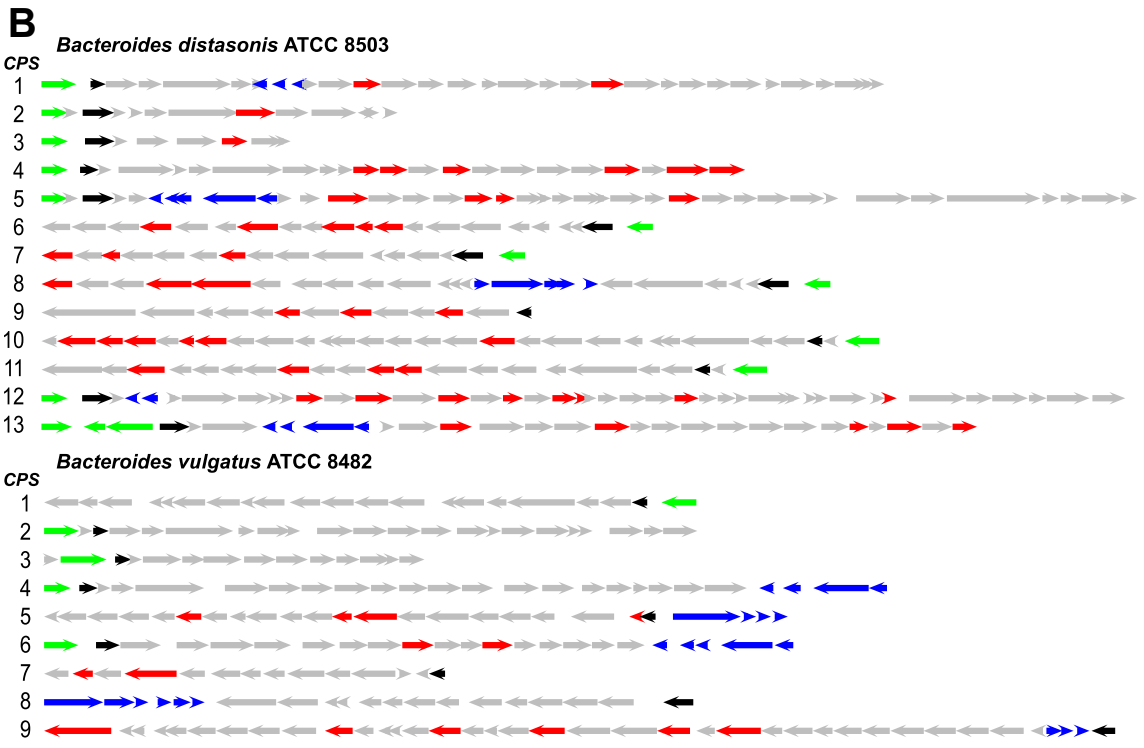
B
Bacteroides distasonis ATCC 8503
CPS
1
2
3
4
5
6
7
8
9
10
11
12
13
Bacteroides vulgatus ATCC 8482
CPS
1
2
3
4
5
6
7
8
9

Figure 5

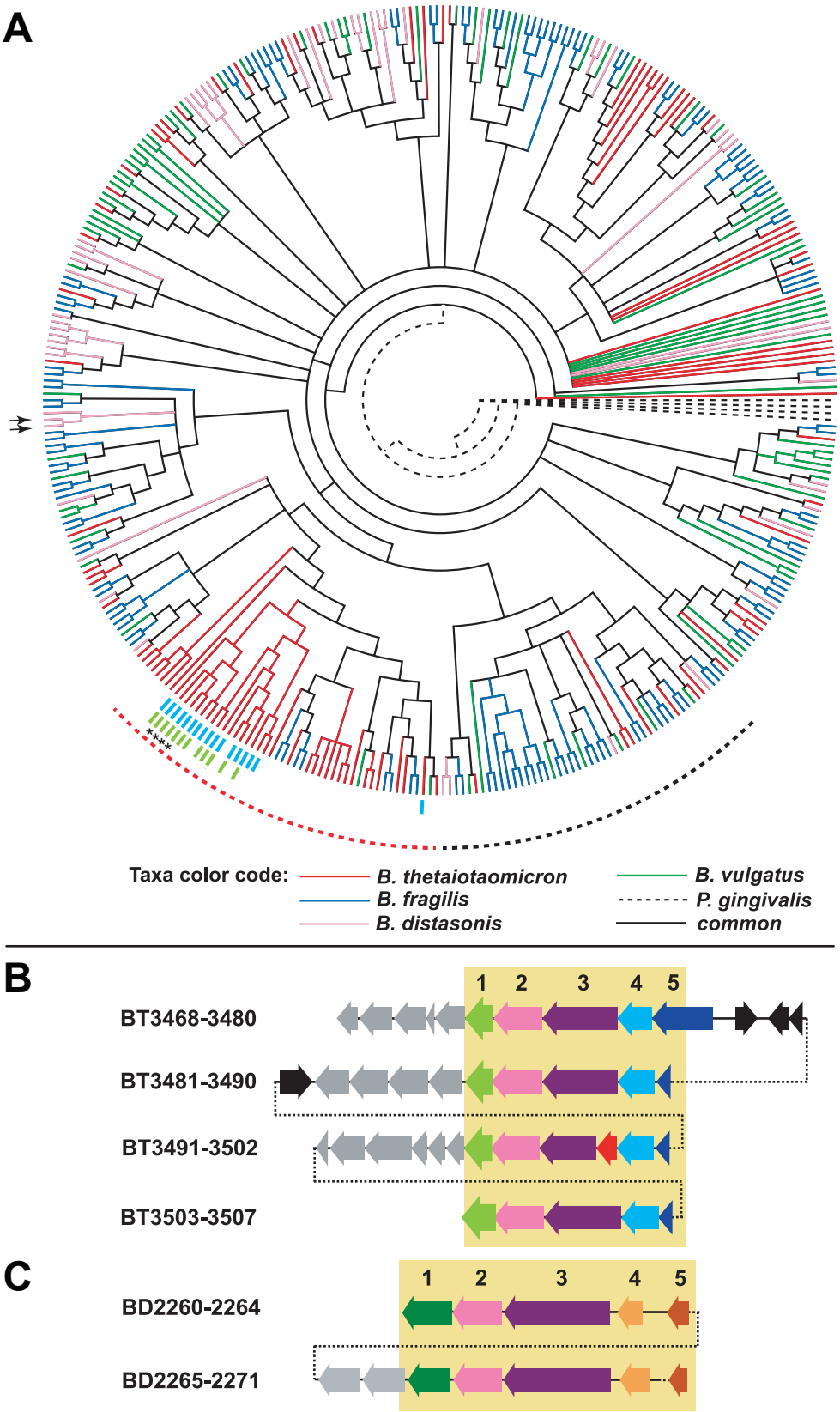
A
Taxa color code:
B. thetaiotaomicron
B. fragilis
B. distasonis
B. vulgatus
P. gingivalis
common
B
BT3468-3480
BT3481-3490
BT3491-3502
BT3503-3507
1 2 3 4 5
C
BD2260-2264
BD2265-2271
1 2 3 4 5

Supplemental Information

Overview of strategy used to identify lateral gene transfer

Many approaches have been used to detect LGT for different applications. For example, compositional methods based on GC content, dinucleotide frequencies, codon usage, and other oligonucleotide frequencies (e.g., [1-5]) are often used to detect transferred genes within a genome. Techniques such as patterns of BLAST hits (e.g., [6-8]) and ratios of sequence divergence between different pairs of genes in different pairs of species (e.g., [9-12]) have also been used in numerous studies. However, these methods for detecting lateral gene transfer are typically seen as surrogates for phylogenetic studies [13], and their sensitivity and specificity have often been criticized. For example, compositional methods are sensitive to equilibration of the gene composition to the genome composition [14-16], and BLAST-based methods are sensitive to loss of paralogs, different rates of evolution, recombination, and many other factors [13,17-21]. Indeed, phylogenetic re-analysis of putative laterally transferred genes that were originally found by reciprocal BLAST hits has indicated that many of these identifications were incorrect (e.g., [22,23]). Similarly, application of parsimony inference to identify gene losses and gains on a species or rRNA tree (e.g., [24-27]) is sensitive to the presence of paralogous sequences and other artifacts [19]. Thus, phylogenetic analysis of individual gene trees, often manually applied, is frequently recommended as the gold standard for lateral gene transfer detection [12,13,17,18,23,28-30].

Phylogenetic analysis itself is subject to many issues, especially because constructing the tree relies on models of sequence evolution that may be simplified or incorrect [31,32], because many protein families lack phylogenetic signal [33], or because of artifacts of tree reconstruction (e.g., [34,35]). There are several formal statistical tests for tree congruence, such as the KH test [36], but these tests require that the two trees to be compared contain the same taxa (i.e. multiple sequences from the same taxon are not allowed).

Because lineage-specific duplications in the Bacteroidetes are common, as shown by our analysis (see **Results**) and previous studies [37-39], applying these tests in an automated fashion becomes exceedingly complex. In particular, choices about which duplicate genes to omit affect the values of the test statistics. Additionally, these tests only measure differences in tree topology, and cannot typically distinguish lateral gene transfer from ancient loss of paralogs or other unusual phylogenetic events. Thus, although the SH test has been extremely useful for identifying genes that lead to poor resolution in whole-genome phylogenies [19], it is less suitable for asking which genes in a genome have undergone lateral gene transfer. Similar comments apply to other global tests for changes in tree topology (e.g., [40-42]) because they cannot handle duplications in any lineage, they cannot be reliably applied on a genome-wide scale. For example, Ge and colleagues were able to find only 297 orthologous gene clusters across 40 species that were suitable for application of their method [41].

Because different methods for detecting lateral gene transfer typically have poor agreement about which genes are detected as transferred [9,12,13,30,43], we decided to use phylogenetic analysis and to focus on the types of transfers it detects best: transfers from within one specific lineage to another specific lineage. In particular, because our 16S rRNA trees showed that the gut Bacteroidetes are well-supported as a monophyletic group, we decided to focus on those genes that were transferred from a specific lineage outside this group to individual species within this group. Since we are in the process of gathering more genomic sequences from Bacteroidetes, we left study of lateral gene transfer within the gut Bacteroidetes for future work because we expect substantially better resolution for detecting lateral gene transfer events when better taxonomic sampling within this group is available.

Our goal was to automatically assign taxon labels to the sequences in individual gene trees, such that unknown sequences would acquire labels from their close relatives in a consistent fashion. In order to achieve this outcome, we treated each taxon label as a

character state, and inferred the ancestral state at each node using the Fitch parsimony algorithm [44]. For example, taxon labels might correspond to bacterial divisions, such as "Firmicutes," or to other taxonomic groups of interest, such as "gut Bacteroidetes" or "non-gut Bacteroidetes". This procedure, which has often been applied either manually or in an automated fashion to reveal lateral gene transfer among specific lineages (e.g., [45-47]), is based on the idea that a lateral gene transfer event followed by speciation should typically be marked by a monophyletic group of sequences from one lineage that stems from within a paraphyletic group of sequences from a single other lineage. In other words, the transfer of a gene from lineage X to lineage Y should give a tree in which the sequences from Y are related to a specific group of sequences within lineage X. We would still count this event as a transfer from X to Y even if there are more sequences in Y than remain in X, for example if Y is a very speciose lineage or is a lineage in which paralogy of the relevant genes is rampant. The parsimony approach we used is related to Brooks Parsimony Analysis, a method used for detecting co-speciation between hosts and parasites [48]. The problem of host-parasite co-speciation is mathematically identical to the problem of relating gene trees to species trees, because both cases require the analysis of phylogenies in which duplication, deletion, and switching between hosts (or genomes) are all possible.

There are two types of events that could conceivably lead to the type of phylogeny in which we are interested (lineage X paraphyletic with respect to lineage Y): lateral transfer from one group to another, and loss of an ancient paralog in all but those two groups. However, because strong selective advantages are required to maintain transferred genes in bacterial populations [49] and because the divergence distances are large (mostly from other bacterial divisions), lateral gene transfer is by far the most likely scenario leading to these trees. We believe that this method is more suitable for detecting a set of high-confidence transfers because global measures of phylogenetic incongruence require rejection over the whole tree, not just for one specific group (potentially leading to high false negative rates), and are influenced by the many factors that can lead to misplacement of taxa not relevant to

our analysis (leading to high false positive rates). We confirmed the likely lateral transfer of these genes by testing that the GC content and codon usage of genes chosen by our method differed from those of randomly chosen genes in the genome. Specifically, we compared the GC contents of transferred and non-transferred genes within each genome (excluding unresolved genes) using two-sample *t* tests with Welch's correction for unequal variances, and compared the codon usage of transferred and non-transferred genes using chi-squared tests. Analysis of the functional categories represented by these genes and presence of groups of genes within apparent genomic islands provided additional supporting evidence of LGT (see **Results**).

Supplemental References

1. Karlin S, Mrazek J, Campbell AM (1998) Codon usages in different gene classes of the Escherichia coli genome. Mol Microbiol 29: 1341-1355.

2. Lawrence JG, Ochman H (1998) Molecular archaeology of the Escherichia coli genome. Proc Natl Acad Sci U S A 95: 9413-9417.

3. Wang HC, Badger J, Kearney P, Li M (2001) Analysis of codon usage patterns of bacterial genomes using the self-organizing map. Mol Biol Evol 18: 792-800.

4. Hooper SD, Berg OG (2002) Detection of genes with atypical nucleotide sequence in microbial genomes. J Mol Evol 54: 365-375.

5. Sandberg R, Branden CI, Ernberg I, Coster J (2003) Quantifying the species-specificity in genomic signatures, synonymous codon choice, amino acid usage and G+C content. Gene 311: 35-42.

6. Nelson KE, Clayton RA, Gill SR, Gwinn ML, Dodson RJ, et al*et al*. (1999) Evidence for lateral gene transfer between Archaea and bacteria from genome sequence of Thermotoga maritima. Nature 399: 323-329.

7. Lander ES, Linton LM, Birren B, Nusbaum C, Zody MC, et al*et al*. (2001) Initial sequencing and analysis of the human genome. Nature 409: 860-921.

8. Pallen MJ, Beatson SA, Bailey CM (2005) Bioinformatics analysis of the locus for enterocyte effacement provides novel insights into type-III secretion. BMC Microbiol 5: 9.

9. Syvanen M (2002) On the occurrence of horizontal gene transfer among an arbitrarily chosen group of 26 genes. J Mol Evol 54: 258-266.

10. Farahi K, Whitman WB, Kraemer ET (2003) RED-T: utilizing the Ratios of Evolutionary Distances for determination of alternative phylogenetic events. Bioinformatics 19: 2152-2154.

11. Novichkov PS, Omelchenko MV, Gelfand MS, Mironov AA, Wolf YI, et al*et al*. (2004) Genome-wide molecular clock and horizontal gene transfer in bacterial evolution. J Bacteriol 186: 6575-6585.

12. Kechris KJ, Lin JC, Bickel PJ, Glazer AN (2006) Quantitative exploration of the occurrence of lateral gene transfer by using nitrogen fixation genes as a case study. Proc Natl Acad Sci U S A 103: 9584-9589.

13. Ragan MA (2001) On surrogate methods for detecting lateral gene transfer. FEMS Microbiol Lett 201: 187-191.

14. Lawrence JG, Ochman H (1997) Amelioration of bacterial genomes: rates of change and exchange. J Mol Evol 44: 383-397.

15. Koski LB, Morton RA, Golding GB (2001) Codon bias and base composition are poor indicators of horizontally transferred genes. Mol Biol Evol 18: 404-412.

16. Wang B (2001) Limitations of compositional approach to identifying horizontally transferred genes. J Mol Evol 53: 244-250.

17. Ochman H (2001) Lateral and oblique gene transfer. Curr Opin Genet Dev 11: 616-619.

18. Doolittle WF, Boucher Y, Nesbo CL, Douady CJ, Andersson JO, et al*et al*. (2003) How big is the iceberg of which organellar genes in nuclear genomes are but the tip? Philos Trans R Soc Lond B Biol Sci 358: 39-57; discussion 57-38.

19. Lerat E, Daubin V, Moran NA (2003) From gene trees to organismal phylogeny in prokaryotes: the case of the gamma-Proteobacteria. PLoS Biol 1: E19.

20. Philippe H, Douady CJ (2003) Horizontal gene transfer and phylogenetics. Curr Opin Microbiol 6: 498-505.

21. Andersson JO (2005) Lateral gene transfer in eukaryotes. Cell Mol Life Sci 62: 1182-1197.

22. Kinsella RJ, McInerney JO (2003) Eukaryotic genes in Mycobacterium tuberculosis? Possible alternative explanations. Trends Genet 19: 687-689.

23. Genereux DP, Logsdon JM, Jr. (2003) Much ado about bacteria-to-vertebrate lateral gene transfer. Trends Genet 19: 191-195.

24. Jordan IK, Makarova KS, Spouge JL, Wolf YI, Koonin EV (2001) Lineage-specific gene expansions in bacterial and archaeal genomes. Genome Res 11: 555-565.

25. Mirkin BG, Fenner TI, Galperin MY, Koonin EV (2003) Algorithms for computing parsimonious evolutionary scenarios for genome evolution, the last universal common ancestor and dominance of horizontal gene transfer in the evolution of prokaryotes. BMC Evol Biol 3: 2.

26. Hao W, Golding GB (2004) Patterns of bacterial gene movement. Mol Biol Evol 21: 1294-1307.

27. Pal C, Papp B, Lercher MJ (2005) Horizontal gene transfer depends on gene content of the host. Bioinformatics 21 Suppl 2: ii222-ii223.

28. Eisen JA (2000) Horizontal gene transfer among microbial genomes: new insights from complete genome analysis. Curr Opin Genet Dev 10: 606-611.

29. Kurland CG, Canback B, Berg OG (2003) Horizontal gene transfer: a critical view. Proc Natl Acad Sci U S A 100: 9658-9662.

30. Ragan MA, Harlow TJ, Beiko RG (2006) Do different surrogate methods detect lateral genetic transfer events of different relative ages? Trends Microbiol 14: 4-8.

31. Lio P, Goldman N (1998) Models of molecular evolution and phylogeny. Genome Res 8: 1233-1244.

32. Bollback JP (2002) Bayesian model adequacy and choice in phylogenetics. Mol Biol Evol 19: 1171-1180.

33. Teichmann SA, Mitchison G (1999) Is there a phylogenetic signal in prokaryote proteins? J Mol Evol 49: 98-107.

34. Doolittle WF (1999) Phylogenetic classification and the universal tree. Science 284: 2124-2129.

35. Thornton JW, DeSalle R (2000) Gene family evolution and homology: genomics meets phylogenetics. Annu Rev Genomics Hum Genet 1: 41-73.

36. Kishino H, Hasegawa M (1989) Evaluation of the maximum likelihood estimate of the evolutionary tree topologies from DNA sequence data, and the branching order in hominoidea. J Mol Evol 29: 170-179.

37. Coyne MJ, Weinacht KG, Krinos CM, Comstock LE (2003) Mpi recombinase globally modulates the surface architecture of a human commensal bacterium. Proc Natl Acad Sci U S A 100: 10446-10451.

38. Kuwahara T, Yamashita A, Hirakawa H, Nakayama H, Toh H, et al*et al*. (2004) Genomic analysis of Bacteroides fragilis reveals extensive DNA inversions regulating cell surface adaptation. Proc Natl Acad Sci U S A 101: 14919-14924.

39. Xu J, Bjursell MK, Himrod J, Deng S, Carmichael LK, et al*et al*. (2003) A genomic view of the human-Bacteroides thetaiotaomicron symbiosis. Science 299: 2074-2076.

40. Daubin V, Ochman H (2004) Quartet mapping and the extent of lateral transfer in bacterial genomes. Mol Biol Evol 21: 86-89.

41. Ge F, Wang LS, Kim J (2005) The cobweb of life revealed by genome-scale estimates of horizontal gene transfer. PLoS Biol 3: e316.

42. Planet PJ, Sarkar IN (2005) mILD: a tool for constructing and analyzing matrices of pairwise phylogenetic character incongruence tests. Bioinformatics 21: 4423-4424.

43. Lawrence JG, Ochman H (2002) Reconciling the many faces of lateral gene transfer. Trends Microbiol 10: 1-4.

44. Fitch WM (1970) Distinguishing homologous from analogous proteins. Syst Zool 20: 406-416.

45. Hooper SD, Berg OG (2003) Duplication is more common among laterally transferred genes than among indigenous genes. Genome Biol 4: R48.

46. Kunin V, Ouzounis CA (2003) GeneTRACE-reconstruction of gene content of ancestral species. Bioinformatics 19: 1412-1416.

47. Daubin V, Ochman H (2004) Bacterial genomes as new gene homes: the genealogy of ORFans in E. coli. Genome Res 14: 1036-1042.

48. Brooks DR (1981) Hennig's parasitological method: a proposed solution. Syst Zool 30: 229-249.

49. Berg OG, Kurland CG (2002) Evolution of microbial genomes: sequence acquisition and loss. Mol Biol Evol 19: 2265-2276.

50. Sonnenburg ED, Sonnenburg JL, Manchester JK, Hansen EE, Chiang HC, et al*et al*. (2006) A hybrid two-component system protein of a prominent human gut symbiont couples glycan sensing in vivo to carbohydrate metabolism. Proc Natl Acad Sci U S A 103: 8834-8839.

Supplemental Figure Legends

Figure S1. *B. distasonis* ATCC 8503 (A) and *B. vulgatus* ATCC 8482 (B) chromosomes. The coding potential of the leading and lagging strands is relatively unbiased. Circles shown in the figure represent, from inside out, GC skew, GC content variation, rRNA operons, tRNA genes, conjugative transposons (CTns), *CPS* loci, extra-cytoplasmic function (ECF) σ factors, SusC paralogs, and all predicted genes with assigned functions on reverse and forward strands, respectively. Color codes for genes are based on their COG functional classification.

Figure S2. COG-based characterization of all proteins with annotated functions in the proteomes of sequenced Bacteroidetes. The term, 'Bacteroides orthologs' refers to the 1,416 orthologs shared by the sequenced gut Bacteroidetes (*B. vulgatus, B. distasonis, B. thetaiotaomicron,* plus the two *B. fragilis* strains). Color codes are the same as **Figure S1**.

Figure S3. Pair-wise alignments of the human gut Bacteroidetes genomes reveal rapid deterioration of global synteny with increasing phylogenetic distance. Each data point on the Dotplot represents one pair of mutual best hits (BLASTP) between the two genomes, plotted by pair-wise genome location. Diagonal lines indicate synteny.

Figure S4. *CPS* loci are the most polymorphic regions in the gut Bacteroidetes genomes. High-resolution synteny map of *CPS* loci and flanking regions in the two sequenced *B. fragilis* strains**.** There are 9 *CPS* loci in each genome. Each data point represents a pair of orthologs (mutual best hits; e-value cutoff: 10^{-6}). Brackets define the coordinates for component genes within a given locus (some pairs are missing due to gene loss or gain): X-axis, coordinate of the middle point of the gene on the NCTC 9343 chromosome; Y-Axis, coordinate of the middle point of the gene on YCH 46 chromosome. With the exception of *CPS* locus 5, which is strictly conserved, the 9 *CPS* loci are affected by non-homologous gene replacement and rearrangement.

Supplemental Figures

Figure S1A.

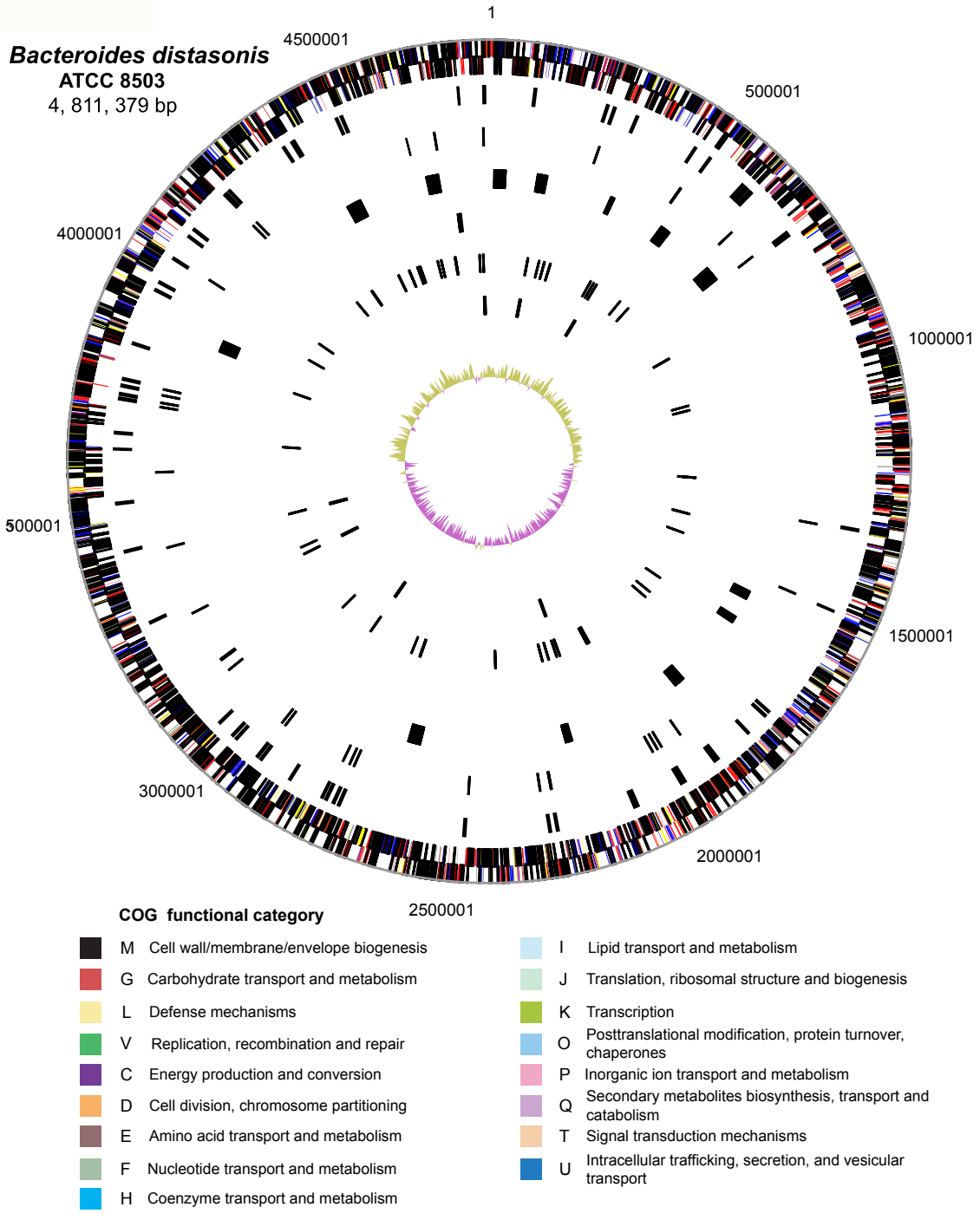

Figure S1B.

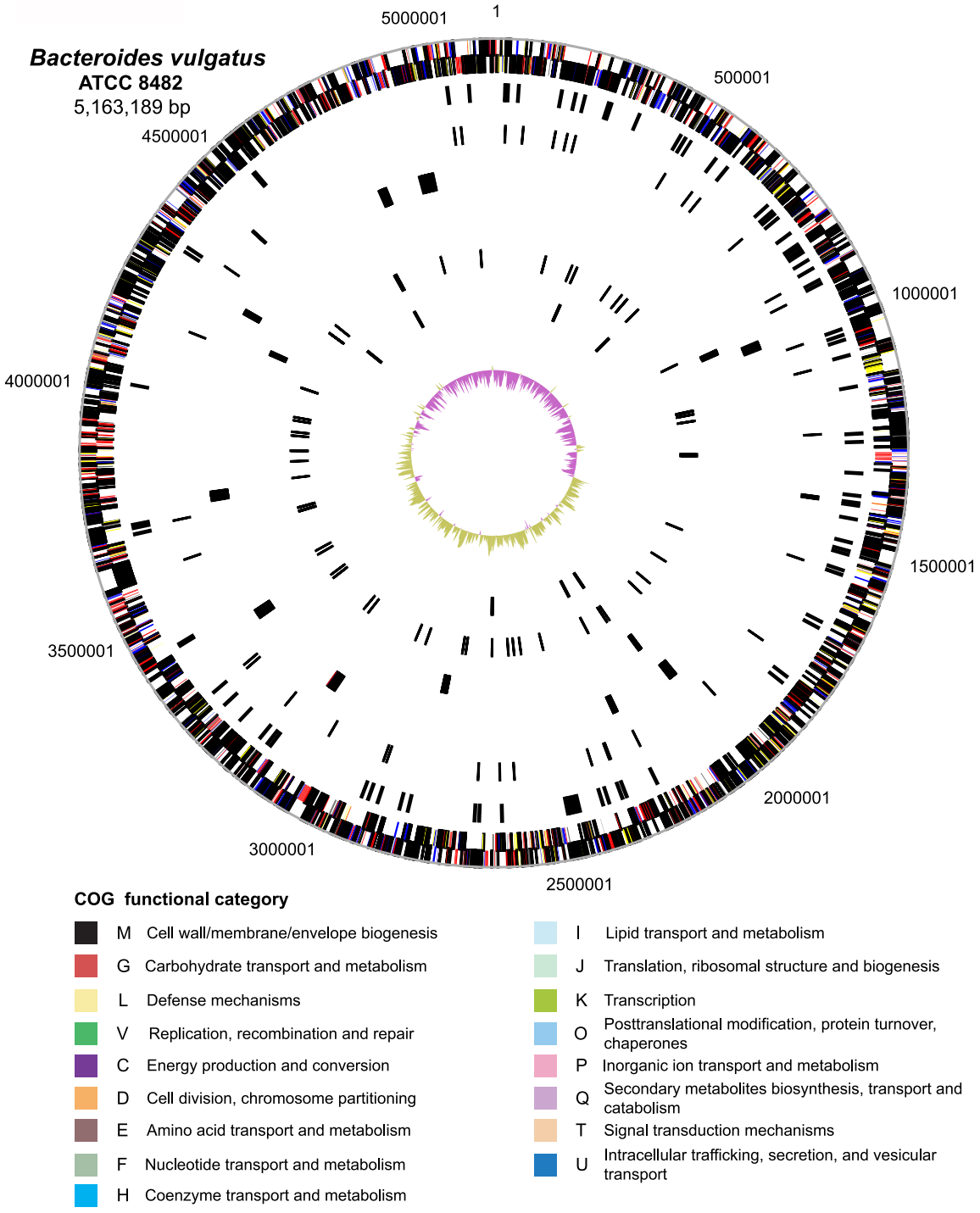
Bacteroides vulgatus
ATCC 8482
5,163,189 bp
1
500001
1000001
1500001
2000001
2500001
3000001
3500001
4000001
4500001
5000001
COG functional category
M Cell wall/membrane/envelope biogenesis
G Carbohydrate transport and metabolism
L Defense mechanisms
V Replication, recombination and repair
C Energy production and conversion
D Cell division, chromosome partitioning
E Amino acid transport and metabolism
F Nucleotide transport and metabolism
H Coenzyme transport and metabolism
I Lipid transport and metabolism
J Translation, ribosomal structure and biogenesis
K Transcription
O Posttranslational modification, protein turnover, chaperones
P Inorganic ion transport and metabolism
Q Secondary metabolites biosynthesis, transport and catabolism
T Signal transduction mechanisms
U Intracellular trafficking, secretion, and vesicular transport

Figure S2.

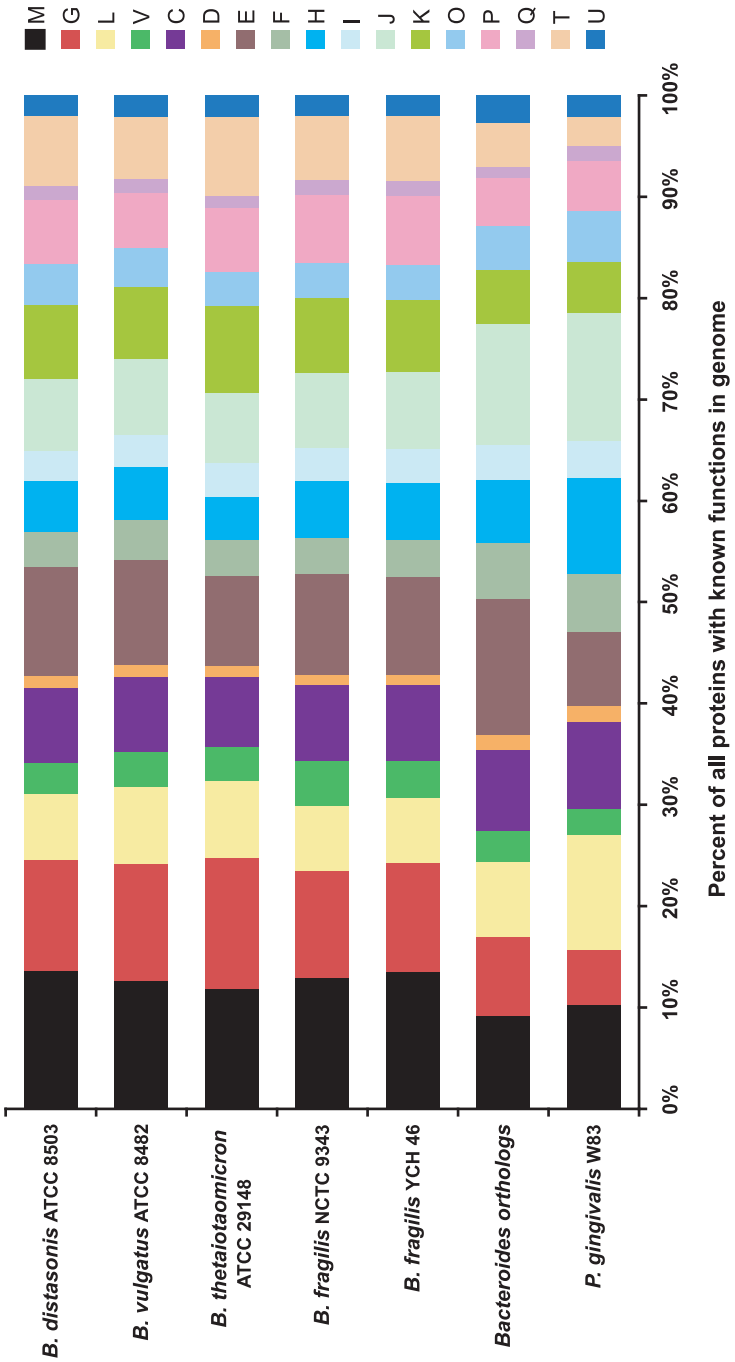
M
G
L
V
C
D
E
F
H
I
J
K
O
P
Q
T
U
0%
10%
20%
30%
40%
50%
60%
70%
80%
90%
100%
Percent of all proteins with known functions in genome
B. distasonis ATCC 8503
B. vulgatus ATCC 8482
B. thetaiotaomicron ATCC 29148
B. fragilis NCTC 9343
B. fragilis YCH 46
Bacteroides orthologs
P. gingivalis W83

Figure S3.

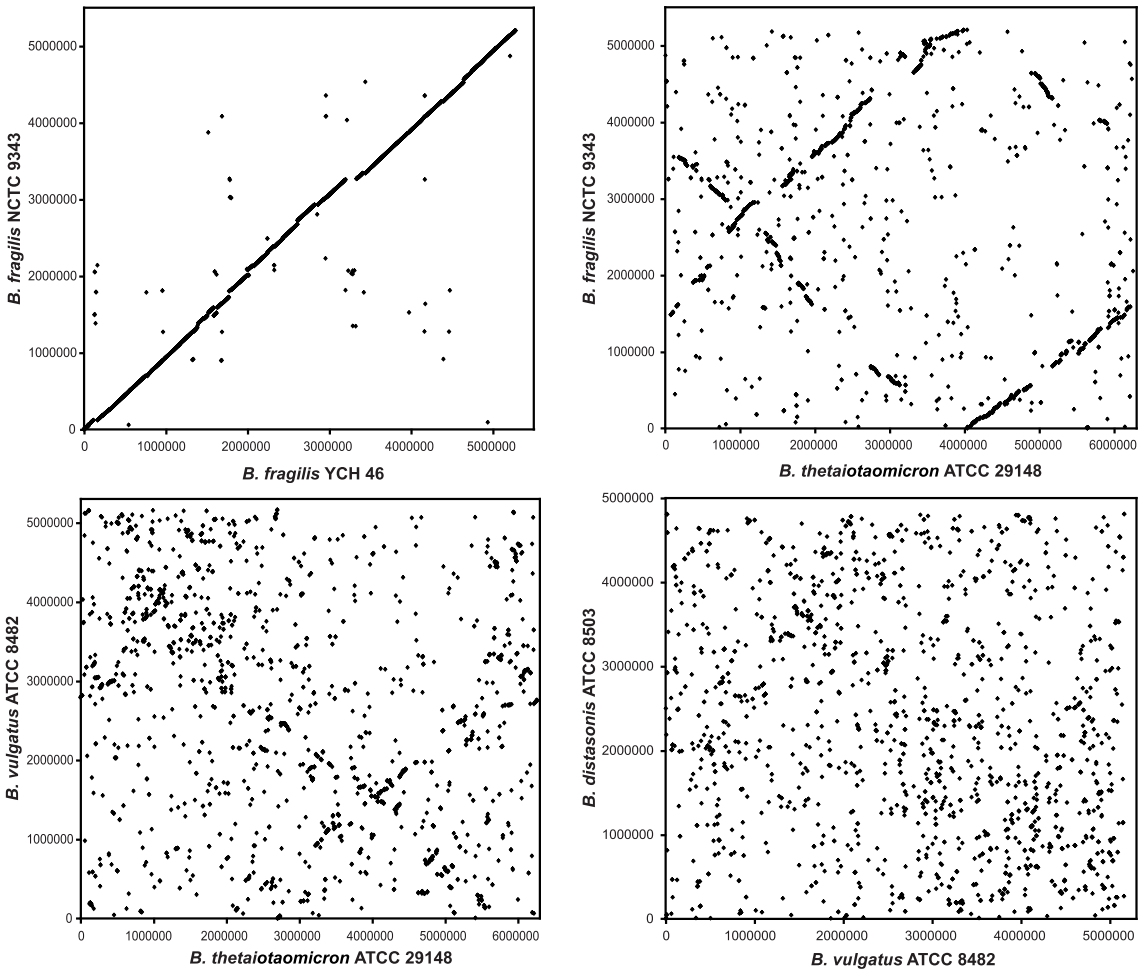
B. fragilis NCTC 9343
B. fragilis YCH 46
B. fragilis NCTC 9343
B. thetaiotaomicron ATCC 29148
B. vulgatus ATCC 8482
B. thetaiotaomicron ATCC 29148
B. distasonis ATCC 8503
B. vulgatus ATCC 8482

Figure S4.

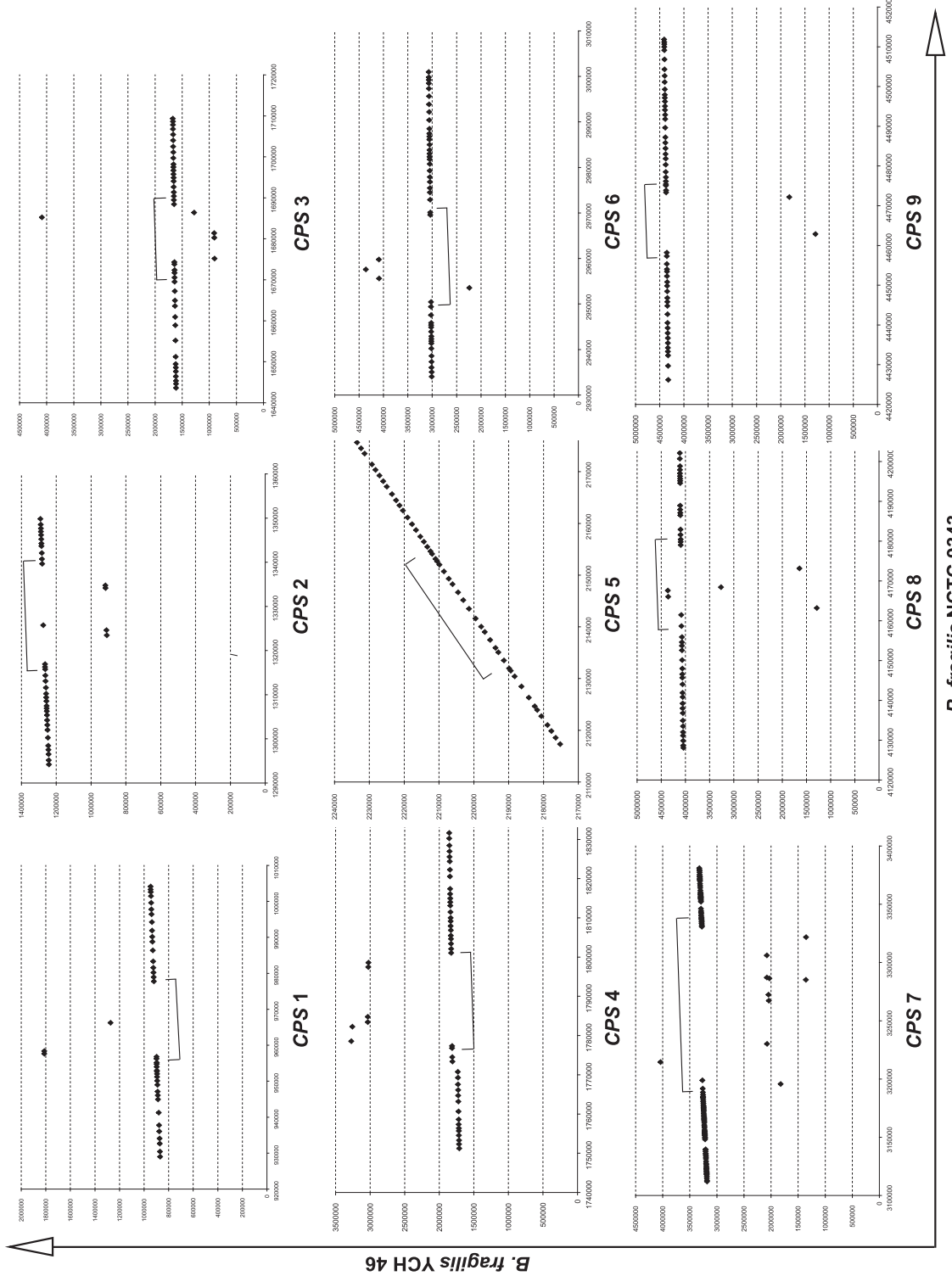
B. fragilis YCH 46
B. fragilis NCTC 9343
CPS 1
CPS 2
CPS 3
CPS 4
CPS 5
CPS 6
CPS 7
CPS 8
CPS 9

Supplemental Table Legends

Table S1. Comparison of genome parameters for *B. distasonis* ATCC 8503, *B. vulgatus* ATCC 8482, *B. thetaiotaomicron* ATCC 29148, *B. fragilis* NCTC 9343 and *B. fragilis* YCH 46. '*', the numbers of SusC/SusD homologs provided are based on BLASTP e-value $\leq 10^{-20}$; the numbers shown in parentheses are based on criteria described in *SusC/SusD alignments* in **Materials and Methods**. See http://gordonlab.wustl.edu/BvBd.html for complete lists of SusC/SusD homologs. A hybrid two-component system protein contains all of the domains present in classical two-component systems but in one polypeptide [50].

Table S2. Shared orthologs in *B. distasonis* ATCC 8503, *B. vulgatus* ATCC 8482, *B. thetaiotaomicron* ATCC 29148, and *B. fragilis* strains NCTC 9343 and YCH 46. For an explanation of COG-based functional codes, see **Figure S1**.

Table S3. Glycoside hydrolases found in ***B. distasonis*** ATCC 8503, ***B. vulgatus*** ATCC 8482, ***B. thetaiotaomicron*** ATCC 29148 and ***B. fragilis*** strains NCTC 9343 and YCH 46. The classification scheme used is described in the Carbohydrate-Active enZYme (CAZy) database.

Table S4. List of putative xenologs in *B. distasonis* ATCC 8503 (A), *B. vulgatus* ATCC 8482 (B), *B. thetaiotaomicron* ATCC 29148 (C), *B. fragilis* NCTC 9343 (D), and *B. fragilis* YCH 46 (E). For an explanation of COG-based functional codes, see **Figure S1**. The lateral gene transfer (LGT) column defines the predicted evolutionary history of the coding sequence: LGT-in, laterally transferred into the genome; LGT-out, laterally transferred out of the genome; LGT-unresolved, laterally transferred but direction unknown. See **Materials and Methods** for detailed explanations.

Table S5. *CPS* loci of *B. distasonis* ATCC 8503 (A), *B. vulgatus* ATCC 8482 (B), *B. thetaiotaomicron* ATCC 29148 (C), *B. fragilis* NCTC 9343 (D) and *B. fragilis* YCH 46 (E). Shown are Gene ID, annotated function, GC content (%) and the predicted evolu-

tionary history of the coding sequence. Code: NOVEL, no homologs found in any other genomes in public databases; NO, not laterally transferred; UNRESOLVED, whether laterally transferred or not is not resolved; LGT-in, laterally transferred into the genome; LGT-out, laterally transferred out of the genome; LGT-unresolved, laterally transferred but direction unknown. See **Materials and Methods** for detailed explanations. Color codes are the same as in **Figure 4B**.

Table S6. *CPS* loci are among the most polymorphic regions in the two *B. fragilis* genomes. The P value is based on the tail probability of a binomial distribution. Gene loss/gain events (3,531 in total) are counted as the difference between the total number of genes and the total number of genes shared between the two genomes.

Table S7. ECF-σ factor-containing polysaccharide utilization gene clusters in *B. distasonis* ATCC 8503 (A) and *B. vulgatus* ATCC 8482 (B). The three columns represent Gene ID, functional annotation and predicted evolutionary history of the gene (labeled as in **Table S5**).

Table S1. Comparison of genome parameters for *B. distasonis* ATCC 8503, *B. vulgatus* ATCC 8482, *B. thetaiotaomicron* ATCC 29148, *B. fragilis* NCTC 9343 and *B. fragilis* YCH 46.

Feature	*B. distasonis* ATCC 8503	*B. vulgatus* ATCC 8482	*B. thetaiotaomicron* ATCC 29148	*B. fragilis* NCTC 9343	*B. fragilis* YCH 46
Genome size (bp)	**4,811,379**	**5,163,189**	6,260,361	5,205,140	5,277,274
G + C (%)	**45.1**	**42.2**	42.8	43.2	43.3
Protein coding (%)	**90.3**	**89.1**	89.5	89.3	90.1
Gene density (no. of CDS per Kb)	**0.804**	**0.792**	0.763	0.818	0.867
Average CDS length (bp)	**1,123**	**1,126**	1,173	1,091	1,039
Protein-coding genes (no.)	**3,867**	**4,088**	4,778	4,189	4,578
CDS with functional assignment	**2,427**	**2,505**	2,709	2,753	2,959
CDS without functional asignment	**1,440**	**1,583**	2,069	1,436	1,619
conserved hypothetical protein	**1,005**	**1,123**	1,532	858	950
hypothetical protein	**435**	**460**	537	578	669
Ribosomal RNA loci	**7**	**7**	5	6	6
Transfer RNAs	**83**	**85**	71	73	74
Conjugative transposons	**1**	**4**	4	2	2
Transposases	**61**	**121**	109	47	60
Phages	**5**	**3**	5	2	4
Glycoside hydrolases (GH)	**97**	**159**	226	126	132
Polysaccharide lyases (PL)	**0**	**7**	15	1	1
Glycosyltransferases (GT)	**78**	**76**	85	79	81
SusC homologs*	**63 (60)**	**89 (86)**	107 (107)	88 (88)	77 (77)
SusD homologs*	**48 (54)**	**74 (80)**	57 (102)	48 (71)	47 (65)
ECF-σ factors	**36**	**41**	50	42	41
Anti-σ factors	**23**	**21**	25	25	25
Hybrid two-component systems	**7**	**22**	32	14	12

Legend: '*', the numbers of SusC/SusD homologs provided are based on BLASTP e-value $\leq 10^{-20}$; the numbers shown in parentheses are based on criteria described in SusC/SusD alignments in **Materials and Methods**. See http://gordonlab.wustl.edu/BvBd.html for complete lists of SusC/SusD homologs. A hybrid two-component system protein contains all of the domains present in classical two-component systems but in one polypeptide (Xu, *et al,* Science 299:2074-6, 2003).

Table S2.

Please access provided CD for this information.

Table S3.

Family ID	*B. distasonis* ATCC 8503	*B. vulgatus* ATCC 8482	*B. thetaiotaomicron* ATCC 29148	*B. fragilis* NCTC 9343	*B. fragilis* YCH 46
Glycosidases and Transglycosidases					
2	11	25	33	15	16
3	8	5	10	10	10
5	0	2	1	1	1
10	0	1	0	0	0
13	9	4	7	6	6
15	1	1	0	0	0
16	1	1	3	6	6
18	0	2	7	2	2
20	6	9	14	12	13
23	3	3	3	3	3
24	1	2	0	0	1
25	0	1	1	1	1
26	1	0	0	2	2
27	0	1	5	3	3
28	1	13	9	0	0
29	1	10	9	9	9
30	2	2	2	0	0
31	1	4	6	4	4
32	1	1	4	2	2
33	1	3	1	3	3
35	1	1	3	4	4
36	2	2	3	3	3
38	1	0	2	1	1
42	0	1	1	0	0
43	7	22	32	9	9
51	3	3	4	2	2
53	0	0	1	0	0
57	1	1	1	1	1
63	1	2	0	0	1
65	0	0	0	1	1
66	0	0	1	0	0
67	0	1	1	0	0
73	3	1	1	1	2
76	1	0	10	3	3
77	1	1	1	1	1
78	7	5	6	2	2
84	1	1	1	1	1
88	0	3	4	1	1
89	0	1	3	1	1
92	14	9	23	8	9
93	0	0	1	0	0
95	1	4	5	4	4
97	3	9	10	4	4
99	0	0	1	0	0
Unclassified	2	2	0	0	0
Sub-total	**97**	**159**	**226**	**126**	**132**
Polysaccharide Lyases					
1	0	1	5	0	0
4	0	1	0	0	0
8	0	0	3	1	1
9	0	2	2	0	0
10	0	1	1	0	0
11	0	2	1	0	0
12	0	0	2	0	0
13	0	0	1	0	0
Sub-total	**0**	**7**	**15**	**1**	**1**

Legend: The classification scheme used is described in the Carbohydrate-Active Enzymes database (CAZy) at http://afmb.cnrs-mrs.fr/CAZY/.

Table S4.

Please access provided CD for this information.

Table S5

Please access provided CD for this information.

Table S6

Table S6. *CPS* loci are among the most polymorphic regions in the two *B. fragilis* genomes.

	***B. fragilis* NCTC 9343**	***B. fragilis* YCH 46**
Number of genes in genome	4189	4578
Number of genes in *CPS* loci	170	204
Number of gene loss/gain events	658	1047
Number of gene loss/gain events in *CPS* loci	77	109
Probability	8.8E-20	3.3E-21

Legend: The probability value is based on the tail probability of a binomial distribution. Gene loss/gain events are counted as the difference between the total number of genes in a given strain and the total number of genes shared between the two strains (3,531 in total).

Table S7. ECF-σ factor-containing polysaccharide utilization gene clusters in *B. distasonis* ATCC 8503 (A) and *B. vulgatus* ATCC 8482 (B).

(A). ECF-σ factor-containing polysaccharide utilization gene clusters in *B. distasonis* ATCC 8503

Cluster 1		
Bd0229	putative RNA polymerase ECF-type sigma factor	UNRESOLVED
Bd0230	putative anti-sigma factor	UNRESOLVED
Bd0231	putative outer membrane protein, probably involved in nutrient binding	NO
Bd0232	putative outer membrane protein probably involved in nutrient binding	UNRESOLVED
Bd0233	conserved hypothetical protein	NO
Bd0234	glycoside hydrolase family 38, distantly related to alpha-mannosidases	NO
Bd0235	putative sodium-dependent transporter	NO
Bd0236	helicase domain protein	LGT-in
Bd0237	conserved hypothetical protein	LGT-in
Bd0238	conserved hypothetical protein	LGT-in
Bd0239	putative exonuclease	NOVEL
Bd0240	conserved hypothetical protein	NO
Bd0241	putative acetyltransferase	NOVEL
Cluster 2		
Bd1126c	two-component system sensor histidine kinase	NO
Bd1127c	conserved hypothetical protein	UNRESOLVED
Bd1128c	probable NADH-dependent dehydrogenase	NO
Bd1129c	oxidoreductase, Gfo/Idh/MocA family	NO
Bd1130c	putative arylsulfatase	NO
Bd1131c	putative outer membrane protein, probably involved in nutrient binding	NO
Bd1132c	putative outer membrane protein, probably involved in nutrient binding	NO
Bd1133c	putative anti-sigma factor	NO
Bd1134c	putative RNA polymerase ECF-type sigma factor	NO
Cluster 3		
Bd1642c	mucin-desulfating sulfatase	NO
Bd1643c	arylsulfatase A	LGT-unresolved
Bd1644c	putative outer membrane protein, probably involved in nutrient binding	NO
Bd1645c	putative outer membrane protein, probably involved in nutrient binding	NO
Bd1646c	putative anti-sigma factor	NO
Bd1647	conserved hypothetical protein	NO
Bd1648c	RNA polymerase ECF-type sigma factor	NO
Cluster 4		
Bd2026	RNA polymerase ECF-type sigma factor	NO
Bd2027	putative anti-sigma factor	NO
Bd2028	putative outer membrane protein probably involved in nutrient binding	NO
Bd2029	putative outer membrane protein probably involved in nutrient binding	NO
Bd2030	putative sulfatase	NO
Bd2031	arylsulfatase A	UNRESOLVED
Bd2032	putative aminotransferase	NO
Bd2033	peptidyl-prolyl cis-trans isomerase SlyD, FKBP-type	NO
Bd2034	chorismate synthase	NO
Bd2035	putative multidrug resistance protein	LGT-in
Cluster 5		
Bd2259c	conserved hypothetical protein	NO
Bd2260c	arylsulfatase A	LGT-in
Bd2261c	putative outer membrane protein probably involved in nutrient binding	NO
Bd2262c	putative outer membrane protein probably involved in nutrient binding	NO

Bd2263c	putative anti-sigma factor	NO
Bd2264c	RNA polymerase ECF-type sigma factor	NO
Cluster 6		
Bd2265c	putative secreted sulfatase precursor	UNRESOLVED
Bd2266c	arylsulfatase A	UNRESOLVED
Bd2267c	arylsulfatase A	LGT-unresolved
Bd2268c	conserved hypothetical protein, probably involved in nutrient binding	NO
Bd2269c	putative outer membrane protein, probably involved in nutrient binding	NO
Bd2270c	putative anti-sigma factor	NO
Bd2271c	RNA polymerase ECF-type sigma factor	NO
Cluster 7		
Bd2277c	putative 1-acyl-sn-glycerol-3-phosphate acyltransferase	NO
Bd2278c	glycoside hydrolase family 92, related to an ill-defined alpha-1,2-mannosidase	UNRESOLVED
Bd2279c	putative outer membrane protein, probably involved in nutrient binding	NO
Bd2280c	putative outer membrane protein, probably involved in nutrient binding	UNRESOLVED
Bd2281c	putative anti-sigma factor	NO
Bd2282	RNA polymerase ECF-type sigma factor	UNRESOLVED
Cluster 8		
Bd2405c	hypothetical protein	NOVEL
Bd2406c	conserved hypothetical protein	LGT-unresolved
Bd2407c	conserved hypothetical protein	UNRESOLVED
Bd2408c	glycoside hydrolase family 28, related to polygalacturonases	UNRESOLVED
Bd2409c	putative outer membrane protein, probably involved in nutrient binding	UNRESOLVED
Bd2410c	putative outer membrane protein, probably involved in nutrient binding	UNRESOLVED
Bd2411c	putative anti-sigma factor	UNRESOLVED
Bd2412c	RNA polymerase ECF-type sigma factor	UNRESOLVED
Cluster 9		
Bd2413c	putative dehydrogenase	NO
Bd2414c	putative glycosylhydrolase (putative secreted protein)	UNRESOLVED
Bd2415c	putative outer membrane protein, probably involved in nutrient binding	NO
Bd2416c	putative outer membrane protein, probably involved in nutrient binding	NO
Bd2417c	putative anti-sigma factor	NO
Bd2418	RNA polymerase ECF-type sigma factor	NO
Cluster 10		
Bd3036	RNA polymerase ECF-type sigma factor	UNRESOLVED
Bd3037	putative anti-sigma factor	UNRESOLVED
Bd3038	putative outer membrane protein probably involved in nutrient binding	NO
Bd3039	putative outer membrane protein, probably involved in nutrient binding	UNRESOLVED
Bd3040	conserved hypothetical protein with endonuclease/exonuclease/phosphatase family domain	UNRESOLVED
Bd3041	conserved hypothetical protein with endonuclease/exonuclease/phosphatase family domain	NO
Cluster 11		
Bd3042	RNA polymerase ECF-type sigma factor	UNRESOLVED
Bd3043	putative anti-sigma factor	NO
Bd3044	putative outer membrane protein probably involved in nutrient binding	NO
Bd3045	putative outer membrane protein probably involved in nutrient binding	NO
Bd3046	conserved hypothetical protein	LGT-in
Bd3047	hypothetical protein	NOVEL
Bd3048	glycoside hydrolase family 2, candidate beta-glycosidase	UNRESOLVED
Bd3049c	glycoside hydrolase family 2, candidate beta-glycosidase	NO
Bd3050	conserved hypothetical protein	NO
Bd3051	putative transmembrane protein	UNRESOLVED

Cluster 12		
Bd3052	RNA polymerase ECF-type sigma factor	NO
Bd3053	putative anti-sigma factor	NO
Bd3054	putative outer membrane protein, probably involved in nutrient binding	NO
Bd3055	putative outer membrane protein, probably involved in nutrient binding	NO
Bd3056	conserved hypothetical protein	LGT-unresolved
Bd3057	glycoside hydrolase family 97, related to alpha-glucosidases	UNRESOLVED
Bd3058	putative lysophospholipase L1 and related esterase	NO
Cluster 13		
Bd3059	RNA polymerase ECF-type sigma factor	NO
Bd3060	putative anti-sigma factor	UNRESOLVED
Bd3061	putative outer membrane protein, probably involved in nutrient binding	UNRESOLVED
Bd3062	putative outer membrane protein, probably involved in nutrient binding	UNRESOLVED
Bd3063	conserved hypothetical protein	UNRESOLVED
Bd3064	putative integrase/transposase	UNRESOLVED
Bd3065	conserved hypothetical protein	UNRESOLVED
Bd3066	hypothetical protein	UNRESOLVED
Bd3067	glycoside hydrolase family 78, related to alpha-L-rhamnosidases	NO
Bd3068	glycoside hydrolase family 92, related to an ill-defined alpha-1,2-mannosidase	NO
Cluster 14		
Bd3260c	putative exported protein	NO
Bd3261c	conserved hypothetical protein	UNRESOLVED
Bd3262c	conserved hypothetical protein	NO
Bd3263c	putative outer membrane protein, probably involved in nutrient binding	NO
Bd3264c	putative outer membrane protein, probably involved in nutrient binding	NO
Bd3265c	putative anti-sigma factor	NO
Bd3266c	putative ECF-type RNA polymerase sigma factor	NO
Cluster 15		
Bd3386	putative RNA polymerase ECF-type sigma factor	NO
Bd3387	conserved hypothetical protein	NO
Bd3388	hypothetical protein	LGT-unresolved
Bd3389	putative outer membrane protein probably involved in nutrient binding	NO
Bd3390	putative outer membrane protein probably involved in nutrient binding	UNRESOLVED
Bd3391	conserved hypothetical protein	LGT-in
Bd3392	hypothetical protein	NOVEL
Bd3393c	putative permease	NO
Cluster 16		
Bd3859	RNA polymerase ECF-type sigma factor	NO
Bd3860	putative anti-sigma factor	NO
Bd3861	putative outer membrane protein, probably involved in nutrient binding	NO
Bd3862	putative outer membrane protein, probably involved in nutrient binding	UNRESOLVED
Bd3863	arylsulfatase precursor	UNRESOLVED
Bd3864	N-acetylgalactosamine 6-sulfatase (GALNS)	UNRESOLVED

(B). ECF-σ factor-containing polysaccharide utilization gene clusters in *B. vulgatus* ATCC 8482

Cluster 1		
Bv0103c	hypothetical protein	NOVEL
Bv0104c	conserved hypothetical protein, possible ATP/GTP-binding site	UNRESOLVED
Bv0105c	putative oxidoreductase	NO
Bv0106c	putative outer membrane protein, probably involved in nutrient binding	NO
Bv0107c	putative outer membrane protein, probably involved in nutrient binding	NO
Bv0108c	putative anti-sigma factor	NO
Bv0109c	RNA polymerase ECF-type sigma factor	NO
Cluster 2		
Bv0110c	putative thiol:disulfide interchange protein DsbE	NO
Bv0111c	putative thiol:disulfide interchange protein	NO
Bv0112c	conserved hypothetical protein	NO
Bv0113c	conserved hypothetical protein	NO
Bv0114c	putative regulatory protein	NO
Bv0115c	glycoside hydrolase family 88, candidate delta-4,5 unsaturated glucuronyl hydrolase	NO
Bv0116c	glycoside hydrolase family 43, candidate beta-xylosidase/alpha-L-arabinofuranosidase	NO
Bv0117c	glycoside hydrolase family 97, related to alpha-glucosidases	NO
Bv0118c	conserved hypothetical protein	NO
Bv0119c	putative beta-lactamase class C and other penicillin binding proteins	LGT-in
Bv0120c	conserved hypothetical protein	NO
Bv0121c	glycoside hydrolase family 28, distantly related to polygalacturonases	LGT-out
Bv0122c	conserved hypothetical protein	NO
Bv0123c	conserved hypothetical protein	NO
Bv0124c	glycoside hydrolase family 28, distantly related to polygalacturonases	NO
Bv0125c	putative outer membrane protein, probably involved in nutrient binding	NO
Bv0126c	putative outer membrane protein, probably involved in nutrient binding	NO
Bv0127c	RNA polymerase ECF-type sigma factor	NO
Cluster 3		
Bv0132c	glycoside hydrolase family 92, related to an ill-defined alpha-1,2-mannosidase	UNRESOLVED
Bv0133c	glycoside hydrolase family 97, related to alpha-glucosidases	NO
Bv0134c	putative outer membrane protein, probably involved in nutrient binding	UNRESOLVED
Bv0135c	putative outer membrane protein, probably involved in nutrient binding	NO
Bv0136c	putative RNA polymerase ECF-type sigma factor	UNRESOLVED
Cluster 3		
Bv0293c	glycoside hydrolase family 2, related to beta-galactosidases	UNRESOLVED
Bv0294c	glycoside hydrolase family 63, distantly related to alpha-glycosidases	UNRESOLVED
Bv0295c	putative outer membrane protein, probably involved in nutrient binding	UNRESOLVED
Bv0296c	putative outer membrane protein, probably involved in nutrient binding	NO
Bv0297c	putative anti-sigma factor	NO
Bv0298c	putative RNA polymerase ECF-type sigma factor	NO
Cluster 4		
Bv0342c	histidyl-tRNA synthetase	NO
Bv0343c	putative ABC transporter, periplasmic sugar-binding protein	LGT-in
Bv0344c	transposase	UNRESOLVED
Bv0345c	ABC-type sugar transport system, periplasmic component	LGT-in
Bv0346c	putative integral membrane protein	NO
Bv0347c	conserved hypothetical protein	LGT-unresolved
Bv0348c	glycerol kinase 2 (ATP:glycerol 3-phosphotransferase 2)	LGT-unresolved
Bv0349c	transketolase, C-terminal subunit	LGT-unresolved
Bv0350c	transketolase, N-terminal subunit	LGT-unresolved
Bv0351c	transcriptional regulator of sugar metabolism	LGT-in

Bv0352c	3,4-dihydroxy-2-butanone 4-phosphate synthase (cyclohydrolase II)	LGT-unresolved
Bv0353c	conserved hypothetical protein	LGT-unresolved
Bv0354c	two-component system sensor histidine kinase/response regulator, hybrid ('one-component system')	NO
Bv0355c	putative outer membrane protein, probably involved in nutrient binding	UNRESOLVED
Bv0356c	putative outer membrane protein, probably involved in nutrient binding	NO
Bv0357c	conserved hypothetical protein, putative anti-sigma factor	NO
Bv0358c	RNA polymerase ECF-type sigma factor	NO
Cluster 5		
Bv0377	putative RNA polymerase ECF-type sigma factor	NO
Bv0378	putative anti-sigma factor	NO
Bv0379	putative outer membrane protein, probably involved in nutrient binding	NO
Bv0380	putative outer membrane protein, probably involved in nutrient binding	NO
Bv0381	glycoside hydrolase family 2, candidate beta-glycosidase	UNRESOLVED
Bv0382	glycoside hydrolase family 20, distantly related to beta-N-acetylhexosaminidases	LGT-unresolved
Bv0383	glycoside hydrolase family 2, candidate beta-glycosidase	NO
Bv0384	arylsulfatase	NO
Bv0385	hypothetical protein	LGT-in
Bv0386	NADH-ubiquinone oxidoreductase subunit	NOVEL
Bv0387	hypothetical protein	NOVEL
Cluster 6		
Bv0472c	conserved hypothetical protein	UNRESOLVED
Bv0473c	glycoside hydrolase family 31, candidate alpha-glycosidase; related to beta-	NO
Bv0474c	putative outer membrane protein, probably involved in nutrient binding	NO
Bv0475c	putative outer membrane protein, probably involved in nutrient binding	NO
Bv0476c	two-component system response regulator	NO
Bv0477c	glycoside hydrolase family 35, candidate beta-glycosidase; related to beta-galactosidases	NO
Bv0478c	glycoside hydrolase family 51, related to alpha-L-arabinofuranosidases	NO
Bv0479c	glycoside hydrolase family 43, modular protein with N-terminal domain distantly related to beta-glycosidases and C-terminal related to beta-xylosidases/alpha-L-arabinofuranosidases	UNRESOLVED
Bv0480c	glycoside hydrolase family 30, candidate beta-glycosidase	NO
Bv0481c	putative outer membrane protein, probably involved in nutrient binding	NO
Bv0482c	putative outer membrane protein, probably involved in nutrient binding	NO
Bv0483c	putative anti-sigma factor	NO
Bv0484c	putative RNA polymerase ECF-type sigma factor	NO
Cluster 7		
Bv0593c	putative oxidoreductase	NO
Bv0594c	conserved hypothetical protein	NO
Bv0595c	putative signal transducer	NO
Bv0596c	conserved hypothetical protein	NO
Bv0597c	exo-alpha sialidase	NO
Bv0598c	conserved hypothetical protein	NO
Bv0599c	glycoside hydrolase family 18, related to chitinases	NO
Bv0600c	conserved hypothetical protein	NO
Bv0601c	putative outer membrane protein, probably involved in nutrient binding	NO
Bv0602c	glycoside hydrolase family 97, related to alpha-glucosidases	NO
Bv0603c	putative endonuclease/exonuclease/phosphatase family protein	NO
Bv0604c	conserved hypothetical protein	NO
Bv0605c	putative outer membrane protein, probably involved in nutrient binding	NO
Bv0606c	glycoside hydrolase family 92, related to an ill-defined alpha-1,2-mannosidase	NO
Bv0607c	glycoside hydrolase family 92, related to an ill-defined alpha-1,2-mannosidase	NO

Bv0608c	putative anti-sigma factor	NO
Bv0609c	RNA polymerase ECF-type sigma factor	NO
Cluster 8		
Bv0709c	hypothetical protein	NOVEL
Bv0710c	conserved hypothetical protein	NO
Bv0711c	conserved hypothetical protein	LGT-in
Bv0712c	putative outer membrane protein, probably involved in nutrient binding	NO
Bv0713c	putative outer membrane protein, probably involved in nutrient binding	NO
Bv0714c	putative anti-sigma factor	NO
Bv0715c	RNA polymerase ECF-type sigma factor	NO
Bv0716c	glycoside hydrolase family 36, candidate alpha-glycosidase; related to alpha-galactosidases	NO
Cluster 9		
Bv0915c	RNA polymerase ECF-type sigma factor	NO
Bv0916	putative anti-sigma factor	NO
Bv0917	putative outer membrane protein, probably involved in nutrient binding	NO
Bv0918	putative outer membrane protein, probably involved in nutrient binding	UNRESOLVED
Bv0919	conserved hypothetical protein	NO
Bv0920	conserved hypothetical protein	NO
Bv0921	putative oxidoreductase (putative secreted protein)	LGT-unresolved
Cluster 10		
Bv1025	RNA polymerase ECF-type sigma factor	NO
Bv1026	putative anti-sigma factor	NOVEL
Bv1027	putative outer membrane protein, probably involved in nutrient binding	NO
Bv1028	hypothetical protein	NO
Bv1029c	erythronate-4-phosphate dehydrogenase	NO
Bv1030	glycosyltransferase family 9, related to glycosyltransferases	NO
Bv1031	putative acetyltransferase	NO
Bv1032	putative LPS biosynthesis related UDP-galactopyranose mutase	NO
Bv1033	conserved hypothetical protein	NO
Bv1034	conserved hypothetical protein	UNRESOLVED
Bv1035	glycosyltransferase family 2, related to beta-glycosyltransferases	NO
Bv1036	glycosyltransferase family 2, distantly related to beta-glycosyltransferases	UNRESOLVED
Bv1037	glycosyltransferase family 14, related to beta-glycosyltransferases	NO
Bv1038	glycosyltransferase family 4, related to alpha-glycosyltransferases	NO
Cluster 11		
Bv1124	putative ECF sigma factor	NO
Bv1125	putative membrane protein	NO
Bv1126	putative outer membrane protein, probably involved in nutrient binding	NO
Bv1127	putative outer membrane protein, probably involved in nutrient binding	NO
Bv1128	sulfatase	LGT-unresolved
Bv1129	arylsulfatase precursor	NO
Bv1130	putative ATP-binding ABC transporter protein	NO
Cluster 12		
Bv1663c	RNA polymerase ECF-type sigma factor	NO
Bv1664	putative anti-sigma factor	NO
Bv1665	putative outer membrane protein, probably involved in nutrient binding	NO
Bv1666	putative outer membrane protein, probably involved in nutrient binding	UNRESOLVED
Bv1667	glycerophosphoryl diester phosphodiesterase	NO
Cluster 13		
Bv1721c	glycoside hydrolase family 28, related to polygalacturonases	UNRESOLVED
Bv1722c	glycoside hydrolase family 2, candidate beta-glycosidase	NO
Bv1723c	glycoside hydrolase family 28, related to polygalacturonases	UNRESOLVED

Bv1724	hypothetical protein	NOVEL
Bv1725c	iduronate 2-sulfatase precursor	NO
Bv1726c	putative outer membrane protein, probably involved in nutrient binding	NO
Bv1727c	putative outer membrane protein, probably involved in nutrient binding	NO
Bv1728c	putative anti-sigma factor	NO
Bv1729	RNA polymerase ECF-type sigma factor	NO
Cluster 14		
Bv1733	putative ECF-type RNA polymerase sigma factor	NO
Bv1734	putative anti-sigma factor	NO
Bv1735	putative outer membrane protein, probably involved in nutrient binding	NO
Bv1736	putative outer membrane protein, probably involved in nutrient binding	NO
Bv1737	conserved hypothetical protein	NO
Bv1738	conserved hypothetical protein	NO
Bv1739	glycoside hydrolase family 2, candidate beta-glycosidase	UNRESOLVED
Bv1740	hypothetical protein	NOVEL
Bv1741	glycoside hydrolase family 78, distantly related to alpha-L-rhamnosidases	UNRESOLVED
Bv1742	two-component system response regulator	NO
Bv1743	aldehyde dehydrogenase A	LGT-unresolved
Bv1744	glycoside hydrolase family 43, related to beta-xylosidases/alpha-L-	NO
Bv1745	conserved hypothetical protein	NO
Bv1746	conserved hypothetical protein	NO
Bv1747	conserved hypothetical protein	NO
Cluster 15		
Bv1758	putative RNA polymerase ECF-type sigma factor	NO
Bv1759	putative anti-sigma factor	NO
Bv1760	putative outer membrane protein, probably involved in nutrient binding	NO
Bv1761	putative outer membrane protein, probably involved in nutrient binding	NO
Bv1762	glycoside hydrolase family 2, candidate beta-glycosidase	LGT-out
Bv1763	glycoside hydrolase family 2, candidate beta-glycosidase	NO
Bv1764	glycoside hydrolase family 31, candidate alpha-glycosidase	UNRESOLVED
Bv1765	conserved hypothetical protein	UNRESOLVED
Bv1766c	putative pectin degradation protein	LGT-in
Bv1767	polysaccharide lyase family 10, related to pectate lyases	LGT-in
Bv1768	conserved hypothetical protein	NO
Bv1769	carbohydrate esterase family 8, modular protein with N-terminal domain distantly related to pectin acetylesterases and C-terminal domain related to pectin methylesterases	NO
Bv1770	two-component system sensor histidine kinase/response regulator, hybrid ('one-component system')	NO
Bv1771	hypothetical protein	NO
Bv1772	dipeptidyl peptidase IV	NO
Cluster 16		
Bv1927c	putative thiol-disulfide oxidoreductase	UNRESOLVED
Bv1928c	putative disulphide-isomerase	NO
Bv1929c	putative outer membrane protein, probably involved in nutrient binding	UNRESOLVED
Bv1930c	putative outer membrane protein, probably involved in nutrient binding	UNRESOLVED
Bv1931c	putative anti-sigma factor	NO
Bv1932c	RNA polymerase ECF-type sigma factor	UNRESOLVED
Bv1933c	glycoside hydrolase family 43, candidate beta-xylosidase/alpha-L-arabinofuranosidase	NO
Bv1934c	conserved hypothetical protein	NO
Bv1935c	glycoside hydrolase family 28, related to polygalacturonases	NO
Cluster 17		
Bv1972	RNA polymerase ECF-type sigma factor	NO

Bv1973	putative anti-sigma factor	NO
Bv1974	putative outer membrane protein, probably involved in nutrient binding	UNRESOLVED
Bv1975	putative outer membrane protein, probably involved in nutrient binding	UNRESOLVED
Bv1976	hypothetical protein	NOVEL
Bv1977	ABC transporter ATP-binding protein	NO
Bv1978	putative endothelin-converting enzyme	NO
Bv1979	conserved hypothetical protein	NO
Bv1980	putative metal resistance related exported protein	NO
Bv1981	AcrB/AcrD/AcrF family cation efflux system protein	NO
Bv1982	conserved hypothetical protein	NO
Bv1983	ThiJ/PfpI family protein	NO
Bv1984	putative nitroreductase	NO
Cluster 18		
Bv2160	RNA polymerase ECF-type sigma factor	UNRESOLVED
Bv2161	putative anti-sigma factor	NO
Bv2162	putative outer membrane protein, probably involved in nutrient binding	NO
Bv2163	putative outer membrane protein, probably involved in nutrient binding	UNRESOLVED
Bv2164	putative thiol-disulfide oxidoreductase	UNRESOLVED
Bv2165	putative thiol-disulfide oxidoreductase	UNRESOLVED
Bv2166	glycoside hydrolase family 2, candidate beta-glycosidase	NO
Bv2167	aldose 1-epimerase precursor	NO
Cluster 19		
Bv2384c	L-serine dehydratase	NO
Bv2385c	conserved hypothetical protein	NO
Bv2386c	putative outer membrane protein, probably involved in nutrient binding	NO
Bv2387c	putative outer membrane protein, probably involved in nutrient binding	NO
Bv2388c	putative anti-sigma factor	NO
Bv2389c	RNA polymerase ECF-type sigma factor	UNRESOLVED
Cluster 20		
Bv4006c	conserved hypothetical protein	NO
Bv4007c	putative outer membrane protein, probably involved in nutrient binding	NO
Bv4008c	putative outer membrane protein, probably involved in nutrient binding	NO
Bv4009c	putative anti-sigma factor	NO
Bv4010c	RNA polymerase ECF-type sigma factor	NO

Legend: The three columns represent Gene ID, functional annotation and predicted evolutionary history of the gene (labeled as in **Table S5**).

Chapter 3

Characterizing a model human gut microbiota composed of members of its two dominant phyla

Chapter 3

Michael A. Mahowald[1], Federico E. Rey[1], Henning Seedorf[1], Robert S. Fulton[2], Aye Wollam[2], Neha Shah[2], Chunyan Wang[2], Vincent Magrini[2], Richard K. Wilson[2], Brandi L. Cantarel[3,4], Pedro M. Coutinho[3], Bernard Henrissat[3,4], Lara W. Crock[1], Alison Russell[5], Nathan C. Verberkmoes[5], Robert L. Hettich[5], and Jeffrey I. Gordon[1]

[1]Center for Genome Sciences, [2]Genome Sequencing Center, Washington University School of Medicine, St. Louis, MO 63108

[3]Universités Aix-Marseille I and II, Marseille, France and [4]CNRS, UMR6098, Marseille, France, [5]Organic and Biological Mass Spectrometry Group, Oak Ridge National Laboratory, Oak Ridge, TN 37830

Correspondence to: jgordon@wustl.edu

Key words: human gut Firmicutes and Bacteroidetes; gut microbiome; gnotobiotic mice; functional genomics and proteomics; carbohydrate metabolism; nutrient sharing

Eubacterium rectale ATCC 33656 and *Eubacterium eligens* ATCC 27750 genome sequences have been deposited in GenBank under accession numbers CP001107 and CP001104-CP001106, respectively.

Abstract

The adult human gut microbial community is dominated by two bacterial phyla, the Firmicutes and the Bacteroidetes. Little is known about the factors that govern the interactions between their members. We have examined the niches (professions) of representatives of both phyla *in vivo*. Finished genome sequences were generated from *E. rectale* and *E. eligens,* which belong to Clostridium Cluster XIVa, one of the most common gut Firmicute clades. Comparison of these and 16 other gut Firmicutes to gut Bacteroidetes indicated that the former possess smaller genomes and a disproportionately smaller number of glycan-degrading enzymes. Germ-free mice were then colonized with *E. rectale* and/or a prominent human gut Bacteroidetes, *Bacteroides thetaiotaomicron*, followed by whole genome transcriptional profiling of both organisms in their distal gut (cecal) habitat, high resolution proteomic analyses of their cecal contents, and biochemical assays of their metabolism. *B. thetaiotaomicron* adapts to *E. rectale* by upregulating expression of a variety of polysaccharide utilization loci (PULs), encoding numerous glycoside hydrolase gene families, so that it can degrade an increased variety of glycans that *E. rectale* cannot access, including those derived from the host. *E. rectale* responds to *B. thetaiotaomicron* by decreasing production of its glycan-degrading enzymes, altering its expression of sugar and amino acid transporters, and facilitating glycolysis by increasing its ratio of NAD^+ to NADH in part via generation of butyrate from acetate, which in turn is utilized by the gut epithelium. In contrast, co-colonization of germ-free mice with *B. thetaiotaomicron* and another human gut Bacteroidetes, *B. vulgatus*, produces minimal changes in the former's glycobiome, while *B. vulgatus* upregulates genes uniquely represented in its genome that are involved in the metabolism of pectin and xylans. These models of the human gut microbiota illustrate niche specialization and functional redundancy within the Bacteroidetes, the adaptable niche specialization that likely underlies the success of Firmicutes in this habitat, and the importance of host glycans as a nutrient foundation that ensures ecosystem stability.

Introduction

The adult human gut houses a bacterial community containing trillions of members comprising hundreds to thousands of species-level phylogenetic types (phylotypes). Culture-independent surveys of this community have revealed remarkable interpersonal variations in strain- and species-level phylotypes, but a consistent pattern of domination of this ecosystem, at the phylum level, by the Firmicutes and the Bacteroidetes [1, 2]. This domination is not a unique feature of humans: a global survey of the guts of 59 other mammalian species showed a similar phylum level pattern [3].

Finished genomes are available for several members of the human gut Bacteroidetes. Each contains a large repertoire of genes involved in the acquisition and metabolism of polysaccharides: this includes: (i) up to hundreds of glycoside hydrolases (GHs) and polysaccharide lyases (PLs); (ii) myriad paralogs of SusC and SusD, outer membrane targeted proteins involved in recognition and import of specific carbohydrate structures [4]; and (iii) a large array of environmental sensors and regulators [5]. Each of these human gut Bacteroidetes assembles these genes into multiple, similarly organized, selectively regulated polysaccharide utilization loci (PULs) that encode functions necessary to detect, bind, degrade and import carbohydrates encountered in the gut habitat – either from the diet or from host glycans associated with mucus and the surfaces of epithelial cells [6, 7]. Studies of germ-free mice colonized with *Bacteroides thetaiotaomicron* alone have demonstrated that this organism can vary its pattern of PUL expression of as a function of diet: e.g., during the transition from mother's milk to a polysaccharide-rich chow encountered when mice are weaned [6], or when adult mice are switched from a diet rich in plant polysaccharides to a diet devoid of these glycans and replete with simple sugars (under the latter conditions, the organism forages host glycans, a strategy that likely contributes to ecosystem stability [7, 8].

Our previous functional genomic studies of the responses of *B. thetaiotaomicron* to colonization of the guts of gnotobiotic mice with *Bifidobacterium longum,* a member of the Actinobacteria that is prominently represented in the gut microbiota of infants, or with *Lactobacillus casei*, a probiotic present in a number of fermented diary products, have shown that *B. thetaiotaomicron* responds to the presence of these other microbes by modifying expression of its PULs in ways that expand the breadth of its carbohydrate foraging activities [9].

These observations underscore the notion that gut microbes live at the intersection of two forms of selective pressure: bottom-up selection, where fierce competition between members of a community that approaches a population density of 10^{11} organisms/ml of colonic contents drives phylotypes to assume distinct functional roles; and top-down selection, where the host selects for functional redundancy to insure against the failure of bioreactor functions that could prove highly deleterious [10, 11].

The content, genomic arrangement and functional properties of PULs in sequenced gut Bacteroidetes illustrate the specialization and functional redundancy within members of this phylum. They also emphasize how the combined metabolic activities of members of the microbiota undoubtedly result in interactions that are both very dynamic and overwhelmingly complex (at least to the human observer), involving multiple potential pathways for the processing of substrates (including the order of substrate processing), varying patterns of physical partitioning of microbes relative to substrates within the ecosystem, and various schemes for utilization of products of bacterial metabolism. Such a system likely provides multiple options for processing of a given metabolite, and for the types of bacteria that can be involved in these activities.

All of this means that the task of defining the interactions of members of the human gut microbiota is daunting, as is the task of identifying general principles that govern the operation of this system. In the present study, we have taken a reductionist approach

to begin to define interactions between members of the Firmicutes and the Bacteroidetes that are commonly represented in the human gut microbiota. In the human colon, members of Clostridium cluster XIVa are one of two abundantly represented clusters of Firmicutes. Therefore, we have generated the initial two complete genome sequences for members of the genus *Eubacterium* in Clostridium cluster XIVa, (the human gut-derived *E. rectale* strain ATCC 33656 and *E. eligens* strain ATCC 27750) and compared them with the draft sequences of 25 other sequenced human gut bacteria belonging to the Firmicutes and the Bacteroidetes. The interactions between *E. rectale* and *B. thetaiotaomicron* were then characterized by performing whole genome transcriptional profiling of each species after colonization of the distal guts of gnotobiotic mice with each organism alone or in combination. The gene expression data were verified by mass spectrometry of cecal proteins, plus biochemical assays of carbohydrate metabolism. The responses of each organism were compared to the niche adaptations of *B. thetaiotaomicron* to another sequenced human gut *Bacteroides, B. vulgatus*. These defined model human gut microbiotas ('synthetic microbiomes') likely illustrate general themes about how members of the dominant gut bacterial phyla are able to co-exist.

Results and Discussion

Comparative genomic studies of human gut-associated Firmicutes and Bacteroidetes

We produced finished genome sequences for *Eubacterium rectale,* which contains a single 3,449,685 bp chromosome encoding 3,627 predicted proteins, and *Eubacterium eligens* which contains a 2,144,190 bp chromosome specifying 2,071 predicted proteins, plus two plasmids (**Tables S1-S3**).

We classified the predicted proteins in these two genomes using Gene Ontology (GO) terms generated via Interproscan, and then applied a binomial test to identify functional categories of genes that are either over- or under-represented within (i) 9 sequenced

human gut-derived Bacteroidetes [includes the finished genomes of *B. thetaiotaomicron*, *B. fragilis, B. vulgatus, and Parabacteroides distasonis,* plus deep draft assemblies of the *B. caccae, B. ovatus*, *B. uniformis B. stercoris* and *P. merdae* genomes generated as part of the human gut microbiome initiative (HGMI; http://genome.wustl.edu/hgm/HGM_front-page.cgi], and (ii) 16 other human gut Firmicutes where deep draft assemblies were available through the HGMI (see **Figure S1** for a phylogenetic tree).

While the sequenced gut Bacteroidetes all harbor large sets of polysaccharide sensing, acquisition and degradation genes, the gut Firmicutes, including *E. rectale* and *E. eligens,* have smaller genomes and a significantly smaller proportion of genes involved in glycan degradation (**Figure S2**). As noted above, the gut-associated Bacteroidetes possess large families of SusC and SusD paralogs involved in binding and import of glycans, while the genomes of *E. rectale* and other gut Firmicutes are enriched for phosphotransferase systems and ABC transporters (**Figure S2**). Lacking adhesive organelles, the ability of gut Bacteroidetes to attach to nutrient platforms consisting of small food particles and host mucus via glycan-specific SusC/SusD outer membrane binding proteins likely increases the efficiency of oligo- and monosaccharide harvest by adaptively expressed bacterial GHs, as well as preventing washout from the gut bioreactor [12]. Unlike the surveyed Bacteroidetes, several Firmicutes, notably *E. rectale, E. eligens*, *E. siraeum,* and *Anaerotruncus colihominis* (the later belongs to the *Clostridium leptum* cluster) possess genes specifying components of flagellae (**Figure S2**): these organelles may contribute to persistence within the gut ecosystem and/or enable these species to move to different microhabitats to access their preferred nutrient substrates.

Table S4 lists predicted GHs and PLs present in the Firmicutes and Bacteroidetes surveyed, sorted into families according to the scheme incorporated into the Carbohydrate Enzymes (CAZy) database (www.cazy.org). The Firmicutes have significantly fewer total polysaccharide-degrading enzymes than the Bacteroidetes. Nonetheless, most of the sampled Firmicutes have sets of carbohydrate active enzyme families that are more abundant

in their genomes than in any known gut Bacteroidetes (highlighted lines of **Table S4**). For example, while *E. rectale* and *E. eligens* lack a variety of enzymes to degrade host-derived glycans present in mucus and/or the apical surfaces of gut epithelial cells (e.g., fucosidases and hexosaminidases), *E. rectale* has a disproportionately large number of predicted α–amylases (GH family 13; **Table S4** and **Figure S3**). *E. eligens* has fewer of the latter, but possesses many enzymes for degrading pectins (e.g. GH family 28, PL families 1 and 9) (**Table S4**). Among the Bacteroidetes 'glycobiomes', there is also evidence of niche specialization: while *B. vulgatus* has fewer GHs and PLs overall than *B. thetaiotaomicron*, it has a larger assortment of enzymes for degrading pectins (GH family 28 and PL families 1, 10 and 11) and possesses enzymes, which *B. thetaiotaomicron* lacks, that should enable it to degrade certain xylans [GH family 10 and Carbohydrate esterase (CE) family 15] (**Figure S3** and **Table S4**). *In vitro* assays of the growth of *B. thetaiotaomicron, B. vulgatus* and *E. rectale* in defined medium containing mono- di- and polysaccharides produced results broadly consistent with these predictions (**Table S5**).

We chose *E. rectale* and *B. thetaiotaomicron* as representatives of these two phyla for further characterization of their niches *in vivo*, because of their prominence in culture-independent surveys of the distal human gut microbiota [1, 10] and because of the pattern of representation of carbohydrate active enzymes in their glycobiomes. We chose *B. vulgatus* as a second representative of the Bacteroidetes because of its distinct repertoire of GHs compared to *B. thetaiotaomicron*. These choices set the stage for 'arranged marriages' between a Firmicute and a Bacteroidetes, and between two Bacteroidetes, hosted by formerly germ-free mice.

Creating a minimal human gut microbiota in gnotobiotic mice

Young adult male germ-free mice belonging to the NMRI inbred strain were colonized with *B. thetaiotaomicron* or *E. rectale,* or both species together. 10-14 d after inoculation by gavage, both species colonized the ceca of recipient germ-free mice fed a standard

chow diet rich in plant polysaccharides at levels that were not significantly different (n=4-5 mice/treatment group in each of 3 independent experiments; **Figure S4A**).

Functional genomic analyses of the minimal human gut microbiome

B. thetaiotaomicron's response to E. rectale - A custom, multispecies, human gut microbiome Affymetrix GeneChip was designed (**Tables S6, S7** plus *Supplemental Methods*), and used to compare the transcriptional profile of each bacterial species when it was the sole inhabitant of the cecum (mono-asociated), and when it co-existed together with the other species (co-colonization). 55 of the 106 *B. thetaiotaomicron* genes that satisfied our criteria for being differentially expressed with *E. rectale* colonization in a statistically significant manner (*Methods*) were located in PULs: of these, 51 (93%) were upregulated (**Figure S4B;** see **Table S8** for a complete list of differentially regulated *B. thetaiotaomicron* genes).

As noted in the *Introduction,* two previous studies from our lab examined changes in *B. thetaiotaomicron's* transcriptome in the ceca of mono-associated gnotobiotic mice when they were switched from a diet rich in plant polysaccharides to a glucose-sucrose chow [7], or in suckling mice consuming mother's milk as they transitioned to a standard chow diet [6]. In both situations, in the absence of dietary plant polysaccharides, *B. thetaiotaomicron* adaptively forages on host glycans.

The transcriptional changes induced in *B. thetaiotaomicron* by co-colonization with *E. rectale* overlap with those noted in these two previous datasets (**Figure S4C**). In addition, they involve several of the genes upregulated during growth on minimal medium containing porcine gastric mucin (PGM) as the sole carbon source [8]. For example, in co-colonized mice and *in vitro*, *B. thetaiotaomicron* upregulates two operons (BT3787-BT3792; BT3774-BT3777; **Figure S4D)** used in degrading α–mannans, a component of host O-glycans. (Note that *E. rectale* is unable to grow in defined medium containing α-mannan or mannose as the sole carbon sources; **Table S5**). *B. thetaiotaomicron* also up-

regulates expression of its starch utilization system (Sus) PUL in the presence of *E. rectale* (BT 3698-3704; **Figure S4D).** This well-characterized PUL is essential for degradation of starch molecules containing ≥6 glucose units [4].

Thus, it appears that *B. thetaiotaomicron* adapts to the presence of *E. rectale* by upregulating expression of a variety of PULs, so that it can broaden its niche and degrade an increased variety of glycan substrates, including those derived from the host that *E. rectale* is unable to access. The capacity to access host glycans likely represents an important trait underpinning microbiota function and stability: glycans in the mucus gel are not only abundant but consistently represented; mucus could serve as a microhabitat for Bacteroidetes spp. to embed in (and adhere to via SusD paralogs) thereby avoiding washout; the products of polysaccharide digestion/fermentation generated by Bacteroidetes spp. can be shared with other members of the microbiota that are located in close proximity, including the Firmicutes.

E. rectale's response to B. thetaiotaomicron - *E. rectale's* response to *B. thetaiotaomicron* in the mouse cecum is in marked contrast to *B. thetaiotaomicron*'s response to *E. rectale*. Carbohydrate metabolism genes, and particularly GHs, are significantly overrepresented among *E. rectale* genes that are downregulated in the presence of *B. thetaiotaomicron* compared to monoassociation**;** i.e. 12 of *E. rectale's* predicted 51 GHs are downregulated while only two are upregulated **(Figure 1A,B**; see **Table S9** for a complete list of *E. rectale* genes regulated by the presence of *B. thetaiotaomicron***)**. The two upregulated GH genes [EUBREC_1072, a 6-P-β-glucosidase (GH family 1) and EUBREC_3687, a cellobiose phosphorylase (GH family 94)], lack export signals and are predicted to break down cellobiose. Three simple sugar transport systems with predicted specificity for celluobiose, galactoside, and arabinose/lactose (EUBREC_3689, EUBREC_0479, and EUBREC_1075-6, respectively) are among the most strongly upregulated genes (highlighted with arrowheads in **Figure 1C**).

Evidence for nutrient sharing

The concurrent upregulation of sugar transporters and downregulation of GHs not only suggest that *E. rectale* is more selective in its sugar degradation in the presence of *B. thetaiotaomicron*, but that it may benefit by harvesting sugars released by *B. thetaiotaomicron* glycosidases. *In vitro* studies support the latter notion. Approximately 10^7 colony-forming units (CFU) of *B. thetaiotaomicron* were plated onto the center of agar plates containing defined medium with various carbon sources plus 10^2 to 10^4 CFU of *E. rectale*. *E. rectale* colonies grew to a larger size the closer they were to *B. thetaiotaomicron*. This effect was most pronounced on plates with dextran as the carbon source, a glucan that can be utilized by *B. thetaiotaomicron* but not by *E. rectale* **(Figure S5, Table S5).** In the presence of a simple sugar that both organisms can utilize (glucose), a simple sugar only utilized by *B. thetaiotaomicron* (D-arabinose; **Table S5**), or plating on tryptone alone without a carbohydrate, the growth effect was considerably reduced (**Figure S5**).

Transcriptional and biochemical data obtained from gnotobiotic mice further support the idea that *E. rectale* is better able to access nutrients in the presence of *B. thetaiotaomicron*. In the presence of *B. thetaiotaomicron, E. rectale* upregulates a significant proportion of genes involved in biosynthetic and amino acid metabolic functions (listed in **Figure 1A**). Phosphoenolpyruvate carboxykinase (EUBREC_2002) is also upregulated with co-colonization. This enzyme catalyzes an energy conserving reaction that produces oxaloacetate from phosphoenolpyruvate. In a subsequent transanimase reaction oxaloacetate can be converted to aspartate, linking this branching of the glycolytic pathway with amino acid biosynthesis. In addition, a number of peptide and amino acid transporters in *E. rectale* are upregulated when it encounters *B. thetaiotaomicron*, as are the central carbon and nitrogen regulatory genes CodY (EUBREC_1812), glutamate synthase (EUBREC_1829) and glutamine synthetase (EUBREC_2543) (**Figure 1B**). Moreover, the expression profile of *E. rectale* in the ceca of co-colonized mice is intermediate between that observed when it alone colonizes the cecum, and during its exponential phase growth in tryptone-glucose

(T-G) medium: i.e., 80% of the genes that are differentially regulated between monoassociation and co-colonization are regulated in the same direction between growth on T-G, and monoassociation **(Table S10**). Among these are genes involved in translation, cell envelope biogenesis and amino acid biosynthesis. All of these data suggest that the presence of *B. theta* increases nutrient availability for *E. rectale*.

Changes in* E. rectale's *fermentative pathways - *E. rectale* harbors genes (EUBREC_733-737 and EUBREC_1017) for the production of butyrate that show high similarity to genes from other Clostridia. This pathway involves the condensation of two molecules of acetylCoA to form butyrate. Transcriptional and high resolution proteomic analyses (see below) indicate that enzymes involved in the production of butyrate are among the most highly expressed in cecal extracts prepared from *E. rectale* colonized mice (**Table S2 and S11**).

In vitro studies have shown that *E. rectale* consumes large amounts of acetate for butyrate production in the presence of carbohydrates [13]. Several observations suggest that *E. rectale* utilizes acetate produced by *B. thetaiotaomicron* to generate increased amounts of butyrate *in vivo*: *First, E. rectale* upregulates a phosphate acetyltransferase (EUBREC_1443; EC 2.3.1.8), one of two enzymes involved in the interconversion of acetylCoA and acetate (**Table S9**; GeneChip data verified by qRT-PCR assays in 2 independent experiments involving 3-4 mice/treatment group). *Second*, cecal acetate levels are significantly lower in co-colonized mice compared to *B. thetaiotaomicron* monoassociated mice (**Figure 2B**). *Third*, although cecal butyrate levels are similar in *E. rectale* monoassociated and co-colonized animals (**Figure 2C**), expression of mouse *Mct-1*, encoding a monocarboxylate transporter whose inducer and preferred substrate is butyrate [14, 15], is significantly higher in the distal gut of co-colonized versus *E. rectale* monoassociated mice ($p<0.05$; **Figure 2D).** The cecal concentrations of butyrate observed are similar to levels known to upregulate Mct-1 in colonic epithelial cell lines [14]. *Fourth*, higher levels of acetate (i.e. those encountered in *B. thetaiotaomicron* monoassociated mice) are insufficient

to induce any change in Mct-1 expression compared to germ-free controls **(Figure 2B** and **2D**). *Fifth*, levels of other monocarboxylates transported by Mct-1 are unchanged (lactate, succinate) or significantly decreased (proprionate) in the ceca of co-colonized compared to *E. rectale* monoassociated mice (**Figure 2E,** and data not shown).

Conversion of acetate to butyrate is accompanied by the oxidation of two molecules of NADH to NAD^+, which is required for glycolysis. The butyrylCoA dehydrogenase/ electron transfer flavoprotein (Bcd/Etf) complex (EC 1.3.99.2) in the butyrate production pathway also offers a recently discovered additional pathway for energy conservation, via a bifurcation of electrons from NADH to crotonylCoA and ferredoxin [16]. The reduced ferredoxin in turn may be reoxidized via hydrogenases, or via the membrane-bound oxidoreductase, Rnf, which generates sodium-motive force. While our GeneChip data indicated no significant difference in expression of the operon encoding the Bcd/Etf complex (EUBREC_0735-0737) in *E. rectale* monoassociated versus co-colonized mice, we observed downregulation of genes that catalyze both of these reduced ferredoxin-dependent reactions (hydrogenases [EUBREC_1227 and EUBREC_2390, EC:1.12.7.2] and Rnf [EUBREC_1641–1646]). This indicates that more of the NADH generated through glycolysis might be reoxidized in the reduction of crotonylCoA rather than by reduction of ferredoxin.

Consistent with these observations, we found that the NAD^+/NADH ratio in cecal contents was significant increased with co-colonization (**Figure 2A**). A high NAD^+/NADH ratio promotes high rates of glycolysis, since NAD^+ is a required cofactor. This shift, therefore, may represent an adaptation by *E. rectale* to the increased nutrient uptake discussed above. **Figure 3** summarizes the metabolic responses of *E. rectale* to *B. thetaiotaomicron***.**

The pathway for acetate metabolism observed in the model human gut community composed of *B. thetaiotaomicron* and *E. rectale* differs markedly from what is seen in mice that harbor *B. thetaiotaomicron* and the principal human gut methanogenic archaeon,

Methanobrevibacter smithii. When *B. thetaiotaomicron* encounters *M. smithii* in the ceca of gnotobiotic mice, there is increased production of acetate by *B. thetaiotaomicron*, no diversion to butyrate (and no induction of Mct-1; [17] and B. Samuel and J. Gordon, unpublished observations), increased serum acetate levels, and increased adiposity compared to *B. thetaiotaomicron* monoassociated controls. In contrast, serum acetate levels and host adiposity (as measured by fat pad to body weight ratios) are not significantly different between *B. thetaiotaomicron* monoassociated and *B. thetaiotaomicron-E. rectale* co-colonized animals (n=4-5 animals/group; n=3 independent experiments; data not shown).

Proteomic studies of this simplified two-component model of the human gut microbiome

Model communities, such as the one described above, constructed in gnotobiotic mice, where microbiome gene content is precisely known and transcriptional data are obtained under controlled conditions, provide a way to test the efficacy of mass spectrometric methods for characterizing gut microbial community proteomes. Therefore, we assayed luminal contents, collected from the ceca of 8 gnotobiotic mice: (germ-free, monoassociated, and co-colonized; n=2 mice/treatment group representing two independent biological experiments). Samples were processed by a small sample method, in which cells were lysed with 6M Guanidine/10mM DTT and heat, proteins were denatured, reduced, and digested with trypsin, and samples analyzed (in triplicate) using tandem mass spectrometry with a linear ion trap. All MS/MS spectra were searched with SEQUEST [18] against a combined database containing predicted proteins from *E. rectale*, *B. thetaiotaomicron*, mouse, plant components of the diet (e.g., rice), and common contaminants (e.g. trypsin). All 8 samples were coded, and MS measurements conducted in a blinded fashion.

The measured proteomes had high reproducibility in terms of total number of proteins observed and spectra matching to each species. Differentiating unique peptides and thus unique proteins between *E. rectale* and *B. thetaiotaomicron* was straightforward since

there are no shared predicted peptides between the two. The resultant microbial species distributions were exactly as expected from the coded samples. **Table 1** summarizes our results, including the percentage of mRNAs called present in the GeneChip datasets for which there was an identified protein product. The most abundant identified proteins from both microbes included ribosomal proteins, elongation factors, chaperones, and proteins involved in energy metabolism (for a full list of identified proteins, see **Table S11** and http://compbio.ornl.gov/mouse_cecal_microbial_metaproteome/; note that **Tables S8** and **S9,** which list differentially expressed genes in co-colonization experiments, indicate whether protein products from the transcripts were identified in these mass spectrometry datasets; in addition, **Table S2,** which lists the genome annotation for *E. rectale,* describes the number of times each protein was identified in our replicate MS/MS analyses). Many conserved hypothetical and pure hypothetical proteins were identified, as well as 10 genes in *B. thetaiotaomicron* whose presence had not been predicted in our initial annotation of the finished genome **(Table S12**). Together, these results provide validation of experimental and computational procedures for proteomic assays of a model gut microbiota, and also illustrate some of the benefits in obtaining this type of information.

Putting the niche adaptations of *B. thetaiotaomicron* and *E. rectale* in perspective: a model gut community containing *B. thetaiotaomicron* and *B. vulgatus*

In a final set of experiments, we colonized adult male NMRI mice consuming a standard polysaccharide-rich chow diet with *B. thetaiotaomicron* alone, *B. vulgatus* alone, or with both organisms together. Animals were sacrificed 14d after gavage. As with *E. rectale* and *B. thetataiomicron*, co-colonization produced similar cecal population densities of both organisms. Moreover, these levels did not differ significantly from what was observed with monoassociation (**Figure S6A**).

The number of genes whose expression was significantly different in co-colonization compared to monoassociation was very modest: only 7 in the case of *B. thetaiotaomicron*

(6 upregulated; see **Table S13** for complete list) and 52 in *B. vulgatus* (60% upregulated) (see **Table S14** for a complete list). This is consistent with the fact that these two human gut Bacteroidetes have largely similar capacities to utilize different polysaccharides. Remarkably, all of the differentially expressed genes in *B. vulgatus* that had functional annotations were located in predicted operons involved in carbohydrate utilization. The upregulated genes included several involved in degradation/metabolism of pectin and xylans **(Figure S6B,C)**: i.e., the same genes identified as distinctively represented in the glycobiome of *B. vulgatus* compared to *B. thetaiotaomicron*.

Prospectus

These studies of model human gut microbiotas created in gnotobiotic mice support a view of the Bacteroidetes, whose genomes contain a disproportionately large number of glycan-degrading enzymes compared to sequenced Firmicutes, as responding to increasing diversity by modulating expression of their vast array of PULs. *B. vulgatus* adapts to the presence of *B. thetaiotaomicron* by increasing expression of its unique and enriched classes of GHs. *B. thetaiotaomicron* responds to *E. rectale* by upregulating a variety of loci specific for host-derived mucin glycans that *E. rectale* is unable to utilize (e.g. α–mannans). *E. rectale,* which like other Firmicutes has a more specialized capacity for glycan degradation, broadly downregulates its available GHs in the presence of *B. thetaiotaomicron*, even though it does not grow efficiently in the absence of carbohydrates. It becomes more selective in its harvest of sugars, while its transcriptional profile suggests improved access to nutrients, with a generalized upregulation of biosynthetic genes, including those involved translation, as well as a set of nutrient transporters that can harvest peptides as well as carbohydrate products liberated by gut Bacteroidetes-derived GHs and PLs: i.e., it becomes, in part, a 'secondary consumer' of the buffet of glycans available in the cecum.

We have previously used gnotobiotic mice to show that the efficiency of fermentation of dietary polysaccharides to short chain fatty acids by *B. thetaiotaomicron* increases

in the presence of *M. smithii* [17]. Co-colonization increases the density of colonization of the distal gut by both organisms, increases production of formate and acetate by *B. thetaiotaomicron* and allows *M. smithii* to use H_2 and formate produce methane, thereby preventing the build-up of these fermentation end-products (including NADH) in the gut bioreactor, and improving the efficiency of carbohydrate metabolism [17]. Removal of H_2 by methanogenic Archaea, by phylogenetically diverse acetogens that use the Wood-Ljungdhal pathway for synthesis of acetyl CoA from CO_2, and/or by Proteobacteria that reduce sulfate to sulfide, allows *B. thetaiotaomicron*'s hydrogenase to oxidize NADH to NAD^+, which can then be used for glycolysis. This situation constitutes a mutualism, in which both members show a clear benefit. The present study, characterizing the interaction between *B. thetaiotaomicron* and *E. rectale,* describes a more nuanced interaction where there are not significant changes in the level of colonization of either species. It is currently difficult to determine the benefit versus cost of these interactions. The cost to *B. thetaiotaomicron* of liberating simple sugars in excess of what it can absorb may not be large enough to allow selection against it. Alternatively, *B. thetaiotaomicron* may benefit from its interaction with *E. rectale* in ways as yet uncharacterized.

It seems likely that as the complexity of the gut community increases, interactions between *B. thetaiotaomicron* and *E. rectale* will either by subsumed or magnified by other 'similar' phylogenetic types (as defined by their 16S rRNA sequence and/or by their glycobiomes). Constructing model human gut microbiotas of increasing the complexity in gnotobiotic mice using sequenced members of our intestinal communities should be very useful for exploring two ecologic concepts: (i) the neutral theory of community assembly which posits that most species will share the same general niche (profession), and thus are likely to be functionally redundant [19], and (ii) the idea that *both* bottom-up selection, where fierce competition between members of the microbiota drives phylotypes to assume distinct functional roles, and top-down selection, where the host selects for functional redundancy to insure against failure of bioreactor functions, operate in our guts [2].

Materials and Methods

Genome comparisons

All nucleotide sequences from all contigs of completed assemblies containing both capillary sequencing and pyrosequencer data, produced as part of the HGMI were downloaded from the Washington University Genome Sequencing Center's website (http://genome.wustl.edu/pub/organism/Microbes/Human_Gut_Microbiome/) on September 27, 2007. The finished genome sequences of *B. thetaiotaomicron* VPI-5482, *Bacteroides vulgatus* ATCC 8482, and *B. fragilis* NCTC9343 were obtained from GenBank.

For comparison purposes, protein-coding genes were identified in all genomes using YACOP [20]; nonredundant NCBI nucleotide (NT) database dated 9/27/2007). Each proteome was assigned InterPro numbers and GO terms using InterProScan release 16.1 [21]. Statistical comparisons between genomes were then carried out, as described previously [5] using perl scripts that are available upon request from the authors.

GeneChip Analysis

RNA was isolated from a 100-300 mg aliquot of frozen cecal contents, and cDNA synthesized, biotinylated and hybridized to GeneChips, as described previously [17], except that 0.1mm zirconia/silica beads (Biospec Products, Bartlesville, OK) were used for lysis in a bead beater (Biospec) for 4 min at high speed. Genes in a given bacterial species that were differentially expressed in mono- versus co-colonization were identified using CyberT (default parameters) following probe masking and scaling with the MAS5 algorithm (Affymetrix; for details of the methods used to create the mask, see the *Methods* section of Supplementary Information)**.**

Other methods

Details about bacterial culture, genome sequencing and finishing, animal husbandry, quantitative PCR assays of the level of colonization of the ceca of gnotobiotic mice, GeneChip design and masking, plus proteomic and metabolite assays of cecal contents are described in the *Methods* section of Supplementary Information.

Acknowledgements

We are indebted to Maria Karlsson, David O'Donnell for help with gnotobiotic husbandry, Jan Crowley, Janaki Guruge, Jill Manchester, and Sabrina Wagoner for outstanding technical assistance, Peter Turnbaugh, Janaki Guruge, and Eric Martens for invaluable suggestions, Jian Xu, Sandra Clifton, and our other colleagues at the Washington University Genome Sequencing Center for assistance with genome sequencing, plus Laura Kyro for help with graphics. This work was supported by grants from the NSF (0333284) and NIH (DK30292, DK70977, and DK52574). M.A.M is a member of the Washington University Medical Scientist Training Program (GM07200) and was also supported by NIH training grant T32-AI07172.

References

1. Eckburg, P.B., E.M. Bik, C.N. Bernstein, E. Purdom, L. Dethlefsen, M. Sargent, S.R. Gill, K.E. Nelson, and D.A. Relman, 2005. Diversity of the human intestinal microbial flora. *Science*, **308** (5728), p. 1635-8.

2. Ley, R.E., D.A. Peterson, and J.I. Gordon, 2006. Ecological and evolutionary forces shaping microbial diversity in the human intestine. *Cell*, **124** (4), p. 837-48.

3. Ley, R.E., M. Hamady, C. Lozupone, P.J. Turnbaugh, R.R. Ramey, J.S. Bircher, M.L. Schlegel, T.A. Tucker, M.D. Schrenzel, R. Knight, and J.I. Gordon, 2008. Evolution of mammals and their gut microbes. *Science*, **320** (5883), p. 1647-51.

4. Koropatkin, N.M., E.C. Martens, J.I. Gordon, and T.J. Smith, 2008. Starch catabolism by a prominent human gut symbiont is directed by the recognition of amylose helices. *Structure*, **16** (7), p. 1105-15.

5. Xu, J., M.A. Mahowald, R.E. Ley, C.A. Lozupone, M. Hamady, E.C. Martens, B. Henrissat, P.M. Coutinho, P. Minx, P. Latreille, H. Cordum, A. Van Brunt, K. Kim, R.S. Fulton, L.A. Fulton, S.W. Clifton, R.K. Wilson, R.D. Knight, and J.I. Gordon, 2007. Evolution of Symbiotic Bacteria in the Distal Human Intestine. *PLoS Biol*, **5** (7), p. e156.

6. Bjursell, M.K., E.C. Martens, and J.I. Gordon, 2006. Functional genomic and metabolic studies of the adaptations of a prominent adult human gut symbiont, Bacteroides thetaiotaomicron, to the suckling period. *J Biol Chem*, **281** (47), p. 36269-79.

7. Sonnenburg, J.L., J. Xu, D.D. Leip, C.H. Chen, B.P. Westover, J. Weatherford, J.D. Buhler, and J.I. Gordon, 2005. Glycan foraging in vivo by an intestine-adapted bacterial symbiont. *Science*, **307** (5717), p. 1955-9.

8. Martens, E.C., H.C. Chiang, and J.I. Gordon, 2008. Mucosal Glycan Foraging Enhances the Fitness and Transmission of a Saccharolytic Human Gut Symbiont. *submitted*.

9. Sonnenburg, J.L., C.T. Chen, and J.I. Gordon, 2006. Genomic and metabolic studies of the impact of probiotics on a model gut symbiont and host. *PLoS Biol*, **4** (12), p. e413.

10. Ley, R.E., P.J. Turnbaugh, S. Klein, and J.I. Gordon, 2006. Microbial ecology: human gut microbes associated with obesity. *Nature*, **444** (7122), p. 1022-3.

11. Lozupone, C.A., M. Hamady, B.L. Cantarel, P.M. Coutinho, B. Henrissat, J.I. Gordon, and R. Knight, 2008. The Convergence of Carbohydrate Active Gene Repertoires in Human Gut Microbes. *submitted*.

12. Sonnenburg, J.L., L.T. Angenent, and J.I. Gordon, 2004. Getting a grip on things: how do communities of bacterial symbionts become established in our intestine? *Nat Immunol*, **5** (6), p. 569-73.

13. Duncan, S.H. and H.J. Flint, 2008. Proposal of a neotype strain (A1-86) for Eubacterium rectale. Request for an Opinion. *Int J Syst Evol Microbiol*, **58** (Pt 7), p. 1735-6.

14. Cuff, M.A., D.W. Lambert, and S.P. Shirazi-Beechey, 2002. Substrate-induced regulation of the human colonic monocarboxylate transporter, MCT1. *J Physiol*, **539** (Pt 2), p. 361-71.

15. Ritzhaupt, A., I.S. Wood, A. Ellis, K.B. Hosie, and S.P. Shirazi-Beechey, 1998. Identification and characterization of a monocarboxylate transporter (MCT1) in pig and human colon: its potential to transport L-lactate as well as butyrate. *J Physiol*, **513 (Pt 3)** p. 719-32.

16. Li, F., J. Hinderberger, H. Seedorf, J. Zhang, W. Buckel, and R.K. Thauer, 2008. Coupled ferredoxin and crotonyl coenzyme A (CoA) reduction with NADH catalyzed by the butyryl-CoA dehydrogenase/Etf complex from Clostridium kluyveri. *J Bacteriol*, **190** (3), p. 843-50.

17. Samuel, B.S. and J.I. Gordon, 2006. A humanized gnotobiotic mouse model of host-archaeal-bacterial mutualism. *Proc Natl Acad Sci U S A*, **103** (26), p. 10011-6.

18. Eng, J.K., A.L. McCormack, and J.R. Yates III, 1994. An approach to correlate tandem mass spectral data of peptides with amino acid sequences in a protein database. *J. Am. Mass Spectrom.*, **5** p. 976-989.

19. Hubbell, S.P., 2006. Neutral theory and the evolution of ecological equivalence. *Ecology*, **87** (6), p. 1387-98.

20. McHardy, A.C., A. Goesmann, A. Puhler, and F. Meyer, 2004. Development of joint application strategies for two microbial gene finders. *Bioinformatics*, **20** (10), p. 1622-31.

21. Quevillon, E., V. Silventoinen, S. Pillai, N. Harte, N. Mulder, R. Apweiler, and R. Lopez, 2005. InterProScan: protein domains identifier. *Nucleic Acids Res*, **33** (Web Server issue), p. W116-20.

22. Sonenshein, A.L., 2007. Control of key metabolic intersections in Bacillus subtilis. *Nat Rev Microbiol*, **5** (12), p. 917-27.

23. Commichau, F.M., K. Forchhammer, and J. Stulke, 2006. Regulatory links between carbon and nitrogen metabolism. *Curr Opin Microbiol*, **9** (2), p. 167-72.

Figure Legends

Figure 1. **Response of *E. rectale* to co-colonization with *B. thetaiotaomicron***. **(A)** Genes assigned to GO terms for carbohydrate metabolism (GO:0005975), transporters (GO: GO:0006810) and predicted GHs are all significantly overrepresented among down-regulated genes while genes with GO terms for biosynthesis (GO:0044249), in particular amino acid metabolism (GO:0006520), are significantly overrepresented among upregulated genes. All categories shown are significantly different from the genome as a whole. *P<0.05; **P<0.01; ***P<0.001 (binomial test). **(B)** Heat map from GeneChip data showing: (i) all significantly regulated GH genes (top), with all but two are downregulated (both cytoplasmic cellobiose processing enzymes); (ii) upregulation of global regulator genes (i) CodY, a repressor of starvation-response genes, and (ii) glutamate synthase, and (iii) glutamine synthetase, which require adequate carbon and nitrogen supplies for activation [22, 23]. (**C**) Heat map of all significantly regulated genes assigned to the GO term for transporters (GO:0006810) illustrates that a number of simple sugar transporters are downregulated upon co-colonization, while peptide and amino acid transporters as well as three predicted simple sugar transporters (arrows; EUBREC_0479, a galactoside ABC transporter; EUBREC_1075-6, a lactose/arabinose transport system, and EUBREC_3689, a predicted cellobiose transporter) are upregulated. Differentially regulated genes were identified using the MAS5 algorithm and Cyber-T (see **Table S9** and *Materials and Methods*). Genes whose differential expression with co-colonization was further validated by qRT-PCR are highlighted with red lettering (2 independent experiments, n=4-5 mice per group, 2-3 measurements per gene).

Figure 2. Co-colonization affects the efficiency of fermentation with an increased NAD^+:NADH ratio and increased acetate production. (**A**) NAD^+:NADH ratios are increased in co-colonization relative to either monoassociation or germ-free mice (n=7-9 per group). (**B,C**) GC-MS assays of cecal acetate and butyrate levels (n=6-8 per group). (**D**) Expression of Mct-1, a monocarboxylate transporter whose preferred substrate and inducer is butyrate, in the proximal colon (n=3-5 per group). (**E**) Cecal propionate concentrations (n=7-9 per group). Mean values ± s.e.m. are plotted; *, p<0.05, **, p<0.01, *** p<0.001 compared with co-colonization (1-way analysis of variance with

Bonferroni correction)**.**

Figure 3. Proposed model of the metabolic responses of *E. rectale* to *B. thetaiotaomicron*. *B. thetaiotaomicron* increases its break down of complex host glycans (HG) and dietary polysaccharides (DP) into monosaccharides (MS) that *E. rectale* efficiently takes up using phosphotransferase systems (Pts) and ABC transporters. Fermentative pathways in *B. thetaiotaomicron* generate acetate that *E. rectale* consumes. *E. rectale* increases its production of butyrate, which is formed from acetyl-CoA in several reductive steps. This regenerates NAD^+ that is reduced during glycolysis, leading to an increase in the NAD^+/NADH ratio. The downregulation of hydrogenase and Rnf may indicate that *E. rectale* uses NADH to produce butyrate rather than to generate reduced ferredoxin or subsequently H_2 (via hydrogenase) or sodium motive force (via Rnf). The butyrate in turn induces the monocarboxylate transporter Mct-1 in the host epithelium, causing an increased uptake of this short chain fatty acid. The constant removal of butyrate from the colon keeps its concentration low, thus favoring *E. rectale's* production of butyrate.

Figures

Figure 1.

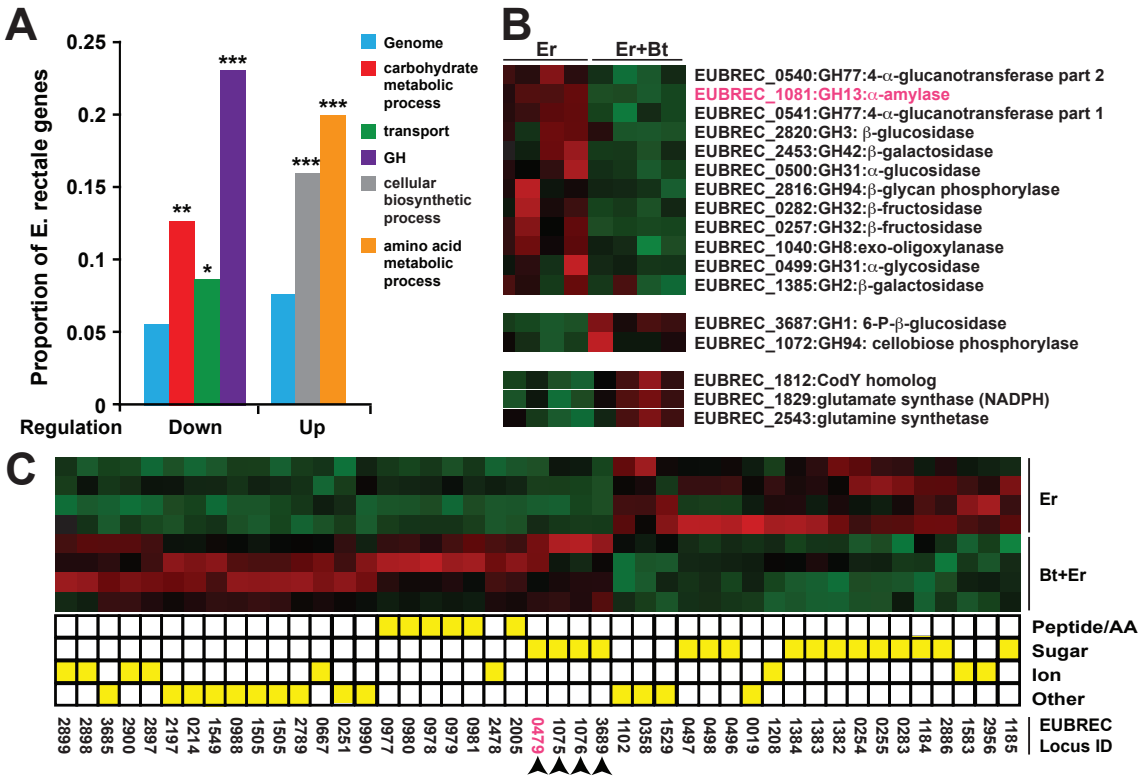

Figure 2.

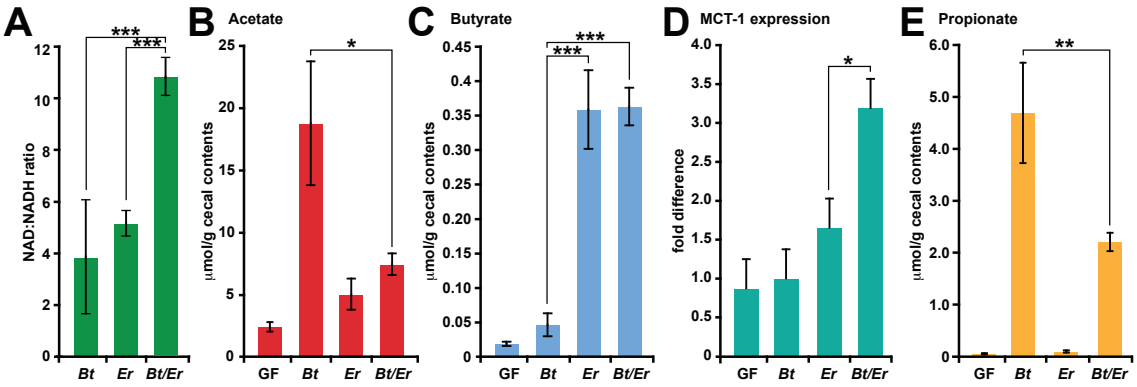
A
NAD:NADH ratio
***
***
Bt
Er
Bt/Er
B
Acetate
µmol/g cecal contents
*
GF
Bt
Er
Bt/Er
C
Butyrate
µmol/g cecal contents
***
***
GF
Bt
Er
Bt/Er
D
MCT-1 expression
fold difference
*
GF
Bt
Er
Bt/Er
E
Propionate
µmol/g cecal contents
**
GF
Bt
Er
Bt/Er

Figure 3.

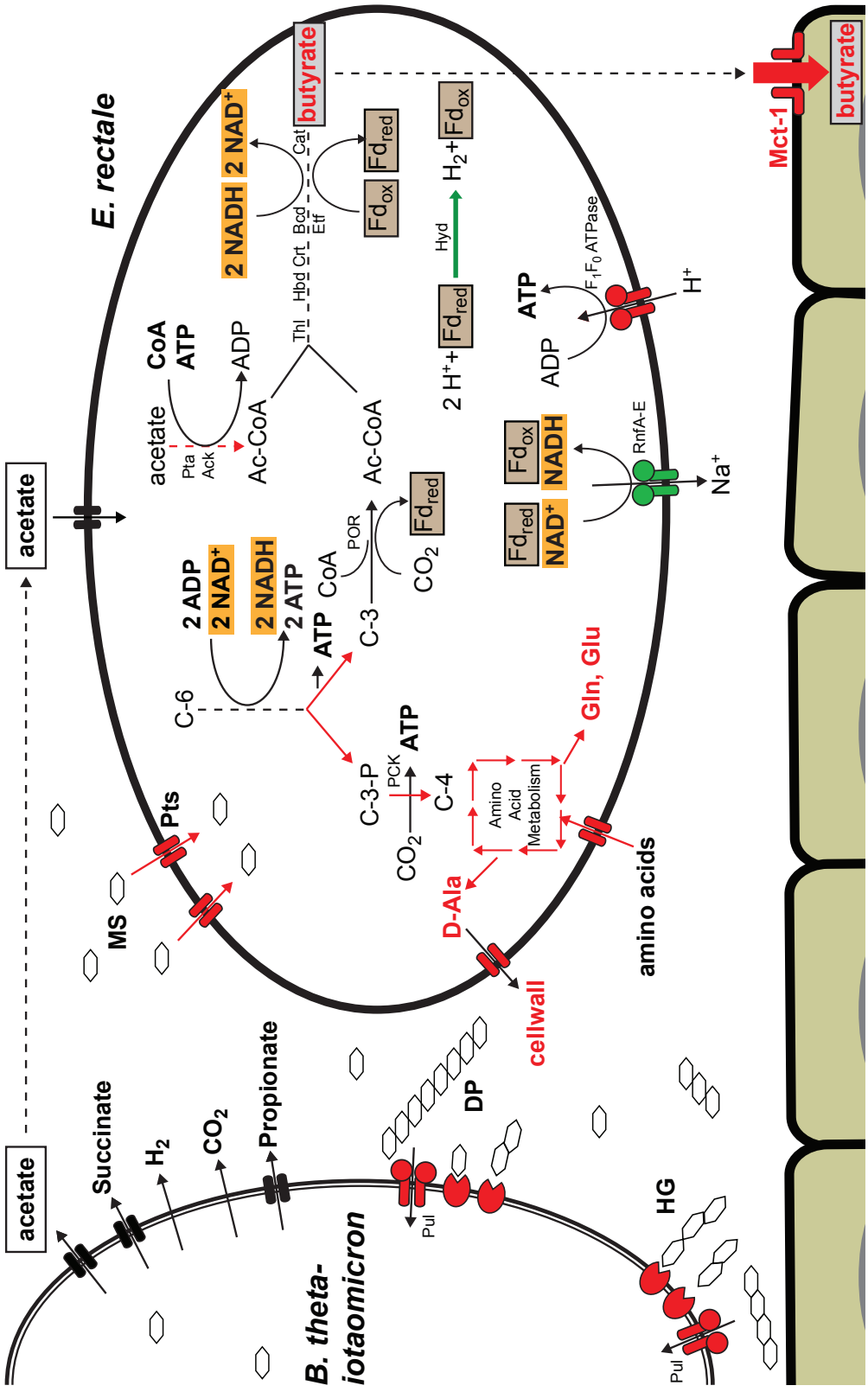
E. rectale
B. theta-iotaomicron
acetate
Succinate
H2
CO2
Propionate
MS
Pts
DP
Pul
HG
cellwall
D-Ala
amino acids
Gln, Glu
Amino Acid Metabolism
C-3-P
PCK
ATP
C-4
CO2
C-6
2 ADP
2 NAD+
2 NADH
2 ATP
ATP
C-3
CoA
POR
Fdred
CO2
Ac-CoA
acetate
Pta
Ack
CoA
ATP
ADP
Ac-CoA
Thl
Hbd
Crt
Bcd
Etf
2 NADH
2 NAD+
butyrate
Cat
Fdox
Fdred
Hyd
H2+Fdox
2 H++Fdred
Fdox
NADH
Fdred
NAD+
RnfA-E
Na+
ATP
ADP
F1F0 ATPase
H+
Mct-1
butyrate

Table Legends

Table 1. Detection of proteins and protein expression by tandem mass spectrometry and gene chip compared. Mono=Monoassociated mouse cecal contents; Biassoc=Biassociated cecal contents. Chip -: less than 75% of gene chips with "Present" call for a gene; for E. rectale this number includes genes not covered by gene chip; in parentheses is the number of chip-negative genes excluding those not on the chip.

Table 1

	E. rectale			***B. thetaiotaomicron***		
	Mono	Biassoc	Total	Mono	Biassoc	Total
Detected by MSMS	661	453	680	1608	1367	1687
75% present by gene chip	2139 91%	2010 85%	2150 91%	3798 78%	3865 79%	3995 82%
Chip - / MS/MS +[a]	132 (7)	83 (7)	135 (8)	40	21	23
MS/MS- / Chip +	1608	1638	1603	2280	2569	2357

Supplemental Information

Methods

Bacterial culture

Bacterial strains were stored frozen at -80°C in a pre-reduced mixture of two parts TYG medium [1] to one part glycerol. Bacteria were routinely cultured in TYG medium in an anaerobic chamber (Coy Lab Products, Grass Lake, MI) under an atmosphere of 40% CO_2, 58% nitrogen, and 2% H_2. To assay growth of *E. rectale* on specific carbon sources, the organism was cultured on medium containing 1% tryptone, 100mM potassium phosphate buffer (pH 7.2), 15 mM NaCl, 180μM $CaCl_2$, 100 μM $MgCl_2$, 50 μM $MnCl_2$, 42 μM $CoCl_2$ and 15 μM $FeSO_4$, 1% trace element mix (ATCC), 2μg/ml folinic acid (calcium salt), 1.2 μg/ml hematin, and 1mg/ml menadione. Growth curves for different carbon sources were acquired at 37°C in the Coy anaerobic chamber using a 96-well plate spectrophotometer (Tecan Sunrise, Tecan U.S., Durham, NC). Growths were scored as positive if the OD_{600} measurement rose by ≥0.2 over a 72 h incubation at 37°C.

Genome sequencing

E. rectale and *E. eligens* were grown to late log phase under anaerobic conditions in TYG medium. Cells were pelleted from 50 ml cultures and lysed in 11 ml Buffer B1 (Qiagen Genomic DNA buffer set; Qiagen) with 2.2 mg RNAse A, 50 U lysozyme, 50 U mutanolysin, and 600 U achromopeptidase (all from Sigma) for 30 min at 37°C. Four ml of Buffer B2 (Qiagen) was added with 10 mg (300 U) proteinase K (Sigma) and incubated at 50°C for 2 h. The DNA was precipitated by adding 1.5 ml of 3M sodium acetate and 30 ml isopropanol, removed with a sterile glass hook, and washed several times with ethanol.

Unlike *E. eligens*, genomic DNA from *E. rectale* was very resistant to standard cloning techniques. This cloning bias made efforts to produce fosmids ineffective, and left

vast regions of the genome uncloned in our primary sequencing vector, pOT. Only half (1.7 Mb) of its genome was represented in our initial assembly containing 228 contigs from >9X plasmid shotgun reads with a ABI 3730 capillary instrument. Therefore, we generated >40X coverage of the *E. rectale* genome through pyrosequencing with a 454 GS20 instrument, and used an additional vector (pJAZZ) for capillary sequencing in order to obtain a finished genome sequence. Significant manual closure efforts including PCR and sequencing of products across gaps, manual manipulation of sequence assemblies to resolve misassemblies, and sequence editing to ensure accurate base calling. were employed to produce a final, hand-curated, base-perfect sequence. In our experience, the effort required was far more extensive than for most finished microbial genomes, due to the repetitive, highly clone-biased nature of this assembly.

Protein-coding genes were subsequently identified using Glimmer 2.13 [2] and GeneMarkS [3] using the start site predicted by GeneMarkS where the two overlapped. 'Missed' genes were then added by using a translated BLAST of intergenic regions against the NCBI nonredundant protein database to find conserved ORFs. Additional missed genes were added to the *E. rectale* genome using YACOP (trained by Glimmer 2.13) [4]. tRNA, rRNA and other non-coding RNAs were identified and annotated using tRNAscan-SE [5], RNAMMER [6], and RFAM [7], respectively. Protein-coding genes were annotated with the KEGG Orthology group definition using a NCBI BLASTP search [8] of the KEGG genes database [9] (Mar. 10, 2008), with a minimum bit score of 60.

Animal husbandry

All experiments using mice were performed using protocols approved by the animal studies committee of Washington University. NMRI-KI mice [10] were maintained in flexible plastic film isolators under a strict 12h light cycle, and fed a standard polysaccharide-rich chow (BK, Zeigler, UK). For colonizations involving *B. vulgatus and B. thetaiotaomicron*, mice were maintained on this diet for the duration of the experiment. 6-8

week old males were placed on an irradiated polysaccharide-rich chow diet (Harlan-Teklad #2918, Madison, WI) 10 to 14d prior to colonizations involving *B. thetaiotaomicron and E. rectale*.

Animals were colonized via gavage with 10^8 CFU from an overnight culture of a *B. thetaiotaomicron* or *B. vulgatus*, or a log-phase culture of *E. rectale*. Gavage with *E. rectale* was repeated on three successive days using cells from separate log-phase cultures begun from separate colonies. Cecal contents and colon tissue were flash frozen in liquid nitrogen immediately after animals were killed.

Quantitative PCR measurements of colonization

A total of 100–300 mg of frozen cecal contents from each gnotobiotic mouse was added to 2 ml tubes containing 250 μl 0.1mm-diameter zirconia/silica beads (Biospec Products), 0.5 ml of Buffer A (200 mM NaCl 20 mM EDTA), 210 μl of 20% SDS, and 0.5 ml of a mixture of phenol:chloroform:isoamyl alcohol (25:24:1; pH 7.9; Ambion, Austin, TX). Samples were lysed by using a bead beater (BioSpec; ''high'' setting for 4 min at room temperature). The aqueous phase was extracted following centrifugation (8,000 x *g* at 4°C for 3 min), and the extraction repeated with another 0.5 ml of phenol:chloroform:isoamyl alcohol and 1 min of vortexing. DNA was precipitated with 0.1 volume of 3M sodium acetate (pH 5) and 1 volume of isopropanol (on ice for 20 min), pelleted (14,000 x g, 20 min at 4°C) and washed with ethanol. The resulting pellet was resuspended in water and one half (for *E. rectale* monoassociations) or one tenth of the DNA (for *B. thetaiotaomicron* colonized samples) further cleaned up using a DNAEasy column (Qiagen). qPCR was performed using (i) primers specific to the 16S rRNA gene of *B. thetaiotaomicron* [11] and the *Clostridium coccoides/E. rectale* group (forward: 5'-CGGTACCTGACTAAGAAGC-3'; reverse: 5'-AGTTT(C/T)ATTCTTGCGAACG-3') [12] and (ii) conditions described previously for *B. thetaiotaomicron* [11]. The amount of DNA from each genome in each PCR was computed by comparison to a standard curve of genomic DNA prepared in the same

manner. Data were converted to genome equivalents by calculating the mass of each finished genome (2.8 x 10^5 genome equivalents (GEq) per ng *E. rectale* DNA, and 1.5 x 10^5 GEq per ng *B. thetaiotaomicron* DNA).

GeneChip design, hybridization and data analysis

A custom, six-species human gut microbiome Affymetrix GeneChip was designed using the finished genome sequences of *B. thetaiotaomicron, B. vulgatus, P. distasonis* and *M. smithii* genomes [13-15], plus draft versions of the *E. rectale* and *E. eligens* genomes. Gene predictions for the Firmicute assemblies were made using Glimmer3 [2]. The design included 14 probe pairs (perfect match plus mismatch) per CDS (protein coding sequence) in each draft assembly, and 11 probe pairs for each CDS in a finished genome. The resulting coverage, after soft pruning against all 6 microbial genomes and the mouse genome, is summarized in **Table S6.**

Non-specific cross-hybridization was controlled in three ways. *First*, probe masks for each genome were developed as follows. For analyses involving organisms for which the finished genomes were used for GeneChip design (*B. thetaiotaomicron-B. vulgatus* co-colonizations), a new GeneChip description file (CDF) was created using the Bio::Affymetrix::CDF perl module obtained from www.cpan.org [16], that included all genes from the genome of interest. *Second,* for analyses involving *E. rectale-B. thetaiotaomicron* co-colonizations, additional probes were removed to avoid cross-hybridization resulting from misassembly and missing sequences in the *E. rectale* draft assembly. NCBI BLASTN [8] was used, with parameters adjusted for small query size (word size 7, no filtering or gaps), to identify probesets that either failed to find a perfect match in the finished genomes (once the *E. rectale* genome was completed), or that registered a hit to more than one sequence feature with a bit score ≥ 38 (using the default scoring parameters for BLASTN). This mask reduced the proportion of probesets exhibiting a spurious 'Present' call (by Affymetrix software) by 36%**.** The resulting CDF file was imported into BioCon-

ductor using the altcdfenvs package [17], and all expression analyses were performed using the MAS5 algorithm implemented in BioConductor's 'Affy package' [18], following masking of GeneChip imperfections with Harshlight [19] - in both cases using the default parameters. *Third,* for all analyses we also identified all probesets that registered a 'Present' call when hybridized to targets generated from the cecal contents of mice that had been monoassociated with either *E. rectale*, or *B. thetaiotaomicron*, or *B. vulgatus*. These probesets were also excluded from further analyses and are listed in **Table S7.**

Proteomic analyses of cecal contents

Cecal contents were pelleted by centrifugation, and the cell pellets processed via a single tube cell lysis and protein digestion method as follows. Briefly, the cell pellet was resuspended in 6M Guanidine/10 mM DTT, heated at 60°C for 1 h followed by an overnight incubation at 37°C to lyse cells and denature proteins. The guanidine concentration was diluted to 1 M with 50mM Tris/10mM $CaCl_2$ (pH 7.8) and sequencing grade trypsin (Promega, Madison, WI) was added (1:100; wt/wt). Digestions were run overnight at 37°C. Fresh trypsin was then added followed by an additional 4 h incubation at 37°C. The complex peptide solution was subsequently de-salted (Sep-Pak C_{18} solid phase extraction; Waters, Milford, MA), concentrated, filtered, aliquoted and frozen at -80°C. All eight samples were coded and mass spectrometry measurements conducted in a blinded fashion.

Cecal samples were analyzed in technical triplicates using a two-dimensional (2D) nano-LC MS/MS system with a split-phase column (SCX-RP) [20] on a linear ion trap (Thermo Fisher Scientific) with each sample consuming a 22 h run as detailed elsewhere [21, 22]. The linear ion trap (LTQ) settings were as follows: dynamic exclusion set at one; and five data-dependent MS/MS. Two microscans were averaged for both full and MS/MS scans and centroid data were collected for all scans. All MS/MS spectra were searched with the SEQUEST algorithm [23] against a database containing the entire mouse genome, plus the *B. thetaiotaomicron*, *E. rectale*, rice, and yeast genomes (common contaminants

such as keratin and trypsin were also included). The SEQUEST settings were as follows: enzyme type, trypsin; Parent Mass Tolerance, 3.0; Fragment Ion Tolerance, 0.5; up to 4 missed cleavages allowed (internal lysine and arginine residues), and fully tryptic peptides only (both ends of the peptide must have arisen from a trypsin specific cut, except N and C-termini of proteins). All datasets were filtered at the individual run level with DTASelect [24] [Xcorrs of at least 1.8 (+1 ions), 2.5 (+2 ions) 3.5 (+3 ions)]. Only proteins identified with two fully tryptic peptides were considered. Previous studies with reverse database searching have shown this filter level to generally give a false positive rate less than 1% even with large databases [21, 25, 26].

Biochemical analyses

Measurements of acetate, butyrate, propionate, NAD^+, NADH, lactate, succinate, and formate in cecal contents were performed as described previously [11], with the exception that acetic acid-1-$^{13}C,d_4$ (Sigma) was used as a standard to control for acetate recovery rather than the isomer listed in the reference.

Supplemental References

1. Holdeman, L.V., E.P. Cato, and W.E.C. Moore, *Anerobe Laboratory Manual*. 4th Ed. ed. 1977, Blacksburg, VA: Virginia Polytechnic Institute and State University.

2. Delcher, A.L., D. Harmon, S. Kasif, O. White, and S.L. Salzberg, 1999. Improved microbial gene identification with GLIMMER. *Nucleic Acids Res*, **27** (23), p. 4636-41.

3. Besemer, J., A. Lomsadze, and M. Borodovsky, 2001. GeneMarkS: a self-training method for prediction of gene starts in microbial genomes. Implications for finding sequence motifs in regulatory regions. *Nucleic Acids Res*, **29** (12), p. 2607-18.

4. McHardy, A.C., A. Goesmann, A. Puhler, and F. Meyer, 2004. Development of joint application strategies for two microbial gene finders. *Bioinformatics*, **20** (10), p. 1622-31.

5. Lowe, T.M. and S.R. Eddy, 1997. tRNAscan-SE: a program for improved detection of transfer RNA genes in genomic sequence. *Nucleic Acids Res*, **25** (5), p. 955-64.

6. Lagesen, K., P. Hallin, E.A. Rodland, H.H. Staerfeldt, T. Rognes, and D.W. Ussery, 2007. RNAmmer: consistent and rapid annotation of ribosomal RNA genes. *Nucleic Acids Res*, **35** (9), p. 3100-8.

7. Griffiths-Jones, S., S. Moxon, M. Marshall, A. Khanna, S.R. Eddy, and A. Bateman, 2005. Rfam: annotating non-coding RNAs in complete genomes. *Nucleic Acids Res*, **33** (Database issue), p. D121-4.

8. Altschul, S.F., T.L. Madden, A.A. Schaffer, J. Zhang, Z. Zhang, W. Miller, and D.J. Lipman, 1997. Gapped BLAST and PSI-BLAST: a new generation of protein database search programs. *Nucleic Acids Res*, **25** (17), p. 3389-402.

9. Kanehisa, M., S. Goto, M. Hattori, K.F. Aoki-Kinoshita, M. Itoh, S. Kawashima, T. Katayama, M. Araki, and M. Hirakawa, 2006. From genomics to chemical

genomics: new developments in KEGG. *Nucleic Acids Res*, **34** (Database issue), p. D354-7.

10. Bry, L., P.G. Falk, T. Midtvedt, and J.I. Gordon, 1996. A model of host-microbial interactions in an open mammalian ecosystem. *Science*, **273** (5280), p. 1380-3.

11. Samuel, B.S. and J.I. Gordon, 2006. A humanized gnotobiotic mouse model of host-archaeal-bacterial mutualism. *Proc Natl Acad Sci U S A*, **103** (26), p. 10011-6.

12. Rinttila, T., A. Kassinen, E. Malinen, L. Krogius, and A. Palva, 2004. Development of an extensive set of 16S rDNA-targeted primers for quantification of pathogenic and indigenous bacteria in faecal samples by real-time PCR. *J Appl Microbiol*, **97** (6), p. 1166-77.

13. Samuel, B.S., E.E. Hansen, J.K. Manchester, P.M. Coutinho, B. Henrissat, R. Fulton, P. Latreille, K. Kim, R.K. Wilson, and J.I. Gordon, 2007. Genomic and metabolic adaptations of Methanobrevibacter smithii to the human gut. *Proc Natl Acad Sci U S A*, **104** (25), p. 10643-8.

14. Xu, J., M.A. Mahowald, R.E. Ley, C.A. Lozupone, M. Hamady, E.C. Martens, B. Henrissat, P.M. Coutinho, P. Minx, P. Latreille, H. Cordum, A. Van Brunt, K. Kim, R.S. Fulton, L.A. Fulton, S.W. Clifton, R.K. Wilson, R.D. Knight, and J.I. Gordon, 2007. Evolution of Symbiotic Bacteria in the Distal Human Intestine. *PLoS Biol*, **5** (7), p. e156.

15. Xu, J., M.K. Bjursell, J. Himrod, S. Deng, L.K. Carmichael, H.C. Chiang, L.V. Hooper, and J.I. Gordon, 2003. A genomic view of the human-Bacteroides thetaiotaomicron symbiosis. *Science*, **299** (5615), p. 2074-6.

16. Hammond, J.P., M.R. Broadley, D.J. Craigon, J. Higgins, Z.F. Emmerson, H.J. Townsend, P.J. White, and S.T. May, 2005. Using genomic DNA-based probe-selection to improve the sensitivity of high-density oligonucleotide arrays when

applied to heterologous species. *Plant Methods*, **1** (1), p. 10.

17. Gautier, L., M. Moller, L. Friis-Hansen, and S. Knudsen, 2004. Alternative mapping of probes to genes for Affymetrix chips. *BMC Bioinformatics*, **5** p. 111.

18. Gautier, L., L. Cope, B.M. Bolstad, and R.A. Irizarry, 2004. affy--analysis of Affymetrix GeneChip data at the probe level. *Bioinformatics*, **20** (3), p. 307-15.

19. Suarez-Farinas, M., M. Pellegrino, K.M. Wittkowski, and M.O. Magnasco, 2005. Harshlight: a "corrective make-up" program for microarray chips. *BMC Bioinformatics*, **6** p. 294.

20. McDonald, W.H., R. Ohi, D.T. Miyamoto, T.J. Mitchison, and J.R. Yates III, 2002. Comparison of three directly coupled HPLC MS/MS strategies for identification of proteins from complex mixtures: single-dimension LC-MS/MS, 2-phase MudPIT, and 3-phase MudPIT. *Int. J. Mass Spectrom.*, **219** p. 245-251.

21. Thompson, M.R., N.C. VerBerkmoes, K. Chourey, M. Shah, D.K. Thompson, and R.L. Hettich, 2007. Dosage-dependent proteome response of Shewanella oneidensis MR-1 to acute chromate challenge. *J Proteome Res*, **6** (5), p. 1745-57.

22. VerBerkmoes, N.C., M.B. Shah, P.K. Lankford, D.A. Pelletier, M.B. Strader, D.L. Tabb, W.H. McDonald, J.W. Barton, G.B. Hurst, L. Hauser, B.H. Davison, J.T. Beatty, C.S. Harwood, F.R. Tabita, R.L. Hettich, and F.W. Larimer, 2006. Determination and comparison of the baseline proteomes of the versatile microbe Rhodopseudomonas palustris under its major metabolic states. *J Proteome Res*, **5** (2), p. 287-98.

23. Eng, J.K., A.L. McCormack, and J.R. Yates III, 1994. An approach to correlate tandem mass spectral data of peptides with amino acid sequences in a protein database. *J. Am. Mass Spectrom.*, **5** p. 976-989.

24. Tabb, D.L., W.H. McDonald, and J.R. Yates, 3rd, 2002. DTASelect and Contrast: tools for assembling and comparing protein identifications from shotgun proteomics. *J Proteome Res*, **1** (1), p. 21-6.

25. Lo, I., V.J. Denef, N.C. Verberkmoes, M.B. Shah, D. Goltsman, G. DiBartolo, G.W. Tyson, E.E. Allen, R.J. Ram, J.C. Detter, P. Richardson, M.P. Thelen, R.L. Hettich, and J.F. Banfield, 2007. Strain-resolved community proteomics reveals recombining genomes of acidophilic bacteria. *Nature*, **446** (7135), p. 537-41.

26. Ram, R.J., N.C. Verberkmoes, M.P. Thelen, G.W. Tyson, B.J. Baker, R.C. Blake, 2nd, M. Shah, R.L. Hettich, and J.F. Banfield, 2005. Community proteomics of a natural microbial biofilm. *Science*, **308** (5730), p. 1915-20.

27. DeSantis, T.Z., Jr., P. Hugenholtz, K. Keller, E.L. Brodie, N. Larsen, Y.M. Piceno, R. Phan, and G.L. Andersen, 2006. NAST: a multiple sequence alignment server for comparative analysis of 16S rRNA genes. *Nucleic Acids Res*, **34** (Web Server issue), p. W394-9.

28. Ludwig, W., O. Strunk, R. Westram, L. Richter, H. Meier, Yadhukumar, A. Buchner, T. Lai, S. Steppi, G. Jobb, W. Forster, I. Brettske, S. Gerber, A.W. Ginhart, O. Gross, S. Grumann, S. Hermann, R. Jost, A. Konig, T. Liss, R. Lussmann, M. May, B. Nonhoff, B. Reichel, R. Strehlow, A. Stamatakis, N. Stuckmann, A. Vilbig, M. Lenke, T. Ludwig, A. Bode, and K.H. Schleifer, 2004. ARB: a software environment for sequence data. *Nucleic Acids Res*, **32** (4), p. 1363-71.

29. Ley, R.E., P.J. Turnbaugh, S. Klein, and J.I. Gordon, 2006. Microbial ecology: human gut microbes associated with obesity. *Nature*, **444** (7122), p. 1022-3.

30. Eckburg, P.B., E.M. Bik, C.N. Bernstein, E. Purdom, L. Dethlefsen, M. Sargent, S.R. Gill, K.E. Nelson, and D.A. Relman, 2005. Diversity of the human intestinal microbial flora. *Science*, **308** (5728), p. 1635-8.

31. Benjamini, Y. and Y. Hochberg, 1995. Controlling the False Discovery Rate: A Practical and Powerful Approach to Multiple Testing. *Journal of the Royal Statistical Society. Series B (Methodological)*, **57** (1), p. 289-300.

32. Martens, E.C., H.C. Chiang, and J.I. Gordon, 2008. Mucosal Glycan Foraging Enhances the Fitness and Transmission of a Saccharolytic Human Gut Symbiont. *submitted*.

33. Reeves, A.R., G.R. Wang, and A.A. Salyers, 1997. Characterization of four outer membrane proteins that play a role in utilization of starch by Bacteroides thetaiotaomicron. *J Bacteriol*, **179** (3), p. 643-9.

Supplemental Figure Legends

Figure S1. Phylogenic relationships of human gut-associated Firmicutes and Bacteroidetes surveyed in the present study. A phylogeny, based on 16S rRNA gene sequences, showing the relationships between representatives from two dominant bacterial phyla in the gut microbiota. Green, genomes generated by the Human Gut Microbiome Initiative (www.genome.gov/Pages/Research/Sequencing/SeqProposals/HGMISeq.pdf). Black, other available related genomes. Red, organisms used for co-colonization studies described in the present study. The phylogenetic tree was created by aligning 16S rRNA gene sequences from each genome using the NAST aligner [27], importing the alignment into Arb [28], and then adding them to an existing database of 16S rRNA sequences derived from enumerations of the human gut [29, 30].

Figure S2. Genes involved in carbohydrate metabolism and energy production whose representation is significant enriched or depleted in sequenced human gut-associated Firmicutes and Bacterodetes. The number of genes assigned to each GO term in each genome is shown. Significance is judged by a binomial test, with multiple hypothesis testing correction (see *Methods*) comparing the proportion of genes assigned to a GO term in one genome versus the average number assigned to the same GO term across all the Firmicutes. Protein-coding genes were identified using YACOP. Each proteome was assigned InterPro numbers and GO terms. The Firmicutes also use distinct mechanisms for environmental sensing and membrane transport. The Bacteroidetes employ a large number of paralogs of the SusC/D system to bind and import sugars (classified as receptors, GO:0004872), while the Firmicutes use ABC transporters and phosphotransferase systems (classified as active membrane transporters, GO:0022804). Color code: red: enriched; blue: depleted; dark, $p<0.001$; light, $p<0.05$) relative to the average of all Bacteroidetes genomes (excluding the one tested).

Figure S3. Comparison of glycoside hydrolases and polysaccharide lyases repertoires of *E. rectale, E. eligens*, *B. vulgatus* and *B. thetaiotaomicron.* The number of genes in each genome in each CAZy GH or PL family are shown. Families that are significantly depleted relative to *B. thetaiotaomicron* are colored blue ($p<0.001$), as judged by a binomial test followed by Benjamini-Hochberg correction [31]. Families in which the other genomes have more members are colored yellow. Families that are absent in *B. thetaiotaomicron* are orange. *B. thetaiotaomicron* has a larger genome and a disproportionately larger assortment of GHs. Both Firmicutes have a reduced capacity to utilize host-derived glycans (hexosaminidases, mannosidases, and fucosidases; GH20, GH29, GH78, GH95). *E. rectale* has a large number of starch-degrading enzymes (GH13), while *E. eligens* has a capacity to degrade pectins (PL9, GH28, GH53). See **Table S4** or a complete list of all CAZy enzymes among the sequenced gut Bacteroidetes and Firmicutes examined.

Figure S4. Creation of a minimal synthetic human gut microbiota composed of a sequenced Firmicute (*E. rectale*) and a sequenced Bacteroidetes (*B. thetaiotaomicron*). **(A)** Levels of colonization of the ceca of 11 week-old male gnotobiotic mice colonized for 14d with one or both organisms. Animals were given an irradiated polysaccharide-rich chow diet *ad libitum*. *B. thetaiotaomicron* and *E. rectale* colonize the ceca of mice to similar levels in both monoassociation and bi-association. Error bars denote standard error of the mean of 2-3 measurements per mouse, 4 mice per group. Results are representative of 3 independent experiments. **(B)** Summary of genes showing upregulation in *B. thetaiotaomicron* with co-colonization. 55 of the 106 genes are within PULs, and of these, 51 (93%) were upregulated. **(C)** Summary of *B. thetaiotaomicron* PUL-associated genes upregulated with co-colonization and their representation in datasets of genes upregulated during the suckling-weaning transition, and when adult gnotobiotic mice are switched from a polysaccharide-rich diet to one devoid of complex glycans and containing simple sugars (glucose, sucrose). The latter two datasets are composed of all genes upregulated ≥10-fold relative to log-phase growth in minimal glucose medium [32]. **(D)** Heat map of GeneChip

data from three loci upregulated by *B. thetaiotaomicron* upon colonization with *E. rectale*; two are involved in degradation of α-mannans (left; [32]) which *E. rectale* cannot access; the third is the Starch-utilization system (Sus) locus [33], which targets a substrate that both species can utilize. Maximal relative expression across a row is red; minimal is green**.** Differential expression was judged using the MAS5 algorithm and CyberT (see **Table S9** and *Methods).*

Figure S5. *In vitro* plate-based assay showing that sugars released by *B. thetaiotaomicron* are utilized by *E. rectale,* allowing its colonies to grow larger. *E. rectale* cells from an overnight culture were plated on tryptone agar with the indicated carbon sources. Ten μl of an overnight culture of *B. thetaiotaomicron* were then spotted in the middle of the plate (at the right edge of each panel). Note that colonies of *E. rectale* located closest to *B. thetaiotaomicron* grow larger on dextran, a glucose polymer that *E. rectale* is unable to degrade. This growth phenotype is due to *E. rectale'*s ability to acquire glucose monomers released during the degradation of dextran and not to other growth factors produced by *B. thetaiotaomicron* since the effect is not observed in tryptone medium alone (bottom panel), or in medium with D-arabinose, a simple sugar that *E. rectale* cannot utilize. Boxed areas in the upper panels are shown at higher magnification in the lower panels. Bars, 2 mm.

Figure S6. *B. vulgatus* adapts to the presence of *B. thetaiotaomicron* by upregulating its unique repertoire of polysaccharide degrading enzymes. (A) *B. vulgatus* and *B. thetaiotaomicron* colonize germ-free NRMI mice to similar levels in mono- and bi-association. Colony forming units (CFU) were measured in the cecum 14 d after gastric gavage with 10^8 CFU of one or both bacterial species (n=4 mice/group, 2–3 replicates per mouse; mean values ± SEM are plotted). **(B)** Heat map showing three *B. vulgatus* loci containing genes involved in xylan and xylose utilization that are significantly upregulated upon co-colonization with *B. thetaiotaomicron*. Each column represents one GeneChip hybridized to cecal contents from one mouse (n=4 per group). **(C)** A depiction of the predicted xylose-utilization pathway encoded by the operon displayed in panel B**.** Red indicates significant

upregulation, while violet indicates a level of upregulation that failed to meet the FDR threshold.

Supplemental Figures

Figure S1.

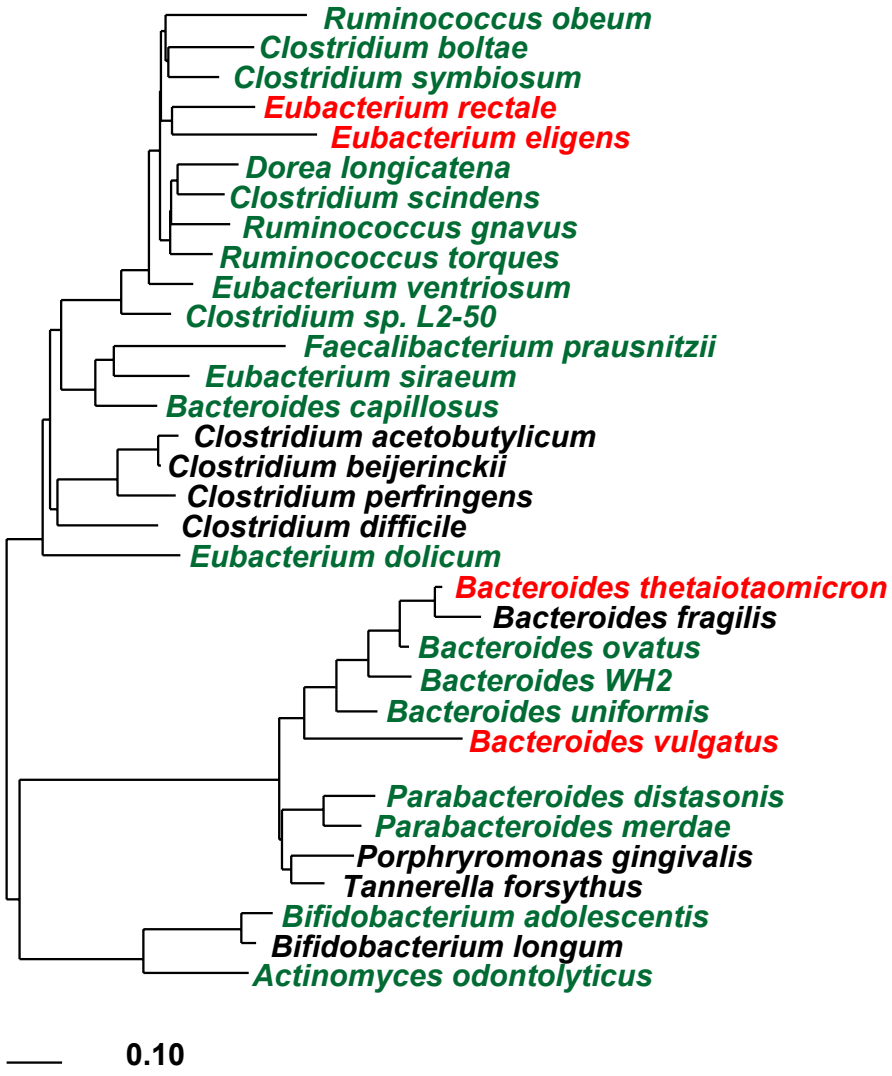

Figure S2.

GO Category
Description
Total genes
B. caccae
B. ovatus
B. stercoris
B. uniformis
B. fragilis
B. theta
B. vulgatus
P. distasonis
P. merdae
C. boltae
C. scindens
C. sp. L2-50
C. symbiosum
R. gnavus
R. obeum
R. torques
C. eutactus
D. longicatena
A. colihominis
B. capillosus
F. prausnitzii
R. micros
E. dolichum
E. siraeum
E. ventriosum
E. eligens
E. rectale
Poly-saccharide metabolism
Energy production
Mobile elements
Oxygen sensitivity
Environ-mental sensing and regulation
Transport
Motility
Bacteroidetes
Firmicutes

Figure S3.

CAZy Family		*B. theta*	*B. vulgatus*	*E. rectale*	*E. eligens*
GH2	various	32	25	3	2
GH20	hexosaminidase	20	8	0	0
GH43	furanosidase	31	22	2	3
GH92	α-1-2-mannosidase	23	9	0	0
GH76	α-1-6-mannosidase	10	0	0	0
GH97	a-glucosidase	10	7	0	0
GH18	chitinase/ glucosaminidase	12	2	1	1
GH28	galacturonase	9	13	0	3
GH29	α-fucosidase	9	8	0	0
GH1	6-P-ß-glucosidase	0	0	1	1
GH25	lysozyme	1	1	4	5
GH94	phosphorylase	0	0	3	1
PL9	pectate lyase	2	0	0	4
GH8	oligoxylanase	0	0	1	0
GH13	α-amylase	7	4	13	6
GH24	lysozyme	0	1	1	0
GH42	ß-galactosidase	1	1	2	0
GH53	endo-1,4- galactanase	1	0	2	0
GH77	amylomaltase	1	1	3	1
GH112	galacto-N-biose phosphorylase	0	0	1	0
GH10	xylanase	0	1	0	0
GH15	α-glycosidase	0	1	0	0
GH63	α-glucosidase	0	2	0	0

Total GH	**255**	**167**	**52**	**30**
Total PL	**17**	**7**	**0**	**7**

Figure S4.

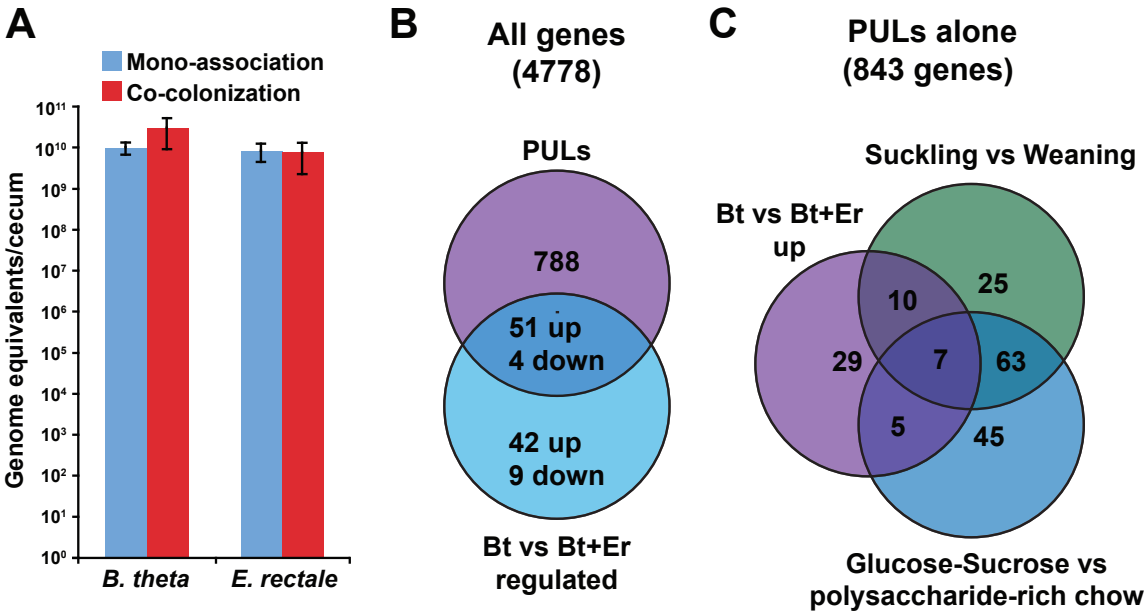
A
Mono-association
Co-colonization
Genome equivalents/cecum
B. theta
E. rectale
B
All genes
(4778)
PULs
788
51 up
4 down
42 up
9 down
Bt vs Bt+Er
regulated
C
PULs alone
(843 genes)
Suckling vs Weaning
Bt vs Bt+Er
up
10
25
29
7
63
5
45
Glucose-Sucrose vs
polysaccharide-rich chow

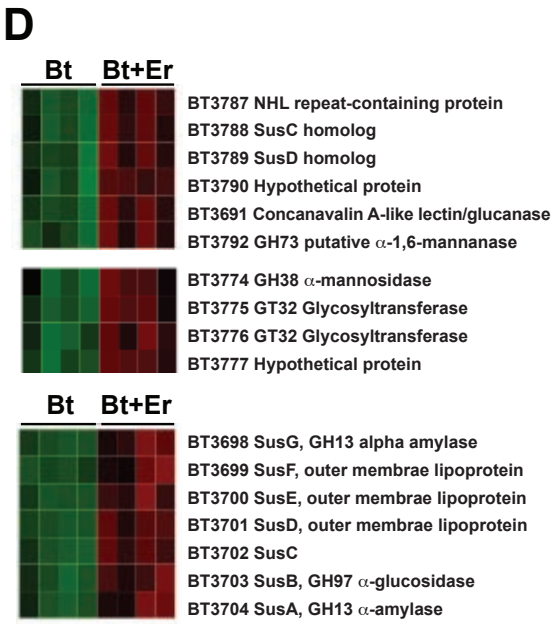
D
Bt
Bt+Er
BT3787 NHL repeat-containing protein
BT3788 SusC homolog
BT3789 SusD homolog
BT3790 Hypothetical protein
BT3691 Concanavalin A-like lectin/glucanase
BT3792 GH73 putative α-1,6-mannanase
BT3774 GH38 α-mannosidase
BT3775 GT32 Glycosyltransferase
BT3776 GT32 Glycosyltransferase
BT3777 Hypothetical protein
Bt
Bt+Er
BT3698 SusG, GH13 alpha amylase
BT3699 SusF, outer membrae lipoprotein
BT3700 SusE, outer membrae lipoprotein
BT3701 SusD, outer membrae lipoprotein
BT3702 SusC
BT3703 SusB, GH97 α-glucosidase
BT3704 SusA, GH13 α-amylase

Figure S5.

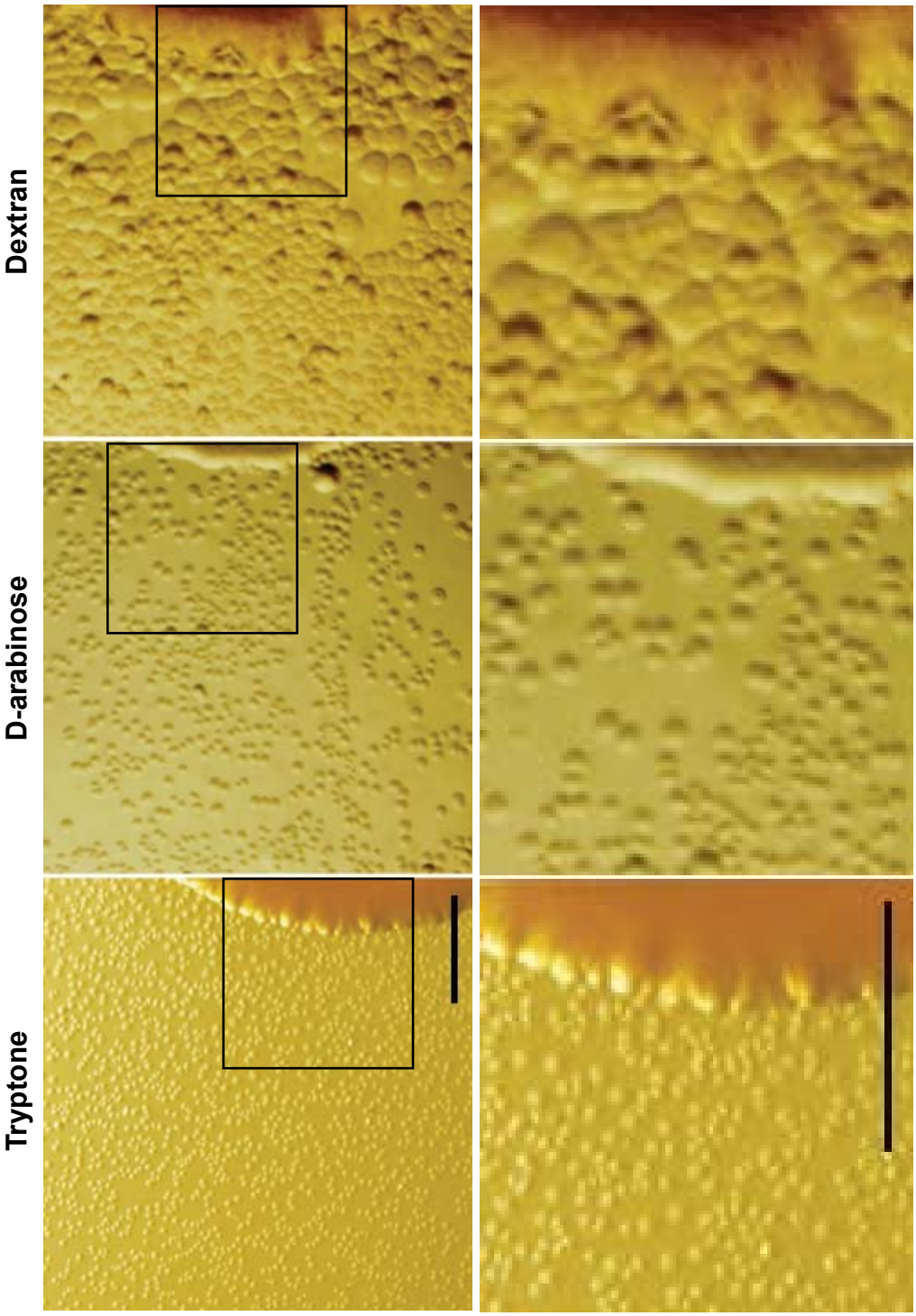

Figurs S6.

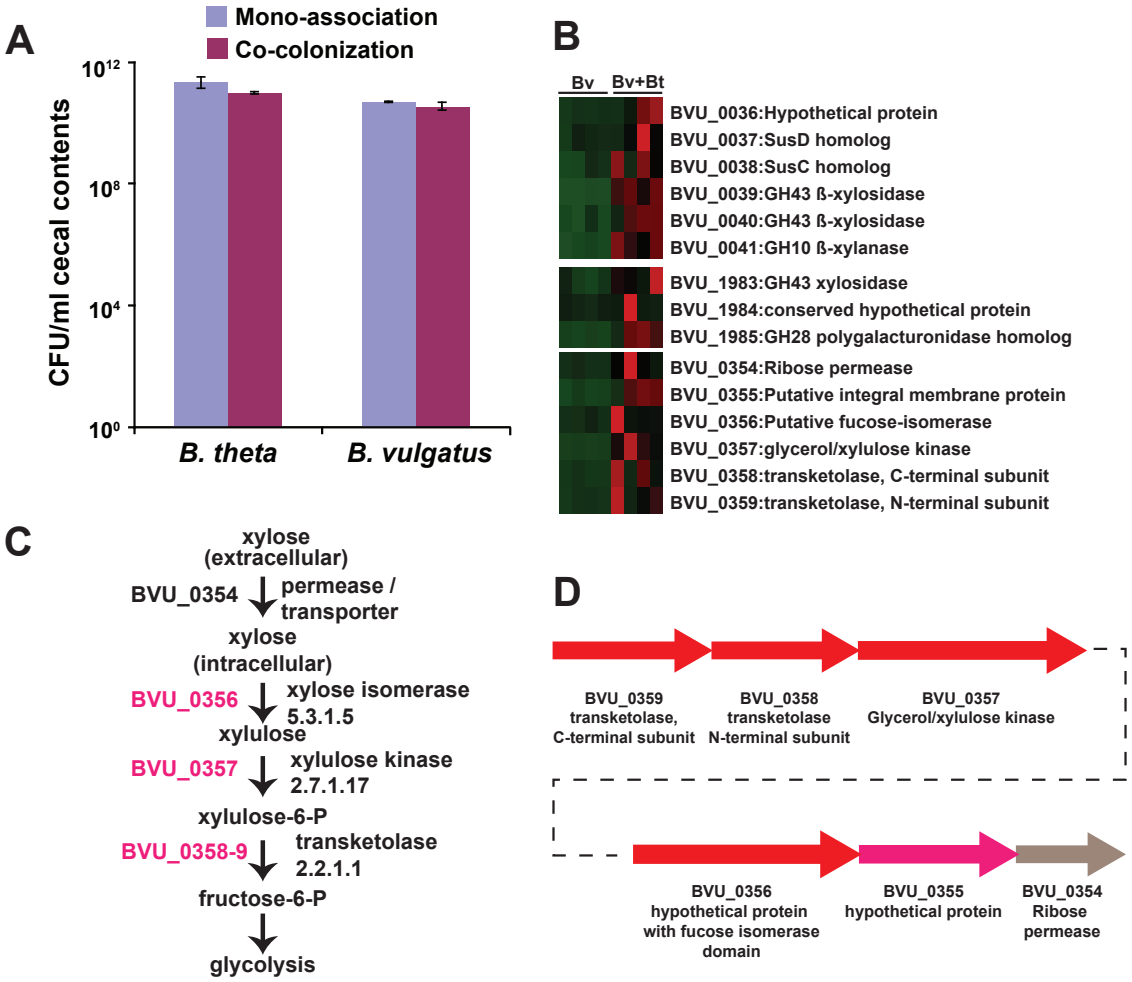
A
Mono-association
Co-colonization
CFU/ml cecal contents
10^12
10^8
10^4
10^0
B. theta
B. vulgatus
B
Bv
Bv+Bt
BVU_0036:Hypothetical protein
BVU_0037:SusD homolog
BVU_0038:SusC homolog
BVU_0039:GH43 ß-xylosidase
BVU_0040:GH43 ß-xylosidase
BVU_0041:GH10 ß-xylanase
BVU_1983:GH43 xylosidase
BVU_1984:conserved hypothetical protein
BVU_1985:GH28 polygalacturonidase homolog
BVU_0354:Ribose permease
BVU_0355:Putative integral membrane protein
BVU_0356:Putative fucose-isomerase
BVU_0357:glycerol/xylulose kinase
BVU_0358:transketolase, C-terminal subunit
BVU_0359:transketolase, N-terminal subunit
C
xylose (extracellular)
BVU_0354
permease / transporter
xylose (intracellular)
BVU_0356
xylose isomerase 5.3.1.5
xylulose
BVU_0357
xylulose kinase 2.7.1.17
xylulose-6-P
BVU_0358-9
transketolase 2.2.1.1
fructose-6-P
glycolysis
D
BVU_0359 transketolase, C-terminal subunit
BVU_0358 transketolase N-terminal subunit
BVU_0357 Glycerol/xylulose kinase
BVU_0356 hypothetical protein with fucose isomerase domain
BVU_0355 hypothetical protein
BVU_0354 Ribose permease

Supplemental Table Legends

Table S1. Summary of results of genome finishing for *E. rectale* strain ATCC 33656 and *E. eligens* strain ATCC 27750.

Table S2. Annotated finished genome of *E. rectale* strain ATCC 33656. Mean Expr. Fields give average expression value for each GeneChip condition: T-G = log-phase tryptone-glucose broth; Mono = cecum, monoassociation; BtEr = cecum, co-colonization with *B. thetaiotaomicron*. Abs = "absent" signal; N/A = feature not included in analysis.

Table S3. Annotated finished genome of *E. eligens* strain ATCC 27750.

Table S4. CAZy categorization of glycoside hydrolase and polysaccharide lysase genes in the sequenced human gut-derived bacterial species surveyed. Highlighted categories have increased numbers of genes in gut Firmicutes compared to gut Bacteroidetes.

Table S5. Growth of *B. thetaiotaomicron, B. vulgatus* and *E. rectale* in defined medium with the indicated carbon sources. Differences between *B. thetaiotaomicron* and the other two species are highlighted.

Table S6. Custom GeneChip containing genes from six common human gut microbes, representing two bacterial phyla and two domains of life. Genome sequences are reported here or in earlier reports from our group [13-15]. Numbers in parentheses denote remaining GeneChip features after application of a cross-hybridization probe mask (for details, see *Methods*).

Table S7. GeneChip probesets yielding ≥60% Present calls when hybridized to cDNAs prepared from the cecal contents of mice colonized with the indicated species. These **probesets were excluded from all analyses involving that species.**

Table S8. List of *B. thetaiotaomicron* genes whose expression in the ceca of gnotobiotic mice was significantly affected by *E. rectale*. Significance measured by CyberT; Fold=fold difference in expression in co-colonization relative to monoassociation; PPDE(p)=posterior probability of differential expression for an individual gene; PPDE(<p)= global posterior probability of differential

expression for the set of all genes with PPDE≥PPDE(p). PPDE(<p) ≥ 0.95 was used as a cutoff. Detection by MS/MS lists the number of technical replicates (out of 3) in which each protein was detected.

Table S9. List of *E. rectale* genes whose expression in the ceca of gnotobiotic mice was significantly affected by the presence of *B. thetaiotaomicron.* Significance measured by CyberT; Fold=fold difference in expression in co-colonization relative to monoassociation; PPDE(p)=posterior probability of differential expression for an individual gene; PPDE(<p)= global posterior probability of differential expression for the set of all genes with PPDE≥PPDE(p). PPDE(<p) ≥ 0.95 and ±1.5 minimum fold change were used as cutoffs. Detection by MS/MS lists the number of technical replicates (out of 3) in which each protein was detected.

Table S10. Changes in *E. rectale* gene expression when comparing *E. rectale*'s transcription during logarithmic phase growth on tryptone-glucose (T-G) medium with its transcriptome during mono-colonization of the cecum. Significance measured by CyberT; Fold=fold difference in expression in co-colonization relative to monoassociation; PPDE(p)=posterior probability of differential expression for an individual gene; PPDE(<p)= global posterior probability of differential expression for the set of all genes with PPDE≥PPDE(p). PPDE(<p) ≥ 0.99 was used as a cutoff.

Table S11. Proteomic analysis of the cecal contents of gnotobiotic mice. Spectral counts corresponding to every identfied protein are listed for each of 3 replicates per sample from 2 independent experiments are shown.

Table S12. Summary of the validation of hypothetical and previously unannotated proteins in *E. rectale* and *B. thetaiotaomicron* using tandem mass spectrometry.

Legend

[a] 12 individual MS/MS runs, three from each of two monoassociated and two *B. thetaiotaomicron*/*E. rectale* co-colonnized mice comprising two independent biological experiments, searched using SEQUEST (see *Methods* for details*).*

[b]Assignments to a COG or KEGG orthology group or Interpro number (for details, see *Methods).*

[c]Additional genes were identified using GeneMarkS [3] and added to the search database.

Table S13. List of *B. thetaiotaomicron* genes whose expression in the ceca of gnotobiotic mice was significantly affected by the presence of *B. vulgatus*. Significance measured by CyberT; Fold=fold difference in expression in co-colonization relative to monoassociation; p-value=p-value of Baysian t-test; corrected p-value=p-value with Benjamini-Hochberg multiple hypothesis testing correction applied [31].

Table S14. List of *B. vulgatus* genes whose expression in the ceca of gnotobiotic mice was significantly affected by the presence of *B. thetaiotaomicron*. Significance measured by CyberT; Fold=fold difference in expression in co-colonization relative to monoassociation; PPDE(p)=posterior probability of differential expression for an individual gene; PPDE(<p)= global posterior probability of differential expression for the set of all genes with PPDE≥PPDE(p).

Supplemental Tables

Table S1.

	E. rectale	E. eligens
Genome size (bp)	3,449,685	2,831,389
Plasmids	0	2 (626 kb, 60 kb)
Predicted proteins	3,627	2,766
tRNAs	57	47
rRNAs	15	15
Other features	20	17
ABI 3730xl Plasmid reads	120,005 reads (9.6x)	37,846 reads (4.0x)
454 GS20 Pyrosequencer	120 Mb (40x)	114 Mb (40x)
Finishing reactions	204	104

Table S2.

Please access provided CD for this information.

Table S3.

Please access provided CD for this information.

Table S4.

Glycoside hydrolase / Polysaccharide lyase family	GH Total	PL Total	Bacteroidetes total	Firmicutes total	B. thetaiotaomicron VPI5482	B. fragilis NCTC9343	B. uniformis	B. vulgatus	B. ovatus	B. stercoris	B. caccae	Parabacteroides distasonis	P. merdae	Anaerotruncus colihominis	Clostridium scindens	C. bolteae	Coprococcus eutactus	D. longicatena	Eubacterium dolichum	E. eligens	E. rectale	E. siraeum	E. ventriosum	Faecalibacterium prausnitzii	Clostridium sp. L2-50	Peptostreptococcus micros	Ruminococcus gnavus	R. torques	R. obeum
	1460	80	561	255	132	173	167	299	84	136	96	118	13	24	55	43	29	24	30	52	57	43	31	9	2	59	44	46
GH1	**0**	**29**	0	0	0	0	0	0	0	0	0	0	0	0	4	2	2	4	1	1	0	1	3	0	0	5	5	1
GH2	**182**	**36**	32	15	22	25	37	6	16	11	18	0	1	2	3	2	4	0	2	3	2	2	7	0	0	6	2	2
GH3	**95**	**29**	10	10	23	5	21	5	10	8	3	2	0	2	2	2	2	2	0	3	4	2	2	1	0	4	0	3
GH4	**0**	**9**	0	0	0	0	0	0	0	0	0	0	0	0	3	0	0	2	0	0	0	0	2	0	0	0	2	0
GH5	**20**	**22**	2	1	7	2	7	2	0	0	1	0	0	0	0	2	0	0	1	1	13	2	0	0	0	2	0	1
GH8	**0**	**1**	0	0	0	0	0	0	0	0	0	0	0	0	0	0	0	0	0	1	0	0	0	0	0	0	0	0
GH9	**8**	**2**	0	0	6	0	1	1	0	0	0	0	0	0	0	2	0	0	0	0	0	0	0	0	0	0	0	0
GH10	**7**	**0**	0	0	0	1	6	0	0	0	0	0	0	0	0	0	0	0	0	0	0	0	0	0	0	0	0	0
GH13	**48**	**98**	7	6	7	4	5	6	6	3	8	2	2	6	10	8	6	3	6	13	6	5	3	4	0	9	5	12
GH15	**4**	**0**	0	0	1	1	1	0	0	0	1	0	0	0	0	0	0	0	0	0	0	0	0	1	0	0	0	0
GH16	**30**	**6**	4	6	1	1	1	5	3	7	1	2	0	0	0	1	0	0	0	0	0	4	0	1	0	0	0	0
GH17	**0**	**1**	0	0	0	0	0	0	0	0	0	0	0	0	0	0	0	0	0	0	0	1	0	0	0	0	0	0
GH18	**30**	**17**	12	2	3	2	9	2	0	0	0	0	0	2	3	0	1	0	1	1	0	4	0	0	0	2	2	1
GH20	**92**	**8**	20	12	5	8	13	7	12	6	9	0	0	0	0	0	0	3	0	0	0	0	0	0	0	0	4	1
GH23	**27**	**26**	3	3	3	3	3	3	3	3	3	3	1	2	2	0	3	0	2	1	1	1	1	1	1	4	0	6
GH24	**2**	**2**	0	0	0	1	0	0	0	1	0	0	0	0	1	0	0	0	0	1	0	0	0	0	0	0	0	0
GH25	**7**	**37**	1	1	1	1	1	1	1	1	0	0	6	2	4	3	1	0	5	4	3	2	1	1	0	2	3	0
GH26	**9**	**8**	0	2	3	0	3	0	0	0	1	0	0	0	1	2	0	0	0	0	5	0	0	0	0	0	0	0
GH27	**14**	**2**	5	3	0	1	3	1	1	1	0	0	0	0	0	0	1	0	0	0	1	0	0	0	0	0	0	0
GH28	**50**	**7**	9	0	2	13	14	5	3	1	3	0	0	0	1	0	0	0	3	0	0	0	2	0	0	1	0	0
GH29	**56**	**7**	9	10	2	8	7	4	12	1	3	0	1	0	0	0	0	0	0	0	2	0	0	0	0	2	1	1
GH30	**9**	**1**	1	0	2	2	2	2	0	0	2	0	0	0	0	0	0	0	0	0	0	1	0	0	0	0	0	0
GH31	**41**	**21**	6	4	6	4	11	1	4	2	3	0	0	0	3	1	0	2	0	3	2	4	1	0	0	3	1	1
GH32	**19**	**21**	4	2	4	1	2	2	2	1	1	1	0	0	2	3	4	2	0	2	1	0	0	0	0	3	0	4
GH33	**22**	**4**	2	3	1	2	4	3	3	1	3	0	0	0	0	0	0	0	0	0	0	0	0	0	0	1	3	0
GH35	**18**	**1**	3	4	1	1	2	0	5	1	1	0	0	0	0	0	0	0	0	0	1	0	0	0	0	0	0	0
GH36	**18**	**19**	3	3	1	2	3	1	2	2	1	0	0	0	2	5	0	1	0	3	2	0	1	0	0	2	2	1
GH38	**7**	**2**	2	1	2	0	1	0	0	0	1	0	0	0	1	0	0	0	0	0	0	1	0	0	0	0	0	0

Glycoside hydrolase / Polysaccharide lyase family	Bacteroidetes total	Firmicutes total	B. thetaiotaomicron VPI5482	B. fragilis NCTC9343	B. uniformis	B. vulgatus	B. ovatus	B. stercoris	B. caccae	Parabacteroides distasonis	P. merdae	Anaerotruncus colihominis	Clostridium scindens	C. bolteae	Coprococcus eutactus	D. longicatena	Eubacterium dolichum	E. eligens	E. rectale	E. siraeum	E. ventriosum	Faecalibacterium prausnitzii	Clostridium sp. L2-50	Peptostreptococcus micros	Ruminococcus gnavus	R. torques	R. obeum
GH42	**4**	**8**	1	0	1	17	9	0	0	1	0	0	0	1	0	1	0	0	2	0	0	0	0	0	1	1	2
GH43	**142**	**17**	31	1	1	22	35	2	8	7	11	0	0	1	1	1	0	3	2	6	0	1	0	0	0	0	2
GH50	**3**	**0**	0	0	0	0	3	0	0	0	0	0	0	0	0	0	0	0	0	0	0	0	0	0	0	0	0
GH51	**24**	**6**	4	2	3	3	4	0	2	3	3	0	0	1	1	1	0	0	1	1	0	0	0	0	0	0	0
GH53	**5**	**3**	1	0	1	0	1	1	1	0	0	0	0	1	0	0	0	0	2	0	0	0	0	0	0	1	0
GH55	**2**	**1**	0	0	2	0	0	0	0	0	0	0	0	0	0	0	0	0	0	0	1	0	0	0	0	0	0
GH57	**9**	**0**	1	1	1	1	1	1	1	1	1	0	0	0	0	0	0	0	0	1	0	0	0	0	0	0	0
GH59	**0**	**1**	0	0	0	0	0	0	0	0	0	0	0	0	0	0	0	0	0	1	0	0	0	0	0	0	0
GH63	**7**	**0**	0	0	3	2	0	1	0	1	0	0	0	0	0	0	0	0	0	0	0	1	0	0	0	0	0
GH64	**0**	**1**	0	0	0	0	0	0	0	0	0	0	0	0	0	0	0	0	0	0	1	0	0	0	0	1	0
GH65	**4**	**3**	0	1	1	0	0	2	0	0	0	0	2	0	0	0	0	0	0	0	1	0	0	0	0	0	0
GH66	**3**	**0**	1	0	1	0	1	0	0	0	0	0	0	0	0	0	0	0	0	0	0	0	0	0	0	0	0
GH67	**4**	**0**	1	0	0	1	2	0	0	0	0	0	0	0	0	0	0	0	0	0	0	0	0	0	0	0	0
GH68	**0**	**3**	0	0	0	0	0	0	0	0	0	0	2	1	0	0	0	0	0	0	0	0	0	0	0	0	0
GH73	**16**	**17**	1	1	1	1	2	1	1	3	5	0	2	2	1	1	2	1	1	0	1	0	0	1	1	2	0
GH74	**3**	**1**	0	0	1	0	0	2	0	0	0	0	0	0	0	0	0	0	0	1	0	0	0	0	0	0	0
GH76	**29**	**1**	10	3	5	0	8	1	0	1	1	0	0	0	0	0	0	0	0	1	0	0	0	0	0	0	0
GH77	**9**	**24**	1	1	1	1	1	1	1	1	1	1	2	2	2	2	1	1	3	2	2	1	0	0	1	1	3
GH78	**43**	**5**	6	2	3	5	8	0	2	7	10	0	0	1	0	0	0	0	0	0	0	1	0	0	1	0	2
GH81	**0**	**4**	0	0	0	0	0	0	0	0	0	0	0	0	0	0	0	0	0	0	0	0	0	0	0	0	0
GH84	**7**	**4**	1	1	1	1	0	0	1	1	1	0	0	0	0	0	1	0	0	0	0	0	0	0	0	3	0
GH88	**32**	**4**	4	1	1	3	8	4	6	0	5	0	0	2	0	0	0	0	0	0	0	1	0	0	1	0	0
GH89	**14**	**2**	3	1	0	1	4	0	3	0	2	0	0	0	0	1	0	0	0	0	0	0	0	0	0	1	0
GH91	**2**	**0**	0	0	0	0	1	0	1	0	0	0	0	0	0	0	0	0	0	0	0	0	0	0	0	0	0
GH92	**107**	**1**	23	8	10	9	19	6	5	14	13	0	0	0	0	0	0	0	0	0	1	0	0	0	0	0	0
GH93	**1**	**0**	1	0	0	0	0	0	0	0	0	0	0	0	0	0	0	0	0	0	0	0	0	0	0	0	0
GH94	**1**	**12**	0	0	1	0	0	0	0	0	0	1	0	0	2	0	0	3	2	1	1	0	0	0	0	0	1
GH95	**32**	**8**	5	4	1	4	7	3	4	1	3	0	0	0	0	0	0	1	0	1	0	0	0	0	3	2	1
GH97	**55**	**0**	10	4	9	7	12	3	4	3	3	0	0	0	0	0	0	0	0	0	0	0	0	0	0	0	0
GH98	**1**	**1**	0	0	0	0	1	0	0	0	0	0	0	0	0	0	0	0	0	0	0	0	0	0	1	0	0
GH99	**1**	**0**	1	0	0	0	0	0	0	0	0	0	0	0	0	0	0	0	0	0	0	0	0	0	0	0	0

Glycoside hydrolase / Polysaccharide lyase family	Bacteroidetes total	Firmicutes total	B. thetaiotaomicron VPI5482	B. fragilis NCTC9343	B. uniformis	B. vulgatus	B. ovatus	B. stercoris	B. caccae	Parabacteroides distasonis	P. merdae	Anaerotruncus colihominis	Clostridium scindens	C. bolteae	Coprococcus eutactus	D. longicatena	Eubacterium dolichum	E. eligens	E. rectale	E. siraeum	E. ventriosum	Faecalibacterium prausnitzii	Clostridium sp. L2-50	Peptostreptococcus micros	Ruminococcus gnavus	R. torques	R. obeum
GH101	0	2	0	0	0	0	0	0	0	0	0	0	0	0	0	0	0	0	0	0	0	0	0	0	0	2	0
GH105	39	9	0	2	7	13	3	5	0	2	0	0	0	3	0	0	2	0	0	0	2	0	0	2	0	0	0
GH106	14	0	0	0	3	4	1	1	0	2	0	0	0	0	0	0	0	0	0	0	0	0	0	0	0	0	0
GH108	1	0	0	1	0	0	0	0	0	0	0	0	0	0	0	0	0	0	0	0	0	0	0	0	0	0	0
GH109	22	0	3	3	5	2	1	4	1	1	0	0	0	0	0	0	0	0	0	0	0	0	0	0	0	0	0
GH110	9	0	2	0	2	0	0	2	0	1	0	0	0	0	0	0	0	0	0	0	0	0	0	0	0	0	0
GH112	0	7	0	0	0	0	0	0	0	0	0	0	1	1	0	0	0	0	1	0	0	1	0	1	0	1	0
PL1	21	3	5	0	0	2	9	3	2	0	2	0	0	0	0	0	0	3	0	0	0	0	0	0	0	0	0
PL8	17	0	4	1	1	0	2	3	4	0	2	0	0	0	0	0	0	0	0	0	0	0	0	0	0	0	0
PL9	7	4	2	0	0	0	2	0	3	0	0	0	0	0	0	0	0	4	0	0	0	0	0	0	0	0	0
PL10	5	0	1	0	0	2	1	1	0	0	0	0	0	0	0	0	0	0	0	0	0	0	0	0	0	0	0
PL11	10	1	1	0	0	3	5	1	0	0	0	0	0	0	0	0	0	0	0	0	0	0	0	1	0	0	0
PL12	10	3	2	1	0	0	3	4	0	0	0	0	2	0	0	0	0	0	0	0	0	0	0	1	0	0	0
PL13	3	0	1	0	0	0	1	1	0	0	0	0	0	0	0	0	0	0	0	0	0	0	0	0	0	0	0
PL15	7	0	1	0	0	0	1	5	0	0	0	0	0	0	0	0	0	0	0	0	0	0	0	0	0	0	0

Table S5.

Carbon source	Class	E. rectale	B. thetaiotaomicron	B. vulgatus	source	Sterilization	Comments
empty		-	-	-		FS	
D(-)arabinose	monosaccharide	-	+	+	Sigma A3131	FS	pentose
D(-)fructose	monosaccharide	+	+	+	Sigma F0127	FS	hexose
L(-)fucose	monosaccharide	-	+	+	Sigma F2252	FS	deoxy-hexose
D(+)galactose	monosaccharide	+	+	+	Sigma G0750	FS	hexose
D-galacturonic acid	monosaccharide	-	+	+	Fluka 73960	FS	modified monosaccharide
D-glucuronic acid	monosaccharide	-	+	+	Sigma G8645	FS	modified monosaccharide
D(+)glucosamine	monosaccharide	+	+	marg	Sigma G4875	FS	modified monosaccharide
D(+)glucose	monosaccharide	+	+	+	Sigma G8270	FS	hexose
D(+)mannose	monosaccharide	-	+	+	Sigma M4625	FS	hexose
N-acetylgalactosamine	monosaccharide	-	+	+	Sigma A2795	FS	modified monosaccharide
N-acetylglucosamine (GlcNAC)	monosaccharide	+	+	+	Sigma A3286	FS	modified monosaccharide
N-acetylmuramic acid (MurNAC)	monosaccharide	-	-	-	Sigma A3007	FS	modified monosaccharide
N-acetylneuraminic acid (IV-S)	monosaccharide	-	-	+	Sigma A0812	FS	modified monosaccharide (Sialic Acid)
L-rhamnose	monosaccharide	-	+	+	Sigma R3875	FS	deoxy-hexose
D(-)ribose	monosaccharide	-	+	-	Sigma R7500	FS	pentose
D(+)xylose	monosaccharide	+	+	+	Sigma X3877	FS	pentose
D(+)cellobiose	disaccharide	+	-	-	Sigma C7252	FS	ß(1-4) glucose disaccharide
sucrose	disaccharide	-	+	+	Fisher S5	FS	Fru(alpha1-2)Glc disaccharide
lactose (b-lactose)	disaccharide	+	+	+	Sigma L3750	FS	Gal(ß1-4)Glc disaccharide
chondroitin sulfate A/C (bovine trachea)	host, GAG	-	+	-	Sigma C9819	AC	

Carbon source	Class	E. rectale	B. thetaiotaomicron	B. vulgatus	source	Sterilization	Comments
dermatan sulfate	host, GAG	-	+	-	Sigma C3788	AC	
heparin (porcine mucosa)	host, GAG	-	+	-	Sigma H0777	AC	
hyaluronan (rooster comb)	host, GAG	-	+	-	Sigma H5388	AC	
arabinan (sugar beet)	plant, pectin	-	+	+	Megazyme P-ARAB	AC	
arabinogalactan (larch)	plant, pectin	-	+	-	Megazyme P-ARGAL	AC	plant cell wall
pectic galactan (potato)	plant, pectin	-	+	+	Megazyme P-GAPT	AC	
polygalacturonate (citrus peel)	plant, pectin	-	+	+	Megazyme P-GACT	AC	
rhamnogalacturonan I (potato pectin)	plant, pectin	-	-	+	Megazyme P-RHAM1	AC	
arabinoxylan (wheat)	plant, hemicellulose	-	-	-	Megazyme P-WAXYL	AC	arabinose, xylose branched
b-glucan (barley)	plant, hemicellulose	-	-	-	Megazyme P-BGBL	AC	
galactomannan (carob)	plant, hemicellulose	marg	-	-	Megazyme P-GALML	AC	galactose, mannan branched
glucomannan (konjac)	plant, hemicellulose	marg	-	-	Megazyme P-GLCML	AC	glucose, mannan linear
methyl glucoronyl xylan	plant, hemicellulose	-	-	+	Sigma M5144	AC	
xylan (oat spelt) (clarified)	plant, hemicellulose	marg	-	-	Fluka 95590	AC	hemicellulose
xyloglucan (tamarind)	plant, hemicellulose	-	-	-	Megazyme P-XYGLN	AC	hemicellulose
carboxymethyl cellulose	plant, cellulose	-	-	-	Fluka 21902	AC	
a-mannan (*S. cerevisiae*)	other	-	+	-	Sigma M7504	AC	fungal cell wall
alginate (brown algae)	other	-	-	-	Sigma 180947	AC	
colominic acid (*E. coli*)	other	-	-	-	Sigma C5762	AC	
dextran (*L. mesenteroides*)	other	-	+	-	Sigma D5251	AC	bacterial secreted

Carbon source	Class	E. rectale	B. thetaiotaomicron	B. vulgatus	source	Sterilization	Comments
DNA (salmon sperm)	other	-	-	-	Sigma D1626	AC	
inulin (chicory)	other	-	+	+	Sigma I2255	AC	B(2-1) fructose poly
l-carrageenan (seaweed)	other	-	-	-	Sigma C1867	AC	galactose poly
pullulan (*A. pullulans*)	other	-	+	+	Sigma P4516	AC	fungal cell wall
RNA (torula yeast, type IV)	other	-	-	-	Sigma R6625	AC	
soluble starch	plant starch	+	+	+	Sigma S9765	AC	

Table S6

Species	*B. theta*	*B. vulgatus*	*P. distasonis*	*E. rectale*	*E. eligens*	*M. smithii*
Genes	5059	4557	4140	3699	2852	1838
Proteins	4973	4445	4057	3627	2773	1796
Probe pairs	54961 (53876)	57313	52355	36943 (32794)	25934	25425
Probe sets	4998 (4924)	9400	8441	2644 (2382)	1860	3445
Genes covered	4927 (4922)	4303	4008	2600 (2367)	1786	1815
Proteins covered	4900 (4896)	4303	4008	2557 (2348)	1773	1782
Intergenic probes	0	8508	7198	0	0	4931
% of proteins covered	99% (98%)	97%	99%	71% (65%)	64%	99%

Table S7.

***B. theta* probe sets cross-hybridizing with *B. vulgatus* cDNA**	***B. vulgatus* probe sets cross-hybridizing with *B. theta* cDNA**	***B. theta* probe sets cross-hybridizing with *E. rectale* cDNA**	***E. rectale* probe sets cross-hybridizing with *B. theta* cDNA**
BT0174_at	Bv_tRNA21_x_at	BT0101_at	Er-060123-0150_at
BT0216_at	Bv_tRNA22_x_at	BT0133_at	Er-060123-0898_at
BT0332_at	Bv_tRNA31_x_at	BT0136_at	Er-060123-0918_at
BT0351_at	Bv_tRNA46_x_at	BT0154_at	Er-060123-0953_at
BT0353_at	Bv_tRNA70_x_at	BT0317_at	Er-060123-1056_at
BT0413_at	Bv_tRNA73_x_at	BT0332_at	Er-060123-1145_at
BT0422_at	Bv_tRNA74_x_at	BT0366_at	Er-060123-1250_at
BT0433_at	Bv_tRNA84_x_at	BT0535_at	Er-060123-1311_at
BT0623_at	Bv0006c_at	BT0733_at	Er-060123-1330_at
BT0701_at	Bv0046c_at	BT0753_at	Er-060123-1481_at
BT0703_at	Bv0100_at	BT0897_at	Er-060123-1503_at
BT0756_at	Bv0205c_at	BT0968_at	Er-060123-1748_at
BT0790_at	Bv0230c_at	BT1003_at	Er-060123-2049_at
BT0804_at	Bv0326_at	BT1012_at	Er-060123-2292_at
BT0827_at	Bv0584c_at	BT1095_at	Er-060123-2382_at
BT1088_at	Bv0602c_at	BT1105_s_at	Er-060123-2406_at
BT1103_s_at	Bv0797c_s_at	BT1107_s_at	Er-060123-2446_at
BT1104_s_at	Bv0903_at	BT1449_at	Er-060123-2496_at
BT1105_s_at	Bv0923c_at	BT1533_at	Er-060123-tRNA12_x_at
BT1107_s_at	Bv1199_at	BT1607_at	Er-060123-tRNA17_x_at
BT1108_s_at	Bv1322_at	BT1683_at	Er-060123-tRNA50_at
BT1109_s_at	Bv1361c_at	BT16S_rRNA1_copy1_a_at	
BT1110_s_at	Bv1547c_at	BT16S_rRNA1_copy2_a_at	
BT1337_at	Bv1567c_at	BT16S_rRNA1_copy3_a_at	
BT1470_at	Bv1615c_at	BT16S_rRNA1_copy4_a_at	
BT1523_at	Bv1621_at	BT1734_at	
BT1550_at	Bv1625_at	BT1814_at	
BT1627_at	Bv1630_at	BT1851_at	
BT1691_at	Bv1652c_at	BT2053_at	
BT16S_rRNA1_copy1_a_at	Bv1872c_at	BT2099_at	
BT16S_rRNA1_copy2_a_at	Bv1978_at	BT2271_at	
BT16S_rRNA1_copy3_a_at	Bv2075_at	BT23S_rRNA1_a_at	
BT16S_rRNA1_copy4_a_at	Bv2090_at	BT2448_at	
BT1766_at	Bv2157_at	BT2505_at	
BT1833_at	Bv2214_at	BT2524_at	
BT1882_at	Bv2256c_at	BT2862_at	
BT1966_at	Bv2325c_s_at	BT3189_at	
BT2002_at	Bv2384c_at	BT3254_at	
BT2026_at	Bv23s_RNA1_a_at	BT3411_at	
BT2157_at	Bv2428c_at	BT3552_at	
BT2163_at	Bv2548_at	BT3644_at	
BT2191_at	Bv2573c_s_at	BT3688_at	
BT2238_at	Bv2841_at	BT3800_at	
BT23S_rRNA1_a_at	Bv2891_at	BT3856_at	
BT2532_at	Bv3373_at	BT3935_at	
BT2553_at	Bv3402_at	BT3950_at	
BT2712_at	Bv3409_at	BT4047_at	
BT2737_at	Bv3434c_s_at	BT4064_at	
BT3020_at	Bv3468c_at	BT4106_at	
BT3055_at	Bv3472c_at	BT4162_at	
BT3116_at	Bv3473c_at	BT4289_at	

***B. theta* probe sets cross-hybridizing with *B. vulgatus* cDNA**	***B. vulgatus* probe sets cross-hybridizing with *B. theta* cDNA**	***B. theta* probe sets cross-hybridizing with *E. rectale* cDNA**	***E. rectale* probe sets cross-hybridizing with *B. theta* cDNA**
BT3254_at	Bv3526_at	BT4522_at	
BT3272_at	Bv3622c_at	BT4649_at	
BT3299_at	Bv3891_at	BT4696_at	
BT3644_at	Bv3957c_at	BT4736_at	
BT3759_at	Bv-GM2025_x_at	BT4772_at	
BT3871_at	Bv-GM2278_at	BT-GM1094_at	
BT3991_at	Bv-GM3714_s_at	BT-GM2964_at	
BT4028_at	Bv-GM4208_x_at	BT-tRNA45_x_at	
BT4059_at		BT-tRNA64_x_at	
BT4121_at			
BT4195_at			
BT4404_at			
BT4461_at			
BT4496_at			
BT4555_at			
BT4557_at			
BT4666_at			
BT-GM1625_at			
BT-GM2011_at			
BT-GM2011_x_at			
BT-GM2028_at			
BT-tRNA1_x_at			
BT-tRNA41_s_at			
BT-tRNA45_x_at			
BT-tRNA5_at			
BT-tRNA5_x_at			
BT-tRNA55_x_at			
BT-tRNA58_x_at			

Table S8.

Locus tag	Probe set	Mono-association average	Bi-association average	Fold change	PPDE (<p)	Detection by MS/MS: Mono-association rep. 1	Mono-association rep. 2	Co-colonization rep. 1	Co-colonization rep. 2	Description
BT_0125	BT0125_at	66	168	2.56	0.99	0	0	0	0	NADH:ubiquinone oxidoreductase subunit
BT_0172	BT0172_at	114	274	2.41	0.95	0	0	0	0	hypothetical protein
BT_0212	BT0212_at	33	172	5.28	0.97	0	0	0	0	protease
BT_0213	BT0213_at	23	104	4.46	0.98	0	0	0	0	conserved hypothetical protein
BT_0292	BT0292_at	14	74	5.49	0.98	0	0	0	0	hypothetical protein
BT_0293	BT0293_at	11	69	6.47	0.99	0	0	0	0	conserved hypothetical protein
BT_0294	BT0294_at	52	570	10.91	1.00	0	1	0	3	conserved hypothetical protein with Carboxypeptidase regulatory domain
BT_0361	BT0361_at	569	1359	2.39	0.96	3	3	3	3	SusD homolog
BT_0636	BT0636_at	902	420	-2.15	0.97	0	0	0	0	putative transcriptional regulator
BT_0639	BT0639_at	106	41	-2.56	0.99	0	0	0	0	hypothetical protein
BT_0865	BT0865_at	1393	4119	2.96	1.00	3	3	1	3	putative chitobiase
BT_0866	BT0866_at	733	2916	3.98	1.00	3	3	3	3	SusD homolog
BT_0867	BT0867_at	1017	3734	3.67	1.00	3	3	3	3	SusC homolog
BT_1024	BT1024_at	73	170	2.32	0.98	0	0	0	0	SusD homolog
BT_1025	BT1025_at	67	155	2.32	0.98	0	0	0	0	SusC homolog
BT_1026	BT1026_at	89	215	2.41	0.99	0	0	0	0	hypothetical protein
BT_1273	BT1273_at	371	907	2.45	0.95	3	3	2	2	L-fucose isomerase
BT_1501	BT1501_at	144	351	2.44	0.99	0	0	0	0	major outer membrane protein OmpA
BT_1502	BT1502_at	1321	2430	1.84	0.95	3	3	1	3	conserved hypothetical protein
BT_1507	BT1507_at	154	387	2.50	0.99	3	3	2	3	conserved hypothetical protein
BT_1541	BT1541_at	82	185	2.25	0.99	0	0	0	0	homologous to putative transmembrane protein
BT_1644	BT1644_at	10	44	4.29	0.97	0	0	0	0	putative CPS biosynthesis glycosyltransferase
BT_1646	BT1646_at	16	71	4.33	0.96	0	0	0	0	glycoside transferase family 2
BT_1647	BT1647_at	22	62	2.83	0.99	0	0	0	0	conserved hypothetical protein, putative integral membrane protein
BT_1648	BT1648_at	33	102	3.12	0.99	0	0	0	0	glycoside transferase family 2
BT_1649	BT1649_at	52	158	3.04	1.00	0	0	0	0	glycoside transferase family 25
BT_1650	BT1650_at	32	98	3.05	0.98	0	0	0	0	putative teichoic acid biosynthesis protein F
BT_1651	BT1651_at	34	117	3.45	1.00	0	0	0	0	pyrophosphorylase
BT_1652	BT1652_at	25	120	4.77	1.00	0	0	0	0	lipopolysaccharide biosynthesis protein
BT_1653	BT1653_at	34	120	3.52	1.00	0	0	0	0	conserved hypothetical protein with Lipopolysaccharide biosynthesis domain
BT_1654	BT1654_at	31	119	3.81	1.00	3	3	3	3	polysialic acid transport protein kpsD precursor
BT_1656	BT1656_at	99	618	6.27	1.00	0	0	0	0	putative transcriptional regulator
BT_1682	BT1682_at	258	606	2.35	0.96	0	0	1	0	SusD homolog
BT_1689	BT1689_at	744	1474	1.98	0.97	0	0	0	0	oxaloacetate decarboxylase beta chain
BT_1719	BT1719_at	20	57	2.84	0.97	0	0	0	0	sulfopyruvate decarboxylase subunit beta
BT_1725	BT1725_at	10	42	4.39	0.97	0	0	0	0	putative transcriptional regulator
BT_1824	BT1824_at	57	122	2.14	0.96	0	0	0	0	conserved hypothetical protein, putative permease
BT_2132	BT2132_at	77	294	3.81	1.00	0	0	0	0	homologous to Cyclic nucleotide-binding
BT_2155	BT2155_at	3348	1667	-2.01	0.96	0	0	0	0	hypothetical protein
BT_2170	BT2170_at	2288	676	-3.38	1.00	0	0	0	0	conserved hypothetical protein
BT_2171	BT2171_at	1543	502	-3.07	1.00	1	0	0	0	putative anti-sigma factor
BT_2172	BT2172_at	316	65	-4.82	1.00	0	0	0	0	SusC homolog
BT_2173	BT2173_at	122	26	-4.69	0.99	0	0	0	0	SusD homolog
BT_2392	BT2392_at	41	100	2.43	0.97	3	0	1	0	NHL repeat-containing protein
BT_2393	BT2393_at	36	91	2.54	0.98	3	0	3	0	SusC homolog
BT_2394	BT2394_at	28	81	2.94	0.99	2	0	0	0	SusD homolog
BT_2395	BT2395_at	63	140	2.21	0.98	0	0	0	0	hypothetical protein

Locus tag	Probe set	Mono-association average	Bi-association average	Fold change	PPDE (<p)	Detection by MS/MS: Mono-association rep. 1	Mono-association rep. 2	Co-colonization rep. 1	Co-colonization rep. 2	Description
BT_2486	BT2486_at	128	290	2.27	0.99	0	0	0	0	hypothetical protein
BT_2665	BT2665_at	206	87	-2.36	0.98	3	3	3	0	TonB
BT_2927	BT2927_at	75	168	2.24	0.98	0	0	0	0	homologous to putative cell wall-associated protein precursor
BT_3020	BT3020_at	35	75	2.14	0.95	0	0	0	0	hypothetical protein
BT_3024	BT3024_at	78	176	2.27	0.97	0	0	1	0	SusC homolog
BT_3025	BT3025_at	89	200	2.24	0.97	0	0	0	0	SusD homolog
BT_3026	BT3026_at	105	207	1.97	0.95	1	0	0	0	glycoside hydrolase family 30
BT_3027	BT3027_at	152	359	2.36	0.98	0	0	0	0	hypothetical protein
BT_3029	BT3029_at	92	188	2.05	0.95	0	0	0	0	Na+/glucose symporter
BT_3221	BT3221_at	775	89	-8.67	1.00	0	0	0	0	hypothetical protein
BT_3222	BT3222_at	10014	884	-11.32	1.00	3	3	0	1	hypothetical protein
BT_3223	BT3223_at	4475	293	-15.26	1.00	3	3	0	0	hypothetical protein
BT_3224	BT3224_at	1143	221	-5.18	1.00	0	0	0	0	putative lysine decarboxylase
BT_3225	BT3225_at	325	66	-4.93	1.00	0	0	0	0	conserved hypothetical protein
BT_3474	BT3474_at	112	229	2.04	0.95	0	0	0	0	SusD homolog
BT_3581	BT3581_at	151	319	2.11	0.97	0	2	1	1	putative dehydrogenases and relate proteins
BT_3614	BT3614_at	117	265	2.26	0.98	0	0	0	1	putative oxidoreductase
BT_3619	BT3619_at	85	189	2.22	0.96	0	0	0	0	homologous to putative transmembrane protein
BT_3669	BT3669_at	59	139	2.37	0.98	0	0	0	0	hypothetical protein
BT_3670	BT3670_at	56	126	2.24	0.96	0	0	0	0	SusC homolog
BT_3672	BT3672_at	46	111	2.42	0.98	0	0	0	0	hypothetical protein
BT_3698	BT3698_at	116	493	4.24	1.00	2	3	1	2	glycoside hydrolase family 13
BT_3699	BT3699_at	734	1901	2.59	1.00	3	3	3	3	outer membrane protein SusF
BT_3700	BT3700_at	368	1594	4.33	1.00	2	1	1	3	outer membrane protein SusE
BT_3701	BT3701_at	466	1894	4.06	1.00	3	3	3	3	SusD, outer membrane protein
BT_3702	BT3702_at	692	2607	3.77	1.00	3	3	3	3	SusC, outer membrane protein involved in starch binding
BT_3703	BT3703_at	659	2112	3.21	1.00	3	3	3	3	glycoside hydrolase family 97
BT_3704	BT3704_at	576	1774	3.08	1.00	2	3	2	2	glycoside hydrolase family 13
BT_3774	BT3774_at	226	447	1.97	0.95	3	3	2	3	glycoside hydrolase family 38
BT_3775	BT3775_at	90	322	3.56	1.00	0	0	0	0	glycoside transferase family 32
BT_3776	BT3776_at	118	313	2.66	0.99	0	0	0	0	glycoside transferase family 32
BT_3777	BT3777_at	330	717	2.17	0.99	0	0	0	0	hypothetical protein
BT_3787	BT3787_at	935	2667	2.85	1.00	3	3	3	3	homologous to NHL repeat-containing protein
BT_3788	BT3788_at	793	1991	2.51	1.00	3	3	3	3	SusC homolog
BT_3789	BT3789_at	1102	2414	2.19	0.99	3	3	3	3	SusD homolog
BT_3790	BT3790_at	890	1818	2.04	0.99	1	0	2	0	hypothetical protein
BT_3791	BT3791_at	1092	2453	2.25	0.99	0	0	2	0	hypothetical protein
BT_3792	BT3792_at	679	1643	2.42	0.99	1	0	3	1	glycoside hydrolase family 73
BT_3868	BT3868_at	313	613	1.95	0.98	3	3	3	3	glycoside hydrolase family 20
BT_4187	BT4187_at	220	483	2.20	0.98	2	0	1	0	glycoside hydrolase family 28
BT_4220	BT4220_at	548	1143	2.09	0.99	3	3	3	3	flotillin-like protein
BT_4227	BT4227_at	20	89	4.51	0.96	0	0	0	0	hypothetical protein
BT_4266	BT4266_at	25	123	4.88	0.99	0	0	0	1	hypothetical protein
BT_4267	BT4267_at	20	112	5.54	1.00	2	2	3	2	SusC homolog
BT_4268	BT4268_at	42	167	4.01	1.00	2	1	0	1	SusD homolog
BT_4269	BT4269_at	19	89	4.55	0.98	0	0	0	0	hypothetical protein
BT_4270	BT4270_at	37	153	4.18	1.00	1	0	0	2	homologous to putative chitobiase
BT_4271	BT4271_at	43	92	2.16	0.96	0	0	0	0	hypothetical protein
BT_4272	BT4272_at	78	157	2.01	0.95	0	0	0	0	conserved hypothetical protein with Coagulation factor 5/8 type, C-terminal domain

Locus tag	Probe set	Mono-association average	Bi-association average	Fold change	PPDE (<p)	Detection by MS/MS: Mono-association rep. 1	Mono-association rep. 2	Co-colonization rep. 1	Co-colonization rep. 2	Description
BT_4283	BT4283_at	18	68	3.87	0.96	0	0	0	0	conserved hypothetical protein
BT_4284	BT4284_at	88	257	2.92	0.99	0	0	0	0	hypothetical protein
BT_4285	BT4285_at	137	375	2.73	0.99	0	0	0	0	hypothetical protein
BT_4286	BT4286_at	172	473	2.75	0.99	0	0	0	0	hypothetical protein
BT_4298	BT4298_at	2256	4056	1.80	0.95	3	3	3	3	SusC homolog
BT_4575	BT4575_at	106	224	2.11	0.97	0	0	0	0	conserved hypothetical protein with Peptidase M, neutral zinc metallopeptidases, zinc-binding site domain
BT_4631	BT4631_at	77	261	3.39	0.99	0	0	0	0	putative arylsulfatase precursor
BT_4632	BT4632_at	79	279	3.55	1.00	0	0	0	0	putative galactose oxidase precursor
BT_4633	BT4633_at	77	322	4.18	1.00	0	0	0	0	SusD homolog
BT_4634	BT4634_at	86	335	3.92	1.00	0	1	0	0	SusC homolog

Table S9.

Locus tag	Probe set	Mono-association average	Bi-association average	Fold change	PPDE (<p)	Detection by MS/MS: Mono-assoc. rep. 1	Mono-assoc. rep. 2	Cocol-onization rep. 1	Cocol-onization rep. 2	Description
EUBREC_3638	Er-060123-0025_at	91	144	1.57	0.96	0	0	0	0	Hypothetical protein
EUBREC_3616	Er-060123-0037_at	25	9	-2.62	0.95	0	0	0	0	Hypothetical protein
EUBREC_3613	Er-060123-0038_at	177	109	-1.62	0.95	0	0	0	0	Hypothetical protein
EUBREC_3612	Er-060123-0039_at	197	105	-1.87	1.00	0	0	0	0	chromosome partitioning protein
EUBREC_3611	Er-060123-0040_at	286	145	-1.97	1.00	0	0	0	0	chromosome partitioning protein, ParB family
EUBREC_3606	Er-060123-0042_at	666	306	-2.17	1.00	0	0	0	0	Hypothetical protein
EUBREC_3605	Er-060123-0043_at	239	111	-2.15	1.00	0	0	0	0	Hypothetical protein
EUBREC_3604	Er-060123-0044_at	437	174	-2.51	1.00	0	0	0	0	DNA replication protein DnaC
EUBREC_3602	Er-060123-0046_at	312	113	-2.75	1.00	0	0	0	0	type IV secretion system protein VirD4
EUBREC_3601	Er-060123-0047_at	183	110	-1.66	0.98	0	0	0	0	site-specific DNA recombinase
EUBREC_3599	Er-060123-0048_at	60	28	-2.10	0.98	0	0	0	0	Hypothetical protein
EUBREC_3598	Er-060123-0049_at	71	36	-1.96	0.98	0	0	0	0	DNA primase
EUBREC_3597	Er-060123-0050_at	134	85	-1.58	0.95	0	0	0	0	Hypothetical protein
EUBREC_3593	Er-060123-0051_at	251	95	-2.64	1.00	0	0	0	0	type IV secretion system protein VirD4
EUBREC_3591	Er-060123-0052_at	639	387	-1.65	0.99	0	0	0	0	GntR family transcriptional regulator
EUBREC_3590	Er-060123-0053_at	503	296	-1.70	0.99	0	0	0	0	ABC-2 type transport system ATP-binding protein
EUBREC_3586	Er-060123-0056_at	42	13	-3.20	0.99	0	0	0	0	Hypothetical protein
EUBREC_3578	Er-060123-0064_at	942	589	-1.60	0.99	0	0	0	0	site-specific DNA recombinase
EUBREC_3576	Er-060123-0065_at	206	75	-2.75	1.00	0	0	0	0	Hypothetical protein
EUBREC_3574	Er-060123-0066_at	132	53	-2.49	1.00	0	0	0	0	Hypothetical protein
EUBREC_3573	Er-060123-0068_at	192	94	-2.04	1.00	0	0	0	0	Hypothetical protein
EUBREC_3571	Er-060123-0069_at	123	45	-2.72	1.00	0	0	0	0	Hypothetical protein
EUBREC_3569	Er-060123-0071_at	87	34	-2.57	1.00	0	0	0	0	Hypothetical protein
EUBREC_3566	Er-060123-0073_at	133	55	-2.40	1.00	0	0	0	0	Hypothetical protein
EUBREC_3563	Er-060123-0075_at	85	41	-2.08	0.98	0	0	0	0	Hypothetical protein
EUBREC_3547	Er-060123-0088_at	82	36	-2.25	1.00	0	0	0	0	Hypothetical protein
EUBREC_3543	Er-060123-0089_at	625	351	-1.78	1.00	0	0	0	0	DNA polymerase V
EUBREC_3529	Er-060123-0093_at	398	258	-1.54	0.99	0	0	0	0	site-specific DNA recombinase
EUBREC_3528	Er-060123-0094_at	254	109	-2.33	1.00	0	0	0	0	site-specific DNA recombinase
EUBREC_3527	Er-060123-0095_at	350	180	-1.95	1.00	0	0	0	0	site-specific DNA recombinase
EUBREC_3484	Er-060123-0123_at	85	52	-1.64	0.95	0	0	0	0	Hypothetical protein
EUBREC_3695	Er-060123-0147_at	298	173	-1.72	0.96	0	0	0	0	Hypothetical protein
EUBREC_3698	Er-060123-0149_at	249	444	1.79	1.00	3	1	0	0	chromosome partitioning protein, ParB family
EUBREC_3704	Er-060123-0153_at	2020	1212	-1.67	0.99	3	3	3	0	haloalkane dehalogenase
EUBREC_3708	Er-060123-0157_at	295	538	1.82	0.99	3	3	3	3	spoIIIJ-associated protein
EUBREC_3709	Er-060123-0158_at	336	682	2.03	1.00	0	0	0	0	preprotein translocase YidC subunit
EUBREC_0001	Er-060123-0159_at	370	593	1.60	1.00	0	0	0	0	chromosomal replication initiator protein DnaA
EUBREC_0002	Er-060123-0160_at	886	1354	1.53	0.99	0	1	1	0	DNA polymerase
EUBREC_0017	Er-060123-0173_at	168	40	-4.15	1.00	1	0	0	0	DeoR family transcriptional regulator, fructose operon transcriptional repressor
EUBREC_0018	Er-060123-0174_at	565	198	-2.86	1.00	0	1	0	0	1-phosphofructokinase
EUBREC_0019	Er-060123-0175_at	891	306	-2.91	0.99	3	3	2	0	protein-Np-phosphohistidine-sugar phosphotransferase
EUBREC_0028	Er-060123-0185_at	194	106	-1.83	0.99	0	0	0	0	Hypothetical protein
EUBREC_0056	Er-060123-0203_at	825	1454	1.76	0.95	0	0	0	0	N-acetylmuramoyl-L-alanine amidase
EUBREC_0057	Er-060123-0205_at	370	776	2.10	1.00	3	3	3	1	ornithine carbamoyltransferas
EUBREC_0058	Er-060123-0206_at	205	428	2.09	1.00	1	0	0	0	biotin-[acetyl-CoA-carboxylase] ligase / BirA family transcriptional regulator, biotin operon repressor
EUBREC_0060	Er-060123-0207_at	250	454	1.81	1.00	2	1	0	0	type III pantothenate kinase
EUBREC_0061	Er-060123-0208_at	158	346	2.18	1.00	0	1	0	0	Hypothetical protein
EUBREC_0062	Er-060123-0209_at	273	594	2.18	1.00	3	3	3	2	transcription elongation factor GreA
EUBREC_0063	Er-060123-0210_at	346	680	1.97	1.00	3	3	3	1	lysyl-tRNA synthetase, class II

Locus tag	Probe set	Mono-association average	Bi-association average	Fold change	PPDE (<p)	Detection by MS/MS				Description
						Mono-assoc. rep. 1	Mono-assoc. rep. 2	Cocol-onization rep. 1	Cocol-onization rep. 2	
EUBREC_0069	Er-060123-0215_at	1063	636	-1.67	1.00	0	0	0	0	Hypothetical protein
EUBREC_0079	Er-060123-0218_at	1577	1008	-1.56	0.99	0	0	0	0	integrase/recombinase XerC
EUBREC_0159	Er-060123-0270_at	523	333	-1.57	0.99	0	0	0	0	Hypothetical protein
EUBREC_0163	Er-060123-0271_at	1628	1003	-1.62	1.00	0	0	0	0	DNA (cytosine-5-)-methyltransferase
EUBREC_0166	Er-060123-0275_at	534	338	-1.58	0.98	0	0	0	0	Hypothetical protein
EUBREC_0167	Er-060123-0276_at	578	352	-1.64	0.99	0	0	0	0	Hypothetical protein
EUBREC_0168	Er-060123-0277_at	337	217	-1.55	0.97	0	0	0	0	Hypothetical protein
EUBREC_0175	Er-060123-0279_at	332	216	-1.53	0.98	0	0	0	0	Hypothetical protein
EUBREC_0190	Er-060123-0290_at	56	98	1.73	0.96	1	0	2	0	tyrosyl-tRNA synthetase
EUBREC_0198	Er-060123-0297_at	306	617	2.01	1.00	0	0	0	0	deoxyribonuclease IV
EUBREC_0214	Er-060123-0305_at	87	161	1.86	0.99	0	0	0	0	multidrug resistance protein, MATE family
EUBREC_1937	Er-060123-0323_at	283	980	3.47	1.00	0	0	0	0	N-acetylmuramoyl-L-alanine amidase
EUBREC_1935	Er-060123-0324_at	262	609	2.32	1.00	3	3	3	3	polyribonucleotide nucleotidyltransferase
EUBREC_1926	Er-060123-0333_at	82	127	1.56	0.95	0	0	0	0	adenosylcobyric acid synthase
EUBREC_1924	Er-060123-0335_at	80	144	1.79	0.98	0	0	0	0	adenosylcobinamide kinase / adenosylcobinamide-phosphate guanylyltransferase
EUBREC_1903	Er-060123-0352_at	174	389	2.24	1.00	1	0	0	0	ribosomal protein L11 methyltransferase
EUBREC_1902	Er-060123-0353_at	191	334	1.75	0.99	0	0	0	0	hypothetical protein
EUBREC_1901	Er-060123-0354_at	128	299	2.33	1.00	0	0	0	0	cysteine desulfurase
EUBREC_1900	Er-060123-0355_at	201	475	2.36	1.00	0	0	0	0	thiamine biosynthesis protein ThiI
EUBREC_1897	Er-060123-0356_at	193	392	2.02	1.00	0	0	0	0	2-alkenal reductase
EUBREC_1889	Er-060123-0360_at	34	62	1.85	0.96	0	0	0	0	Hypothetical protein
EUBREC_1869	Er-060123-0378_at	460	720	1.57	0.99	0	0	0	0	Hypothetical protein
EUBREC_1868	Er-060123-0380_at	587	944	1.61	1.00	3	3	3	3	glycyl-tRNA synthetase, class II
EUBREC_1866	Er-060123-0381_at	500	286	-1.75	0.99	0	0	0	0	signal peptidase I
EUBREC_1865	Er-060123-0382_at	2143	1337	-1.60	0.99	0	0	0	0	Hypothetical protein
EUBREC_1863	Er-060123-0384_at	796	513	-1.55	0.97	0	0	0	0	sortase A
EUBREC_1859	Er-060123-0388_at	1205	795	-1.52	0.96	0	0	0	0	Hypothetical protein
EUBREC_1838	Er-060123-0403_at	259	467	1.81	1.00	0	0	0	0	Hypothetical protein
EUBREC_1830	Er-060123-0409_at	418	696	1.67	1.00	3	3	3	0	ferredoxin--NADP+ reductase
EUBREC_1829	Er-060123-0410_at	568	895	1.57	0.99	3	3	3	3	glutamate synthase (NADPH)
EUBREC_1813	Er-060123-0425_at	133	230	1.72	0.99	1	1	0	0	DNA topoisomerase I
EUBREC_1812	Er-060123-0426_at	99	192	1.94	0.99	2	0	0	0	pleiotropic transcriptional repressor CodY
EUBREC_1796	Er-060123-0437_at	954	1499	1.57	1.00	0	0	0	0	Hypothetical protein
EUBREC_1795	Er-060123-0438_at	959	1479	1.54	0.99	0	0	0	0	flagellar motor switch protein FliM
EUBREC_1759	Er-060123-0470_at	47	96	2.04	0.99	0	0	0	0	Hypothetical protein
EUBREC_1746	Er-060123-0480_at	282	449	1.59	0.99	0	0	0	0	DNA repair protein RadC
EUBREC_1743	Er-060123-0483_at	267	408	1.53	0.97	0	0	0	0	Hypothetical protein
EUBREC_1701	Er-060123-0509_at	1967	1104	-1.78	1.00	2	0	0	0	repressor LexA
EUBREC_1699	Er-060123-0510_at	175	378	2.16	1.00	0	0	0	0	nicotinate-nucleotide adenylyltransferase
EUBREC_1698	Er-060123-0511_at	140	294	2.10	1.00	0	0	0	0	nicotinate-nucleotide adenylyltransferase
EUBREC_1696	Er-060123-0512_at	136	284	2.09	1.00	1	1	2	0	GTP-binding protein
EUBREC_1691	Er-060123-0514_at	211	331	1.57	0.99	0	0	0	0	Hypothetical protein
EUBREC_1690	Er-060123-0515_at	212	345	1.63	0.99	0	0	0	0	Hypothetical protein
EUBREC_1677	Er-060123-0527_at	365	552	1.51	0.99	1	0	0	0	site-specific DNA-methyltransferase (adenine-specific)
EUBREC_1675	Er-060123-0528_at	326	497	1.53	0.99	0	1	0	0	2-alkenal reductase
EUBREC_1673	Er-060123-0529_at	469	837	1.79	1.00	2	0	0	0	guanylate kinase
EUBREC_1657	Er-060123-0538_at	159	279	1.75	0.98	0	0	0	0	Hypothetical protein
EUBREC_1655	Er-060123-0539_at	195	341	1.75	0.99	0	0	0	0	holliday junction DNA helicase RuvA
EUBREC_1652	Er-060123-0540_at	302	560	1.86	1.00	0	1	0	0	2-alkenal reductase
EUBREC_1651	Er-060123-0541_at	253	477	1.89	1.00	0	0	0	0	glutamate-5-semialdehyde dehydrogenase
EUBREC_1650	Er-060123-0543_at	204	383	1.88	1.00	0	0	0	0	5-formyltetrahydrofolate cyclo-ligase

Locus tag	Probe set	Mono-association average	Bi-association average	Fold change	PPDE (<p)	Detection by MS/MS				Description
						Mono-assoc. rep. 1	Mono-assoc. rep. 2	Cocol-onization rep. 1	Cocol-onization rep. 2	
EUBREC_1648	Er-060123-0544_at	183	344	1.88	0.99	0	0	0	0	glutamate 5-kinase
EUBREC_1646	Er-060123-0546_at	1853	1183	-1.57	0.99	0	1	1	0	electron transport complex protein RnfB
EUBREC_1645	Er-060123-0547_at	1542	955	-1.62	0.99	0	0	0	0	electron transport complex protein RnfA
EUBREC_1637	Er-060123-0555_at	85	150	1.77	0.99	0	0	0	0	4-hydroxy-3-methylbut-2-enyl diphosphate reductase
EUBREC_1636	Er-060123-0556_at	91	182	2.01	0.99	1	1	0	1	cytidylate kinase
EUBREC_1635	Er-060123-0557_at	80	128	1.59	0.97	0	0	0	0	Hypothetical protein
EUBREC_1596	Er-060123-0559_at	684	445	-1.54	0.99	0	0	0	0	Hypothetical protein
EUBREC_0748	Er-060123-0615_at	135	62	-2.19	0.99	0	0	0	0	bleomycin hydrolase
EUBREC_0747	Er-060123-0616_at	112	39	-2.85	1.00	0	0	0	0	Hypothetical protein
EUBREC_0745	Er-060123-0617_at	152	83	-1.84	0.98	0	0	0	0	Hypothetical protein
EUBREC_0744	Er-060123-0618_at	162	81	-2.00	0.99	0	0	0	0	Hypothetical protein
EUBREC_0740	Er-060123-0619_at	366	163	-2.25	1.00	0	0	0	0	Hypothetical protein
EUBREC_0732	Er-060123-0627_at	845	1303	1.54	0.99	3	3	3	2	carbamoyl-phosphate synthase
EUBREC_0731	Er-060123-0628_at	654	987	1.51	0.99	2	2	3	0	carbamoyl-phosphate synthase
EUBREC_0721	Er-060123-0636_at	391	664	1.70	1.00	0	0	0	0	Hypothetical protein
EUBREC_0716	Er-060123-0638_at	337	539	1.60	0.99	1	0	1	0	carboxyl-terminal processing protease
EUBREC_0710	Er-060123-0643_at	2924	5045	1.73	0.99	0	0	0	0	Hypothetical protein homologous to chitinase
EUBREC_0708	Er-060123-0644_at	338	663	1.96	1.00	0	0	0	0	hypothetical protein
EUBREC_0707	Er-060123-0645_at	252	435	1.73	1.00	0	0	0	0	Hypothetical protein
EUBREC_0704	Er-060123-0647_at	268	146	-1.84	1.00	0	0	0	0	thymidylate synthase
EUBREC_0703	Er-060123-0648_at	286	447	1.56	0.98	2	1	1	0	Glycosyltransferase Family 51 candidate bifunctional family GT51 b-glycosyltransferase/PBP transpeptidase (candidate murein polymerase)
EUBREC_0693	Er-060123-0659_at	86	157	1.84	0.99	0	0	0	0	excinuclease ABC subunit C
EUBREC_0667	Er-060123-0675_at	493	812	1.65	0.99	2	2	0	0	phosphate:Na+ symporter, PNaS family
EUBREC_0646	Er-060123-0691_at	90	155	1.72	0.96	0	0	0	0	Hypothetical protein
EUBREC_0624	Er-060123-0709_at	48	24	-1.98	0.96	0	0	0	0	Hypothetical protein
EUBREC_0609	Er-060123-0717_at	147	80	-1.83	0.98	0	0	0	0	DNA segregation ATPase FtsK/SpoIIIE, S-DNA-T family
EUBREC_2663	Er-060123-0760_at	365	565	1.55	0.97	0	0	0	0	undecaprenyl-phosphate galactose phosphotransferase
EUBREC_2662	Er-060123-0761_at	713	1168	1.64	0.99	2	0	0	0	Hypothetical protein
EUBREC_2659	Er-060123-0762_at	261	531	2.04	1.00	0	0	0	0	Glycosyltransferase Family 4 candidate a-glycosyltransferase
EUBREC_2658	Er-060123-0763_at	405	636	1.57	0.98	1	1	0	0	Glycosyltransferase Family 4 distantly related to a-glycosyltransferases
EUBREC_2657	Er-060123-0764_at	760	1144	1.51	0.98	0	0	0	0	serine O-acetyltransferase
EUBREC_2655	Er-060123-0766_at	389	703	1.80	1.00	0	0	0	0	lipopolysaccharide cholinephosphotransferase
EUBREC_2653	Er-060123-0768_at	251	409	1.63	0.98	0	0	0	0	Hypothetical protein
EUBREC_2630	Er-060123-0782_at	126	210	1.66	0.97	0	0	0	0	polysaccharide transporter, PST family
EUBREC_2608	Er-060123-0802_at	43	80	1.84	0.97	3	1	0	0	choline kinase / choline-phosphate cytidylyltransferase
EUBREC_2598	Er-060123-0809_at	2097	1337	-1.57	0.99	3	3	0	0	hydrophobic/amphiphilic exporter-1 (mainly G- bacteria), HAE1 family
EUBREC_2547	Er-060123-0848_at	357	628	1.76	1.00	0	0	0	0	putative hemolysin
EUBREC_2545	Er-060123-0850_at	399	796	2.00	1.00	3	3	3	3	malate dehydrogenase
EUBREC_2544	Er-060123-0851_at	129	242	1.87	1.00	0	0	0	0	phosphoribosylformimino-5-aminoimidazole carboxamide ribotide isomerase
EUBREC_2543	Er-060123-0852_at	150	225	1.51	0.96	0	2	0	0	glutamine synthetase
EUBREC_2542	Er-060123-0853_at	153	270	1.77	0.99	0	0	0	0	Hypothetical protein
EUBREC_2538	Er-060123-0855_at	135	295	2.18	1.00	3	3	3	0	GTP-binding protein
EUBREC_2536	Er-060123-0857_at	315	509	1.62	0.99	0	0	0	0	Hypothetical protein
EUBREC_2535	Er-060123-0858_at	249	464	1.87	0.98	3	3	2	2	dihydrodipicolinate synthase
EUBREC_2534	Er-060123-0859_at	532	1068	2.01	1.00	3	1	3	0	dihydrodipicolinate reductase
EUBREC_2155	Er-060123-0882_at	291	445	1.53	0.97	0	0	0	0	Hypothetical protein

Locus tag	Probe set	Mono-association average	Bi-association average	Fold change	PPDE (<p)	Detection by MS/MS				Description
						Mono-assoc. rep. 1	Mono-assoc. rep. 2	Cocol-onization rep. 1	Cocol-onization rep. 2	
EUBREC_2153	Er-060123-0884_at	104	186	1.79	0.99	0	0	0	0	argininosuccinate lyase
EUBREC_2152	Er-060123-0885_at	135	221	1.63	0.99	3	3	3	1	aspartate-semialdehyde dehydrogenase
EUBREC_2149	Er-060123-0887_at	405	610	1.51	0.99	0	0	0	0	Hypothetical protein
EUBREC_2101	Er-060123-0915_at	31	58	1.89	0.96	0	0	0	0	Hypothetical protein
EUBREC_2038	Er-060123-0942_at	22	47	2.16	0.96	0	0	0	0	Hypothetical protein
EUBREC_2032	Er-060123-0948_at	891	566	-1.57	0.99	0	0	0	0	two-component system, response regulator Yes
EUBREC_2016	Er-060123-0962_at	128	219	1.71	0.97	0	0	0	0	Hypothetical protein
EUBREC_2007	Er-060123-0966_at	103	166	1.61	0.96	0	0	0	0	Glycosyltransferase Family 28 related to b-glycosyltransferases
EUBREC_2005	Er-060123-0968_at	33	98	2.98	1.00	1	0	1	0	polar amino acid transport system substrate-binding protein
EUBREC_2002	Er-060123-0971_at	3129	5281	1.69	0.99	3	3	3	3	phosphoenolpyruvate carboxykinase (ATP)
EUBREC_1999	Er-060123-0974_at	313	549	1.75	1.00	3	3	3	1	leucyl-tRNA synthetase
EUBREC_1983	Er-060123-0986_at	36	93	2.60	0.99	1	1	2	0	phenylalanyl-tRNA synthetase
EUBREC_1982	Er-060123-0987_at	101	170	1.67	0.95	0	0	0	0	S-adenosylmethionine:tRNA ribosyltransferase-isomerase
EUBREC_1980	Er-060123-0988_at	103	182	1.76	0.97	0	0	0	0	3-phosphoshikimate 1-carboxyvinyltransferase
EUBREC_1970	Er-060123-0992_at	64	108	1.68	0.96	0	0	0	0	2-isopropylmalate synthase
EUBREC_1966	Er-060123-0996_at	399	672	1.69	1.00	0	0	0	0	Hypothetical protein
EUBREC_1965	Er-060123-0997_at	135	237	1.75	1.00	0	0	0	0	Hypothetical protein
EUBREC_1964	Er-060123-0998_at	215	376	1.75	1.00	0	0	0	0	alanine racemase
EUBREC_2313	Er-060123-1002_at	62	103	1.68	0.97	0	0	0	0	putative pyruvate formate lyase activating enzyme
EUBREC_3197	Er-060123-1012_at	327	177	-1.84	1.00	0	0	0	0	Hypothetical protein
EUBREC_3197	Er-060123-1012_x_at	303	157	-1.93	1.00	0	0	0	0	Hypothetical protein
EUBREC_3218	Er-060123-1029_at	30	13	-2.37	0.97	0	0	0	0	Hypothetical protein
EUBREC_3237	Er-060123-1041_at	820	412	-1.99	1.00	0	0	0	0	transposase
EUBREC_3238	Er-060123-1043_at	159	84	-1.90	0.99	0	0	0	0	transposase
EUBREC_3280	Er-060123-1075_at	188	302	1.60	0.98	1	1	0	0	Hypothetical protein
EUBREC_3287	Er-060123-1080_at	72	169	2.33	1.00	1	0	0	0	ATP-dependent RNA helicase DeaD
EUBREC_2820	Er-060123-1085_at	1900	1262	-1.51	0.97	1	3	1	0	Glycoside Hydrolase Family 3 candidate b-glucosidase
EUBREC_2816	Er-060123-1088_at	155	101	-1.53	0.95	0	0	0	0	Glycoside Hydrolase Family 94 distantly related to b-glycan phosphorylases
EUBREC_2815	Er-060123-1089_at	112	69	-1.63	0.95	0	0	0	0	AraC family transcriptional regulator
EUBREC_2804	Er-060123-1096_at	161	243	1.51	0.96	0	0	0	0	Hypothetical protein
EUBREC_2800	Er-060123-1100_at	412	684	1.66	1.00	0	1	0	0	lysophospholipase
EUBREC_2789	Er-060123-1109_at	296	651	2.20	1.00	3	3	3	3	preprotein translocase SecA subunit
EUBREC_2786	Er-060123-1112_at	1024	1562	1.52	1.00	3	3	3	3	rod shape-determining protein MreB and related proteins
EUBREC_2785	Er-060123-1113_at	232	428	1.85	0.99	0	0	0	0	competence protein ComFC
EUBREC_2745	Er-060123-1149_at	340	574	1.69	0.99	0	0	0	0	Hypothetical protein
EUBREC_1253	Er-060123-1154_at	1538	910	-1.69	0.99	3	3	3	1	Hypothetical protein
EUBREC_1319	Er-060123-1192_at	124	189	1.52	0.96	0	0	0	0	phospho-N-acetylmuramoyl-pentapeptide-transferase
EUBREC_1343	Er-060123-1208_at	357	951	2.66	1.00	0	0	0	0	Hypothetical protein
EUBREC_1345	Er-060123-1209_at	277	961	3.47	1.00	0	0	0	0	Hypothetical protein
EUBREC_1346	Er-060123-1210_at	264	870	3.30	1.00	0	0	0	0	Hypothetical protein
EUBREC_1349	Er-060123-1212_at	79	170	2.17	1.00	0	0	0	0	two-component system, CitB family, cit operon sensor histidine kinase CitA
EUBREC_1350	Er-060123-1213_at	578	1934	3.34	1.00	0	0	0	0	Hypothetical protein
EUBREC_1353	Er-060123-1214_at	409	1548	3.78	1.00	0	0	0	0	Hypothetical protein
EUBREC_1376	Er-060123-1234_at	933	618	-1.51	0.98	0	0	0	0	Hypothetical protein
EUBREC_1379	Er-060123-1236_at	784	323	-2.43	1.00	0	1	0	0	Hypothetical protein
EUBREC_1381	Er-060123-1237_at	471	274	-1.72	0.96	0	0	0	0	AraC family transcriptional regulator, L-rhamnose operon transcriptional activator RhaR

Locus tag	Probe set	Mono-association average	Bi-association average	Fold change	PPDE (<p)	Detection by MS/MS				Description
						Mono-assoc. rep. 1	Mono-assoc. rep. 2	Cocol-onization rep. 1	Cocol-onization rep. 2	
EUBREC_1382	Er-060123-1238_at	2469	1155	-2.14	1.00	2	3	2	0	lactose/L-arabinose transport system substrate-binding protein
EUBREC_1383	Er-060123-1239_at	1139	626	-1.82	0.99	0	0	0	0	lactose/L-arabinose transport system permease protein
EUBREC_1384	Er-060123-1240_at	666	291	-2.29	1.00	0	0	0	0	lactose/L-arabinose transport system permease protein
EUBREC_1385	Er-060123-1241_at	214	123	-1.74	0.97	0	0	0	0	Glycoside Hydrolase Family 2 candidate b-galactosidase
EUBREC_1387	Er-060123-1243_at	1344	811	-1.66	1.00	3	3	3	3	galactokinase
EUBREC_3031	Er-060123-1259_at	3686	6231	1.69	0.98	3	3	3	3	Hypothetical protein
EUBREC_3015	Er-060123-1269_at	133	375	2.83	0.97	0	0	0	0	Hypothetical protein
EUBREC_3014	Er-060123-1270_at	181	614	3.39	0.99	0	0	0	0	putative membrane protein
EUBREC_3013	Er-060123-1271_at	283	613	2.16	0.96	0	0	0	0	Hypothetical protein
EUBREC_3012	Er-060123-1272_at	102	159	1.57	0.96	0	0	0	0	Hypothetical protein
EUBREC_3003	Er-060123-1277_at	270	410	1.52	0.99	0	0	0	0	aspartate aminotransferase
EUBREC_3002	Er-060123-1278_at	215	357	1.66	0.99	2	0	0	0	RNA methyltransferase, TrmH family, group 2
EUBREC_2992	Er-060123-1286_at	287	484	1.69	1.00	0	0	0	0	X-Pro aminopeptidase
EUBREC_2989	Er-060123-1288_at	112	215	1.91	0.99	1	0	0	0	putative acetyltransferase
EUBREC_2974	Er-060123-1299_at	304	195	-1.56	0.99	0	0	0	0	Hypothetical protein
EUBREC_2956	Er-060123-1310_at	85	37	-2.30	0.99	0	0	0	0	phosphate transport system permease protein
EUBREC_2947	Er-060123-1319_at	76	43	-1.79	0.96	0	0	0	0	phosphate transport system protein
EUBREC_2944	Er-060123-1322_at	150	305	2.04	1.00	0	0	0	0	Hypothetical protein
EUBREC_2943	Er-060123-1323_at	83	262	3.14	1.00	0	0	0	0	ATP-binding cassette, sub-family F, member 3
EUBREC_2934	Er-060123-1329_at	89	141	1.59	0.97	0	0	0	0	GMP synthase (glutamine-hydrolysing)
EUBREC_2922	Er-060123-1341_at	355	200	-1.77	1.00	0	0	0	0	endonuclease
EUBREC_2919	Er-060123-1344_at	170	293	1.72	0.99	0	0	0	0	Hypothetical protein
EUBREC_2912	Er-060123-1350_at	106	173	1.63	0.96	0	0	0	0	Hypothetical protein
EUBREC_2463	Er-060123-1362_at	245	112	-2.18	1.00	0	1	0	0	DeoR family transcriptional regulator, fructose operon transcriptional repressor
EUBREC_2478	Er-060123-1375_at	547	962	1.76	1.00	0	0	0	0	Na+:H+ antiporter, NhaC family
EUBREC_2479	Er-060123-1376_at	515	820	1.59	0.99	3	2	3	1	dihydroorotate oxidase
EUBREC_2480	Er-060123-1377_at	395	685	1.73	1.00	1	0	1	1	dihydroorotate dehydrogenase electron transfer subunit
EUBREC_2481	Er-060123-1378_at	549	840	1.53	0.99	3	3	3	3	orotidine-5'-phosphate decarboxylase
EUBREC_2505	Er-060123-1391_at	1349	846	-1.59	0.99	0	0	0	0	Hypothetical protein
EUBREC_2522	Er-060123-1406_at	620	937	1.51	0.99	0	0	0	0	Hypothetical protein
EUBREC_2527	Er-060123-1411_at	146	246	1.68	0.98	3	3	2	0	thiamine biosynthesis protein ThiC
EUBREC_2528	Er-060123-1413_at	89	182	2.03	1.00	2	2	1	1	hydroxymethylpyrimidine kinase / phosphomethylpyrimidine kinase
EUBREC_2529	Er-060123-1415_at	70	127	1.81	0.97	0	0	0	0	thiamine-phosphate pyrophosphorylase
EUBREC_0351	Er-060123-1418_at	480	735	1.53	0.99	3	3	3	1	aldose 1-epimerase
EUBREC_0354	Er-060123-1420_at	127	211	1.66	0.99	0	0	0	0	Hypothetical protein
EUBREC_0358	Er-060123-1423_at	9416	4578	-2.06	1.00	3	2	3	2	Hypothetical protein
EUBREC_0373	Er-060123-1431_at	2307	3974	1.72	0.99	2	1	1	0	transcriptional antiterminator NusG
EUBREC_0376	Er-060123-1434_at	2312	3661	1.58	0.97	3	3	3	3	large subunit ribosomal protein L10
EUBREC_0385	Er-060123-1440_at	965	617	-1.56	0.99	0	0	0	0	Hypothetical protein
EUBREC_0389	Er-060123-1443_at	79	43	-1.83	0.98	0	0	0	0	integrase/recombinase XerC
EUBREC_0390	Er-060123-1444_at	45	18	-2.45	0.98	0	0	0	0	Hypothetical protein
EUBREC_0418	Er-060123-1462_at	1226	2441	1.99	1.00	3	3	3	3	large subunit ribosomal protein L3
EUBREC_0419	Er-060123-1463_at	921	1570	1.70	0.98	3	3	3	3	large subunit ribosomal protein L4
EUBREC_1101	Er-060123-1482_at	2307	1468	-1.57	0.99	0	0	0	0	Hypothetical protein
EUBREC_1102	Er-060123-1483_at	1759	1166	-1.51	0.99	0	0	0	0	pilus assembly protein CpaF
EUBREC_1109	Er-060123-1489_at	995	660	-1.51	0.99	0	0	0	0	Hypothetical protein
EUBREC_1119	Er-060123-1497_at	59	117	1.97	0.98	3	0	2	0	glycine hydroxymethyltransferase
EUBREC_1395	Er-060123-1545_at	270	420	1.56	0.99	1	0	0	0	DNA helicase II / ATP-dependent DNA helicase PcrA
EUBREC_1390	Er-060123-1548_at	265	418	1.58	0.99	0	0	0	0	histidinol-phosphate aminotransferase

Locus tag	Probe set	Mono-association average	Bi-association average	Fold change	PPDE (<p)	Detection by MS/MS				Description
						Mono-assoc. rep. 1	Mono-assoc. rep. 2	Cocol-onization rep. 1	Cocol-onization rep. 2	
EUBREC_2841	Er-060123-1560_at	241	129	-1.86	1.00	1	0	0	0	3-dehydroquinate dehydratase
EUBREC_2854	Er-060123-1568_at	483	246	-1.96	0.97	0	0	0	0	molecular chaperone DnaJ
EUBREC_2874	Er-060123-1587_at	831	483	-1.72	0.99	1	0	0	0	Hypothetical protein
EUBREC_2878	Er-060123-1588_at	1116	580	-1.93	1.00	0	0	0	0	Hypothetical protein
EUBREC_2880	Er-060123-1590_at	86	48	-1.80	0.98	0	0	0	0	Hypothetical protein
EUBREC_2883	Er-060123-1594_at	77	43	-1.80	0.97	0	0	0	0	Hypothetical protein
EUBREC_2886	Er-060123-1597_at	186	97	-1.91	0.99	0	0	0	0	multiple sugar transport system permease protein
EUBREC_2887	Er-060123-1598_at	703	383	-1.84	1.00	0	0	0	0	two-component system, response regulator YesN
EUBREC_2888	Er-060123-1599_at	608	370	-1.64	0.99	0	0	0	0	two-component system, sensor histidine kinase YesM
EUBREC_2889	Er-060123-1600_at	551	313	-1.76	1.00	0	0	0	0	Hypothetical protein
EUBREC_2897	Er-060123-1606_at	81	147	1.82	0.99	3	3	3	1	F-type H+-transporting ATPase beta chain
EUBREC_2898	Er-060123-1607_at	67	118	1.76	0.97	0	0	0	0	Na+-transporting two-sector ATPase
EUBREC_2899	Er-060123-1608_at	83	149	1.79	0.97	1	2	0	0	F-type H+-transporting ATPase alpha chain
EUBREC_2900	Er-060123-1609_at	57	129	2.27	1.00	0	0	0	0	Hypothetical protein
EUBREC_0885	Er-060123-1635_at	81	131	1.63	0.97	0	0	0	0	type I restriction enzyme, S subunit
EUBREC_0886	Er-060123-1636_at	120	225	1.87	0.99	0	0	0	0	type I restriction enzyme
EUBREC_0893	Er-060123-1643_at	209	124	-1.69	0.98	0	0	0	0	thioredoxin reductase (NADPH)
EUBREC_0895	Er-060123-1645_at	318	198	-1.60	0.99	0	0	0	0	coenzyme F420 hydrogenase
EUBREC_0902	Er-060123-1648_at	128	196	1.53	0.96	0	0	0	0	uroporphyrin-III C-methyltransferase / precorrin-2 dehydrogenase / sirohydrochlorin ferrochelatase
EUBREC_2267	Er-060123-1687_at	23	72	3.15	0.98	0	0	0	0	antibiotic transport system ATP-binding protein
EUBREC_2265	Er-060123-1689_at	50	102	2.04	0.96	0	0	0	0	Hypothetical protein
EUBREC_2261	Er-060123-1692_at	1122	1787	1.59	0.99	3	3	3	3	Hypothetical protein
EUBREC_2257	Er-060123-1694_at	81	147	1.82	0.97	0	0	0	0	Hypothetical protein
EUBREC_2244	Er-060123-1707_at	3236	2112	-1.53	0.98	1	2	0	0	metallo-beta-lactamase family protein
EUBREC_2243	Er-060123-1708_at	641	383	-1.68	0.99	0	0	0	0	Hypothetical protein
EUBREC_2242	Er-060123-1709_at	962	619	-1.55	0.99	0	0	0	0	putative two-component system response regulator
EUBREC_2229	Er-060123-1718_at	84	188	2.23	1.00	3	2	1	0	peptide chain release factor RF-3
EUBREC_2223	Er-060123-1724_at	56	101	1.80	0.98	3	2	1	0	3-deoxy-7-phosphoheptulonate synthase
EUBREC_2219	Er-060123-1726_at	87	153	1.77	0.97	0	0	0	0	ribosomal large subunit pseudouridine synthase F
EUBREC_2218	Er-060123-1727_at	105	171	1.63	0.97	0	1	0	0	DNA ligase (NAD+)
EUBREC_3149	Er-060123-1753_at	209	130	-1.61	0.98	0	0	0	0	Hypothetical protein
EUBREC_3152	Er-060123-1756_at	167	90	-1.86	0.99	0	0	0	0	AbrB family transcriptional regulator, stage V sporulation protein T
EUBREC_3158	Er-060123-1762_at	1359	854	-1.59	0.99	2	1	0	0	Hypothetical protein
EUBREC_3169	Er-060123-1774_at	410	269	-1.52	0.98	0	0	0	0	xanthine dehydrogenase accessory factor
EUBREC_3181	Er-060123-1783_at	1061	1887	1.78	1.00	0	0	0	0	Hypothetical protein
EUBREC_3184	Er-060123-1785_at	829	1413	1.70	1.00	0	0	0	0	Hypothetical protein
EUBREC_1197	Er-060123-1790_at	960	581	-1.65	0.99	0	0	0	0	Hypothetical protein
EUBREC_1208	Er-060123-1798_at	535	294	-1.82	0.98	0	0	0	0	arsenical pump membrane protein
EUBREC_1213	Er-060123-1803_at	1361	701	-1.94	1.00	3	3	3	2	5-methyltetrahydropteroyltriglutamate--homocysteine methyltransferase
EUBREC_1227	Er-060123-1808_at	724	275	-2.63	1.00	3	3	3	3	ferredoxin hydrogenase large subunit
EUBREC_1229	Er-060123-1809_at	537	329	-1.63	0.99	0	0	0	0	putative two-component system response regulator
EUBREC_1249	Er-060123-1822_at	269	453	1.68	0.99	1	1	0	0	dihydrofolate reductase
EUBREC_1250	Er-060123-1823_at	217	357	1.64	0.99	0	1	0	0	acetolactate synthase large subunit
EUBREC_1535	Er-060123-1827_at	796	440	-1.81	1.00	0	0	0	0	Hypothetical protein
EUBREC_1529	Er-060123-1830_at	631	415	-1.52	0.97	0	0	0	0	twitching motility protein PilT
EUBREC_1519	Er-060123-1839_at	113	183	1.61	0.97	0	0	0	0	nicotinate phosphoribosyltransferase
EUBREC_1518	Er-060123-1840_at	236	359	1.52	0.98	3	3	3	3	phosphoribosylformylglycinamidine synthase
EUBREC_1509	Er-060123-1847_at	92	178	1.93	0.98	0	0	0	0	tRNA (guanine-N1-)-methyltransferase
EUBREC_1508	Er-060123-1849_at	77	172	2.22	0.97	1	1	0	0	16S rRNA processing protein RimM

Locus tag	Probe set	Mono-association average	Bi-association average	Fold change	PPDE (<p)	Detection by MS/MS				Description
						Mono-assoc. rep. 1	Mono-assoc. rep. 2	Cocol-onization rep. 1	Cocol-onization rep. 2	
EUBREC_1505	Er-060123-1851_at	451	758	1.68	1.00	3	3	1	1	signal recognition particle, subunit SRP54
EUBREC_1486	Er-060123-1868_at	128	194	1.52	0.96	0	0	0	0	hypothetical protein
EUBREC_1471	Er-060123-1881_at	127	197	1.55	0.96	3	0	1	0	Hypothetical protein
EUBREC_1470	Er-060123-1882_at	6928	4394	-1.58	0.97	0	0	0	0	Hypothetical protein
EUBREC_1461	Er-060123-1892_at	183	326	1.78	0.98	0	0	0	0	Hypothetical protein
EUBREC_1458	Er-060123-1894_at	32	76	2.37	0.97	0	0	0	0	Hypothetical protein
EUBREC_1443	Er-060123-1905_at	124	209	1.69	0.98	3	3	3	3	phosphate acetyltransferase
EUBREC_1441	Er-060123-1908_at	66	146	2.20	1.00	0	0	0	0	quanylate kinase
EUBREC_3289	Er-060123-1910_at	687	56	-12.36	1.00	0	0	0	0	putative biotin biosynthesis protein BioY
EUBREC_3296	Er-060123-1918_at	246	148	-1.66	0.98	0	0	0	0	methicillin resistance protein
EUBREC_0832	Er-060123-1939_at	159	264	1.66	0.99	2	1	0	0	Hypothetical protein
EUBREC_0826	Er-060123-1944_at	126	217	1.72	0.97	0	0	0	0	Hypothetical protein
EUBREC_0825	Er-060123-1945_at	461	907	1.97	1.00	0	0	0	0	glucosamine--fructose-6-phosphate aminotransferase (isomerizing)
EUBREC_1038	Er-060123-1960_at	184	371	2.02	1.00	0	0	0	0	multiple sugar transport system substrate-binding protein
EUBREC_1040	Er-060123-1962_at	458	304	-1.51	0.98	0	0	0	0	Glycoside Hydrolase Family 8 candidate reducing-end-xylose releasing exo-oligoxylanase
EUBREC_1043	Er-060123-1965_at	202	129	-1.56	0.96	0	0	0	0	two-component system, response regulator YesN
EUBREC_1053	Er-060123-1977_at	182	285	1.56	0.97	3	2	1	0	isoleucyl-tRNA synthetase
EUBREC_1011	Er-060123-1989_at	264	462	1.75	1.00	0	0	0	0	Hypothetical protein
EUBREC_0996	Er-060123-2001_at	618	371	-1.67	1.00	0	0	0	0	Hypothetical protein
EUBREC_0991	Er-060123-2007_at	171	427	2.50	1.00	1	0	0	1	ATP-dependent Lon protease
EUBREC_0990	Er-060123-2008_at	377	712	1.89	0.99	3	3	1	2	ATP-dependent Clp protease ATP-binding subunit ClpX
EUBREC_0988	Er-060123-2010_at	951	1883	1.98	1.00	3	3	3	3	trigger factor
EUBREC_0984	Er-060123-2012_at	237	400	1.68	0.99	0	0	0	0	Hypothetical protein
EUBREC_0982	Er-060123-2014_at	151	232	1.54	0.97	0	0	0	0	Hypothetical protein
EUBREC_0981	Er-060123-2015_at	284	1117	3.93	1.00	3	2	3	3	peptide/nickel transport system substrate-binding protein
EUBREC_0980	Er-060123-2016_at	123	471	3.83	1.00	3	1	2	1	peptide/nickel transport system ATP-binding protein
EUBREC_0979	Er-060123-2017_at	159	420	2.64	1.00	3	1	2	2	peptide/nickel transport system ATP-binding protein
EUBREC_0978	Er-060123-2018_at	92	325	3.53	1.00	2	2	2	0	peptide/nickel transport system permease protein
EUBREC_0977	Er-060123-2019_at	82	265	3.21	1.00	0	0	0	0	peptide/nickel transport system permease protein
EUBREC_0973	Er-060123-2020_at	52	94	1.81	0.97	0	0	0	0	Hypothetical protein
EUBREC_3107	Er-060123-2059_at	482	245	-1.97	1.00	0	0	0	0	RNA polymerase sigma-70 factor, ECF subfamily
EUBREC_3106	Er-060123-2060_at	773	450	-1.72	0.99	0	0	0	0	Hypothetical protein
EUBREC_3105	Er-060123-2061_at	1083	523	-2.07	1.00	0	0	0	0	ABC-2 type transport system ATP-binding protein
EUBREC_3104	Er-060123-2062_at	833	489	-1.70	0.99	0	0	0	0	Hypothetical protein
EUBREC_3100	Er-060123-2064_at	1727	493	-3.50	1.00	3	2	0	2	hydrogenase 1 maturation protease
EUBREC_1092	Er-060123-2099_at	551	295	-1.87	1.00	0	0	0	0	Hypothetical protein
EUBREC_1081	Er-060123-2110_at	5969	1499	-3.98	1.00	3	3	1	1	Glycoside Hydrolase Family 13 candidate a-amylase with C-terminal cell surface anchor
EUBREC_1076	Er-060123-2115_at	1281	2363	1.85	0.99	0	0	0	0	lactose/L-arabinose transport system permease protein
EUBREC_1075	Er-060123-2117_at	1292	2481	1.92	1.00	0	0	0	0	lactose/L-arabinose transport system permease protein
EUBREC_1072	Er-060123-2120_at	595	905	1.52	0.97	0	0	0	0	Glycoside Hydrolase Family 94 candidate cellobiose phosphorylase
EUBREC_0283	Er-060123-2128_at	160	105	-1.52	0.96	0	0	0	0	multiple sugar transport system substrate-binding protein
EUBREC_0282	Er-060123-2129_at	102	53	-1.95	0.98	0	0	0	0	Glycoside Hydrolase Family 32 related to b-fructosidases and b-fructosyltransferases
EUBREC_1187	Er-060123-2137_at	49	26	-1.87	0.96	0	0	0	0	Hypothetical protein
EUBREC_1185	Er-060123-2139_at	51	23	-2.22	0.97	0	0	0	0	maltose/maltodextrin transport system permease protein
EUBREC_1184	Er-060123-2140_at	88	54	-1.62	0.96	0	0	0	0	maltose/maltodextrin transport system permease protein
EUBREC_1177	Er-060123-2146_at	59	31	-1.90	0.97	0	0	0	0	Lrp/AsnC family transcriptional regulator, leucine-responsive regulatory protein

Locus tag	Probe set	Mono-association average	Bi-association average	Fold change	PPDE (<p)	Detection by MS/MS				Description
						Mono-assoc. rep. 1	Mono-assoc. rep. 2	Cocol-onization rep. 1	Cocol-onization rep. 2	
EUBREC_1175	Er-060123-2148_at	447	826	1.85	1.00	3	1	2	1	citrate synthase
EUBREC_1173	Er-060123-2150_at	326	500	1.54	0.99	0	0	0	0	Hypothetical protein
EUBREC_1141	Er-060123-2169_at	213	140	-1.53	0.97	0	0	0	0	Hypothetical protein
EUBREC_0513	Er-060123-2171_at	248	394	1.59	0.99	0	0	0	0	GntR family transcriptional regulator, transcriptional repressor for pyruvate dehydrogenase complex
EUBREC_0500	Er-060123-2179_at	883	526	-1.68	0.99	1	0	0	0	Glycoside Hydrolase Family 31 candidate a-glucosidase
EUBREC_0499	Er-060123-2180_at	910	384	-2.37	0.98	0	0	0	0	Glycoside Hydrolase Family 31 candidate a-glycosidase
EUBREC_0498	Er-060123-2181_at	749	331	-2.26	0.98	0	0	0	0	multiple sugar transport system permease protein
EUBREC_0497	Er-060123-2182_at	624	265	-2.36	0.98	0	0	0	0	multiple sugar transport system permease protein
EUBREC_0496	Er-060123-2183_at	1317	618	-2.13	0.99	1	0	0	0	multiple sugar transport system substrate-binding protein
EUBREC_0479	Er-060123-2199_at	950	3451	3.63	1.00	3	3	3	3	methyl-galactoside transport system permease protein
EUBREC_0478	Er-060123-2200_at	1001	3564	3.56	1.00	2	2	2	0	methyl-galactoside transport system ATP-binding protein
EUBREC_0477	Er-060123-2201_at	3616	8681	2.40	1.00	3	3	3	3	methyl-galactoside transport system substrate-binding protein
EUBREC_0469	Er-060123-2204_at	597	256	-2.34	1.00	3	3	3	3	formate C-acetyltransferase
EUBREC_2331	Er-060123-2217_at	546	317	-1.72	0.99	3	0	3	0	L-lactate dehydrogenase
EUBREC_2342	Er-060123-2230_at	129	233	1.81	0.99	0	0	0	0	Hypothetical protein
EUBREC_2343	Er-060123-2231_at	158	311	1.97	1.00	0	0	0	0	Sun protein
EUBREC_2344	Er-060123-2232_at	209	386	1.84	1.00	0	0	0	0	Hypothetical protein
EUBREC_2345	Er-060123-2233_at	221	381	1.72	0.99	0	0	1	0	methionyl-tRNA formyltransferase
EUBREC_2347	Er-060123-2235_at	252	420	1.67	0.99	0	0	0	0	primosomal protein N' (replication factor Y) (superfamily II helicase)
EUBREC_2360	Er-060123-2245_at	261	424	1.62	0.99	0	0	0	0	dGTPase
EUBREC_2361	Er-060123-2246_at	44	83	1.87	0.97	0	0	0	0	Hypothetical protein
EUBREC_0937	Er-060123-2255_at	72	121	1.68	0.96	0	0	0	0	two-component system, LytT family, response regulator LytT
EUBREC_0920	Er-060123-2269_at	712	86	-8.30	1.00	3	2	0	0	biotin synthetase
EUBREC_2426	Er-060123-2286_at	2027	1095	-1.85	1.00	2	0	0	0	Glycosyltransferase Family 35 candidate glycogen phosphorylase
EUBREC_2427	Er-060123-2287_at	230	138	-1.67	0.99	0	0	0	0	AraC family transcriptional regulator, L-rhamnose operon transcriptional activator RhaR
EUBREC_1549	Er-060123-2291_at	134	293	2.18	1.00	0	0	0	0	nucleobase:cation symporter-2, NCS2 family
EUBREC_1557	Er-060123-2297_at	139	216	1.56	0.97	0	0	0	0	Hypothetical protein
EUBREC_1573	Er-060123-2309_at	448	731	1.63	0.98	3	2	0	0	molecular chaperone HtpG
EUBREC_1600	Er-060123-2313_at	86	154	1.80	0.98	1	1	0	0	Hypothetical protein
EUBREC_1604	Er-060123-2316_at	121	230	1.90	0.99	0	0	0	0	hypothetical protein
EUBREC_1608	Er-060123-2318_at	58	113	1.95	0.98	1	0	0	0	N-acetyl-gamma-glutamyl-phosphate reductase
EUBREC_1610	Er-060123-2319_at	44	98	2.25	0.98	2	1	0	0	acetylglutamate kinase
EUBREC_1611	Er-060123-2320_at	79	190	2.41	1.00	0	1	0	1	acetylornithine aminotransferase
EUBREC_0258	Er-060123-2344_at	3165	1130	-2.80	1.00	3	3	3	2	fructokinase
EUBREC_0257	Er-060123-2345_at	6388	2704	-2.36	1.00	3	3	3	0	Glycoside Hydrolase Family 32 related to b-fructosidases and b-fructosyltransferases
EUBREC_0256	Er-060123-2346_at	6993	3296	-2.12	1.00	3	3	3	2	multiple sugar transport system substrate-binding protein
EUBREC_0255	Er-060123-2347_at	5440	2538	-2.14	1.00	1	0	0	0	multiple sugar transport system permease protein
EUBREC_0254	Er-060123-2348_at	6496	2848	-2.28	1.00	0	0	0	0	multiple sugar transport system permease protein
EUBREC_0253	Er-060123-2349_at	56	86	1.55	0.95	0	0	0	0	LacI family transcriptional regulator, sucrose operon repressor
EUBREC_0251	Er-060123-2351_at	83	144	1.73	0.98	0	0	0	0	multidrug resistance protein, MATE family
EUBREC_2390	Er-060123-2381_at	5196	1786	-2.91	1.00	3	3	3	3	ferredoxin hydrogenase
EUBREC_0139	Er-060123-2398_at	85	140	1.64	0.95	1	0	0	0	Hypothetical protein
EUBREC_0533	Er-060123-2408_at	111	172	1.54	0.97	0	0	0	0	cell cycle protein MesJ
EUBREC_0534	Er-060123-2410_at	263	405	1.54	0.99	3	3	3	1	hypoxanthine phosphoribosyltransferase

Locus tag	Probe set	Mono-association average	Bi-association average	Fold change	PPDE (<p)	Detection by MS/MS				Description
						Mono-assoc. rep. 1	Mono-assoc. rep. 2	Cocol-onization rep. 1	Cocol-onization rep. 2	
EUBREC_0535	Er-060123-2411_at	379	572	1.51	0.99	2	2	0	0	microtubule-severing ATPase
EUBREC_0540	Er-060123-2414_at	7212	4401	-1.64	0.99	0	0	0	0	Glycoside Hydrolase Family 77 candidate 4-a-glucanotransferase
EUBREC_0541	Er-060123-2415_at	4823	2835	-1.70	0.99	0	0	0	0	Glycoside Hydrolase Family 77 candidate 4-a-glucanotransferase
EUBREC_2453	Er-060123-2439_at	304	170	-1.79	0.99	0	0	0	0	Glycoside Hydrolase Family 42 candidate b-galactosidase
EUBREC_3346	Er-060123-2444_at	4936	2654	-1.86	1.00	0	0	0	0	Hypothetical protein
EUBREC_3345	Er-060123-2445_at	118	203	1.71	0.98	0	0	0	0	lysine decarboxylase
EUBREC_3343	Er-060123-2447_at	372	622	1.67	1.00	0	0	0	0	saccharopine dehydrogenase (NAD+, L-lysine forming)
EUBREC_3341	Er-060123-2449_at	81	133	1.65	0.97	0	0	0	0	agmatine deiminase
EUBREC_0313	Er-060123-2469_at	389	238	-1.64	0.98	0	0	0	0	Hypothetical protein
EUBREC_3685	Er-060123-2478_at	85	425	5.01	1.00	0	0	0	0	multidrug resistance protein, MATE family
EUBREC_3687	Er-060123-2479_at	189	1266	6.71	1.00	0	0	0	0	Glycoside Hydrolase Family 1 candidate 6-P-b-glucosidase
EUBREC_3689	Er-060123-2480_at	1127	3666	3.25	1.00	0	0	0	0	PTS system, cellobiose-specific IIC component
EUBREC_0457	Er-060123-2491_at	244	368	1.50	0.98	0	0	0	0	Hypothetical protein
EUBREC_1957	Er-060123-2501_at	415	628	1.52	0.99	1	1	0	0	methylenetetrahydrofolate dehydrogenase (NADP+)
EUBREC_1953	Er-060123-2505_at	1310	2131	1.63	0.99	3	3	2	2	translation initiation factor IF-3
EUBREC_0234	Er-060123-2508_at	223	38	-5.86	1.00	0	0	0	0	biotin synthetase
EUBREC_0235	Er-060123-2509_at	400	37	-10.75	1.00	0	2	0	0	thiamine biosynthesis ThiH
EUBREC_0236	Er-060123-2510_at	352	58	-6.08	1.00	0	0	0	0	GTP-binding protein
EUBREC_0237	Er-060123-2511_at	371	124	-2.98	1.00	0	0	0	0	Hypothetical protein
EUBREC_0241	Er-060123-2515_at	1242	765	-1.62	0.99	0	0	0	0	Mg-dependent DNase
EUBREC_0292	Er-060123-2519_at	781	478	-1.63	0.97	1	0	0	0	uridine phosphorylase
EUBREC_0293	Er-060123-2520_at	640	384	-1.67	0.98	0	0	0	0	deoxyribose-phosphate aldolase
EUBREC_1583	Er-060123-2526_at	102	34	-2.99	1.00	0	0	0	0	ferrous iron transport protein B
EUBREC_1586	Er-060123-2527_at	68	23	-2.99	0.99	0	0	0	0	Hypothetical protein
EUBREC_1587	Er-060123-2528_at	224	72	-3.13	1.00	0	0	0	0	Hypothetical protein
EUBREC_2197	Er-060123-2532_at	100	222	2.22	1.00	0	0	0	0	neurotransmitter:Na+ symporter, NSS family
EUBREC_2192	Er-060123-2537_at	147	422	2.87	1.00	0	0	0	0	Hypothetical protein
EUBREC_3363	Er-060123-2540_at	109	184	1.70	0.98	0	0	0	0	Hypothetical protein
EUBREC_0682	Er-060123-2545_at	238	377	1.59	0.99	1	1	0	0	Hypothetical protein
EUBREC_0304	Er-060123-2552_at	172	91	-1.89	0.96	0	0	0	0	Hypothetical protein
EUBREC_3318	Er-060123-2561_s_at	151	82	-1.84	0.99	0	0	0	0	Hypothetical protein
EUBREC_3574	Er-060123-2580_s_at	123	31	-3.94	1.00	0	0	0	0	Hypothetical protein
EUBREC_3574	Er-060123-2580_x_at	143	54	-2.64	1.00	0	0	0	0	Hypothetical protein
EUBREC_3574	Er-060123-2584_s_at	78	24	-3.33	1.00	0	0	0	0	Hypothetical protein
EUBREC_2160	Er-060123-tRNA09_at	89	42	-2.10	0.99	0	0	0	0	tRNA-Thr-4
EUBREC_2299	Er-060123-tRNA15_at	479	287	-1.67	0.96	0	0	0	0	tRNA-Trp
EUBREC_0347	Er-060123-tRNA26_at	848	315	-2.69	1.00	0	0	0	0	tRNA-Met
EUBREC_0850	Er-060123-tRNA30_at	140	58	-2.40	0.98	0	0	0	0	tRNA-Glu-3
EUBREC_2363	Er-060123-tRNA44_at	4570	2303	-1.98	0.98	0	0	0	0	tRNA-Leu
EUBREC_2363	Er-060123-tRNA44_x_	4460	2295	-1.94	0.97	0	0	0	0	tRNA-Leu
EUBREC_0916	Er-060123-tRNA49_at	558	251	-2.22	1.00	0	0	0	0	tRNA-His
EUBREC_0916	Er-060123-tRNA49_x_	557	213	-2.61	1.00	0	0	0	0	tRNA-His

Table S10.

Please access provided CD for this information.

Table S11.

Please access provided CD for this information.

Table S12.

		Predicted proteins	Observed by MS/MS[a]
E. rectale			
	Total	3627	680
Without annotation[b]		1111	25
B. thetaiotaomicron			
Original	Total	4778	1687
	Without annotation[b]	1527	293
Additional[c]	Add'l predictions	180	10
	Add'l w/o annotation[b]	173	7

Table S13.

Locus tag	Probe set	Mono-association average	Biassoc-iation average	Fold change	Baysian p-value	Corrected p-value	Description
BT_0866	BT0866_at	1269	291	-4.4	1.4E-05	4.4E-02	SusD homolog
BT_1030	BT1030_at	62	424	6.9	5.0E-04	3.0E-02	conserved hypothetical protein with Fibronectin, type III-like fold domain
BT_3221	BT3221_at	71	2401	33.9	1.8E-03	2.7E-07	hypothetical protein
BT_3222	BT3222_at	356	14984	42.0	7.0E-03	4.9E-06	hypothetical protein
BT_3223	BT3223_at	209	7538	36.0	4.0E-02	2.1E-06	hypothetical protein
BT_3224	BT3224_at	163	1674	10.3	1.6E-03	6.6E-04	homologous to putative lysine decarboxylase
BT_3225	BT3225_at	84	645	7.7	9.4E-04	2.5E-02	conserved hypothetical protein

Table S14.

Probe set name	locus tag	Mono-association mean	Biassoc-iation mean	fold change	PPDE(<p)	Description
Bv-GM2830_at	N/A	56	224	3.97	0.96	Hypothetical protein
Bv-GM3615_at	N/A	8	123	15.27	1.00	Hypothetical protein
Bv-GM4084_at	N/A	724	212	-3.42	0.97	Hypothetical protein
Bv0039c_at	BVU_0039	31	271	8.63	0.97	glycoside hydrolase family 43, candidate beta-xylosidase/alpha-L-arabinofuranosidase
Bv0041c_at	BVU_0041	60	388	6.47	0.99	glycoside hydrolase family 10, candidate beta-xylanase
Bv0157c_at	BVU_0159	48	513	10.74	1.00	conserved hypothetical protein
Bv0165c_at	BVU_0167	115	1298	11.25	0.99	putative outer membrane protein, probably involved in nutrient binding
Bv0173_at	BVU_0175	23	156	6.78	0.99	putative acetyl xylan esterase
Bv0347c_at	BVU_0356	34	285	8.26	0.98	conserved hypothetical protein
Bv0348c_at	BVU_0357	28	242	8.60	0.99	glycerol kinase 2 (ATP:glycerol 3-phosphotransferase 2)
Bv0349c_at	BVU_0358	12	134	11.33	1.00	transketolase, C-terminal subunit
Bv0350c_at	BVU_0359	87	514	5.93	0.95	transketolase, N-terminal subunit
Bv0378_at	BVU_0388	220	752	3.42	0.97	putative anti-sigma factor
Bv0379_at	BVU_0389	247	1060	4.29	0.95	putative outer membrane protein, probably involved in nutrient binding
Bv0472c_at	BVU_0490	203	722	3.56	0.98	conserved hypothetical protein
Bv0473c_at	BVU_0491	141	763	5.42	0.99	glycoside hydrolase family 31, candidate alpha-glycosidase; related to beta-xylosidases
Bv0550_at	BVU_0568	752	3323	4.42	0.95	putative outer membrane protein, probably involved in nutrient binding
Bv0577_at	BVU_0595	131	456	3.49	0.97	rhamnulose kinase/L-fuculose kinase
Bv0579_at	BVU_0597	206	678	3.29	0.98	L-rhamnose/H+ symporter
Bv0716c_at	BVU_0736	12445	164	-75.92	1.00	glycoside hydrolase family 36, candidate alpha-glycosidase; related to alpha-galactosidases
Bv0916_at	BVU_0945	3151	824	-3.82	0.95	putative anti-sigma factor
Bv0917_at	BVU_0946	3941	529	-7.45	1.00	putative outer membrane protein, probably involved in nutrient binding
Bv0918_at	BVU_0947	3762	592	-6.36	1.00	putative outer membrane protein, probably involved in nutrient binding
Bv0919_at	BVU_0948	3546	517	-6.86	1.00	conserved hypothetical protein
Bv0920_at	BVU_0949	2227	450	-4.95	1.00	conserved hypothetical protein
Bv0921_at	BVU_0950	2438	477	-5.11	1.00	putative oxidoreductase (putative secreted protein)
Bv1023_at	BVU_1054	2514	510	-4.93	0.99	putative outer membrane protein, probably involved in nutrient binding
Bv1024_at	BVU_1055	2107	619	-3.40	0.97	conserved hypothetical protein
Bv1085c_at	BVU_1116	28	146	5.20	0.98	polysaccharide lyase family 10, candidate pectate lyase
Bv1087c_at	BVU_1118	84	324	3.86	0.98	hypothetical protein
Bv1088c_at	BVU_1119	62	256	4.14	0.98	putative outer membrane protein, probably involved in nutrient binding
Bv1089c_at	BVU_1120	70	482	6.86	0.99	putative outer membrane protein, probably involved in nutrient binding
Bv1722c_at	BVU_1768	54	356	6.59	0.99	glycoside hydrolase family 2, candidate beta-glycosidase
Bv1727c_at	BVU_1773	181	33	-5.47	0.95	putative outer membrane protein, probably involved in nutrient binding
Bv1741_at	BVU_1787	23	227	9.72	1.00	glycoside hydrolase family 78, distantly related to alpha-L-rhamnosidases
Bv1805_at	BVU_1852	8555	180	-47.50	1.00	putative outer membrane protein, probably involved in nutrient binding
Bv1806_at	BVU_1853	4676	74	-63.21	1.00	putative outer membrane protein, probably involved in nutrient binding
Bv1933c_at	BVU_1983	31	253	8.17	1.00	glycoside hydrolase family 43, candidate beta-xylosidase/alpha-L-arabinofuranosidase

Probe set name	locus tag	Mono-association mean	Biassoc-iation mean	fold change	PPDE(<p)	Description
Bv1935c_at	BVU_1985	117	535	4.58	0.99	glycoside hydrolase family 28, related to polygalacturonases
Bv1966_at	BVU_2021	152	796	5.24	0.96	conserved hypothetical protein
Bv2279_at	BVU_2338	6204	582	-10.66	0.97	RNA polymerase ECF-type sigma factor
Bv2415c_at	BVU_2476	42	250	6.01	0.98	conserved hypothetical protein
Bv2527c_at	BVU_2588	395	83	-4.77	0.95	two-component system response regulator
Bv2528c_at	BVU_2589	902	158	-5.70	1.00	putative two-component system sensor kinase
Bv2529c_at	BVU_2590	9481	1321	-7.18	0.99	conserved hypothetical protein
Bv2530c_at	BVU_2591	10432	1418	-7.35	0.98	conserved hypothetical protein
Bv2531c_at	BVU_2592	8146	1062	-7.67	0.99	conserved hypothetical protein
Bv2849_at	BVU_2922	70	254	3.64	0.98	putative outer membrane protein, probably involved in nutrient binding
Bv2851_at	BVU_2924	20	158	7.96	0.99	putative outer membrane protein, probably involved in nutrient binding
Bv2879_at	BVU_2952	240	726	3.03	0.96	putative epimerase/dehydratase
Bv3820c_at	BVU_3924	991	269	-3.68	0.97	glycosyltransferase family 26, related to beta-glycosyltransferases
Bv3822c_at	BVU_3926	462	113	-4.10	0.97	putative glycosyltransferase

Chapter 4

Future Directions

Chapter 4

As mentioned in Chapter 1, the effects of the gut microbiota on murine adiposity are linked with changes in host gene expression, including decreased expression of the circulating inhibitor of lipoprotein lipase, Fiaf [1, 2]. However, the signal(s) or metabolite(s) responsible for these changes remain unknown. The most direct contributions of the microbiota to energy harvest are the short chain fatty acids (SCFAs) it produces. Studies of germ-free mice colonized with *B. thetaiotaomicron* with and without the methanogen and hydrogen-consumer *Methanobrevibacter smithii* show a correlation between increased adiposity and the amount of SCFAs produced [3]. This is only one of many changes in *B. thetaiotaomicron's* metabolism induced by the presence of *M. smithii,* however, and more generally, methanogen levels have not been correlated with obesity in humans.

The balance between Bacteroidetes and Firmicutes in the gut has been linked with obesity in mice and humans in both genetic and dietary models, as discussed in the Introduction. Transfer of a gut microbiota from obese donors to germ-free mouse recipients produces a larger increase in adiposity than the equivalent transfer from lean donors [4, 5]. The simplified, two-component communities characterized in Chapter 3 provide an opportunity to test whether an increase in the proportion of Firmicutes in a simplified community might likewise produce an increase in obesity. A simplified community would also provide a more experimentally tractable model to assess specific bacterial contributions to host adiposity.

Host adiposity in simplified microbial communities

I observed increased adiposity in mice co-colonized with *E. rectale* and *B. thetaiotaomicron* compared to mice colonized with either species alone or to germ-free controls in two of three experiments (**Figure 1**). The inconsistency between the three experiments

was not due to measurable differences in feed efficiency (weight gain per food consumed); however, this parameter is difficult to measure over the short time frame of the experiments described (data not shown). The observed increases in adiposity were also smaller than those seen after transplantation of an intact cecal microbiota from conventionally-raised lean donors.

While increased power (repetition) might show conclusively that the addition of *E. rectale* to *B. thetaiotaomicron* affects adiposity, I believe that it will be more useful to carefully and incrementally increase the complexity of the community to achieve a more consistent phenotype. As mentioned in Chapter 3, inoculating *B. thetaiotaomicron*-colonized mice with the methanogenic archaeon *Methanobrevibacter smithii* triggered a 100-fold increase in the colonization level of *B. thetaiotaomicron* and 19% increase in mouse adiposity. This was attributed to increased efficiency of fermentation in the presence of *M. smithii* due to its consumption of hydrogen, since cecal and serum acetate levels and cecal formate levels also increased significantly. Rather than consuming hydrogen, *E. rectale* produces large amounts [6], which explains, at least in part, why *B. thetaiotaomicron* does not show a similar syntrophy with *E. rectale*. An alternative hydrogen-consuming pathway is the Wood-Ljungdahl pathway, or acetogenesis, which produces acetate from carbon dioxide and hydrogen or formate. Since acetate is efficiently absorbed by the gut epithelium and metabolized by liver, muscle and fat cells, introduction of this pathway into the gut microbial community may result in increased energy harvest, and thus, increased host adiposity.

Two acetogenic bacteria have been sequenced thus far as part of the Human Gut Microbiome Initiative (HGMI). One, *Bryantella formatexigens,* utilizes formate but not hydrogen, while *Ruminococcus hydrogenotrophicus* uses primarily hydrogen in the production of acetate. While preliminary results indicate no dramatic difference in adiposity between *B. thetaiotaomicron*-colonized mice and those co-colonized with *B. thetaiotaomi-*

cron and either acetogen (F. Rey and J. Gordon, unpublished observations), *B. thetaiotaomicron* does not produce levels of hydrogen that are as high as *E. rectale in vitro* [6, 7].

As discussed in Chapter 3, *E. rectale* consumes acetate during its production of butyrate. Therefore, the combination of a hydrogen-consuming acetogen such as *R. hydrogenotrophicus* and an acetate-consuming hydrogen producer such as *E. rectale* in a two-component simplified microbiota may provide a syntrophic relationship even more beneficial to host energy harvest than the methanogenic archaeon and *B. thetaiotaomicron*. Such an idea has precedence in efforts to improve ruminant feed efficiency through inhibition of methanogenesis [8]. The addition of *B. thetaiotaomicron* to this two-component community may create a microbiota that has an even larger increase in its ability to promote energy harvest, since as described in Chapter 3, *E. rectale* grows more rapidly in the presence of *B. thetaiotaomicron*.

Hydrogen and carbon dioxide are not the only fermentative byproducts whose energy is lost to the host in these simplified models of the human gut microbiota. Lactate is produced in large amounts by *E. rectale* and by *B. thetaiotaomicron in vitro,* and is present in the ceca of *E. rectale* and *B. theta* mono-associated as well as co-colonized mice (1 μmol/g dry weight cecal contents in all three conditions; see [3] for methods). Its level is, on average, higher than that found for butyrate in the ceca of gnotobiotic mice consuming the polysaccharide-rich diet used in the studies described in Chapter 3 (0.35 μmol butyrate per gram wet weight in both *E. rectale*-colonized groups; see Chapter 3). Lactate is not as efficiently absorbed as butyrate [9, 10], but is only detected at low levels in conventional mice. This is thought to be because of the presence of bacteria that reduce it to butyrate [11, 12]. The effect of this conversion may be three-fold: firstly, replacing the supply of one poorly absorbed nutrient for a preferred one may increase the efficiency of host energy harvest. Additionally, butyrate induces expression of intestinal SCFA transporters [13]. Finally, butyrate provides more energy to the host than shorter, more oxidized substrates such as lactate.

One lactate-reducing organism, *Anaerostipes caccae,* has been sequenced as part of the HGMI, and another, related to *E. halii,* is slated for sequencing. Comparing the effect on host energy balance of simplified gut communities both with and without acetogens and lactate reducers will enable further tests of the hypothesis that SCFAs are a major mechanism by which the microbiota contributes to host adiposity. Bacterial SCFA prodution and host absorption can be monitored by biochemical methods. In addition, the known genome sequences of all of these organisms would permit concomitant transcriptional studies to assess the extent to which acetogenesis and lactate reduction contribute to the metabolism of the bacterial community *in vivo*.

Microbial-dependent increases in feed efficiency

In examining the role of the microbiota in energy harvest from these simplified communities, it will be critical to manipulate and define the dietary polysaccharides that are resistant to mouse-derived glycoside hydrolases and accessible to the bacteria. The diets used in the studies described in the Chapter 3 are primarily composed of wheat, corn and soy; their precise polysaccharide content has not been well characterized either before or after sterilization prior to consumption by germ-free mice. It will be helpful to use better-characterized purified diets, composed of components that the bacteria in the gut microbiota can metabolize. A starting point for the design of such diets would be the simplified diets used in the study of diet-induced obesity discussed in the Introduction [4] (**Table 1**). Because the cellulose included in these diets is not accessible to the simplified community, the amount of microbially-accessible polysaccharides can be increased by replacing cellulose with other, more readily fermented polysaccharides. For example, resistant starches, inulin and pectins are common food additives with known structures that are not degraded in the proximal intestine [14] and are fermented by the bacteria studied here (see Chapter 3). Systematically varying the amount of these substrates that is added to purified diets will allow more decisive tests of the relationship between microbial and host energy harvest

and adiposity. Concurrent monitoring of bacterial and host SCFA metabolism both transcriptionally and biochemically, in a manner similar to that described in Chapter 3, would permit more detailed modeling of the factors that drive that relationship.

Developing a more defined dietary platform for assessment of bacterial contributions to adiposity faces several hurdles, but the first is that such a diet must be suitable for coexistence of the members of the simplified microbiota in mice. With this in mind, I have conducted a proof of concept pilot study to assess the feasibility of this approach. Germ-free male NMRI mice co-colonized with *B. thetaiotaomicron* and *E. rectale* were fed one of three diets (n=5 mice/treatment group): either a standard, 18% protein irradiated diet consisting principally of wheat, corn and soy, as in Chapter 3 (3.4 kcal/g), or two purified formulations, a low fat and a "Western" diet, consisting of corn starch, maltodextrin, sucrose, shortening and beef tallow that differ primarily in their caloric density and fat content (**Table 1**). Mice consumed significantly less of either purified diet than the standard chow, and significantly less of the high fat Western diet than the low fat diet (**Figure 2A**). Fecal levels of each bacterium were monitored 4 weeks after co-colonization, using the same qPCR assay developed for the studies described in Chapter 3. The results revealed that all three of these diets support the coexistence of both bacterial strains throughout the course of the experiment (**Figure 2B**). The two purified diets, however, produce a higher ratio of *B. thetaiotoaomicron* to *E. rectale*. These diets probably provide less accessible polysaccharide to the distal gut community, since starch is largely absorbed in the proximal intestine and neither bacterium can degrade cellulose. Thus, *B. thetaiotaomicron's* ability to ferment host-derived glycans likely favors it.

Differences were also observed in fat pad weights, with increased adiposity occurring in both purified diets (**Figure 2C**). The similarity in adiposity between mice fed the two purified diets is surprising, since they differ both in caloric density (**Table 1**) and in their ability to produce diet-induced obesity [4]. This similarity suggests that the increased adiposity produced by the purified diets may be due to increased microbial energy harvest

compared to the standard chow. This possibility can be verified by cecal and serum SCFA measurements as in Chapter 3. Correlating biochemical measurements of SCFA metabolism with bacterial and host transcription will help identify bacterial pathways associated with increased energy harvest. In addition, careful and incremental manipulation of the amount of fermentable polysaccharide in the diet and/or the complexity of the community, as described above, would enable a dissection of the effects of differences in SCFA production and community composition on host energy balance.

Microbial affects on the host: beyond energy balance

A number of bacterial metabolites are thought to have profound effects on colonic and generalized host health. Prominent among these is butyrate. To date, studies that examine the effects of butyrate on the host have been conducted using several approaches: (i) *in vitro* examinations of colonic cell lines; (ii) *in vivo* administration of probiotic strains (i.e., live bacteria that produce the proposed beneficial metabolite, e.g., butyrate); (iii) *in vivo* administration of prebiotics, i.e., polysaccharides known to stimulate the growth of a particular butyrate-producing class of bacteria in a microbial community whose complete composition is unknown; (iv) direct supplementation. For example, *in vivo* models have included supplementation of drinking water with butyrate or infusion of butyrate via injection or enema: unfortunately, such studies preclude studying butyrate utilization long-term and at physiological levels. Alternatively, some workers have added resistant starches or inulin, which stimulate butyrate production by a 'normal' microbiota. It is impossible from such experimental designs to determine whether any changes seen in the host or microbial community reflect direct or indirect effects. However, as described in the Introduction, these different techniques result in contradictory phenotypes. Resolving the contradictions requires a more physiological and more easily manipulated model of butyrate production.

The construction of simplified microbial communities, composed of sequenced members of the human gut microbiota in gnotobiotic mice, provides a means to conduct

more direct tests of the effect of this intriguing bacterial metabolite, as well as others. The phylogeny of butyrate production suggests that it has evolved (or been lost) many times over the evolution of the Firmicutes (see Introduction Figure 2 and [15, 16]). In the setting of gnotobiotic mice, this presents the advantage that phenotypically and phylogenetically similar bacteria can be studied that differ in few known ways other than their production of butyrate. For instance, the *R. obeum*-related strains SR1/1 and SR1/5 [17] are 99% identical to each other based on their 16S rRNA gene sequences, but only the SR1/1 strain produces butyrate. Similarly, *Clostridium nexile* and *C.* sp. A2-232 are 98% identical in their 16S rRNA sequence, but only sp. 2-232 produces butyrate [17]. Both members of the latter pair are part of the HGMI. Identifying matched strains such as SR1/1 and SR1/5 for targeted whole genome sequencing will facilitate more careful study of the evolution of butyrate production as well as its effect on the host. An experimental paradigm substituting such matched strains for each other in gnotobiotic mice harboring suitably constructed simplified models of the human gut microbiota (e.g., adding them alone, or together with *B. thetaiotaomicron* and/or *R. hydrogenotrophicus*), combined with careful transcriptional, biochemical, calorimetric and proteomic monitoring of both host and microbe, should enable dissection of the effects of butyrate from other effects of these organisms on the host.

Butyrate production is not the only example of a trait with highly variable representation within the Firmicutes; several other phenotypes of known importance to host physiology show a similarly 'scattered phylogeny'. Among these is the Wood-Ljungdahl pathway of acetogenesis [18]. A similar approach can therefore be used to examine the effect of acetogenesis upon the microbial community and its host.

References

1. Backhed, F., J.K. Manchester, C.F. Semenkovich, and J.I. Gordon, 2007. Mechanisms underlying the resistance to diet-induced obesity in germ-free mice. *Proc Natl Acad Sci U S A*, **104** (3), p. 979-84.

2. Backhed, F., H. Ding, T. Wang, L.V. Hooper, G.Y. Koh, A. Nagy, C.F. Semenkovich, and J.I. Gordon, 2004. The gut microbiota as an environmental factor that regulates fat storage. *Proc Natl Acad Sci U S A*, **101** (44), p. 15718-23.

3. Samuel, B.S. and J.I. Gordon, 2006. A humanized gnotobiotic mouse model of host-archaeal-bacterial mutualism. *Proc Natl Acad Sci U S A*, **103** (26), p. 10011-6.

4. Turnbaugh, P.J., F. Backhed, L. Fulton, and J.I. Gordon, 2008. Diet-induced obesity is linked to marked but reversible alterations in the mouse distal gut microbiome. *Cell Host Microbe*, **3** (4), p. 213-23.

5. Turnbaugh, P.J., R.E. Ley, M.A. Mahowald, V. Magrini, E.R. Mardis, and J.I. Gordon, 2006. An obesity-associated gut microbiome with increased capacity for energy harvest. *Nature*, **444** (7122), p. 1027-31.

6. Duncan, S.H. and H.J. Flint, 2008. Proposal of a neotype strain (A1-86) for Eubacterium rectale. Request for an Opinion. *Int J Syst Evol Microbiol*, **58** (Pt 7), p. 1735-6.

7. McKay, L.F., W.P. Holbrook, and M.A. Eastwood, 1982. Methane and hydrogen production by human intestinal anaerobic bacteria. *Acta Pathol Microbiol Immunol Scand [B]*, **90** (3), p. 257-60.

8. Miller, T.L. and M.J. Wolin, 2001. Inhibition of growth of methane-producing bacteria of the ruminant forestomach by hydroxymethylglutaryl-SCoA reductase inhibitors. *J Dairy Sci*, **84** (6), p. 1445-8.

9. Ganapathy, V., M. Thangaraju, E. Gopal, P.M. Martin, S. Itagaki, S. Miyauchi, and P.D. Prasad, 2008. Sodium-coupled monocarboxylate transporters in normal tissues and in cancer. *Aaps J*, **10** (1), p. 193-9.

10. Ritzhaupt, A., I.S. Wood, A. Ellis, K.B. Hosie, and S.P. Shirazi-Beechey, 1998. Identification and characterization of a monocarboxylate transporter (MCT1) in pig and human colon: its potential to transport L-lactate as well as butyrate. *J Physiol*, **513 (Pt 3)** p. 719-32.

11. Belenguer, A., S.H. Duncan, A.G. Calder, G. Holtrop, P. Louis, G.E. Lobley, and H.J. Flint, 2006. Two routes of metabolic cross-feeding between Bifidobacterium adolescentis and butyrate-producing anaerobes from the human gut. *Appl Environ Microbiol*, **72** (5), p. 3593-9.

12. Duncan, S.H., P. Louis, and H.J. Flint, 2004. Lactate-utilizing bacteria, isolated from human feces, that produce butyrate as a major fermentation product. *Appl Environ Microbiol*, **70** (10), p. 5810-7.

13. Cuff, M.A., D.W. Lambert, and S.P. Shirazi-Beechey, 2002. Substrate-induced regulation of the human colonic monocarboxylate transporter, MCT1. *J Physiol*, **539** (Pt 2), p. 361-71.

14. Roberfroid, M.B., 1999. Caloric Value of Inulin and Oligofructose. *J. Nutrition*, **129** (7 (Supplement)), p. 1436S-1437S.

15. Barcenilla, A., S.E. Pryde, J.C. Martin, S.H. Duncan, C.S. Stewart, C. Henderson, and H.J. Flint, 2000. Phylogenetic relationships of butyrate-producing bacteria from the human gut. *Appl Environ Microbiol*, **66** (4), p. 1654-61.

16. Pryde, S.E., S.H. Duncan, G.L. Hold, C.S. Stewart, and H.J. Flint, 2002. The microbiology of butyrate formation in the human colon. *FEMS Microbiol Lett*, **217** (2), p. 133-9.

17. Louis, P., S.H. Duncan, S.I. McCrae, J. Millar, M.S. Jackson, and H.J. Flint, 2004. Restricted distribution of the butyrate kinase pathway among butyrate-producing bacteria from the human colon. *J Bacteriol*, **186** (7), p. 2099-106.

18. Drake, H.L., K. Küsel, and C. Matthies, *Acetogenic Prokaryotes*, in *Prokaryotes*, M. Dowrkin, S. Falkow, E. Rosenberg, K.H. Schleifer, and E. Stackebrandt, Editors. 2006, Springer: New York. p. 354-420.

Figure Legends

Figure 1. Fat pad to body weight ratios for three independent colonization experiments show a trend toward increased adiposity with co-colonization in two out of three experiments. Each experiment involved 14 d colonizations of 6-10 week old male germ-free NMRI mice as described in Chapter 3; n=4-5 mice per group per experiment. Error bars are ± s.e.m.

Figure 2. The impact of purified diets on membership in a simplified model human gut microbiota. (A) Chow consumption varies proportionally to caloric density: polysaccharide-rich (3.4 kcal/g), low-fat (3.7 kcal/g, and western (4.7 kcal/g). Both purified diets showed significantly less chow consumption over the course of the experiment ($p<0.001$). **(B)** The ratio of genome equivalents of *B. theta* to *E. rectale* in fecal pellets is higher in both purified diets, regardless of caloric density or fat content (see **Table 1**). Fecal pellets from *B. thetaiotaomicron* and *E. rectale* co-colonized mice were assayed for colonization levels after 6 weeks on the indicated diet as described in Chapter 3. **(C)** Fat pad weights eight weeks post-colonization on the purified diets, both low fat and western, compared with the polysaccharide-rich diet. *: $p<0.05$, ** $p<0.01$, *** $p< 0.001$ using a heteroscedastic t-test; error bars are ± standard deviation.

Figures

Figure 1.

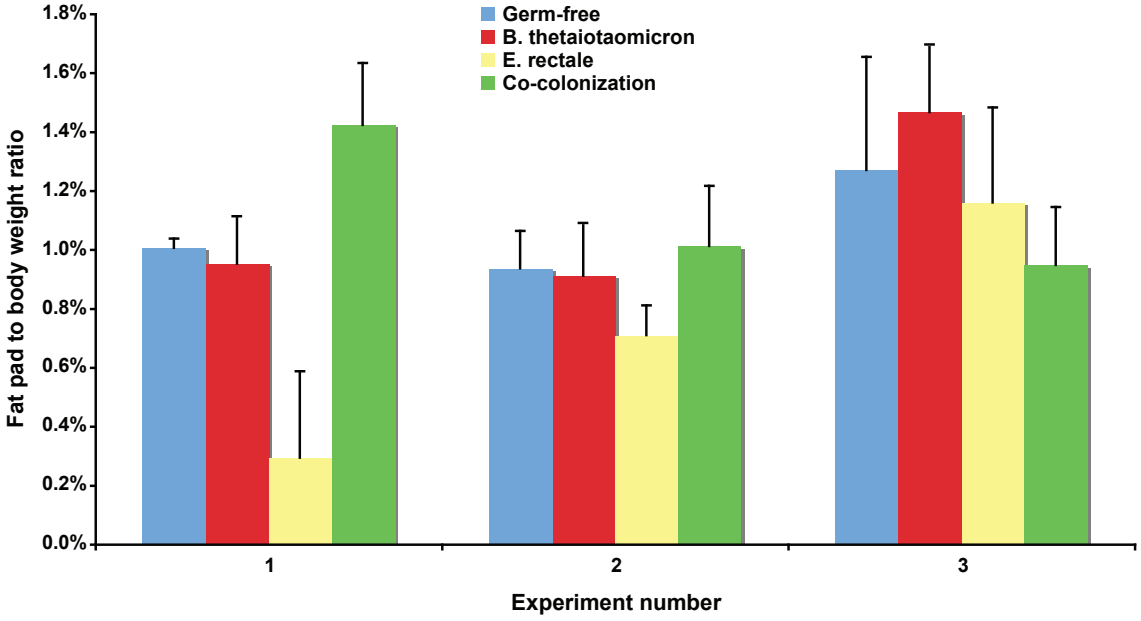

Figure 2.

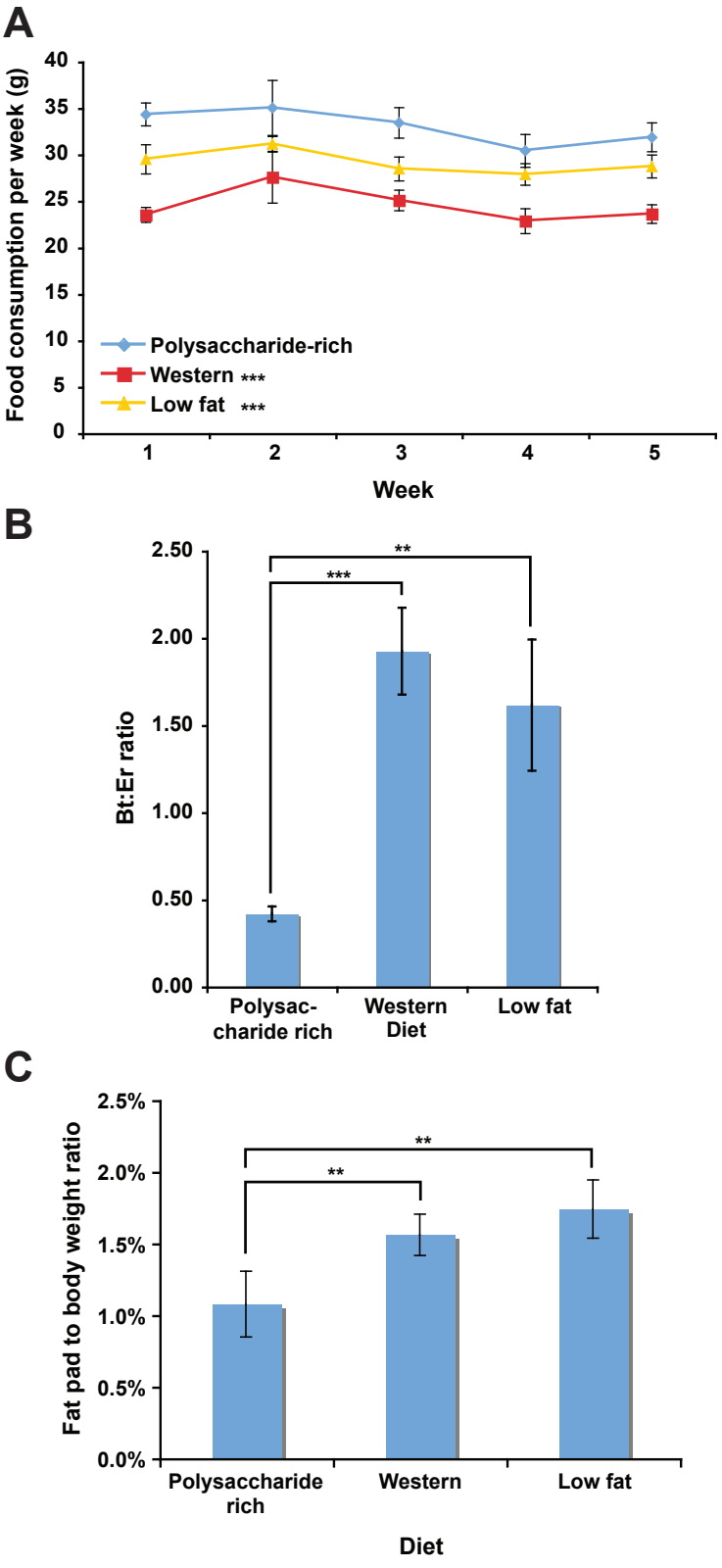
A
Food consumption per week (g)
40
35
30
25
20
15
10
5
0
Polysaccharide-rich
Western ***
Low fat ***
1
2
3
4
5
Week
B
Bt:Er ratio
2.50
2.00
1.50
1.00
0.50
0.00
**
***
Polysac-charide rich
Western Diet
Low fat
C
Fat pad to body weight ratio
2.5%
2.0%
1.5%
1.0%
0.5%
0.0%
**
**
Polysaccharide rich
Western
Low fat
Diet

Table 1.

Composition of a proposed basic diet for examination of microbial community contributions to obesity

Ingredient	Low fat	Western
Casein	200	236
DL-Methionine	3	3.54
Sucrose	182.99	182.62
Corn Starch	340	160
Maltodextrin	120	120
Shortening (Primex)	25	100
Beef Tallow	25	100
Soybean Oil	5	0
Mineral Mix	35	41.3
CaHPO4	4	4.72
Vitamin Mix	10	11.8
Ethoxyquin (antioxidant)	0.01	0.02
Cellulose[1]	**50**	**40**
Calories (kcal/g)	**3.7**	**4.5**

[1] Substituting cellulose for polysaccharides such as pectins, resistant starch and inulin that can be utilized by a gnotobiotic microbial community is suggested in the text.

APPENDIX A

Peter J. Turnbaugh, Ruth E. Ley, Michael A. Mahowald, Vincent Magrini, Elaine R. Mardis and Jeffrey I. Gordon

An obesity-associated gut microbiome with increased capacity for energy harvest

Nature. 2006 Dec 21;**444**(7122):1027-31.

ARTICLES

An obesity-associated gut microbiome with increased capacity for energy harvest

Peter J. Turnbaugh[1], Ruth E. Ley[1], Michael A. Mahowald[1], Vincent Magrini[2], Elaine R. Mardis[1,2] & Jeffrey I. Gordon[1]

The worldwide obesity epidemic is stimulating efforts to identify host and environmental factors that affect energy balance. Comparisons of the distal gut microbiota of genetically obese mice and their lean littermates, as well as those of obese and lean human volunteers have revealed that obesity is associated with changes in the relative abundance of the two dominant bacterial divisions, the Bacteroidetes and the Firmicutes. Here we demonstrate through metagenomic and biochemical analyses that these changes affect the metabolic potential of the mouse gut microbiota. Our results indicate that the obese microbiome has an increased capacity to harvest energy from the diet. Furthermore, this trait is transmissible: colonization of germ-free mice with an 'obese microbiota' results in a significantly greater increase in total body fat than colonization with a 'lean microbiota'. These results identify the gut microbiota as an additional contributing factor to the pathophysiology of obesity.

The human 'metagenome' is a composite of *Homo sapiens* genes and genes present in the genomes of the trillions of microbes that colonize our adult bodies. The latter genes are thought to outnumber the former by several orders of magnitude[1]. 'Our' microbial genomes (the microbiome) encode metabolic capacities that we have not had to evolve wholly on our own[2,3], but remain largely unexplored. These include degradation of otherwise indigestible components of our diet[4], and therefore may have an impact on our energy balance.

Colonization of adult germ-free mice with a distal gut microbial community harvested from conventionally raised mice produces a dramatic increase in body fat within 10–14 days, despite an associated decrease in food consumption[5]. This change involves several linked mechanisms: microbial fermentation of dietary polysaccharides that cannot be digested by the host; subsequent intestinal absorption of monosaccharides and short-chain fatty acids; their conversion to more complex lipids in the liver; and microbial regulation of host genes that promote deposition of the lipids in adipocytes[5]. These findings have led us to propose that the microbiota of obese individuals may be more efficient at extracting energy from a given diet than the microbiota of lean individuals[2,5].

In a previous study, we performed a comparative 16S-rRNA-gene-sequence-based survey of the distal gut microbiota of adult C57BL/6J mice homozygous for a mutation in the leptin gene (Lep^{ob}) that produces obesity, as well as the microbiota of their lean (*ob*/+ and +/+) littermates[6]. Members of two of the 70 known divisions of Bacteria[7,8], the Bacteroidetes and the Firmicutes, consisted of more than 90% of all phylogenetic types in both groups of mice, just as they do in humans[6,9,10]. However, the relative abundance of the Bacteroidetes in *ob/ob* mice was lower by 50%, whereas the Firmicutes were higher by a corresponding degree[6]. These differences were division-wide, and not attributable to differences in food consumption (a runted *ob/ob* mouse weighed less than his *ob/ob* littermates owing to reduced chow consumption, but still exhibited a markedly greater per cent body fat and ratio of Firmicutes to Bacteroidetes)[6].

We have observed analogous differences in the distal gut microbiota of obese versus lean humans; the relative abundance of Bacteroidetes increases as obese individuals lose weight on either a fat- or a carbohydrate-restricted low-calorie diet. Moreover, the increase in Bacteroidetes was significantly correlated to weight loss but not to total caloric intake[9].

To determine if microbial community gene content correlates with, and is a potential contributing factor to obesity, we characterized the distal gut microbiomes of *ob/ob*, *ob*/+, and +/+ littermates by random shotgun sequencing of their caecal microbial DNA. Mice were used for these comparative metagenomics studies to eliminate many of the confounding variables (environment, diet and genotype) that would make such a proof of principle experiment more difficult to perform and interpret in humans. The caecum was chosen as the gut habitat for sampling because it is an anatomically distinct structure, located between the distal small intestine and colon, that is colonized with sufficient quantities of a readily harvested microbiota for metagenomic analysis. The predicted increased capacity for dietary energy harvest by the *ob/ob* microbiome was subsequently validated using biochemical assays and by transplantation of lean and obese caecal microbiotas into germ-free wild-type mouse recipients. These transplantation experiments illustrate the power of marrying metagenomics to gnotobiotics to discover how microbial communities encode traits that markedly affect host biology.

Shotgun sequencing of microbiomes

Bulk DNA was prepared from the caecal contents of two *ob/ob* and +/+ littermate pairs. A lean *ob*/+ mouse from one of the litters was also studied. All caecal microbial community DNA samples were analysed using a 3730xl capillary sequencer (10,500 ± 431 (s.e.m.) unidirectional reads per data set; 752 ± 13.8 (s.e.m.) nucleotides per read; 39.5 Mb from all five plasmid libraries). Material from one of the two obese and lean sibling pairs was also analysed using a highly parallel 454 Life Sciences GS20 pyrosequencer[11]: three runs for the +/+ mouse (known as lean1), and two runs for its *ob/ob* littermate (ob1) produced a total of 160 Mb of sequence (345,000 ± 23,500 (s.e.m.) unidirectional reads per run; 93.1 ± 1.56 (s.e.m.) nucleotides per read) (Supplementary Tables 1–3). Both sequencing platforms have unique advantages and limitations: capillary sequencing allows more confident gene calling (Supplementary Fig. 1) but is affected by cloning bias, whereas pyrosequencing can achieve higher sequence coverage with no cloning bias, but produces shorter reads

[1]Center for Genome Sciences, and [2]Genome Sequencing Center, Washington University, St. Louis, Missouri 63108, USA.

(Supplementary Table 2). The three pyrosequencer runs of the lean1 caecal microbiome (94.9 Mb) yielded 0.44× coverage (on the basis of PROmer sequence alignments[12]) of the 3730xl-derived sequences obtained from the same sample (8.23 Mb), whereas the two pyrosequencer runs of the microbiome of its *ob/ob* littermate (ob1; 65.4 Mb) produced 0.32× coverage of the corresponding 3730xl sequences (8.19 Mb).

Taxonomic analysis of microbiomes

Environmental gene tags (EGTs) are defined as sequencer reads assigned to the NCBI non-redundant, Clusters of Orthologous Groups[13] (COG), or Kyoto Encyclopedia of Genes and Genomes[14] (KEGG) databases (Fig. 1a; Supplementary Fig. 2; Supplementary Table 4). Averaging results from all data sets, 94% of the EGTs assigned to the non-redundant database were bacterial, 3.6% were eukaryotic (0.29% *Mus musculus*; 0.36% fungal), 1.5% were archaeal (1.4% Euryarcheota; 0.07% Crenarcheota), and 0.61% were viral (0.57% double stranded DNA viruses) (Supplementary Table 5). The relative abundance of the eight bacterial divisions identified from EGTs and 16S rRNA gene fragments was comparable to our previous PCR-derived, 16S-rRNA-gene-sequence-based surveys of these caecal samples, including the increased ratio of Firmicutes to Bacteroidetes in obese versus lean littermates (Supplementary Fig. 2). In addition, comparisons of the lean1 and ob1 reads obtained with the pyrosequencer against the finished genome of *Bacteroides thetaiotaomicron* ATCC29148[1], and a deep draft genome assembly of *Eubacterium rectale* ATCC33656 (50% of total contig bases present in contigs ≥75.9 kb; http://gordonlab.wustl.edu/supplemental/Turnbaugh/obob/) provided independent confirmation of the greater relative abundance of Firmicutes in the *ob/ob* microbiota. These organisms were selected for comparison because both are prominently represented in the normal human distal gut microbiota[10] and species related to *B. thetaiotaomicron* (Bacteroidetes division) and *E. rectale* (Firmicutes division) are members of the normal mouse distal gut microbiota[6]. The ratio of sequences homologous to the *E. rectale* versus *B. thetaiotaomicron* genome was 7.3 in the ob1 caecal microbiome compared with 1.5 in the lean1 microbiome.

Intriguingly, there were more EGTs that matched Archaea (Euryarchaeota and Crenarchaeota) in the caecal microbiome of *ob/ob* mice compared with their lean *ob/+* and *+/+* littermates (binomial test of pooled obese versus pooled lean capillary-sequencing-derived microbiomes, $P < 0.001$; Supplementary Table 5).

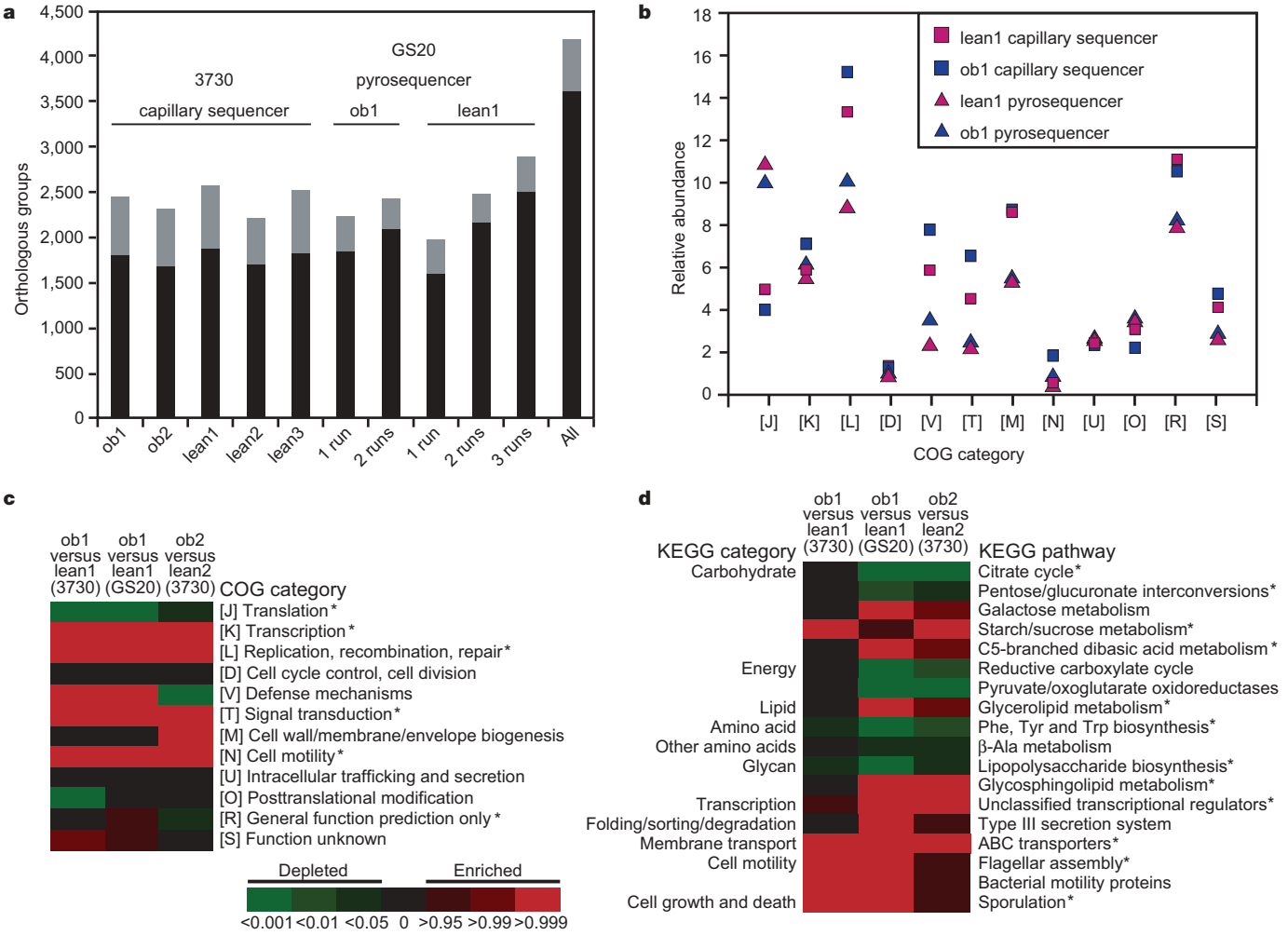

Figure 1 | Comparison of data sets obtained from the caecal microbiomes of obese and lean littermates. **a**, Number of observed orthologous groups in each caecal microbiome. Black indicates the number of observed groups. Grey indicates the number of predicted missed groups. **b**, Relative abundance of a subset of COG categories (BLASTX, *e*-value $< 10^{-5}$) in the lean1 (red) and ob1 (blue) caecal microbiome, characterized by capillary- and pyro-sequencers (squares and triangles, respectively). **c**, **d**, A subset of COG categories (**c**) and all KEGG pathways (**d**) consistently enriched or depleted in the caecal microbiomes of both obese mice compared with their lean littermates. Red denotes enrichment and green indicates depletion on the basis of a cumulative binomial test (brightness indicates the level of significance). Black indicates pathways whose representation is not significantly different. Asterisks indicate groups that were consistently enriched or depleted between both sibling pairs using a more stringent EGT assignment strategy (*e*-value $< 10^{-8}$). For additional details see Supplementary Discussion; Supplementary Figs 5 and 6, and Supplementary Tables 6, 8 and 9.

Methanogenic archaea increase the efficiency of bacterial fermentation by removing one of its end products, H_2. Our recent studies of gnotobiotic normal mice colonized with the principal methanogenic archaeon in the human gut, *Methanobrevibacter smithii*, and/or *B. thetaiotaomicron* revealed that co-colonization not only increases the efficiency, but also changes the specificity of bacterial polysaccharide fermentation, leading to a significant increase in adiposity compared with mice colonized with either organism alone[15].

Comparative metagenomic analysis

Using reciprocal TBLASTX comparisons, we found that the Firmicutes-enriched microbiomes from *ob/ob* hosts clustered together, as did lean microbiomes with low Firmicutes to Bacteroidetes ratios (Fig. 2a). Likewise, Principal Component Analysis of EGT assignments to KEGG pathways revealed a correlation between host genotype and the gene content of the microbiome (Fig. 2b).

Reads were then assigned to COGs and KOs (KEGG orthology terms) by BLASTX comparisons against the STRING-extended COG database[13], and the KEGG Genes database[14] (version 37). We tallied the number of EGTs assigned to each COG or KEGG category, and used the cumulative binomial distribution[3], and a bootstrap analysis[16,17], to identify functional categories with statistically significant differences in their representation in both sets of obese and lean littermates. As noted above, capillary sequencing requires cloned DNA fragments; the pyrosequencer does not, but produces relatively short read lengths. These differences are a likely cause of the shift in relative abundance of several COG categories obtained using the two sequencing methods for the same sample (Fig. 1b). Nonetheless, comparisons of the caecal microbiomes of lean versus obese littermates sequenced with either method revealed similar differences in their functional profiles (Fig. 1c).

The *ob/ob* microbiome is enriched for EGTs encoding many enzymes involved in the initial steps in breaking down otherwise indigestible dietary polysaccharides, including KEGG pathways for starch/sucrose metabolism, galactose metabolism and butanoate metabolism (Fig. 1d; Supplementary Fig. 3 and Supplementary Table 6). EGTs representing these enzymes were grouped according to their functional classifications in the Carbohydrate Active Enzymes (CAZy) database (http://afmb.cnrs-mrs.fr/CAZY/). The *ob/ob* microbiome is enriched ($P < 0.05$) for eight glycoside hydrolase families capable of degrading dietary polysaccharides including starch (CAZy families 2, 4, 27, 31, 35, 36, 42 and 68, which contain α-glucosidases, α-galactosidases and β-galactosidases). Finished genome sequences of prominent human gut Firmicutes have not been reported. However, our analysis of the draft genome of *E. rectale* has revealed 44 glycoside hydrolases, including a significant enrichment for glycoside hydrolases involved in the degradation of dietary starches (CAZy families 13 and 77, which contain α-amylases and amylomaltases; $P < 0.05$ on the basis of a binomial test of *E. rectale* versus the finished genomes of Bacteroidetes—*Bacteroides thetaiotaomicron* ATCC29148, *B. fragilis* NCTC9343, *B. vulgatus* ATCC8482 and *B. distasonis* ATCC8503).

EGTs encoding proteins that import the products of these glycoside hydrolases (ABC transporters), metabolize them (for example, α- and β-galactosidases KO7406/7 and KO1190, respectively), and generate the major end products of fermentation, butyrate and acetate (pyruvate formate-lyase, KO0656, and other enzymes in the KEGG 'Butanoate metabolism' pathway; and formate-tetrahydrofolate ligase, KO1938, the second enzyme in the homoacetogenesis pathway for converting CO_2 to acetate) are also significantly enriched in the *ob/ob* microbiome (binomial comparison of pyrosequencer-derived ob1 and lean1 data sets, $P < 0.05$) (Fig. 1d; Supplementary Fig. 3 and Supplementary Table 6).

As predicted from our comparative metagenomic analyses, the *ob/ob* caecum has an increased concentration of the major fermentation end-products butyrate and acetate (Fig. 3a). This observation is also consistent with the fact that many Firmicutes are butyrate producers[18–20]. Moreover, bomb calorimetry revealed that *ob/ob* mice have significantly less energy remaining in their faeces relative to their lean littermates (Fig. 3b).

Microbiota transplantation

We performed microbiota transplantation experiments to test directly the notion that the *ob/ob* microbiota has an increased capacity to harvest energy from the diet and to determine whether increased adiposity is a transmissible trait. Adult germ-free C57BL/6J mice were colonized (by gavage) with a microbiota harvested

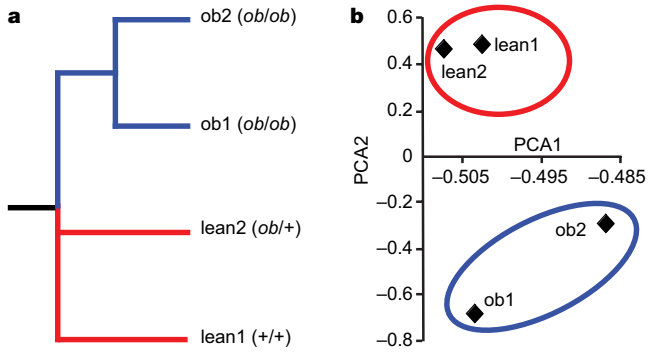

Figure 2 | Microbiomes cluster according to host genotype. a, Clustering of caecal microbiomes of obese and lean sibling pairs based on reciprocal TBLASTX comparisons. All possible reciprocal TBLASTX comparisons of microbiomes (defined by capillary sequencing) were performed from both lean and obese sibling pairs. A distance matrix was then created using the cumulative bitscore for each comparison and the cumulative score for each self–self comparison. Microbiomes were subsequently clustered using NEIGHBOUR (PHYLIP version 3.64). **b**, Principal Component Analysis (PCA) of KEGG pathway assignments. A matrix was constructed containing the number of EGTs assigned to each KEGG pathway in each microbiome (includes KEGG pathways with >0.6% relative abundance in at least two microbiomes, and a standard deviation >0.3 across all microbiomes), PCA was performed using Cluster3.0 (ref. 25), and the results graphed along the first two components.

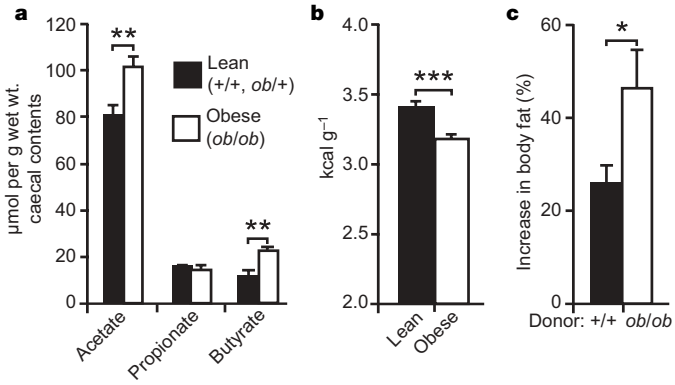

Figure 3 | Biochemical analysis and microbiota transplantation experiments confirm that the *ob/ob* microbiome has an increased capacity for dietary energy harvest. a, Gas-chromatography mass-spectrometry quantification of short-chain fatty acids in the caeca of lean ($n = 4$) and obese ($n = 5$) conventionally raised C57BL/6J mice. **b**, Bomb calorimetry of the faecal gross energy content (kcal g^{-1}) of lean (+/+, *ob*/+; $n = 9$) and obese (*ob/ob*; $n = 13$) conventionally raised C57BL/6J mice. **c**, Colonization of germ-free wild-type C57BL/6J mice with a caecal microbiota harvested from obese donors (*ob/ob*; $n = 9$ recipients) results in a significantly greater percentage increase in total body fat than colonization with a microbiota from lean donors (+/+; $n = 10$ recipients). Total body fat content was measured before and after a two-week colonization, using dual-energy X-ray absorptiometry. Mean values ± s.e.m. are plotted. Asterisks indicate significant differences (two-tailed Student's *t*-test of all datapoints, $^*P < 0.05$, $^{**}P \leq 0.01$, $^{***}P < 0.001$).

from the caecum of obese (*ob/ob*) or lean (+/+) donors (1 donor and 4–5 germ-free recipients per treatment group per experiment; two independent experiments). 16S-rRNA-gene-sequence-based surveys confirmed that the *ob/ob* donor microbiota had a greater relative abundance of Firmicutes compared with the lean donor microbiota (Supplementary Fig. 4 and Supplementary Table 7). Furthermore, the *ob/ob* recipient microbiota had a significantly higher relative abundance of Firmicutes compared with the lean recipient microbiota ($P < 0.05$, two-tailed Student's *t*-test). UniFrac analysis[21] of 16S rRNA gene sequences obtained from the recipients' caecal microbiotas revealed that they cluster according to the input donor community (Supplementary Fig. 4): that is, the initial colonizing community structure did not exhibit marked changes by the end of the two-week experiment. There was no statistically significant difference in (1) chow consumption over the 14-day period (55.4 ± 2.5 g (*ob/ob*) versus 54.0 ± 1.2 g (+/+); caloric density of chow, 3.7 kcal g^{-1}), (2) initial body fat (2.7 ± 0.2 g for both groups as measured by dual-energy X-ray absorptiometry), or (3) initial weight between the recipients of lean and obese microbiotas. Strikingly, mice colonized with an *ob/ob* microbiota exhibited a significantly greater percentage increase in body fat over two weeks than mice colonized with a +/+ microbiota (Fig. 3c; 47 ± 8.3 versus 27 ± 3.6 percentage increase or 1.3 ± 0.2 versus 0.86 ± 0.1 g fat (dual-energy X-ray absorptiometry): at 9.3 kcal g^{-1} fat, this corresponds to a difference of 4 kcal or 2% of total calories consumed).

Discussion

The primary cause of obesity in the *ob/ob* mouse model is increased food consumption due to leptin deficiency. We have used this model to provide direct experimental evidence that at least one type of obesity-associated gut microbiome has an increased capacity for energy harvest from the diet. This finding provides support for the more general concept that the gut microbiome should be considered as a set of genetic factors that, together with host genotype and lifestyle (energy intake and expenditure), contribute to the pathophysiology of obesity. Yet to be answered are the questions of what mechanisms are responsible for mediating the linkage between the relative abundance of the Bacteroidetes to Firmicutes divisions and adiposity in both mice and humans, and to what extent is this relationship self-perpetuating?

Energy balance is an equilibrium between the amount of energy taken in as food and the amount expended during resting metabolism, as well as the thermic effect of food, physical activity, and loss in the faeces and urine. The alteration in efficiency of energy harvest from the diet produced by changes in gut microbial ecology does not have to be great to contribute to obesity, given that small changes in energy balance, over the course of a year, can result in significant changes in body weight[22]. We are aware of only one report showing that obese humans may have an increased capacity to absorb energy from their diet: in this case, analysis of four lean and four obese individuals given three different diets (high protein/high fat, 'average', and high carbohydrate) revealed that on average, the obese individuals lost less energy to stool compared with their lean counterparts. However, the differences did not achieve statistical significance[23].

Our study in mice demonstrates the feasibility and utility of applying comparative metagenomics to mouse models of human physiologic or pathophysiologic states in order to understand the complex interplay between host genetics, microbial community gene content and the biological properties of the resulting 'superorganism'. As such, it opens the door for comparable investigations of the interactions between humans and their microbial communities, including whether there is a core set of genes associated with the microbiomes of obese versus lean individuals; whether these genes are transmitted from mothers to their offspring; what genetic or behavioural traits of the host can reshape the community[24]; how the microbiome changes as body mass index changes within an individual; the degree to which these changes correlate with energy harvest from their diets; and whether germ-free mice can be used as a bioassay to compare the energy harvesting activities encoded in human gut microbiomes. Our results indicate that if the gut microbiome of obese humans is comparable to that of obese mice, then it may be a biomarker, a mediator and a new therapeutic target for people suffering from this increasingly worldwide disease.

METHODS

DNA was isolated from the caeca of *ob/ob*, *ob/*+ and +/+ littermates using a bead beater to mechanically disrupt cells, followed by phenol–chloroform extraction. DNA was sequenced using 3730xl capillary- and GS20 pyro-sequencers: in the case of the latter, DNA was purified further using the Qiaquick gel extraction kit (Qiagen).

Individual reads in the resulting 199.8 Mb data set were directly compared with each other and to reference sequenced gut microbial genomes using MUMmer[12]. Taxonomic assignments were made on the basis of BLASTX searches of the non-redundant database (*e*-value $< 10^{-5}$) and alignment of 16S gene fragments. Reads were also assigned to EGTs (environmental gene tags) by BLASTX searches against the non-redundant database, STRING-extended COG[13], and KEGG[14] (v37) databases. Microbiomes from each animal were clustered according to reciprocal TBLASTX comparisons and their EGT assignments to KEGG pathways. Statistically enriched or depleted COG and KEGG groups were identified using bootstrap[16,17] and cumulative binomial[3] analyses. For the binomial analysis, the probability of observing 'n_1' EGT assignments to a given group in microbiome 1, given 'N_1' EGT assignments to all groups in microbiome 1, was calculated using the cumulative binomial distribution and an expected probability equal to 'n_2/N_2' (the number of EGTs assigned to a given group in microbiome 2 divided by the total number of EGTs assigned to all groups in microbiome 2). Detailed descriptions of these methods and techniques for (1) measuring short-chain fatty acids in caecal samples by gas-chromatography mass-spectrometry, (2) bomb calorimetry of faecal samples, (3) transplanting the caecal microbiota of C57BL/6J *ob/ob* or +/+ donors into 8–9-week-old germ-free +/+ C57BL/6J recipients, (4) measuring the total body fat of transplant recipients, before and after colonization, by dual-energy X-ray absorptiometry, and (5) performing 16S-rRNA-gene-sequence-based surveys of the input (donor) and output (recipient) caecal microbiotas are provided in Supplementary Information.

Received 8 October; accepted 7 November 2006.

1. Xu, J. *et al.* A genomic view of the human–*Bacteroides thetaiotaomicron* symbiosis. *Science* **299,** 2074–2076 (2003).
2. Backhed, F., Ley, R. E., Sonnenburg, J. L., Peterson, D. A. & Gordon, J. I. Host–bacterial mutualism in the human intestine. *Science* **307,** 1915–1920 (2005).
3. Gill, S. R. *et al.* Metagenomic analysis of the human distal gut microbiome. *Science* **312,** 1355–1359 (2006).
4. Sonnenburg, J. L. *et al.* Glycan foraging *in vivo* by an intestine-adapted bacterial symbiont. *Science* **307,** 1955–1959 (2005).
5. Backhed, F. *et al.* The gut microbiota as an environmental factor that regulates fat storage. *Proc. Natl Acad. Sci. USA* **101,** 15718–15723 (2004).
6. Ley, R. E. *et al.* Obesity alters gut microbial ecology. *Proc. Natl Acad. Sci. USA* **102,** 11070–11075 (2005).
7. Ley, R. E. *et al.* Unexpected diversity and complexity of the Guerrero Negro hypersaline microbial mat. *Appl. Environ. Microbiol.* **72,** 3685–3695 (2006).
8. Ley, R. E., Peterson, D. A. & Gordon, J. I. Ecological and evolutionary forces shaping microbial diversity in the human intestine. *Cell* **124,** 837–848 (2006).
9. Ley, R. E., Turnbaugh, P. J., Klein, S. & Gordon, J. I. Human gut microbes associated with obesity. *Nature* doi:10.1038/nature4441023a (this issue).
10. Eckburg, P. B. *et al.* Diversity of the human intestinal microbial flora. *Science* **308,** 1635–1638 (2005).
11. Margulies, M. *et al.* Genome sequencing in microfabricated high-density picolitre reactors. *Nature* **437,** 376–380 (2005).
12. Kurtz, S. *et al.* Versatile and open software for comparing large genomes. *Genome Biol.* **5,** R12 (2004).
13. von Mering, C. *et al.* STRING: known and predicted protein–protein associations, integrated and transferred across organisms. *Nucleic Acids Res.* **33,** D433–D437 (2005).
14. Kanehisa, M., Goto, S., Kawashima, S., Okuno, Y. & Hattori, M. The KEGG resource for deciphering the genome. *Nucleic Acids Res.* **32,** D277–D280 (2004).
15. Samuel, B. S. & Gordon, J. I. A humanized gnotobiotic mouse model of host–archaeal–bacterial mutualism. *Proc. Natl Acad. Sci. USA* **103,** 10011–10016 (2006).
16. DeLong, E. F. *et al.* Community genomics among stratified microbial assemblages in the ocean's interior. *Science* **311,** 496–503 (2006).
17. Rodriguez-Brito, B., Rohwer, F. & Edwards, R. An application of statistics to comparative metagenomics. *BMC Bioinformatics* **7,** 162 (2006).
18. Duncan, S. H., Hold, G. L., Barcenilla, A., Stewart, C. S. & Flint, H. J. *Roseburia intestinalis* sp. nov., a novel saccharolytic, butyrate-producing bacterium from human faeces. *Int. J. Syst. Evol. Microbiol.* **52,** 1615–1620 (2002).

19. Barcenilla, A. *et al.* Phylogenetic relationships of butyrate-producing bacteria from the human gut. *Appl. Environ. Microbiol.* **66,** 1654–1661 (2000).
20. Pryde, S. E., Duncan, S. H., Hold, G. L., Stewart, C. S. & Flint, H. J. The microbiology of butyrate formation in the human colon. *FEMS Microbiol. Lett.* **217,** 133–139 (2002).
21. Lozupone, C., Hamady, M. & Knight, R. UniFrac—an online tool for comparing microbial community diversity in a phylogenetic context. *BMC Bioinformatics* **7,** 371 (2006).
22. Flegal, K. M. & Troiano, R. P. Changes in the distribution of body mass index of adults and children in the US population. *Int. J. Obes. Relat. Metab. Disord.* **24,** 807–818 (2000).
23. Webb, P. & Annis, J. F. Adaptation to overeating in lean and overweight men and women. *Hum. Nutr. Clin. Nutr.* **37,** 117–131 (1983).
24. Rawls, J. F., Mahowald, M. A., Ley, R. E. & Gordon, J. I. Reciprocal gut microbiota transplants from zebrafish and mice to germ-free recipients reveal host habitat selection. *Cell* **127,** 423–433 (2006).
25. de Hoon, M. J., Imoto, S., Nolan, J. & Miyano, S. Open source clustering software. *Bioinformatics* **20,** 1453–1454 (2004).

Supplementary Information is linked to the online version of the paper at www.nature.com/nature.

Acknowledgements We thank our colleagues B. Samuel, F. Backhed, D. O'Donnell, M. Karlsson, M. Hickenbotham, K. Haub, L. Fulton, J. Crowley, T. Coleman, C. Semenkovich, V. Markowitz and E. Szeto for their assistance. This work was supported by grants from the NIH and the W.M. Keck Foundation.

Author Information This Whole Genome Shotgun project has been deposited at DDBJ/EMBL/GenBank under the project accession AATA00000000–AATF00000000. The version described in this paper is the first version, AATA01000000–AATF01000000. All 454 GS20 reads have been deposited in the NCBI Trace Archive. PCR-derived 16S rRNA gene sequences are deposited in GenBank under the accession numbers EF95962-100118. Annotated sequences are also available for further analysis in IMG/M (http://img.jgi.doe.gov/m). Reprints and permissions information is available at www.nature.com/reprints. The authors declare no competing financial interests. Correspondence and requests for materials should be addressed to J.I.G. (jgordon@wustl.edu).

Supplementary Discussion of data presented in Figure 1

Each pyrosequencer run of cecal DNA from lean1 and ob1 littermates yielded 387±95 new groups (s.e.m.) (**Fig. 1A**). The observed relative abundance of COG categories was markedly influenced by sequencing platform (**Fig. 1B**).

As expected, the Firmicutes-enriched, Bacteroidetes-depleted *ob/ob* microbiome is depleted for genes involved in the biosynthesis of lipopolysaccharide (a major component of the outer membrane of Gram-negative bacteria), and enriched for genes involved in cell motility and sporulation (many Firmicutes are motile and form endospores) (**Fig. 1C and 1D; Supplementary Fig. 6**).

EGT assignment notes (**Fig. 1D**): (i) 'Type III secretion systems' are represented by EGTs involved in flagellar assembly (very few EGTs were assigned specifically to the secretion apparatus); (ii) 'Galactose metabolism' includes glycoside hydrolases [alpha-glucosidase (KO1187), beta-galactosidase (KO1190), and alpha-galactosidase (KO7406/7)], and 6-phosphofructokinase (KO0850, catalyzes the rate limiting step in glycolysis); (iii) 'Glycerolipid metabolism' includes glycoside hydrolases [beta-galactosidase (KO1190) and alpha-galactosidase (KO7406/7)] plus glycerol kinase (KO0864, involved in degradation of triglycerides and phospholipids); (iv) 'Glycosphingolipid metabolism' also includes glycoside hydrolases [beta-galactosidase (KO1190) and alpha-galactosidase (KO7406/7)]; (v) 'Reductive carboxylate cycle' and 'Pyruvate/oxoglutarate oxidoreductases' both include genes involved in the citrate cycle [2-oxoglutarate ferrodoxin oxidoreductase (KO0174/5) and succinate dehydrogenase

(KO0238/39/40)], (vi) 'C5-branched dibasic acid metabolism' includes valine and isoleucine biosynthesis from pyruvate [i.e. acetolactate synthase (KO1651/2)[26,27]]. Metabolic capacity is defined based on microbial community gene content. Transcriptomic, proteomic and/or metabolomic data are necessary to confirm predicted activites of genes and their products (e.g. see **Fig. 3**).

Materials and Methods

Animals – All experiments involving mice were performed using protocols approved by the Washington University Animal Studies Committee. Once C57BL/6J *ob/ob*, *ob*/+, and +/+ littermates were weaned, they were housed individually in microisolator cages where they were maintained in a specified pathogen-free state, under a 12-h light cycle, and fed a standard polysaccharide-rich chow diet (PicoLab, Purina) *ad libitum*. Germ-free and colonized animals were maintained in gnotobiotic isolators[28], under a strict 12-h light cycle and fed an autoclaved chow diet (B&K Universal, East Yorkshire, U.K.) *ad libitum*. Fecal samples for bomb calorimetry were collected from mice at 8 or 14 weeks of age, after which time animals were sacrificed.

Community DNA Preparation – The cecal contents used for community DNA sequencing and gas chromatography-mass spectrometry (GC-MS) were obtained, at eight weeks of age, from the same animals used for our previous PCR-based 16S rRNA survey of the gut microbiota[6]: samples had been stored at -80^{o}C (**Supplementary Table 1)**. An aliquot (~10mg) of each sample was suspended while frozen in a solution containing 500 μL of extraction buffer [200 mM Tris (pH 8.0), 200 mM NaCl, 20 mM EDTA], 210 μL of 20% SDS, 500 μL of a mixture of of phenol:chloroform:isoamyl alcohol (25:24:1)], and 500 μL of a slurry of 0.1-mm-diameter zirconia/silica beads (BioSpec Products, Bartlesville, OK). Microbial cells were then lysed by mechanical disruption with a bead beater (BioSpec Products) set on high for 2 min (23^{o}C), followed by extraction with phenol:chloroform:isoamyl alcohol, and precipitation with isopropanol. In order to perform pyrosequencing, DNA was purified further using the Qiaquick gel extraction kit (Qiagen).

Shotgun sequencing and assembly of cecal microbiomes – DNA samples were used to construct plasmid libraries for 3730xl capillary-based sequencing. Pyrosequencing was performed as previously described[11]. Briefly, samples were nebulized to 200 nucleotide fragments, ligated to adaptors, fixed to beads, suspended in a PCR reaction mixture-in-oil emulsion, amplified, and sequenced using a GS20 pyrosequencer (454 Life Sciences, Branford, CT). The Newbler *de novo* shotgun sequence assembler (454 Life Sciences) was used to assemble sequences based on flowgram signal space. This process includes overlap generation, contig layout, and consensus generation. The resulting GS20 contigs were then broken into linked sequences to generate pseudo paired-end reads, and aligned with 3730xl reads using PCAP[29].

Sequences were aligned to reference genomes using the PROmer script in MUMmer[12] (version 3.18). Capillary sequencer reads from each microbiome, the finished genome of the human gut-derived *Bacteroides thetaiotaomicron* type strain ATCC29148[1], and a deep draft genome of the human gut-derived *Eubacterium rectale* type strain ATCC33656 (http://gordonlab.wustl.edu/supplemental/Turnbaugh/obob/) were used as a reference for the pyrosequencer datasets. Coverage was calculated by dividing the sum of all alignment lengths by the length of the reference genome.

Whole genome sequencing and annotation – A draft assembly of *Eubacterium rectale* ATCC33656 was generated from AB36731xl paired end-reads of inserts in whole genome shotgun plasmid and fosmid libraries, as well as from reads produced by the GS20 pyrosequencer. Sequences were assembled using Newbler and PCAP (see above) and ORFs predicted with Glimmer3.01[30] (maximum overlap of 100, minimum length of

110 and a threshold of 30). Each predicted gene sequence was translated, and the resulting protein sequence assigned to InterPro numbers using InterProScan[31] (Release 12.0).

Database search parameters – NCBI BLAST was used to query the non-redundant database (NR), the STRING-extended COG database (179 microbial genomes, version 6.3)[13], a database constructed from 334 genomes available through KEGG (version 37)[14], and the Ribosomal Database Project database (RDP, version 9.33)[32]. Reads with multiple COG/KO hits were counted once for each classification scheme. KO hits were also categorized into CAZy families (http://afmb.cnrs-mrs.fr/CAZY/). KEGG pathway maps are available on-line (http://gordonlab.wustl.edu/supplemental/Turnbaugh/obob/).

NR, COG, and KEGG comparisons were performed using NCBI BLASTX. RDP comparisons were performed using NCBI BLASTN, and microbiomes were directly compared using TBLASTX. A cutoff of e-value < 10^{-5} was used for EGT assignments and sequence comparisons[16] (corresponds to a p-value cutoff of 10^{-12} against the NR and KEGG databases, and 10^{-11} against the COG database). Given this cutoff, we would only expect three false EGT assignments in our combined analyses due to random chance. We also re-analyzed the data using a more stringent cutoff[33] (e-value < 10^{-8}).

Taxonomic assignments of shotgun 16S rRNA gene fragments – Shotgun reads containing a 16S rRNA fragment were identified by BLASTX comparison of each microbiome to the RDP database. 16S rRNA gene fragments were then aligned using the NASTA multi-aligner[34] with a minimum template length of 20 bases and a minimum

percent identity of 75%. The resulting alignment was then imported into an ARB neighbor-joining tree and hypervariable regions were masked using the lanemaskPH filter[35]. Direct BLAST taxonomic assignments were performed through BLASTX comparisons of each microbiome and the NR database. Best-BLAST-hits with an e-value $< 10^{-5}$ were used to assign each read to a given species.

Estimating the total number of orthologous groups – The total estimated number of COGs and NOGs (Non-supervised Orthologous Groups) in each sample was calculated using the lower-limit of the Chao1 95% confidence interval in EstimateS (Version 7.5, R. K. Colwell, http://purl.oclc.org/estimates), based on the number of EGTs assigned to each orthologous group. The number of missed groups was calculated by subtracting the estimated total (Chao1 lower-limit) from the observed number of groups.

Direct comparisons of microbiome sequences – Microbiomes sequenced using the 3730xl instrument were evaluated by reciprocal pairwise TBLASTX comparisons[16]. 8,832 reads were used from each microbiome to limit artifacts that arise from different sized datasets. Each possible pairwise comparison was made by using a BLAST database constructed from each microbiome. Samples were clustered based on the cumulative pairwise BLAST score. An estimate of distance was constructed using the D2 normalization and genome conservation approach previously used for genome clustering[36]. This method calculates a distance score based on the minimum cumulative BLAST score (sum of all best-BLAST-hit scores) between two microbiomes and the weighted average of both self-self comparisons ($D2 = -\ln(\min S_{1v2}, S_{2v1}/\text{average})$. The weighted average is calculated using $\text{average} = \text{squareroot}(2) * S_{1v1} * S_{2v2} / \text{squareroot}(S_{1v1}^2 + S_{2v2}^2)$. The resulting distances were used to create a distance matrix. A tree was

constructed using NEIGHBOR (PHYLIP version 3.64; kindly provided by J. Felsenstein, Department of Genome Sciences, University of Washington, Seattle), and was viewed using Treeview X[37].

Clustering of microbiomes based on predicted metabolic function – Microbiomes were clustered based on the percent representation of EGTs assigned to each COG, KEGG pathway, and phylotype (genome in NR) using Cluster3.0[25]. Percent representation was calculated as the number of EGTs assigned to a given group divided by the number of EGTs assigned to all groups. Single linkage hiearchical clustering via Pearson's correlation was performed on each dataset, and the results were visualized by using the Treeview Java applet[38]. Principal Component Analysis was also performed based on the percent representation of EGTs assigned to KEGG pathways (Cluster3.0[25]), and the data were graphed according to the first two coordinates.

Identification of statistically enriched and depleted metabolic groups – Two methods were used to determine statistically enriched or depleted metabolic groups: the cumulative binomial distribution[3] and a bootstrap analysis[16,17]. The cumulative binomial distribution was used for pairwise comparisons of microbiome COG, KEGG, and taxonomic assignments. The calculation uses the following inputs: number of successes for microbiome 1 (number of EGTs assigned to a given group), number of trials for microbiome 1 (total number of EGTs assigned to all groups), and the expected frequency (number of successes/number of trials for microbiome 2). The probability of having less than or equal to the number of observed EGTs in a given group was then calculated using the cumulative binomial distribution. Depletion was defined as having a probability less than 0.05, 0.01, or 0.001 assuming p equals the expected frequency and that the expected

frequency is normally distributed. Enrichment was defined as having a probability of greater than 0.95, 0.99, or 0.999 given the same assumptions. To minimize false negatives, no corrections for multiple sampling were made. To limit false positives resulting from low sampling, only groups with at least one hit in each microbiome were evaluated.

Xipe[17] (Rodriguez-Brito, version 0.2) was employed for bootstrap analyses of KEGG pathway enrichment and depletion, using the following parameters: 10,000 samples, 10,000 repeats, and three confidence levels (95%, 99%, and 99.9%). Briefly, a dataset composed of the number of EGTs assigned to each KEGG pathway was sampled with replacement from each microbiome 10,000 times. The difference between the number of EGTs per pathway in the first microbiome, and the number of EGTs per pathway in the second microbiome, was calculated for each group. This process was repeated 10,000 times and the median difference calculated for each pathway. A confidence interval was determined by pooling both datasets and comparing 10,000 random samples to 10,000 other random samples. Groups with a larger median difference between microbiomes than the confidence interval were considered significantly different.

Biochemical analyses – Short-chain fatty acids (SCFAs) were measured in nine cecal samples (4 lean, 5 obese) obtained from nine mice that had been used for our previous 16S rRNA gene sequence-based survey [animals C1, C3, C4, C9, C10, C13, C15 (lean2), C17, and C22 in ref. 6]. Two aliquots of each sample were evaluated. SCFA levels were quantified according to previously published protocols[15]: i.e., double diethyl ether extraction of deproteinized cecal contents spiked with isotope-labeled internal

SCFA standards; derivatization of SCFAs with N-tert-butyldimethylsilyl-N-methyltrifluoracetamide (MTBSTFA); and GC-MS analysis of the resulting TBDMS-derivatives.

Bomb calorimetry was performed on 44 fecal samples collected from 22 mice (9 lean, 13 obese). Each mouse was transferred to a clean cage for 24 hours, at which point fecal samples were collected and oven dried at 60^{o}C for 48 hours. Gross energy content was measured using a semimicro oxygen bomb calorimeter, calorimetric thermometer, and semimicro oxygen bomb (Models 6725, 6772 and 1109, respectively, from Parr Instrument Co.). The calorimeter energy equivalent factor was determined using benzoic acid standards. The mean of each distribution was compared using a two-tailed Student's t-Test.

Microbiota transplantation experiments – Germ-free C57BL/6J mice (8-9 weeks old) were colonized with a cecal microbiota obtained from either a lean (+/+) or an obese (*ob/ob*) C57BL/6J donor (n=1 donor and 4-5 recipients/treatment group/experiment; 2 independent experiments). Recipient mice were anesthetized at 0 and 14 days post colonization with an i.p. injection of ketamine (10 mg/kg body weight) and xylazine (10mg/kg) and total body fat content was measured by dual-energy x-ray absorptiometry (Lunar PIXImus Mouse, GE Medical Systems) using previously described protocols[39]. Donor mice were sacrificed at day 0 and recipient mice after the final DEXA on day 14.

16S rRNA sequence-based surveys of the cecal microbiotas of conventionalized mice – Cecal contents were recovered at the time of sacrifice by manual extrusion and frozen immediately at -80°C. DNA was prepared by bead beating,

phenol/chloroform extraction, and gel purification (see above). Five replicate PCRs were performed for each mouse. Each 25 μl reaction contained 50-100 ng of purified DNA from cecal contents, 10 mM Tris (pH 8.3), 50 mM KCl, 2 mM $MgSO_4$, 0.16 μM dNTPs, 0.4 μM of the bacteria-specific primer 8F (5'-AGAGTTTGATCCTGGCTCAG-3'), 0.4 μM of the universal primer 1391R (5'-GACGGGCGGTGWGTRCA-3'), 0.4 M betaine, and 3 units of Taq polymerase (Invitrogen). Cycling conditions were 94°C for 2 min, followed by 35 cycles of 94°C for 1 min, 55°C for 45 sec, and 72°C for 2 min, with a final extension period of 20 min at 72°C. Replicate PCRs were pooled, concentrated with Millipore columns (Montage), gel-purified with the Qiaquick kit (Qiagen), cloned into TOPO TA pCR4.0 (Invitrogen), and transformed into *E. coli* TOP10 (Invitrogen). For each mouse, 384 colonies containing cloned amplicons were processed for sequencing. Plasmid inserts were sequenced bidirectionally using vector-specific primers and the internal primer 907R (5'-CCGTCAATTCCTTTRAGTTT-3').

16S rRNA gene sequences were edited and assembled into consensus sequences using the PHRED and PHRAP software packages within the Xplorseq program[40]. Sequences that did not assemble were discarded and bases with PHRED quality scores <20 were trimmed. Sequences were checked for chimeras using Bellerophon[41] and sequences with greater than 95% identity to both parents were removed (n=535; 13% of aligned sequences). The final dataset (n=4,157 sequences; for ARB alignment and tree see http://gordonlab.wustl.edu/supplemental/Turnbaugh/obob/; for sequence designations see **Supplementary Table 7**) was aligned using the on-line version of the NAST multi-aligner[34] (minimum alignment length=1250; percent identity >75), hypervariable regions were masked using the lanemaskPH filter provided with the ARB database[35], and the

aligned sequences were added to the ARB neighbor-joining tree (based on pairwise distances with the Olsen correction) with the parsimony insertion tool. A phylogenetic tree containing all 16S rRNA gene sequences was exported from ARB and clustered using online UniFrac[21] without abundance weighting.

Supplementary Notes

26. Dailey, F. E. & Cronan, J. E., Jr. Acetohydroxy acid synthase I, a required enzyme for isoleucine and valine biosynthesis in *Escherichia coli K-12* during growth on acetate as the sole carbon source. *J. Bacteriol* **165**, 453-460 (1986).

27. Dailey, F. E., Cronan, J. E., Jr. & Maloy, S. R. Acetohydroxy acid synthase I is required for isoleucine and valine biosynthesis by *Salmonella typhimurium LT2* during growth on acetate or long-chain fatty acids. *J. Bacteriol* **169**, 917-919 (1987).

28. Hooper, L. V. *et al.* (2002) in Molecular Cellular Microbiology, eds. Sansonetti, P. & Zychlinsky, A. (Academic San Diego), Vol. **31**, pp. 559-589.

29. Huang, X., Wang, J., Aluru, S., Yang, S. P. & Hillier, L. PCAP: a whole-genome assembly program. *Genome Res.* **13**, 2164-2170 (2003).

30. Delcher, A. L., Harmon, D., Kasif, S., White, O. & Salzberg, S. L. Improved microbial gene identification with GLIMMER. *Nucleic Acids Res.* **27**, 4636-4641 (1999).

31. Mulder, N. J. *et al.* InterPro, progress and status in 2005. *Nucleic Acids Res.* **33**, D201-205 (2005).

32. Cole, J. R. *et al.* The Ribosomal Database Project (RDP-II): sequences and tools for high-throughput rRNA analysis. *Nucleic Acids Res.* **33**, D294-296 (2005).

33 . Tringe, S. G. *et al.* Comparative metagenomics of microbial communities. *Science* **308**, 554-557 (2005).

34. DeSantis, T. Z. *et al.* NAST: a multiple sequence alignment server for comparative analysis of 16S rRNA genes. *Nucleic Acids Res.* **34**, W394-399 (2006).

35. Ludwig, W. *et al.* ARB: a software environment for sequence data. *Nucleic Acids Res.* **32**, 1363-1371 (2004).

36. Kunin, V., Ahren, D., Goldovsky, L., Janssen, P. & Ouzounis, C. A. Measuring genome conservation across taxa: divided strains and united kingdoms. *Nucleic Acids Res.* **33**, 616-621 (2005).

37. Page, R. D. TreeView: an application to display phylogenetic trees on personal computers. *Comput. Appl. Biosci.* **12**, 357-358 (1996).

38. Saldanha, A. J. Java Treeview--extensible visualization of microarray data. *Bioinformatics* **20**, 3246-3248 (2004).

39. Bernal-Mizrachi, C. *et al.* Respiratory uncoupling lowers blood pressure through a leptin-dependent mechanism in genetically obese mice. *Arterioscler Thromb Vasc Biol.* **22**, 961-968 (2002).

40. Papineau, D., Walker, J. J., Mojzsis, S. J. & Pace, N. R. *Appl. Environ. Microbiol.* **71**, 4822-4832 (2006).

41. Huber, T., Faulkner, G. & Hugenholtz, P. Bellerophon: a program to detect chimeric sequences in multiple sequence alignments. *Bioinformatics* **20**, 2317-2319 (2004).

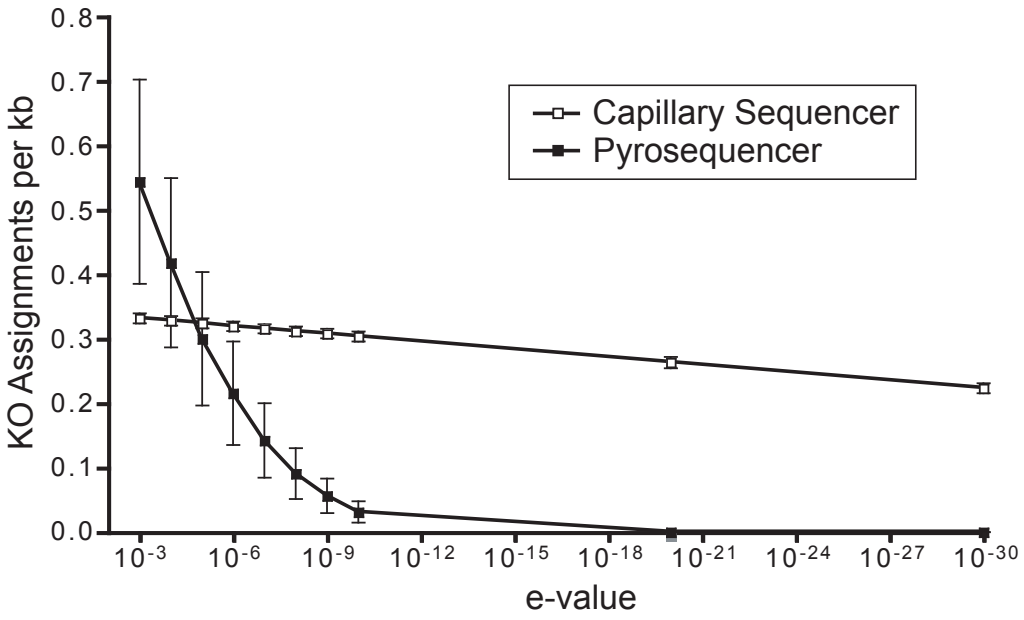

Supplementary Figure 1: The effect of decreasing e-value cut-offs on EGT assignments to the KEGG database from pyrosequencer and capillary sequencer datasets. Points indicate the average number of KO assignments per kb of microbiome sequence. Mean values ± s.e.m. are plotted. The GS20 pyrosequencer and the 3730xl capillary sequencer both resulted in an average 0.3 KO (KEGG orthology) assignments per kb of sequence at an e-value cutoff $<10^{-5}$. However, the number of EGTs present in the pyrosequencer-derived datasets rapidly decays as the e-value cutoff is decreased, whereas the number of EGTs present in the capillary sequencer datasets is relatively stable to $<10^{-30}$.

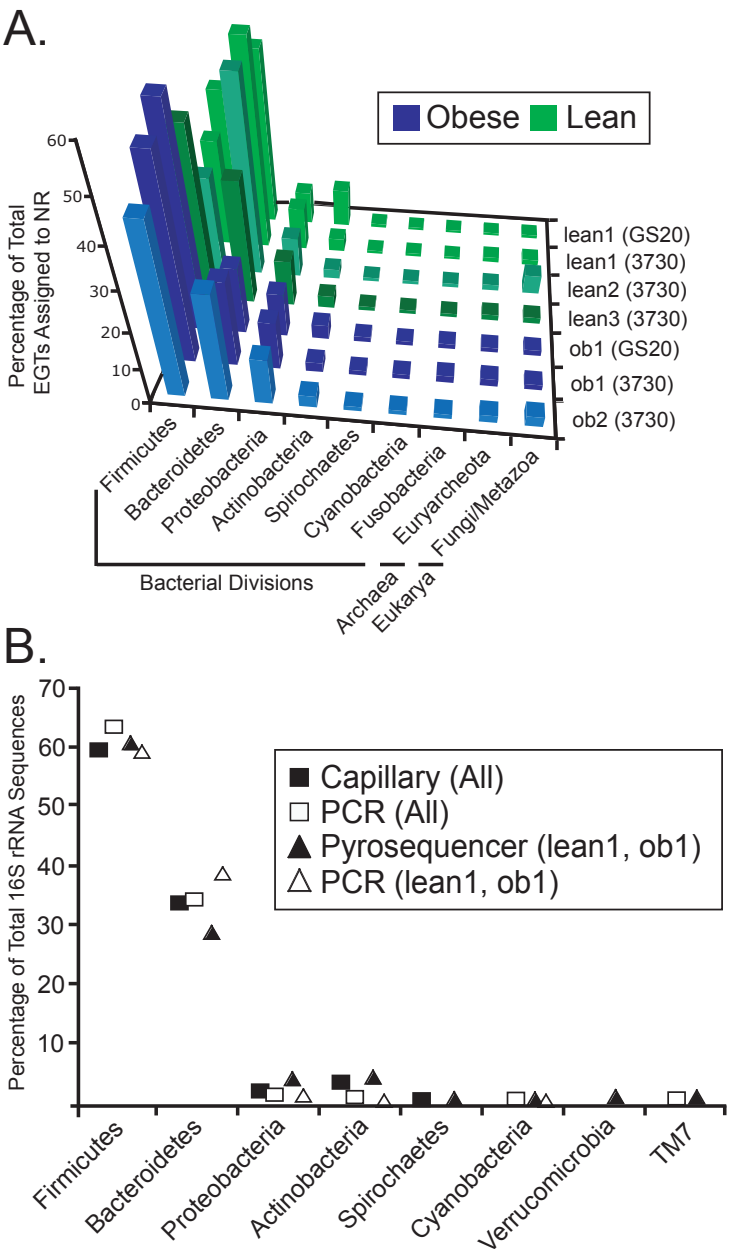

Supplementary Figure 2: Taxonomic assignments of EGTs and 16S rRNA gene fragments. (A) Relative abundance of EGTs (reads assigned to NR, BLASTX with an e-value<10^{-5}) in each cecal microbiome confirms the presence of the indicated bacterial divisions in addition to Euryarcheota. Metazoan sequences (including *Mus musculus* and fungi) are also present at low abundance. Bacterial divisions with greater than 1% representation in at least three microbiomes are shown. (B) Alignment of 16S rRNA gene fragments (black) confirms our previous PCR-derived 16S rRNA gene sequence-based survey[6] (white). Comparisons include all microbiomes sampled with the capillary sequencer (square) and the two microbiomes sampled with the pyro-sequencer (triangle).

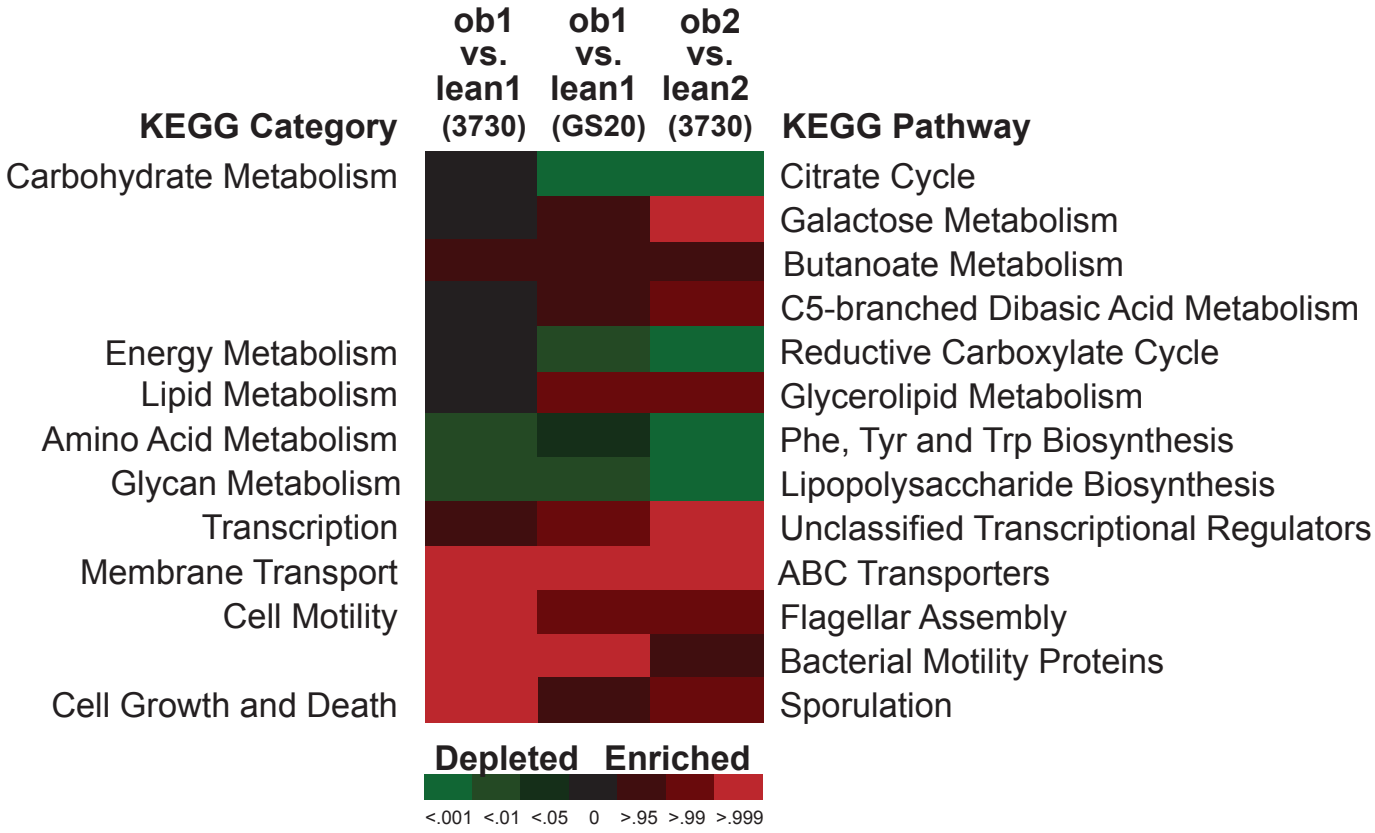

Supplementary Figure 3: KEGG pathways that are enriched or depleted in the cecal microbiomes of both obese versus lean sibling pairs, as indicated by bootstrap analysis of relative gene content. Pathways that are consistently enriched or depleted in the pyrosequencer-based comparison of ob1 versus lean1 littermates, and the capillary sequencer-based comparison of ob2 versus lean2 littermates are shown. Red indicates enrichment and green indicates depletion (brightness denotes level of significance). Black indicates groups that are not significantly changed.

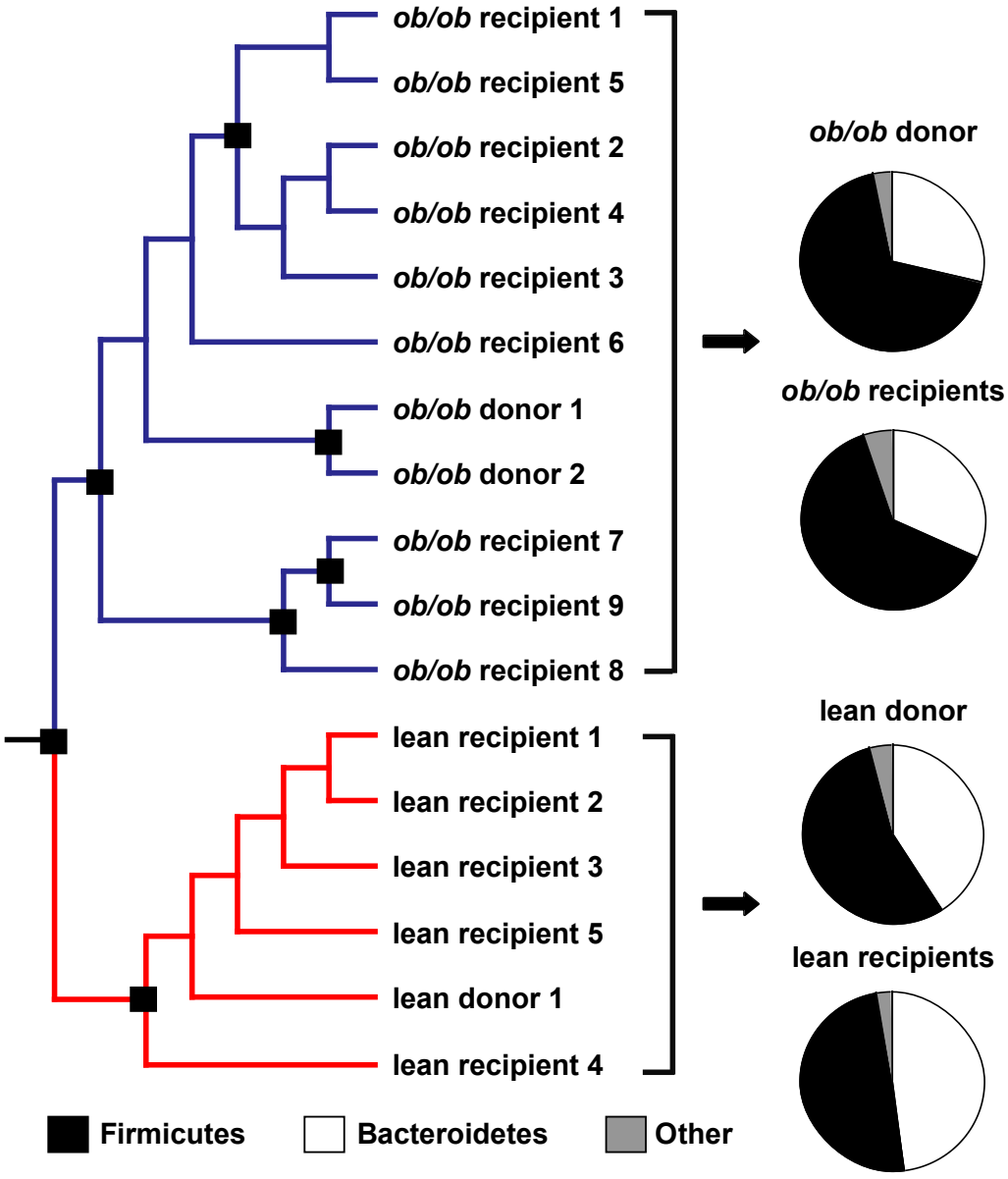

Supplementary Figure 4: Analyses of microbial communities harvested from obese (*ob/ob*) and lean (+/+) C57BL/6J donor mice and colonized gnotobiotic recipients. Online Unifrac clustering[21] of microbial community structure, based on 4,157 16S rRNA gene sequences (see Supplementary Table 7 for number of sequences per sample; ARB tree available at http://gordonlab.wustl.edu/supplemental/Turnbaugh/obob/). Nodes denoted by a black square are robust to sequence number (jackknife values > 0.70, representing the number of times the node was present when 166 sequences were randomly chosen for each mouse for n=100 replicates). Pie charts indicate the average relative abundance of Firmicutes (black), Bacteroidetes (white), and other (grey; includes Verrucomicrobia, Proteobacteria, Actinobacteria, TM7, and Cyanobacteria) in the donor and recipient microbial communities.

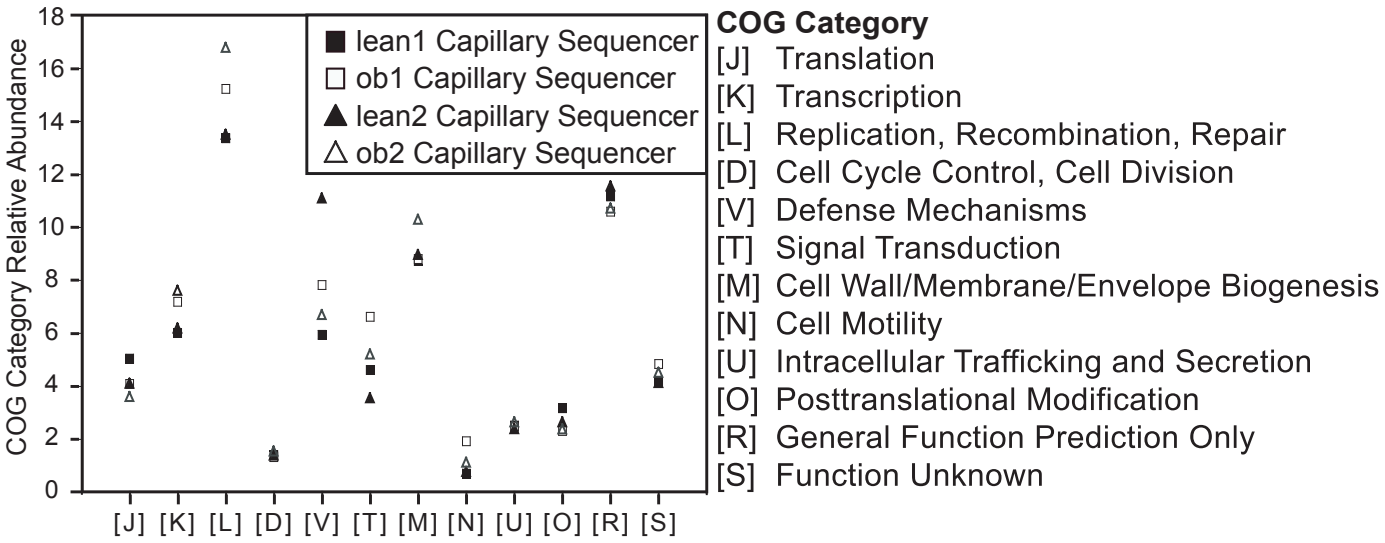

Supplementary Figure 5: Relative abundance of COG categories (percentage of total EGTs assigned to COG using BLASTX and e-value<10^{-5}) in the lean1 (black square), ob1 (white square), lean2 (black triangle), and ob2 (white triangle) cecal microbiomes. Microbiomes were characterized by capillary sequencing.

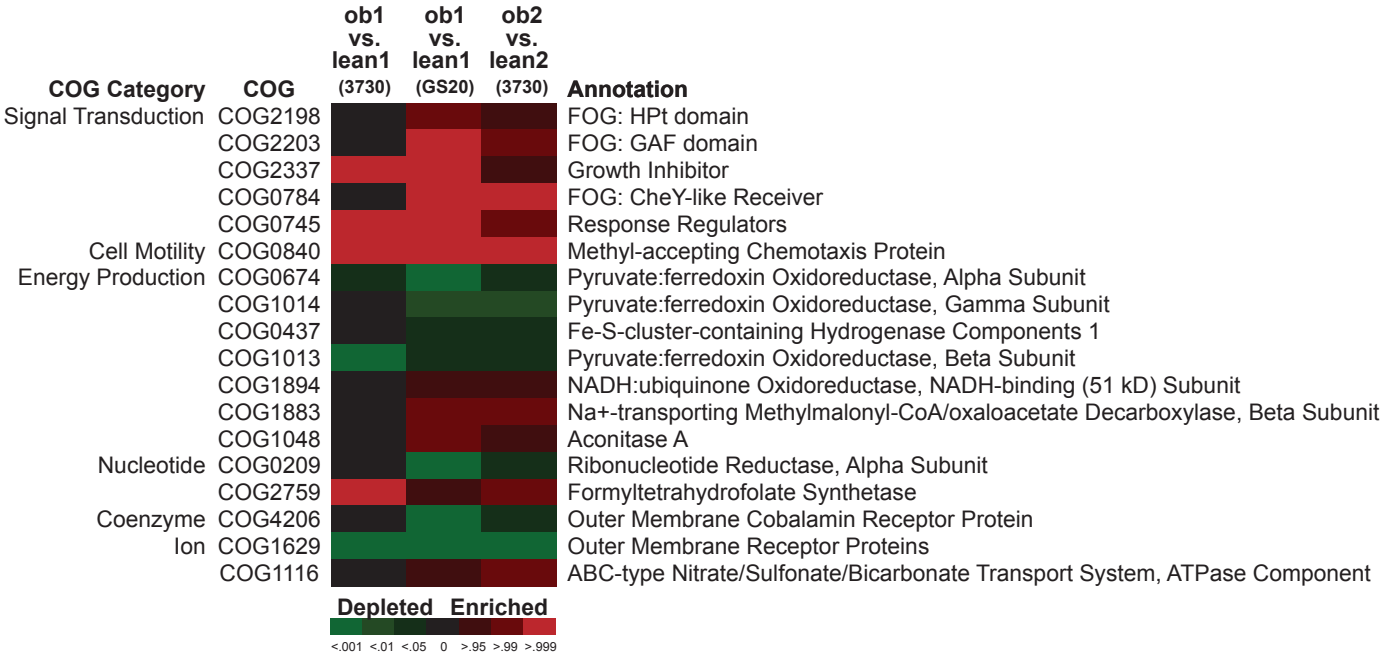

Supplementary Figure 6: COGs that are enriched or depleted in the cecal microbiomes of both obese versus lean sibling pairs, as indicated by binomial comparisons of relative gene content. The COGs shown are enriched or depleted in the pyrosequencer-based comparison of ob1 versus lean1 littermates and the capillary sequencer-based comparison of ob2 versus lean2 littermates. Red indicates enrichment and green indicates depletion (brightness denotes level of significance). Black indicates groups that are not significantly changed.

Supplementary Table 1 – Nomenclature used to designate metagenomic datasets obtained from the cecal microbiota of C57BL/6J *ob/ob*, *ob*/+, and +/+ littermates.

Figure label	Metagenome label	Litter	16S rRNA survey label[1]	Tree label[1]	Host genotype
ob1	PT6	1	C23	M2B-4	*ob/ob*
ob2	PT4	2	C18	M1-2	*ob/ob*
lean1	PT3	1	C21	M2B-1	+/+
lean2	PT8	2	C15	M1-3	*ob*/+
lean3	PT2	2	C16	M1-4	+/+

[1]Samples obtained from our previous 16S rRNA survey (ref. 6).

Supplementary Table 2 – Sequencing results for each cecal microbiome.

Microbiome	Average read length	Number of reads	Sequence
lean1 (GS20)	90.9	1,046,611	94,913,476
ob1 (GS20)	96.4	677,384	65,370,448
lean1 (3730xl)	765	10,752	8,227,047
lean2 (3730xl)	782	11,136	8,705,876
lean3 (3730xl)	706	10,752	7,590,528
ob1 (3730xl)	735	11,136	8,185,880
ob2 (3730xl)	771	8,832	6,811,035
TOTAL	**-**	**1,776,603**	**199,804,290**

Abbrevations: GS20, pyrosequencer; 3730xl, capillary sequencer

Supplementary Table 3 – Assembly of reads from capillary sequencer and pyrosequencer datasets.

Sample	Contigs	Average contig length	Contiged bases[1]	Largest Assembly	N50 contig length (kb)[2]
lean1 (GS20)	102,299	117	11,966,580	2,793	0.109
ob1 (GS20)	56,425	116	6,518,469	2,174	0.109
lean1 (3730xl)	167	1527	254,985	5,500	1.62
lean2 (3730xl)	407	1598	650,499	5,522	1.71
lean3 (3730xl)	224	1528	342,172	3,281	1.59
ob1 (3730xl)	320	1393	445,814	3,225	1.49
ob2 (3730xl)	269	1644	442,210	4,186	1.70
All (3730xl)	2,575	1734	4,465,685	11,213	1.78
All (GS20)	159,245	118	18,809,438	2,708	0.110
All (GS20 and 3730xl)	13,667	898	12,275,469	14,755	0.903

[1]Contiged bases refers to the combined length of all contigs.

[2]N50 contig length refers to the length of the contig, such that 50% of the total contiged bases are present in contigs of greater or equal size.

Assembly of the GS20 pyrosequencer datasets from lean1 (+/+) or ob1 (*ob/ob*) produced very modest contiguity. Note that assembly of all GS20 pyrosequencer data from both lean1 and ob1 did not improve contiguity. However, including the five 3730xl datasets increased the average contig length to 1kb, and the largest contig to >14 kb.

Supplementary Table 4 – Number of EGTs assigned to the NR, COG, and/or KEGG databases.

Microbiome	Total NR EGTs	Total COG EGTs	Total KO EGTs	Total EGTs	Percent unassigned
lean1 (GS20)	48,625	51,481	28,359	56,599	94.6
ob1 (GS20)	33,360	32,819	18,308	39,058	94.2
lean1 (3730xl)	7,973	7,970	2,810	8,462	21.3
lean2 (3730xl)	7,309	7,687	2,723	8,170	26.6
lean3 (3730xl)	7,042	7,119	2,562	7,616	29.2
ob1 (3730xl)	7,331	7,299	2,639	7,859	29.4
ob2 (3730xl)	6,008	6,016	2,053	6,425	27.3

Supplementary Table 5 – Percentage of total assigned reads among each taxonomic domain based on BLASTX searches of the NR database with an e-value cutoff<10^{-5}.

Domain	lean1 3730xl	lean1 GS20	lean2 3730xl	lean3 3730xl	ob1 3730xl	ob1 GS20	ob2 3730xl
Archaea	1.28	0.658	1.55	1.59	2.07	1.23	2.08
Bacteria	95.8	97.9	90.7	95.1	94.4	93.4	92.9
Eukarya	2.36	1.39	7.36	2.74	2.77	4.15	4.19
(Viruses)	0.527	0.065	0.383	0.611	0.709	1.21	0.782

Supplementary Table 6 – KEGG pathways enriched in the pooled *ob/ob* cecal microbiome relative to the pooled lean cecal microbiome (capillary sequencing datasets, ob1+ob2 vs. lean1+lean2+lean3, binomial test, P<0.05).

KEGG Category	KEGG Pathway[1]
Carbohydrate Metabolism	Starch and sucrose metabolism
	Aminosugars metabolism
	Nucleotide sugars metabolism
Amino Acid Metabolism	Lysine biosynthesis
Metabolism of Other Amino Acids	D-Alanine metabolism
Glycan Biosynthesis and Metabolism	N-Glycan degradation
	Glycosaminoglycan degradation
	Glycosphingolipid metabolism
Biosynthesis of Polyketides and Nonribosomal Peptides	Polyketide sugar unit biosynthesis
	Biosynthesis of vancomycin group antibiotics
Transcription	Other and unclassified family transcriptional regulators
Folding, Sorting and Degradation	Type III secretion system
	Membrane Transport
	ABC transporters
Folding, Sorting and Degradation	Phosphotransferase system (PTS)
Signal Transduction	Two-component system
Cell Motility	Bacterial chemotaxis
	Flagellar assembly
	Bacterial motility proteins
Cell Growth and Death	Sporulation

[1]Only pathways with greater than ten hits in both pooled datasets are shown.

Supplementary Table 7 – 16S rRNA gene-sequence libraries from microbiota transplant experiments.

Label in Fig. S4	ARB label	Host Genotype	16S gene sequences
lean donor 1	lean2	+/+	166
ob/ob donor 1	obob1	*ob/ob*	199
ob/ob donor 2	obob2	*ob/ob*	229
lean recipient 1	SWPT11	+/+	248
lean recipient 2	SWPT13	+/+	265
lean recipient 3	SWPT18	+/+	247
lean recipient 4	SWPT19	+/+	278
lean recipient 5	SWPT20	+/+	271
ob/ob recipient 1	SWPT1	+/+	219
ob/ob recipient 2	SWPT2	+/+	268
ob/ob recipient 3	SWPT3	+/+	280
ob/ob recipient 4	SWPT4	+/+	272
ob/ob recipient 5	SWPT5	+/+	290
ob/ob recipient 6	SWPT12	+/+	197
ob/ob recipient 7	SWPT14	+/+	272
ob/ob recipient 8	SWPT15	+/+	198
ob/ob recipient 9	SWPT16	+/+	258
TOTAL	**-**	**-**	**4,157**

Supplementary Table 8 – KEGG pathways depleted in the pooled *ob/ ob* cecal microbiome relative to the pooled lean cecal microbiome (capillary sequencing datasets, ob1+ob2 vs. lean1+lean2+lean3, binomial test, P<0.05).

KEGG Category	KEGG Pathway[1]
Carbohydrate Metabolism	Glycolysis / Gluconeogenesis
	Citrate cycle (TCA cycle)
	Pentose phosphate pathway
	Pentose and glucuronate interconversions
	Fructose and mannose metabolism
Energy Metabolism	Carbon fixation
	Reductive carboxylate cycle (CO2 fixation)
	Pyruvate/Oxoglutarate oxidoreductases
Lipid Metabolism	Fatty acid metabolism
Nucleotide Metabolism	Pyrimidine metabolism
Amino Acid Metabolism	Glutamate metabolism
	Glycine, serine and threonine metabolism
	Cysteine metabolism
	Arginine and proline metabolism
	Phenylalanine, tyrosine and tryptophan biosynthesis
Glycan Biosynthesis and Metabolism	Lipopolysaccharide biosynthesis
Metabolism of Cofactors and Vitamins	Riboflavin metabolism
	Folate biosynthesis
Translation	Ribosome
Folding, Sorting and Degradation	Other ion-coupled transporters

[1]Only pathways with greater than ten hits in both pooled datasets are shown.

Supplementary Table 9 – COG categories involved in information storage and cellular processes that are enriched or depleted in the pooled *ob/ob* cecal microbiome relative to the pooled lean cecal microbiome (capillary sequencing datasets, ob1+ob2 vs. lean1+lean2+lean3, binomial test, P<0.05).

ENRICHED
[K] Transcription
[L] Replication, recombination, repair
[Y] Nuclear structure
[T] Signal transduction
[M] Cell wall/membrane/envelope biogenesis
[N] Cell motility

DEPLETED
[J] Translation
[V] Defense mechanisms
[O] Posttranslational modification, protein turnover, chaperones

APPENDIX B

John F. Rawls, Michael A. Mahowald, Ruth E. Ley and Jeffrey I. Gordon

Reciprocal Gut Microbiota Transplants from Zebrafish and Mice to Germ-free Recipients Reveal Host Habitat Selection

Cell. *2006* Oct 20;**127**(2):423-33.

For supplemental tables please see enclosed CD.

Cell

Reciprocal Gut Microbiota Transplants from Zebrafish and Mice to Germ-free Recipients Reveal Host Habitat Selection

John F. Rawls,[1,2] Michael A. Mahowald,[1] Ruth E. Ley,[1] and Jeffrey I. Gordon[1,*]
[1] Center for Genome Sciences, Washington University School of Medicine, St. Louis, MO 63108 USA
[2] Present address: Department of Cell and Molecular Physiology, University of North Carolina at Chapel Hill, Chapel Hill, NC 27599 USA.
*Contact: jgordon@wustl.edu
DOI 10.1016/j.cell.2006.08.043

SUMMARY

The gut microbiotas of zebrafish and mice share six bacterial divisions, although the specific bacteria within these divisions differ. To test how factors specific to host gut habitat shape microbial community structure, we performed reciprocal transplantations of these microbiotas into germ-free zebrafish and mouse recipients. The results reveal that communities are assembled in predictable ways. The transplanted community resembles its community of origin in terms of the lineages present, but the relative abundance of the lineages changes to resemble the normal gut microbial community composition of the recipient host. Thus, differences in community structure between zebrafish and mice arise in part from distinct selective pressures imposed within the gut habitat of each host. Nonetheless, vertebrate responses to microbial colonization of the gut are ancient: Functional genomic studies disclosed shared host responses to their compositionally distinct microbial communities and distinct microbial species that elicit conserved responses.

INTRODUCTION

Animal evolution has occurred, and is occurring, in a world dominated by microorganisms. As animals evolved to occupy different habitats (addresses) and niches (professions) in our biosphere, they have forged strategic alliances with microorganisms on their body surfaces. The genomes of microbes within these consortia encode physiologic traits that are not represented in host genomes: Microbial-microbial and host-microbial mutualism endows the resulting "super-organisms" with a fitness advantage (Ley et al., 2006b). The majority of these microbes are present in digestive tract communities where, among other things, they contribute to the harvest of dietary nutrients that would otherwise be inaccessible (Bäckhed et al., 2004; Sonnenburg et al., 2005), as well as to the education of the host's immune system (Cebra, 1999).

The advent of massively parallel DNA sequencers provides an opportunity to define the gene content of these indigenous microbial communities with increased speed and economy. These "microbiome" sequencing projects promise to provide a more comprehensive view of the genetic landscape of animal-microbial alliances and testable hypotheses about the contributions of microbial communities to animal biology. The results should allow a number of fundamental questions to be addressed. Is there an identifiable core microbiota and microbiome associated with a given host species? How are a microbiota and its microbiome selected, and how do they evolve within and between hosts? What are the functional correlates of diversity in the membership of a microbiota and in the genetic composition of its microbiome?

Answers to these questions also require model organisms to assess how communities are assembled, to determine how different members impact community function and host biology, and to ascertain the extent of redundancy or modularity within a microbiota. One approach for generating such models is to use gnotobiotics—the ability to raise animals under germ-free (GF) conditions—to colonize them at varying points in their life cycle with a single microbe or more complex collections, and to then observe the effects of host habitat on microbial community structure and function and of the community on the host. Methods for raising and propagating rodents under GF conditions have been available for 50 years (see Wostmann, 1981), although genomic and allied computational methods for comprehensively assessing microbial community composition, gene content, and host-microbial structure/function relationships have only been deployed in the last five years (e.g., Hooper and Gordon, 2001; Ley et al., 2005). Recently, we developed techniques for rearing the zebrafish (*Danio rerio*) under GF conditions (Rawls et al., 2004). In principle, this model organism provides a number of attractive and distinctive features for analyzing host-microbial mutualism. Zebrafish remain transparent until adulthood, creating an opportunity to visualize microbes

in their native gut habitats in real time. A deep draft reference genome sequence of *D. rerio* is available (http://www.sanger.ac.uk/Projects/D_rerio/). In addition, forward genetic tests and chemical screens can be conducted (Patton and Zon, 2001; Peterson and Fishman, 2004) to characterize zebrafish signaling pathways regulated by microbial consortia and/or their component members.

A preliminary functional genomic study of the effects of colonizing GF zebrafish with an unfractionated microbiota harvested from adult conventionally raised (CONV-R) zebrafish revealed 59 genes whose responses were similar to those observed when GF mice were colonized with an adult mouse gut microbiota (Rawls et al., 2004). These genes encode products affecting processes ranging from nutrient metabolism to innate immunity and gut epithelial cell turnover (Rawls et al., 2004). The experiments did not distinguish whether the host responses were evolutionarily conserved and thus present in the last common ancestor of fish and mammals, or if they had been independently derived in mammals and fish. However, the fact that numerous homologous genes and shared cellular changes comprised the "common" response favors the notion of evolutionary conservation over convergence. It was also unclear whether these common host responses were elicited by the same or different bacterial signals in each host or by signals from the whole community versus from specific bacteria.

A recent comprehensive 16S rRNA sequence-based survey of the adult mouse gut disclosed that, as in humans, >99% of the bacterial phylogenetic types (phylotypes) belong to two divisions—the Firmicutes and Bacteroidetes (Ley et al., 2005). In contrast, limited surveys of different fish species indicate that their gut communities are dominated by the Proteobacteria (Cahill, 1990; Huber et al., 2004; Rawls et al., 2004; Bates et al., 2006; Romero and Navarrete, 2006). Fish and mammals live in very different environments, so it is possible that differences in their gut microbiotas arise from "legacy effects" (e.g., local environmental microbial community composition or inheritance of a microbiota from a parent). Furthermore, legacy effects might combine with "gut habitat effects" (e.g., distinct selective pressures arising from differences in anatomy, physiology, immunologic "climate," or nutrient milieu) to shape the different community structures of fish and mammals.

In the present study, we have performed reciprocal microbiota transplantations in GF zebrafish and mice. We provide evidence that gut habitat shapes microbial community structure and that both animal species respond in remarkably similar ways to components of one another's microbiota.

RESULTS

Comparison of the Zebrafish and Mouse Gut Microbiota: Overlapping Bacterial Divisions but Marked Differences at More Shallow Phylogenetic Resolution

Our previous survey of the gut microbiota of adult CONV-R zebrafish was limited to 176 bacterial 16S rRNA gene sequences (Rawls et al., 2004). Therefore, we performed a more comprehensive analysis of intestinal contents pooled from 18 adult male and female C32 zebrafish (comprised of two independent pools, each containing material from 9 animals). A total of 1456 bacterial 16S rRNA sequences formed the final analyzed dataset: 616 from pool 1 and 840 from pool 2 (libraries JFR0503 and JFR0504, respectively, in Table S1 available with this article online). Phylogenetic analysis revealed 198 "species-level" phylotypes defined by 99% pairwise sequence identity. These phylotypes represented a total of 11 bacterial divisions and were dominated by the Proteobacteria (82% ± 22.9% [SD] of all clones averaged across both libraries) and the Fusobacteria (11% ± 15.2%; Figures 1 and 2). The Firmicutes, Bacteroidetes, Verrucomicrobia, Actinobacteria, TM7, Planctomycetes, TM6, Nitrospira, and OP10 divisions were minor components (3.2%–0.6%).

Six of the eleven bacterial divisions found in adult zebrafish are also found in mice (Ley et al., 2005); five of these are also shared by the adult human microbiota (Eckburg et al., 2005; Figure 1A). However, zebrafish community members within these shared divisions are distinct from those in mice and humans at more shallow phylogenetic resolution (Figures 1B–1D).

The Gut Selects Its Microbial Constituents

The composition of the mouse gut microbiota is affected by host genotype, as well as by legacy (it is inherited from the mother; Ley et al., 2005). To determine whether the observed differences between zebrafish and mouse microbiotas reflect host genome-encoded variations in their gut habitats versus differences in the local microbial consortium available for colonization, we colonized (1) adult GF mice with an unfractionated gut microbiota harvested from CONV-R adult zebrafish (yielding "Z-mice") and (2) GF zebrafish larvae with a gut microbiota from CONV-R adult mice ("M-zebrafish"). By comparing the composition of the community introduced into the GF host ("input community") with the community that established itself in the host (Z-mouse or M-zebrafish "output community"), we sought to determine whether gut microbial ecology is primarily influenced by legacy effects (the input community structure would persist in the new host) versus gut habitat effects (the representation changes when certain taxa are selected).

We introduced the pooled intestinal contents of 18 CONV-R adult zebrafish belonging to the C32 inbred strain (pools 1 and 2 above) into adult GF mice belonging to the NMRI inbred strain (n = 6, Table S1, Figure S1). The resulting Z-mice were housed in gnotobiotic isolators and sacrificed 14 days after colonization (i.e., after several cycles of replacement of the intestinal epithelium and its overlying mucus layer). Their cecal contents were harvested and provided community DNA for 16S rRNA sequence-based enumerations. The cecum was selected for this analysis because it is a well-defined anatomic structure located at the junction of the small intestine and colon, and its luminal contents can be readily and

A

Bacterial division	Zebrafish	Mouse	Human
Proteobacteria	+	+	+
Firmicutes	+	+	+
Bacteroidetes	+	+	+
Verrucomicrobia	+	+	+
Actinobacteria	+	+	+
TM7	+	+	
Fusobacteria	+		+
Planctomycetes	+		
TM6	+		
Nitrospira	+		
OP10	+		
Cyanobacteria		+	+
Deferribacteria		+	
Gemmimonoas		+	
Spirochaeates			+
VadinBE97			+

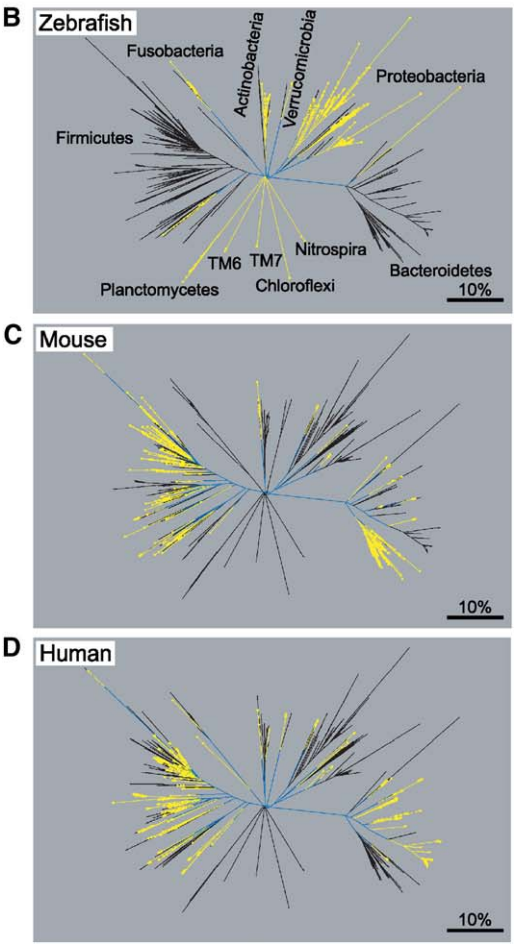

Figure 1. Bacterial Divisions and Their Lineages Detected in the Zebrafish Digestive Tract, Mouse Cecum, and Human Colon

(A) Summary of shared and distinct bacterial divisions in the zebrafish, mouse, and human gut microbiota (data from this study; Rawls et al., 2004; Ley et al., 2005; Eckburg et al., 2005; Bäckhed et al., 2005). Divisions found in the normal gut microbiota of each host are indicated (+). (B–D) Phylogenetic trees constructed from enumeration studies of the zebrafish digestive tract (B), mouse cecal (C), and human colonic (D) microbiotas. The zebrafish data are 1456 16S rRNA gene sequences derived from adult CONV-R C32 fish. The mouse data are 2196 sequences from adult CONV-R C57Bl/6J mice and their mothers (Ley et al., 2005). The human dataset contains 2989 bacterial 16S rRNA sequences from colonic mucosal biopsies and a fecal sample obtained from a healthy adult (Eckburg et al., 2005). Within a given panel, yellow lines indicate lineages unique to the host, blue lines indicate lineages that are shared by at least one other host, while black lines indicate lineages that are absent from the host. The scale bar indicates 10% pairwise 16S rRNA sequence divergence.

reliably recovered. It also harbors a very dense microbial population in CONV-R mice (10^{11}–10^{12} organisms/ml luminal contents) that has been comprehensively surveyed (Ley et al., 2005).

In addition to the 1456 16S rRNA sequences representing 198 phylotypes from the input zebrafish community (libraries JFR0503 and JFR0504; see above), we obtained a total of 1836 sequences representing 179 phylotypes from the Z-mouse cecal community (libraries JFR0507–12; Figures S1 and S2). Only 12% of the phylotypes found in the Z-mouse community, representing 39% of all sequences, were detected in the input zebrafish community. The dominant division in the input zebrafish community (Proteobacteria) persisted but shrank in abundance in the Z-mouse community (82% ± 22.9% in the input versus 41.7% ± 8.9% in the output; Figure 2). The Z-mouse community only contained members of the γ- and β-Proteobacteria subdivisions, whereas the input zebrafish community had also included δ- and α-Proteobacteria. In addition, members of the Bacteroidetes detected in the input zebrafish community were not observed in the Z-mouse community. The Z-mouse community showed a striking amplification of the Firmicutes (1% ± 1.1% of the input, 54.3% ± 6.5% of the Z-mouse output; Figure 2); this amplification included members of Bacilli as well as Clostridia classes.

By comparing communities at multiple thresholds for pairwise percent identity among 16S rRNA gene sequences (%ID), we determined that divergence between the input zebrafish and output Z-mouse communities occurred at 89%ID and higher (Figure 3). This implies that genera represented within the zebrafish and Z-mouse gut microbiotas are different but represent the same major lineages. The analysis also demonstrated that the phylotypes that bloomed in the mouse cecum were minor constituents of the input zebrafish digestive tract community. Despite the difference in genus/species representation, the richness and diversity of the input zebrafish and Z-mouse gut communities remained similar through the shift in microbial community composition (Figure S2 and Table S1).

When a similar analysis was applied to the input mouse and M-mouse communities obtained from a mouse-into-mouse microbiota transplant experiment (Bäckhed et al., 2004), we found that a high degree of similarity was maintained at levels as great as 97%ID (Figure 3). Based on these results, we concluded that (1) the difference in composition of the input zebrafish and output Z-mouse communities is not likely to be due to the microbiota transplantation procedure per se and (2) the adult mouse cecum is able to support a complex foreign microbial consortium by shaping its composition.

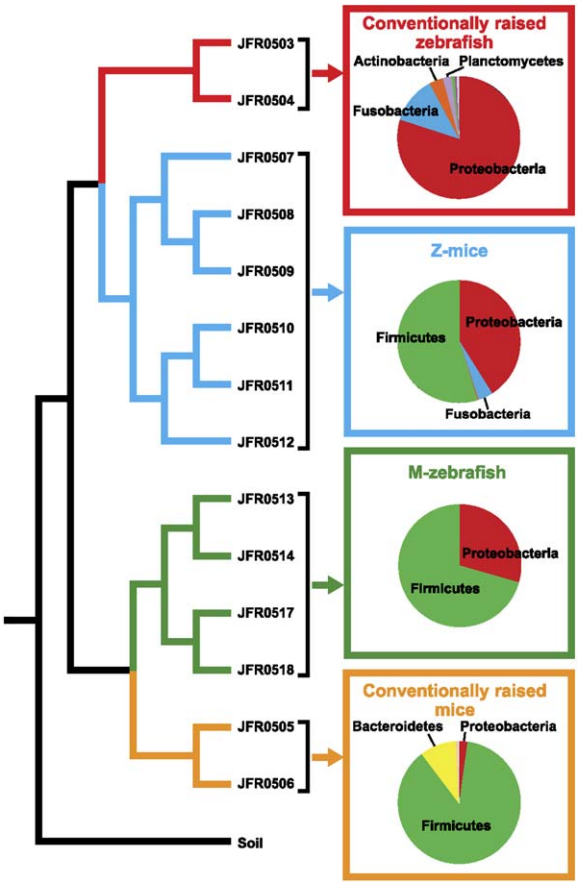

Figure 2. Comparison of Input and Output Communities following Reciprocal Transplantation of Gut Microbiotas in Gnotobiotic Zebrafish and Mice

Tree based on pairwise differences between the following bacterial communities (weighted UniFrac metric, based on a 6379 sequence tree; Lozupone and Knight, 2005): (1) CONV-R zebrafish digestive tract microbiota (conventionally raised zebrafish, red); (2) CONV-R mouse cecal microbiota (conventionally raised mice, yellow); (3) output community from the cecal contents of ex-GF mice that had been colonized with a normal zebrafish microbiota (Z-mice, blue); (4) output community from the digestive tracts from ex-GF zebrafish that had been colonized with a normal mouse microbiota (M-zebrafish, green); and (5) a control soil community that served as an outgroup (Soil; Axelrood et al., 2002). The distance p value for this entire UniFrac tree (UniFrac P, the probability that there are more unique branches than expected by chance, using 1000 iterations) was found to be <0.001, assigning high confidence to the overall structure of the UniFrac tree. 16S rRNA library names are shown next to their respective branch (see Table S1 for additional details about these libraries). The relative abundance of different bacterial divisions within these different communities (replicate libraries pooled) is shown in pie charts with dominant divisions highlighted.

We performed the reciprocal experiment by colonizing recently hatched (3 days post-fertilization [dpf]) GF C32 zebrafish with the pooled cecal contents of three CONV-R adult female mice (libraries JFR0505 and JFR0506 in Table S1) and conducting surveys of the recipients' digestive tract communities 3 or 7 days later (libraries JFR0513-

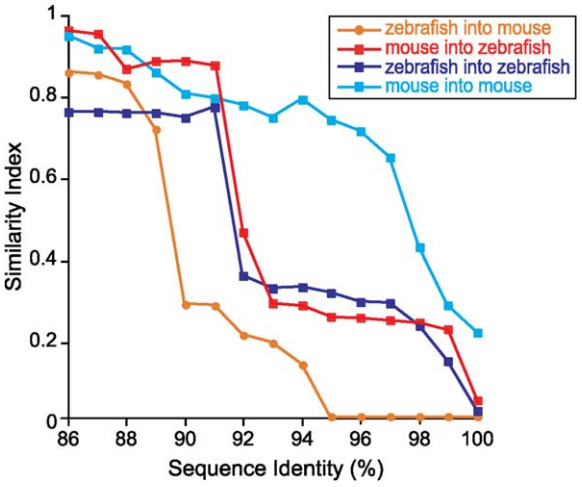

Figure 3. Similarity Indices for Pairwise Comparisons of Communities Defined as Assemblages of Phylotypes Computed at Levels of %ID Ranging from 86%ID to 100%ID and Compared at Each %ID Threshold using the Chao-Jaccard Abundance-Based Similarity Index

Abbreviations: zebrafish into mouse, CONV-R zebrafish compared to Z-mouse microbiotas; mouse into zebrafish, CONV-R mouse compared to M-zebrafish microbiotas; zebrafish into zebrafish, CONV-R zebrafish compared to Z-zebrafish microbiotas (data from Rawls et al., 2004); mouse into mouse, CONV-R mouse compared to M-mouse microbiotas (data from Bäckhed et al., 2004). Similarity indices range from 0 (no overlap in composition) to 1 (identical communities).

18 in Table S1; Figure S1). As in the previous experiment, the dominant bacterial division in the input mouse community (Firmicutes) persisted in the output M-zebrafish community (87.3% ± 2.2% of input, 64.9% ± 41.7% of output; Figure 2). However, only members of Bacilli, the dominant Firmicute class in the zebrafish but not the normal mouse gut microbiota, were retained; other prominent members of the Firmicutes found in the input mouse library (i.e., Clostridia and Mollicutes) were no longer detected in the M-zebrafish gut. Bacteroidetes (9.8% ± 3.3% of input community) were also undetected. Proteobacteria, a minor member of the input mouse community, were amplified markedly in the M-zebrafish gut (2.2% ± 0.6% of input, 35.1% ± 41.7% of output; Figure 2).

In addition to their drastic compositional differences, we also found that the output M-zebrafish community was less rich and less diverse than the input mouse community (Table S1 and Figure S2), indicating that only a small subset of the mouse gut microbial consortium was able to establish and/or thrive in the larval M-zebrafish gut. In contrast to the reciprocal zebrafish-into-mouse experiment where the contents of the adult fish gut were gavaged directly into the stomachs of recipient GF mice, our mouse-into-zebrafish gut microbiota transplantation involved introduction of mouse cecal contents into gnotobiotic zebrafish medium (GZM) containing 3dpf fish. Therefore, environmental factors could operate to select a subset of the input mouse community prior to entry in the recipient fish gut.

The similarities between input mouse and M-zebrafish communities were high, from 86%ID to 91%ID, above which the communities diverged in composition (Figure 3), i.e., different genera were representative of the same deeper phylogenetic lineages. Indeed, there was no overlap between phylotypes with threshold pairwise ≥99%ID in the datasets obtained from the input mouse and M-zebrafish communities. This was due, in part, to the limited degree of coverage (73% for the input community according to Good's method; Good, 1953). Phylotypes that were detected only in the M-zebrafish community were identifiable in the input mouse community using PCR and phylotype-specific primers (e.g., Staphylococcus; data not shown). Compared to the reciprocal zebrafish-into-mouse transplantation experiment, the input mouse and output M-zebrafish communities diverged at a higher %ID cutoff (Figure 3), indicating that they were more similar at a higher taxonomic level than the zebrafish/Z-mouse communities. Part of the drop in similarity could be attributed to the experimental manipulation since a similar analysis of a zebrafish-into-zebrafish transplant (Rawls et al., 2004) revealed a drop in similarity at a comparable %ID (Figure 3).

The similarity indices described above are derived from phylotype abundances at different phylotype thresholds (%IDs). However, an implicit assumption underlying such an analysis is that all phylotypes are treated equally regardless of lineage, even though they may represent similar or very unrelated lineages (Lozupone and Knight, 2005). Another way to compare communities is the UniFrac analysis: In this method, the abundance of each lineage is weighted, such that the abundance of lineages is considered as well as which lineages are present (Lozupone and Knight, 2005). The UniFrac approach circumvents the problem of having to decide at what %ID level to define the phylotype units that we call "different" (the cut-off is likely to vary according to lineage).

UniFrac analysis revealed that replicate Z-mouse datasets are most similar to the input zebrafish datasets with respect to detected lineages (Figure 2). However, the abundance of the Firmicutes in Z-mice expanded to resemble the division's abundance in CONV-R mice, indicating that the input community, although derived from a zebrafish, has been shaped to resemble a native mouse community. Similarly, the M-zebrafish communities are most similar to the mouse input communities by UniFrac, but the Proteobacteria in M-zebrafish expanded to resemble a CONV-R zebrafish community, indicating that the input mouse community has been shaped to resemble a native zebrafish microbiota (Figure 2).

Together, the results from our reciprocal microbiota transplantation experiments disclose that (1) gut habitat sculpts community composition in a consistent fashion, regardless of the input, and (2) stochastic effects are minimal (One notable exception was that γ-Proteobacteria in M-zebrafish [*Escherichia*, *Shigella*, and *Proteus* spp.] were more abundant in one experimental replicate [69.8% ± 20.5%] compared to the other [0.5% ± 0.6%]). The amplified taxa in both sets of transplantation experiments represented dominant divisions in the native gut microbiota of the respective host: Firmicutes in the case of teleostification (zebrafish-into-mouse), Proteobacteria in the case of murinization (mouse-into-zebrafish).

Shared Responses Elicited in Gnotobiotic Mice after Exposure to a Mouse or Zebrafish Gut Microbiota from Conventionally Raised Animals

While the studies described above indicated that the composition of the gut microbiota is sensitive to host habitat, we did not know whether the host response was sensitive to microbial community composition. Therefore, we conducted a GeneChip-based functional genomic analysis of gene expression in the distal small intestines (ileums) of mice that had been subjected to zebrafish-into-mouse (Z-mice) and mouse-into-mouse (M-mice) microbiota transplantations. All animals (n = 3–5/treatment group) were sacrificed 14 days after inoculation, RNA was prepared from the ileum of each mouse, and the cRNA target generated from each RNA sample was hybridized to an Affymetrix 430 v2 mouse GeneChip. Ingenuity Pathways Analysis software (IPA; see Supplemental Data) was then used to compare host responses to these different microbial communities. IPA software was utilized for genes that exhibited a ≥1.5-fold change (increased or decreased) in their expression compared to GF controls (false discovery rate <1%).

Despite the different bacterial compositions of the two input communities, their impact on the mouse was remarkably similar (Figure 4). The number of IPA-annotated mouse genes whose expression changed in response to the two microbiotas was comparable: 500 in response to the native mouse microbiota (Table S7) and 525 in response to the zebrafish microbiota (Table S8 and Figure 4A). Approximately half of the genes (225) were responsive to both microbial communities (Table S10): 217 (96.4%) were regulated in the same direction. Among the two sets of responsive genes, there was shared enrichment of IPA-annotated metabolic pathways involved in (1) biosynthesis and metabolism of fatty acids (sources of energy as well as substrates for synthesis of more complex cellular lipids in an intestinal epithelium that undergoes continuous and rapid renewal); (2) metabolism of essential amino acids (valine, isoleucine, and lysine); (3) metabolism of amino acids that contain the essential trace element selenium (selenocystine/selenomethioinine) and are incorporated into the active sites of selenoproteins such as glutathione peroxidase; (4) metabolism of butyrate (a product of polysaccharide fermentation that is a key energy source for the gut epithelium); and (5) biosynthesis of bile acids needed for absorption of lipids and other hydrophobic nutrients (Figure 4B and Table S12).

Both communities altered expression of a similar set of genes involved in insulin-like growth factor-1 (Igf-1), vascular endothelial growth factor (Vegf), B cell receptor, and interleukin-6 (Il-6) signaling pathways (Figure 4C and Table S13). These results are intriguing: Previous

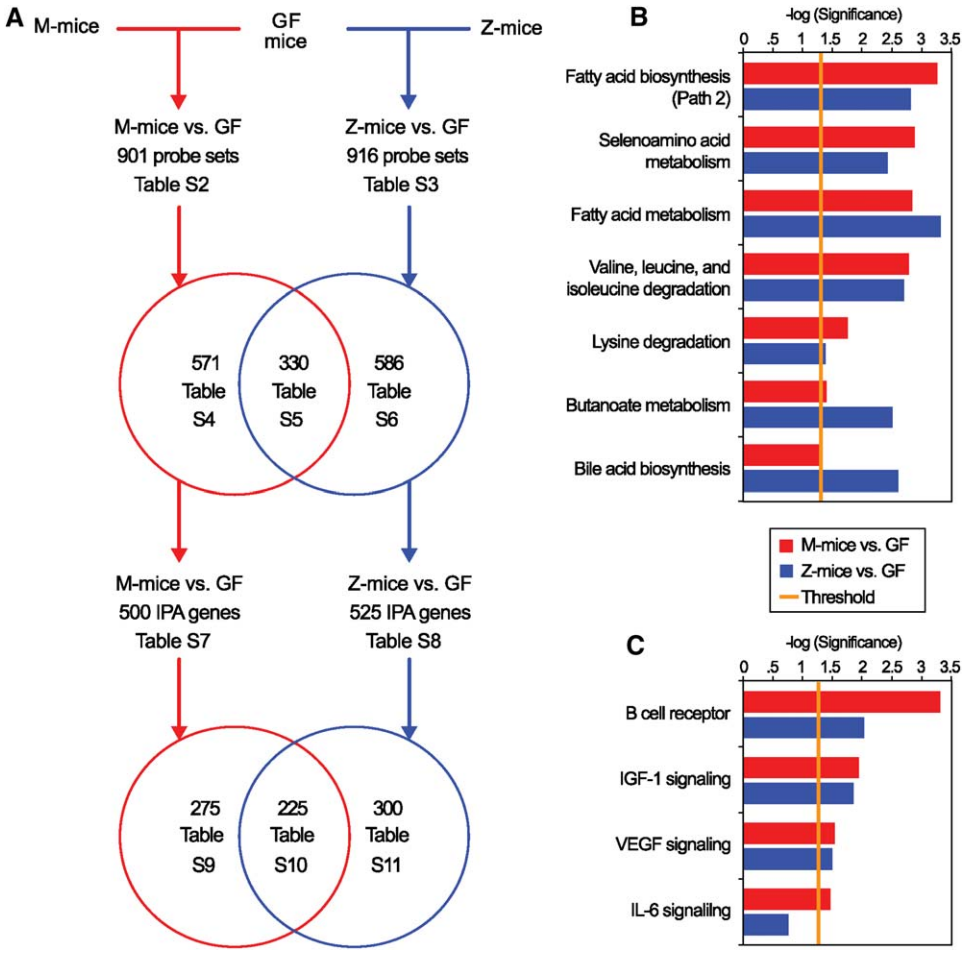

Figure 4. Identifying a Common Response of the Germ-free Mouse Distal Small Intestine to Colonization with Mouse and Zebrafish Gut Microbial Communities

(A) Summary of results of GeneChip analysis of the ileal transcriptome in GF mice versus mice colonized for 14 days with a mouse cecal microbiota (M-mice versus GF; red lines) or a normal zebrafish digestive tract microbiota (Z-mice versus GF; blue lines). Note that only a subset of all Affymetrix GeneChip probe sets are annotated by Ingenuity Pathway Analysis (IPA). Supplemental tables containing GeneChip probe set and IPA gene information are indicated. IPA reveals metabolic pathways (panel B; Table S12) and molecular functions (panel C; Table S13) that are significantly enriched ($p < 0.05$) in the host response to each community. The seven most significant metabolic pathways and the four most significant signaling pathways from the M-mice versus GF mice comparison (red bars) are shown along with corresponding data from the Z-mice versus GF mice comparison (blue bars). (Not shown: the 275 IPA-annotated mouse genes regulated by the mouse microbiota but unchanged by the zebrafish digestive tract microbiota were significantly enriched for components of ERK/MAPK, SAPK/JNK, antigen presentation, and the pentose phosphate pathways [Table S9]. In contrast, the 300 IPA-annotated mouse genes regulated by the zebrafish microbiota but unchanged by the mouse microbiota were enriched for components of glutamate and arginine/proline metabolism, ketone body synthesis/degradation, plus β-adrenergic signaling pathways [Table S11]).

mouse-into-mouse and zebrafish-into-zebrafish transplantations revealed that the microbiota-directed increase in proliferative activity of gut epithelial lineage progenitors is a shared host response (Rawls et al., 2004). The underlying mechanisms are not known. However, we recently found that components of Igf-1, Vegf, B cell receptor, and Il-6 signaling pathways were significantly enriched in mouse small intestinal epithelial progenitors (Giannakis et al., 2006). Thus, it is tempting to speculate that these pathways may be involved in mediating the microbiota's effect on mouse intestinal epithelial renewal.

Taken together, these results reveal a commonality in the transcriptional responses of the mouse to two microbial communities with shared divisions represented by different lineages at a finer phylogenetic resolution (Figure 1). This common response to a microbiota may reflect as yet unappreciated shared functional properties expressed by the two compositionally distinct communities and/or a core response, evolved by the mouse gut to distinct microbial communities.

Comparison of Zebrafish Host Responses to a Zebrafish versus a Mouse Gut Microbiota

Analysis of zebrafish 3 days after colonization with either a zebrafish or a mouse microbiota at 3dpf also demonstrated shared features of the host response to both

microbial communities. To quantify these responses, we selected biomarkers identified from our comparisons of 6dpf GF, CONV-R, and Z-zebrafish (Rawls et al., 2004). Quantitative real-time RT-PCR (qRT-PCR) of biomarkers of lipid metabolism, including *fasting-induced adipose factor* (*fiaf*; circulating inhibitor of lipoprotein lipase, Bäckhed et al., 2004), *carnitine palmitoyltransferase 1a* (*cpt1a*), and the trifunctional enzyme *hydroxyacylCoA dehydrogenase/3-ketoacylCoA thiolase/enoyl CoA hydratase α* (*hadha*), revealed that the mouse microbiota was able to largely recapitulate the effect of the zebrafish microbiota (Figures 5 and S3). In contrast, the zebrafish microbiota, but not the mouse microbiota, prominently increased host expression of (1) innate immune response biomarkers (*serum amyloid a* [*saa*], *myeloperoxidase* [*mpo*; Lieschke et al., 2001; Figure 5], and *complement component factor b* [*bf*; Figure S3]) and (2) *proliferating cell nuclear antigen* (*pcna*; biomarker of epithelial cell renewal; Figure 5).

Selecting Readily Culturable Microbial Species that Are Useful Models for Translating Information about Host-Bacterial Mutualism from Zebrafish to Mice

In order to use gnotobiotic zebrafish as a surrogate for studying the mechanisms underlying host-microbial mutualism in the mammalian gut, we sought culturable bacterial species that were capable of (1) efficiently colonizing the digestive tracts of GF zebrafish and mice and (2) eliciting evolutionarily conserved host responses in both hosts. Therefore, we performed culture-based bacterial surveys of the Z-mouse and M-zebrafish output communities in parallel with our culture-independent 16S rRNA surveys. 16S rRNA sequence-based analysis of 160 different bacterial isolates from the communities of six Z-mice yielded 47 different phylotypes (defined at 97%ID) representing four divisions (Proteobacteria, Fusobacteria, Actinobacteria, and Firmicutes). Similarly, an analysis of 303 isolates recovered from the communities of 18 M-zebrafish yielded 41 phylotypes representing the Proteobacteria and Firmicutes (Tables S1 and S14).

We selected seven primary isolates from the transplantation experiments representing the Firmicutes (*Enterococcus* and *Staphylococcus* spp.) and the Proteobacteria (*Shewanella*, *Aeromonas*, *Citrobacter*, *Plesiomonas*, *Escherichia* spp.). Three laboratory strains of γ-Proteobacteria (*Aeromonas hydrophila* ATCC35654, *Pseudomonas aeruginosa* PAO1, and *E. coli* MG1655) were used as controls (Table S15). These primary isolates and lab strains were selected based on the relative abundance of their phylotypes in our culture-based surveys of input and output communities (Table S14).

3dpf GF zebrafish were exposed to 10^4 CFU of each primary isolate or strain per milliliter of gnotobiotic zebrafish medium (GZM); all reached similar densities in the digestive tract by 6dpf (10^4–10^5 CFU/gut). These densities are similar to those documented in age-matched CONV-R or Z-zebrafish (Rawls et al., 2004).

An epidermal degeneration phenotype that develops in fed (but not fasted) GF zebrafish beginning at 9dpf (Rawls et al., 2004) was ameliorated by colonization with nine of the ten bacterial strains at 3dpf. The *Enterococcus* isolate M2E1F06 was the only tested strain that did not have any detectable effect (Figure S4). We found that epidermal degeneration could also be prevented by placing a mesh bag, containing an autoclaved mixture of activated carbon and cation exchange resin, into the GZM (Figure S4). This latter finding suggests that rescue by most of the tested bacterial strains involves bioremediation of toxic compounds that accumulate when GF zebrafish are exposed to food. Our subsequent analysis of the impact of the Firmicutes (i.e., *Enterococcus* and *Staphylococcus* isolates) on gut gene expression was performed using zebrafish raised in the presence of activated carbon and resin.

qRT-PCR analysis of biomarkers of lipid metabolism, including *fiaf*, *cpt1a*, and *hadha*, revealed that five of the seven primary isolate strains and all of the type strains tested were able to at least partially recapitulate the response obtained after exposure to an unfractionated zebrafish microbiota. Colonization with T1E1C05 (*Shewanella* sp.) and *P. aeruginosa* PAO1 had the largest effects (Figures 5 and S3). Two biomarkers of innate immune responses, *saa* and *bf*, were also responsive to the majority of these strains, but the granulocyte-specific marker *mpo* was relatively specific for *P. aeruginosa* PAO1 (Figures 5 and S3). None of the tested individual bacterial strains, including PAO1, were able to recapitulate the degree of stimulation of cell division in the intestinal epithelium of 6dpf zebrafish seen in the presence of an unfractionated zebrafish microbiota harvested from CONV-R donors, whether judged by qRT-PCR assays of *pcna* expression or by immunohistochemical analysis of the incorporation of BrdU administered 24 hr prior to sacrifice (Figure 5).

We also assessed the host response to colonization with a consortium consisting of an equal mixture of all seven primary isolates (n = 2 groups of 20 GF zebrafish colonized at 3dpf and sacrificed at 6dpf). qRT-PCR indicated that this model microbiota was able to partially recapitulate the nutrient metabolic and innate immune (but not epithelial proliferative) responses to the normal zebrafish microbiota. Importantly, the response to the consortium was a nonadditive representation of the responses to each component strain, and not equivalent to what was observed with a complete microbiota from CONV-R zebrafish (Figures 5 and S3).

qRT-PCR assays established that treatment of 6dpf zebrafish larvae with lipopolysaccharide (LPS) purified from *P. aeruginosa* was able to partially recapitulate innate immune responses seen with live *P. aeruginosa* (Figure 5). In contrast, LPS treatment did not affect expression of biomarkers of nutrient metabolism (Figure 5). This notion of distinct bacterial signaling mechanisms for innate immune and metabolic responses is supported by the observation that some of the tested isolates (e.g, T1E1C05, a *Shewanella* sp.) are able to induce robust nutrient metabolic responses without eliciting innate immune responses

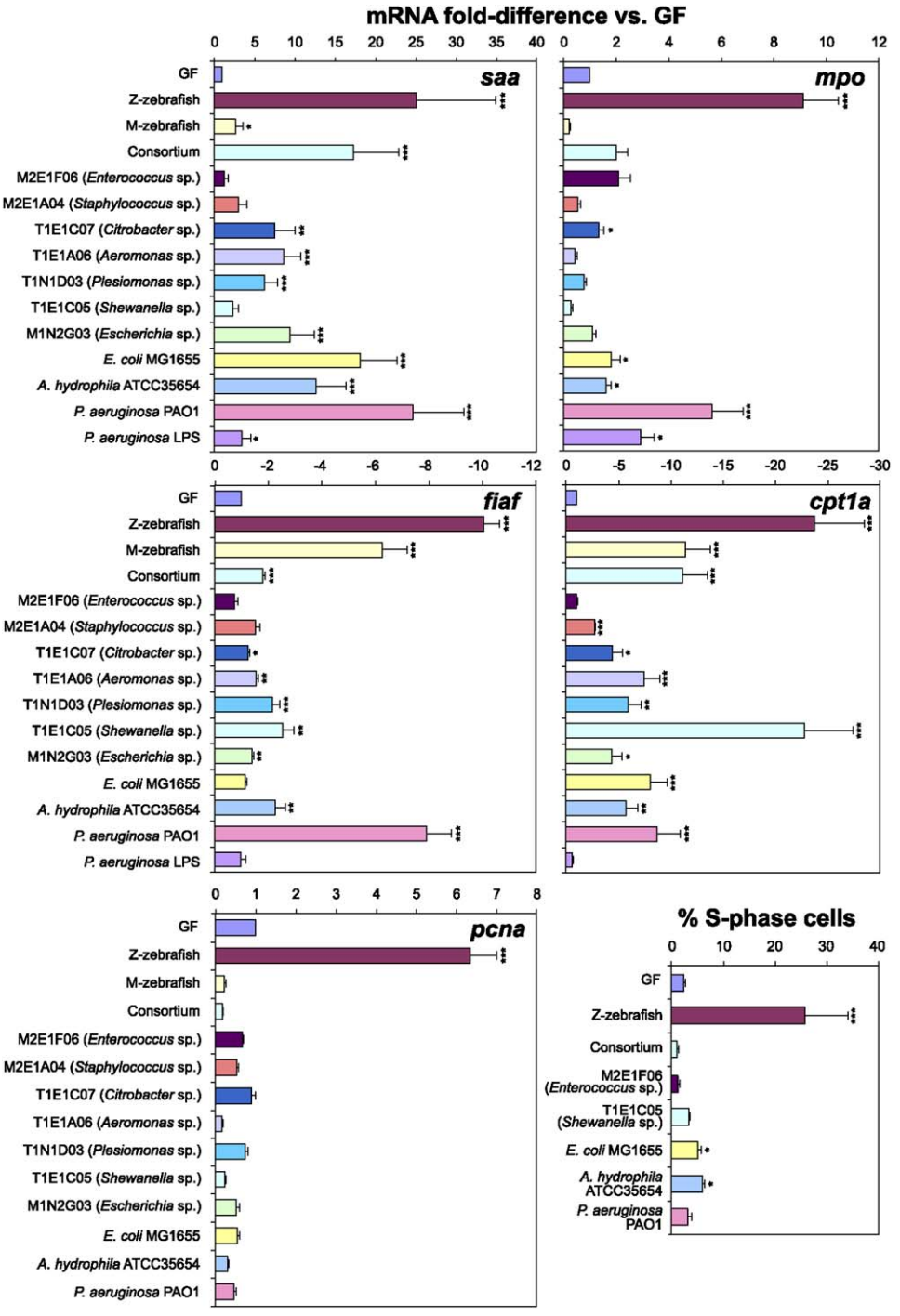

Figure 5. qRT-PCR Assays of the Responses of Germ-free Zebrafish to Colonization with Individual Culturable Members of the Zebrafish and Mouse Gut Microbiotas

Expression levels of *serum amyloid a* (*saa*), *myeloperoxidase* (*mpo*), *fasting-induced adipose factor* (*fiaf*), *carnitine palmitoyltransferase 1a* (*cpt1a*), and *proliferating cell nuclear antigen* (*pcna*) were assessed using RNA extracted from the pooled digestive tracts of 6dpf zebrafish inoculated since 3dpf with a CONV-R zebrafish microbiota (Z-zebrafish), a CONV-R mouse microbiota (M-zebrafish), a consortium of seven primary isolates (Consortium), a primary *Enterococcus* isolate (M2E1F06), a primary *Staphylococcus* isolate (M2E1A04), a primary *Citrobacter* isolate (T1E1C07), a primary *Aeromonas* isolate (T1E1A06), a primary *Plesiomonas* isolate (T1N1D03), a primary *Shewanella* isolate (T1E1C05), a primary *Escherichia* isolate (M1N2G03), an *Escherichia coli* type strain (*E. coli* MG1655), an *Aeromonas hydrophila* type strain (*A. hydrophila* ATCC35654), a *Pseudomonas aeruginosa* type strain (*P. aeruginosa* PAO1), or 0.1 μg/ml *P. aeruginosa* LPS (*P. aeruginosa* LPS). Data from biological duplicate pools (≥ 10 animals per pool) were normalized to 18S rRNA levels and results expressed as mean fold-difference compared to GF controls ± SEM. S phase cells were

(Figures 5 and S3). Moreover, we found that all three classes of host response (innate immunity, nutrient metabolism, and cell proliferation) are strongly attenuated in the absence of an exogenous nutrient supply (See Figure S5).

DISCUSSION

There is considerable interest in how communities assemble at the microbial scale, and how the environment (e.g., local chemistry) and legacy effects (e.g., microbes available to colonize) interact to predict the composition of a community (Hughes-Martiny et al., 2006). Some host-associated microorganisms exhibit patterns of genetic differentiation that are related to the geographic distribution of their hosts (Bala et al., 2003; Falush et al., 2003). This raises the question of how much of the variation is due to habitat differences that correlate with geographic separation, versus the legacy of past communities. Our study directly tests the effect of habitat in assembling a community: We constrained the legacy effect by presenting empty GF hosts with a known microbial community so that observed changes in diversity could be correlated with factors specific to host gut habitat (e.g., either direct effects of the niche space or indirect effects on intercommunity dynamics).

UniFrac showed the output community of the Z-mouse to be made up of zebrafish-specific lineages, but the proportional representation of the divisions was more similar to what is typical of a mouse gut community. Conversely, the M-zebrafish digestive tract community was "teleostified" by a change in the proportions of divisions from the mouse input. Moreover, all ten of the individual cultured strains introduced into the GF host guts took up residence. These results show that the host will "work" with what it gets: We constrained the input by presenting the empty host with a constrained microbiota, and the resulting community took on a relative divisional abundance characteristic of the recipient host's naturally occurring community.

What determines the host's relative abundance of divisions? Its reproducibility regardless of the provenance of the input community underscores the presence of very powerful organizing principles in community composition that have yet to be fully explored. A simple interpretation of these findings is that members of the Firmicutes and Proteobacteria possess division-wide properties that allow them to succeed in the mouse and zebrafish gut, respectively; thus, even distantly related members within a division will respond similarly to habitat effects. If so, the implication is that there is considerable functional and/or physiological redundancy within lineages that are selected for in specific host gut habitats. One obvious difference between the Gram-positive Firmicutes and the Gram-negative Proteobacteria is their cell wall structure, which could be a target for selection. Another trait that may differentiate gut Firmicutes from Proteobacteria is their oxygen tolerence: The larval and adult zebrafish gut is predicted to have higher levels of oxygen than the mouse cecum and might exclude Firmicutes, whose members are more likely to be strictly anaerobic than the Proteobacteria. However, generalizations about division-level traits are conjecture and almost certainly prone to exceptions, particularly since they are based on a severely limited knowledge of the genomic features and phenotypes of gut bacteria. This is highlighted by our observation that the Firmicutes amplified in the ceca of Z-mice were only from the classes Bacilli and Clostridia, while the Proteobacteria amplified in M-zebrafish digestive tracts were only from the γ-Proteobacteria class.

The bacteria that establish themselves in a new host do not necessarily need to be identical by 16S rRNA %ID to be functionally similar ecotypes and to have similar genome content. Closely related phylotypes that form polytomies (i.e., star phylogenies) are common in the environment and in the animal gut (Acinas et al., 2004; Eckburg et al., 2005; Ley et al., 2006a, 2006b): Whole-genome comparisons of gut-dwelling Bacteroidetes species show that their proteomes have similar functional profiles, although they can differ in 16S rRNA %ID by as much as 12% (Xu et al., 2003; J. Xu, M.A.M, R.E.L., and J.I.G., unpublished data).

Curtis and Sloan (2004) state that when a new community is formed, it must be initiated by drawing from the available microbes at random. Two random samples from a log-normal distribution can have quite different compositions. Therefore, physically identical habitats (in this study, genetically identical hosts) will have different communities if they are formed at random from large seeding communities and will only be similar if the seeding community is small enough that the same bacteria arrive by chance (Curtis and Sloan, 2004). However, the input communities (mouse and zebrafish) each contained hundreds of species, making it unlikely that the same bacteria would establish by chance in each recipient GF animal.

In addition to host habitat factors, dynamics within microbial communities will interact with the host habitat to shape the final community. The relative abundance of divisions can be viewed as a simple emergent property of the community that belies underlying, highly complex organizational principles. Community-level interactions such as competition, cooperation, predation, and food web dynamics will all interact to shape a community (Ley et al., 2006b). The host provides the habitat and a basic niche space that the microbial community expands by its physical presence and metabolic activities. It is remarkable that such complex interactions can result in the predictable community structure that we observed at the division

quantified in the intestinal epithelium of 6dpf zebrafish colonized since 3dpf with a CONV-R zebrafish microbiota (Z-zebrafish), a consortium of seven primary isolates (Consortium), or individual species. The percentage of all intestinal epithelial cells in S phase was scored using antibodies directed against BrdU, following incubation in BrdU for 24 hr prior to sacrifice. Data are expressed as the mean of two independent experiments ± SEM (n = 9–15 five micron-thick transverse sections scored per animal, $\geq$7 animals analyzed per experiment). ***, $p < 0.0001$; **, $p < 0.001$; *, $p < 0.05$.

level. The shared host response to reciprocally transplanted zebrafish and mouse gut microbiotas suggests that this predictability of community composition also extends to the functions encoded in their microbiomes.

EXPERIMENTAL PROCEDURES

Animal Husbandry

All experiments using zebrafish and mice were performed using protocols approved by the Washington University Animal Studies Committee.

Conventionally Raised Animals

CONV-R zebrafish belonging to the C32 inbred strain were maintained under a 14 hr light cycle and given a diet described in an earlier publication (Rawls et al., 2004). CONV-R Swiss-Webster mice were purchased from Taconic Labs and fed an irradiated PicoLab chow diet (Purina) ad libitum. Mice were reared in a specific pathogen-free state, in a barrier facility, under a 12 hr light cycle.

Germ-free Animals

Zebrafish were derived as GF and reared using established protocols and diets (Rawls et al., 2004). GF zebrafish were maintained at 28.5°C in plastic gnotobiotic isolators at an average density of 0.3 individuals/ml gnotobiotic zebrafish medium (GZM; Rawls et al., 2004). GF mice belonging to the NMRI inbred strain were housed in plastic gnotobiotic isolators and fed an autoclaved chow diet (B&K Universal) ad libitum (Hooper et al., 2002). GF zebrafish and mice were kept under a 12 hr light cycle and monitored routinely for sterility (Rawls et al., 2004).

Colonization

GF zebrafish were conventionalized at 3dpf with a digestive tract microbiota harvested from CONV-R C32 donors, using established protocols (Rawls et al., 2004). To colonize zebrafish with individual bacterial species, or with defined consortia (see below), cultures were added directly to GZM containing 3dpf GF zebrafish (final density 10^4 CFU/ml). Colonization with members of the Firmicutes was coupled with addition of a cotton mesh bag containing 15 ml of ammonia-removing resin and activated carbon (AmmoCarb, Aquarium Pharmaceuticals) per 100 ml GZM at 3dpf.

To colonize zebrafish with a mouse gut microbiota, cecal contents were pooled from three adult CONV-R Swiss-Webster female mice under aerobic conditions, diluted 1:1200 in PBS, and added directly (1:100 dilution) to GZM containing 3dpf GF zebrafish (final density: 10^2 CFU/ml [aerobic culture]; 10^3 CFU/ml [anaerobic culture], as defined by incubation on BHI-blood agar for 2 days at 28°C).

GF NMRI mice were colonized at 7–11 weeks of age with a microbiota harvested from the cecal contents of adult CONV-R female Swiss-Webster mice (Bäckhed et al., 2004). To colonize mice with a zebrafish microbiota, the pooled digestive tract contents of 18 CONV-R adult C32 zebrafish were diluted 1:4 in sterile PBS under aerobic conditions and a 100 μl aliquot was introduced, with a single gavage (5×10^3 CFU/mouse, as defined by anaerobic and aerobic culture on BHI-blood agar and tryptic soy agar for 2 days at 37°C).

Other Treatments of Zebrafish

GF 3dpf animals were immersed in filter-sterilized GZM containing 0.1 μg/ml LPS purified from *Pseudomonas aeruginosa* ATCC27316 (Sigma, L8643). Sterility during this treatment was monitored routinely by culturing the aquaculture medium under a variety of conditions (Rawls et al., 2004).

To quantify cellular proliferation in the intestinal epithelium, 5dpf zebrafish were immersed in a solution of 5-bromo-2′-deoxyuridine (BrdU; 160 μg/ml of GZM) and 5-fluoro-2′-deoxyuridine (16 μg/ml GZM) for 24 hr prior to sacrifice. S phase cells were detected and scored as described (Rawls et al., 2004).

Phylogenetic and Diversity Analyses

Bulk DNA was obtained from the digestive tracts of zebrafish and the ceca of mice by solvent extraction and mechanical disruption (Ley et al., 2005; Rawls et al., 2004). The DNA was used in replicate PCRs using Bacteria-specific 16S rRNA gene primers. Amplicons from replicate PCRs were pooled and cloned prior to sequencing (See Supplemental Data).

16S rRNA gene sequences were edited and assembled into consensus sequences using PHRED and PHRAP aided by XplorSeq (Daniel Frank, University of Colorado, Boulder, personal communication); bases with a PHRAP quality score of <20 were trimmed. Contiguous sequences with at least 1000 >Q20 bp were checked for chimeras and then aligned to the 16S rRNA prokMSA database using the NAST server (http://greengenes.lbl.gov/cgi-bin/nph-NAST_align.cgi). The resulting multiple sequence alignments were incorporated into a curated Arb alignment (Ludwig et al., 2004) available at http://gordonlab.wustl.edu/supplemental/Rawls/Gut_Micro_Transplant.arb.

Assignment of the majority of sequences to their respective divisions was based on their position after parsimony insertion to the Arb dendrogram (omitting hypervariable portions of the 16S rRNA gene using lanemaskPH provided with the database). Chloroplast sequences were identified in CONV-R zebrafish libraries and removed (i.e., 8 sequences from library JFR0503 and 59 sequences from library JFR0504). Sequences that did not fall within described divisions were characterized as follows. Phylogenetic trees including the novel sequences and reference taxa were constructed by evolutionary distance (using PAUP* 4.0 [Swofford, 2003], a neighbor-joining algorithm with either Kimura two-parameter correction or maximum-likelihood correction with an empirically determined γ distribution model of site-into-site rate variation and empirically determined base frequencies). Bootstrap resampling was used to test the robustness of inferred topologies.

Distance matrices generated in Arb (with hypervariable regions masked, and with Olsen correction [Ley et al., 2006a]) were used to cluster sequences into operational taxonomic units (OTU's) by pairwise identity (%ID) with a furthest-neighbor algorithm and a precision of 0.01 implemented in DOTUR (Schloss and Handelsman, 2005). We use "phylotype" to refer to bins of sequences with $\geq$99% pairwise identity. Collector's curves, Chao1 diversity estimates, and Simpson's diversity index were calculated using DOTUR and Chao-Jaccard Abundance-based diversity indices using EstimateS 7.5 (Colwell, 2005). The percentage of coverage was calculated by Good's method with the equation $(1 - [n/N]) \times 100$, where n is the number of phylotypes in a sample represented by one clone (singletons) and N is the total number of sequences in that sample (Good, 1953).

To cluster the communities from each treatment, we used the UniFrac computational tool (Lozupone and Knight, 2005). To do so, the masked Arb alignment containing 5527 sequences from this study plus 852 sequences obtained from soil (Axelrood et al., 2002) was used to construct a neighbor-joining tree. The neighbor-joining tree was annotated according to the treatment from which each sequence was derived, and the fraction of tree branch length unique to any one treatment in pairwise comparisons (the UniFrac metric) was calculated. The p value for the tree, reflecting the probability that the there are more unqiue branch lengths than expected by chance alone, was calculated by generating 1000 random trees (Lozupone and Knight, 2005).

Functional Genomics

Analyses of gene expression in the mice and zebrafish using Affymetrix GeneChips, quantitative real-time RT-PCR, and Ingenuity Pathways Analysis were performed using methods described in previous publications (Giannakis et al., 2006; Hooper and Gordon, 2001; Rawls et al., 2004). For additional details, see Supplemental Data.

Supplemental Data

Supplemental Data include Experimental Procedures, 5 figures, and 16 tables and can be found with this article online at http://www.cell.com/cgi/content/full/127/2/423/DC1/.

ACKNOWLEDGMENTS

We are grateful to David O'Donnell and Maria Karlsson for assistance with husbandry of gnotobiotic animals, Sabrina Wagoner and Jill Manchester for valuable technical help, plus Fredrik Bäckhed, Peter Crawford, Marios Giannakis, and Justin Sonnenburg for many helpful discussions. This work was supported by the Ellison Medical Foundation, the W.M. Keck Foundation, and the NIH (DK30292, DK62675, DK073695).

Received: May 3, 2006
Revised: June 28, 2006
Accepted: August 25, 2006
Published: October 19, 2006

REFERENCES

Acinas, S.G., Klepac-Ceraj, V., Hunt, D.E., Pharino, C., Ceraj, I., Distel, D.L., and Polz, M.F. (2004). Fine-scale phylogenetic architecture of a complex bacterial community. Nature *430*, 551–554.

Axelrood, P.E., Chow, M.L., Radomski, C.C., McDermott, J.M., and Davies, J. (2002). Molecular characterization of bacterial diversity from British Columbia forest soils subjected to disturbance. Can. J. Microbiol. *48*, 655–674.

Bäckhed, F., Ding, H., Wang, T., Hooper, L.V., Koh, G.Y., Nagy, A., Semenkovich, C.F., and Gordon, J.I. (2004). The gut microbiota as an environmental factor that regulates fat storage. Proc. Natl. Acad. Sci. USA *101*, 15718–15723.

Bäckhed, F., Ley, R.E., Sonnenburg, J.L., Peterson, D.A., and Gordon, J.I. (2005). Host-bacterial mutualism in the human intestine. Science *307*, 1915–1920.

Bala, A., Murphy, P., and Giller, K.E. (2003). Distribution and diversity of rhizobia nodulating agroforestry legumes in soils from three continents in the tropics. Mol. Ecol. *12*, 917–929.

Bates, J.M., Mittge, E., Kuhlman, J., Baden, K.N., Cheesman, S.E., and Guillemin, K. (2006). Distinct signals from the microbiota promote different aspects of zebrafish gut differentiation. Dev. Biol. *297*, 374–386.

Cahill, M.M. (1990). Bacterial flora of fishes: a review. Microb. Ecol. *19*, 21–41.

Cebra, J.J. (1999). Influences of microbiota on intestinal immune system development. Am. J. Clin. Nutr. *69*, 1046S–1051S.

Colwell, R.K. (2005). EstimateS: Statistical estimation of species richness and shared species from samples (http://purl.oclc.org/estimates.

Curtis, T.P., and Sloan, W.T. (2004). Prokaryotic diversity and its limits: microbial community structure in nature and implications for microbial ecology. Curr. Opin. Microbiol. *7*, 221–226.

Eckburg, P.B., Bik, E.M., Bernstein, C.N., Purdom, E., Dethlefsen, L., Sargent, M., Gill, S.R., Nelson, K.E., and Relman, D.A. (2005). Diversity of the human intestinal microbial flora. Science *308*, 1635–1638.

Falush, D., Wirth, T., Linz, B., Pritchard, J.K., Stephens, M., Kidd, M., Blaser, M.J., Graham, D.Y., Vacher, S., Perez-Perez, G.I., et al. (2003). Traces of human migrations in *Helicobacter pylori* populations. Science *299*, 1582–1585.

Giannakis, M., Stappenbeck, T.S., Mills, J.C., Leip, D.G., Lovett, M., Clifton, S.W., Ippolito, J.E., Glasscock, J.I., Arumugam, M., Brent, M.R., and Gordon, J.I. (2006). Molecular properties of adult mouse gastric and intestinal epithelial progenitors in their niches. J. Biol. Chem. *281*, 11292–11300.

Good, I.J. (1953). The population frequencies of species and the estimation of population parameters. Biometrika *40*, 237–264.

Hooper, L.V., and Gordon, J.I. (2001). Commensal host-bacterial relationships in the gut. Science *292*, 1115–1118.

Hooper, L.V., Mills, J.C., Roth, K.A., Stappenbeck, T.S., Wong, M.H., and Gordon, J.I. (2002). Combining gnotobiotic mouse models with functional genomics to define the impact of the microflora on host physiology. Mol. Cell. Microbiol. *31*, 559–589.

Huber, I., Spanggaard, B., Appel, K.F., Rossen, L., Nielsen, T., and Gram, L. (2004). Phylogenetic analysis and in situ identification of the intestinal microbial community of rainbow trout (*Oncorhynchus mykiss*, Walbaum). J. Appl. Microbiol. *96*, 117–132.

Hughes-Martiny, J.B., Bohannan, B.J., Brown, J.H., Colwell, R.K., Fuhrman, J.A., Green, J.L., Horner-Devine, M.C., Kane, M., Krumins, J.A., Kuske, C.R., et al. (2006). Microbial biogeography: putting microorganisms on the map. Nat. Rev. Microbiol. *4*, 102–112.

Ley, R.E., Bäckhed, F., Turnbaugh, P., Lozupone, C.A., Knight, R.D., and Gordon, J.I. (2005). Obesity alters gut microbial ecology. Proc. Natl. Acad. Sci. USA *102*, 11070–11075.

Ley, R.E., Harris, J.K., Wilcox, J., Spear, J.R., Miller, S.R., Bebout, B.M., Maresca, J.A., Bryant, D.A., Sogin, M., and Pace, N.R. (2006a). Unexpected diversity and complexity from the Guerrero Negro hypersaline microbial mat. Appl. Environ. Microbiol. *72*, 3685–3695.

Ley, R.E., Peterson, D.A., and Gordon, J.I. (2006b). Ecological and evolutionary forces shaping microbial diversity in the human intestine. Cell *124*, 837–848.

Lieschke, G.J., Oates, A.C., Crowhurst, M.O., Ward, A.C., and Layton, J.E. (2001). Morphologic and functional characterization of granulocytes and macrophages in embryonic and adult zebrafish. Blood *98*, 3087–3096.

Lozupone, C., and Knight, R. (2005). UniFrac: a new phylogenetic method for comparing microbial communities. Appl. Environ. Microbiol. *71*, 8228–8235.

Ludwig, W., Strunk, O., Westram, R., Richter, L., Meier, H., Yadhukumar, Buchner, A., Lai, T., Steppi, S., Jobb, G., et al. (2004). ARB: a software environment for sequence data. Nucleic Acids Res. *32*, 1363–1371.

Patton, E.E., and Zon, L.I. (2001). The art and design of genetic screens: zebrafish. Nat. Rev. Genet. *2*, 956–966.

Peterson, R.T., and Fishman, M.C. (2004). Discovery and use of small molecules for probing biological processes in zebrafish. Methods Cell Biol. *76*, 569–591.

Rawls, J.F., Samuel, B.S., and Gordon, J.I. (2004). Gnotobiotic zebrafish reveal evolutionarily conserved responses to the gut microbiota. Proc. Natl. Acad. Sci. USA *101*, 4596–4601.

Romero, J., and Navarrete, P. (2006). 16S rDNA-based analysis of dominant bacterial populations associated with early life stages of coho salmon (*Oncorhynchus kisutch*). Microb. Ecol. *51*, 422–430.

Schloss, P.D., and Handelsman, J. (2005). Introducing DOTUR, a computer program for defining operational taxonomic units and estimating species richness. Appl. Environ. Microbiol. *71*, 1501–1506.

Sonnenburg, J.L., Xu, J., Leip, D.D., Chen, C.H., Westover, B.P., Weatherford, J., Buhler, J.D., and Gordon, J.I. (2005). Glycan foraging *in vivo* by an intestine-adapted bacterial symbiont. Science *307*, 1955–1959.

Swofford, D.L. (2003). PAUP*, Phylogenetic Analysis Using Parsimony (*and Other Methods) (http://paup.csit.fsu.edu/) (Sunderland, MA: Sinauer Associates).

Wostmann, B.S. (1981). The germfree animal in nutritional studies. Annu. Rev. Nutr. *1*, 257–279.

Xu, J., Bjursell, M.K., Himrod, J., Deng, S., Carmichael, L.K., Chiang, H.C., Hooper, L.V., and Gordon, J.I. (2003). A genomic view of the human-*Bacteroides thetaiotaomicron* symbiosis. Science *299*, 2074–2076.

Accession Numbers

16S rRNA sequences have been deposited in GenBank under accession numbers DQ813844–DQ819377. GeneChip datasets have been deposited in Gene Expression Omnibus under accession number GSE5198.

Cell, Volume *127*
Supplemental Data

Reciprocal Gut Microbiota Transplants from Zebrafish and Mice to Germ-free Recipients Reveal Host Habitat Selection

John F. Rawls, Michael A. Mahowald, Ruth E. Ley, and Jeffrey I. Gordon

Supplemental Experimental Procedures

16S rRNA Gene Sequencing

Luminal contents from the ceca of CONV-R adult mice and Z-mice, and the intact digestive tracts of CONV-R adult zebrafish and 6dpf/10dpf M-zebrafish were removed immediately after animals were killed, and homogenized in sterile PBS under aerobic conditions (see **Fig. S1, Table S1**). An aliquot of each homogenate was used immediately for culture-based enumeration (see below): the remainder was frozen at –80^{o}C until use.

A frozen aliquot of each sample was thawed, centrifuged at 18,000 x g for 30 min at 4^{o}C to pellet material, and the pellet was then pulverized with a sterile pestle in 700µL filter-sterilized extraction buffer [100mM NaCl, 10mM Tris-Cl (pH 8.0), 25mM EDTA (pH 8.0), 0.5% (w/v) SDS, 0.1 mg/mL proteinase K (Sigma)]. Following a 40 min incubation at 37^{o}C for 40 min, 500µL of 0.1mm-diamter zirconia/silica beads (Biospec Products) plus 500µL of a mixture of phenol:chloroform (Ambion) were added to each sample, and the sample was disrupted mechanically for 2 min at 23^{o}C with a bead beater (Mini-Beadbeater, BioSpec Products Inc.; using the instrument's highest setting). Samples were centrifuged at 18,000 x g at 4^{o}C for 3 min. The aqueous phase was subjected to one additional round of phenol:chlorofom extraction prior to precipitation of DNA with isopropanol. Isolated genomic DNA was further purified over Montage PCR Centrifugal Filters (Millipore).

For each sample, three replicate 25µL polymerase chain reactions were performed, each containing 1-200 ng of purified genomic DNA, 20mM Tris-HCl (pH 8.4), 50mM KCl, 300uM $MgCl_2$, 400mM Betaine, 160µM dNTPs, 3 units of Taq DNA polymerase (Invitrogen), and 400nM of universal 16S rRNA primers 27F (5'-AGAGTTTGATCCTGGCTCAG-3') and 1491R (5'-GGTTACCTTGTTACGACTT-3'). Reactions were incubated initially at 94^{o}C for 10 min, followed by 30 cycles of 94^{o}C for 1 min, 52^{o}C for 1 min, and 72^{o}C for 2 min, and a final extension step at 72^{o}C for 10 min. Replicate reactions were pooled and purified over Montage PCR Centrifugal Filters (Millipore), and pooled PCR products cloned into pCR4-TOPO (TOPO TA Cloning Kit for Sequencing, Invitrogen). DNA extraction of control samples from GF animals did not yield detectable 16S rRNA PCR products or colonies. Clones were sequenced in BigDye Terminator reactions using 16S rRNA primers [27F, 1491R, and 907R (5'-CCGTCAATTCCTTTRAGTTT-3')]. 16S rRNA sequences derived from these culture-independent surveys were submitted to GenBank under accession numbers DQ813844-DQ819370.

Culture-Based Enumerations

To recover culturable bacteria from microbial consortia, homogenates of pooled zebrafish digestive tracts or individual mouse ceca were plated under aerobic conditions in a dilutional series on BHI-blood agar, tryptic soy agar, PEA-blood agar, nutrient agar, marine agar, and cholera agar (Becton Dickinson), and grown at 37°C and/or 28.5°C under aerobic and anaerobic conditions. Colonies were picked in a non-random manner into the corresponding liquid media under aerobic conditions, and grown under the same conditions that led to their initial detection. Liquid cultures were frozen as glycerol stocks in 96-well microtiter plates.

Aliquots (1μL) of these glycerol stocks were used directly as templates for 25μL PCR with the 27F and 1491R primers described above. PCR products were purified over Perfectprep PCR Cleanup 96-well plates (Eppendorf), and partial 16S rRNA sequences were generated using 27F primer. The resulting 16S rRNA sequences with ≥700 Phred >Q20 bp were aligned in Arb and analyzed as described above. These 575 16S rRNA sequences are available on our lab website at http://gordonlab.wustl.edu/supplemental/Rawls/Cultured_Clone_Seqs_FastA.txt. A subset of these cultured clones were subsequently recovered from glycerol stocks and re-sequenced using both 27F and 1491R primers to confirm their identity and to provide more complete sequence coverage (GenBank accession numbers DQ819371-DQ819377).

Functional Genomics

To compare gene expression in zebrafish reared under different conditions, two biological duplicate pools of animals from each group were analyzed. For zebrafish reared in gnotobiotic isolators, digestive tracts were removed *en bloc* under a dissecting microscope and pooled (n= 10-40/pool). For zebrafish reared in tissue culture flasks, intact larvae were pooled (n= 6-17/pool). Each pooled collection was homogenized by repeated passage through a 20-gauge needle, and total RNA was then extracted (TRIzol reagent; Invitrogen).

To compare gene expression in mice reared under different conditions, 3-5 animals were analyzed per treatment group. Immediately after each animal was killed, its small intestine was removed, divided into 16 equal-size segments, and segment 14 (ileal sample) was taken. The segment was homogenized, and RNA was extracted (Rneasy Miniprep Kit; Qiagen).

The quantity and quality of zebrafish and mouse gut RNA were assessed with a NanoDrop ND-1000 Spectrophotometer (NanoDrop Technologies) and Agilent 2100 Bioanalyzer (Agilent Technologies). RNA preparations were then used as templates for generating cDNAs (Superscript II reverse transcriptase; random primers; Invitrogen).

qRT-PCR assays were performed as described (Rawls et al., 2004), except that each 25μL reaction mixture contained cDNA corresponding to 2ng of total RNA from zebrafish digestive tracts, plus 900 nM gene-specific primers (except zebrafish 18S rRNA-specific control primers which were used at 300 nM) (**Table S16**). Assays were performed in triplicate using Absolute SYBR Green ROX Mix (ABgene) and a MX3000P QPCR Instrument (Stratagene). Data were normalized to 18S rRNA ($\Delta\Delta C_T$ analysis).

Whole genome transcriptional profiling was performed using Affymetrix GeneChips. cRNA targets were prepared, and hybridized (40 μg/sample) to 430 v2 mouse GeneChips using established protocols (Hooper et al., 2001). CEL files were normalized using RMA (Bolstad, 2004; http://rmaexpress.bmbolstad.com/), and all probesets with an average intensity across all arrays >50 were analyzed using Significance Analysis of Microarrays software (SAM version 2.21; Tusher et al., 2001). For M-mice vs. GF mice and Z-mice vs. GF mice comparisons, a false-discovery rate of <1% and a post-analysis fold-change cut-off of ≥1.5 were used, and all genes with ≥50% present calls (calculated using Affymetrix Microarray Suite 5.0) across all

replicate experimental or reference arrays were culled for further analysis. The resulting datasets were analyzed using the Ingenuity Pathways Analysis (IPA) software tool (http://www.ingenuity.com) according to Giannakis et al. (2006). IPA annotations take into account Gene Ontology (GO) annotations, but are distinct and based on a proprietary knowledge base of over 1,000,000 protein-protein interactions. The IPA output includes metabolic and signaling pathways: statistical assessments of the significance of their representation are based on a right-tailed Fisher's Exact Test, which is used to calculate the probability that genes participate in a given pathway relative to their occurrence in all other pathway annotations.

References

Axelrood, P. E., Chow, M. L., Radomski, C. C., McDermott, J. M., and Davies, J. (2002). Molecular characterization of bacterial diversity from British Columbia forest soils subjected to disturbance. Can. J. Microbiol. *48*, 655-674.

Bäckhed, F., Ding, H., Wang, T., Hooper, L. V., Koh, G. Y., Nagy, A., Semenkovich, C. F., and Gordon, J. I. (2004). The gut microbiota as an environmental factor that regulates fat storage. Proc. Natl. Acad. Sci. USA *101*, 15718-15723.

Bolstad, B. M. (2004) Low Level Analysis of High-density Oligonucleotide Array Data: Background, Normalization and Summarization, University of California – Berkeley.

Giannakis, M., Stappenbeck, T. S., Mills, J. C., Leip, D. G., Lovett, M., Clifton, S. W., Ippolito, J. E., Glasscock, J. I., Arumugam, M., Brent, M. R., and Gordon, J. I. (2006). Molecular properties of adult mouse gastric and intestinal epithelial progenitors in their niches. J. Biol. Chem. *281*, 11292-11300.

Good, I. J. (1953). The population frequencies of species and the estimation of population parameters. Biometrika *40*, 237-264.

Hooper, L. V., and Gordon, J. I. (2001). Commensal host-bacterial relationships in the gut. Science *292*, 1115-1118.

Ley, R. E., Harris, J. K., Wilcox, J., Spear, J. R., Miller, S. R., Bebout, B. M., Maresca, J. A., Bryant, D. A., Sogin, M., and Pace, N. R. (2006). Unexpected diversity and complexity from the Guerrero Negro hypersaline microbial mat. Appl. Environ. Microbiol. *72*, 3685-3695.

Lozupone, C., and Knight, R. (2005). UniFrac: a new phylogenetic method for comparing microbial communities. Appl. Environ. Microbiol. *71*, 8228-8235.

Rawls, J. F., Samuel, B. S., and Gordon, J. I. (2004). Gnotobiotic zebrafish reveal evolutionarily conserved responses to the gut microbiota. Proc. Natl. Acad. Sci. USA *101*, 4596-4601.

Schloss, P. D., and Handelsman, J. (2005). Introducing DOTUR, a computer program for defining operational taxonomic units and estimating species richness. Appl. Environ. Microbiol. *71*, 1501-1506.

Tusher, V. G., Tibshirani, R., and Chu, G. (2001). Significance analysis of microarrays applied to the ionizing radiation response. Proc. Natl. Acad. Sci. USA *98*, 5116-5121.

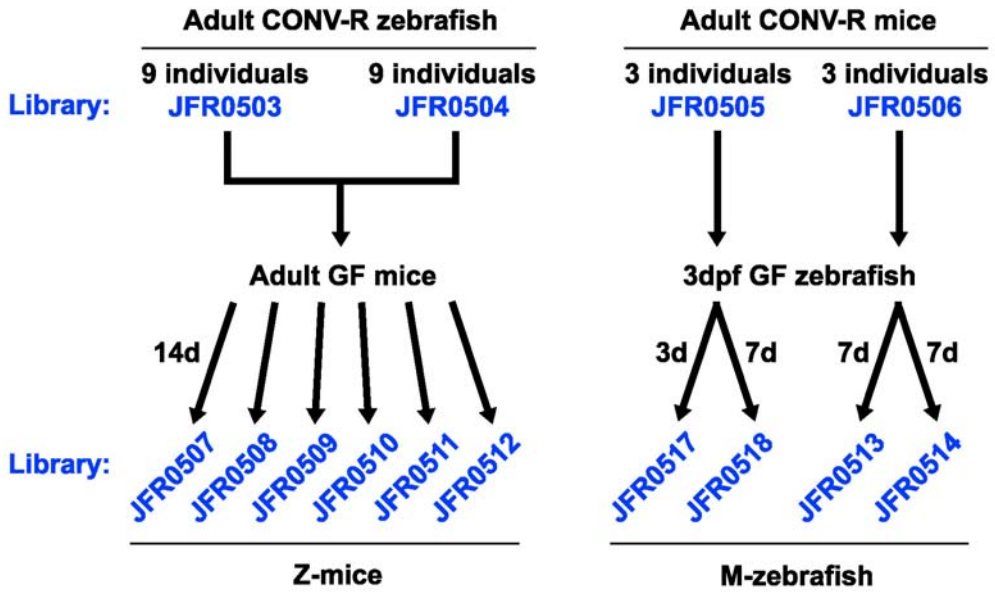

Figure S1. Flow Chart of Reciprocal Transplantation Experimental Design

The gut microbiota from two independent pools of 9 adult conventionally-raised (CONV-R) zebrafish were harvested, combined, and used to colonize 6 adult germ-free (GF) mice, yielding Z-mice. 14 days later, the cecal contents from individual Z-mice were harvested for analysis. The gut microbiota from 3 adult conventionally-raised mice were harvested and used to colonize 3dpf germ-free zebrafish, yielding M-zebrafish. 3 or 7 days later, the gut contents from groups of M-zebrafish were harvested. As indicated, this mouse-into-zebrafish experiment was performed in duplicate. Culture-independent 16S rRNA libraries generated from these different samples (Library) are indicated in blue text.

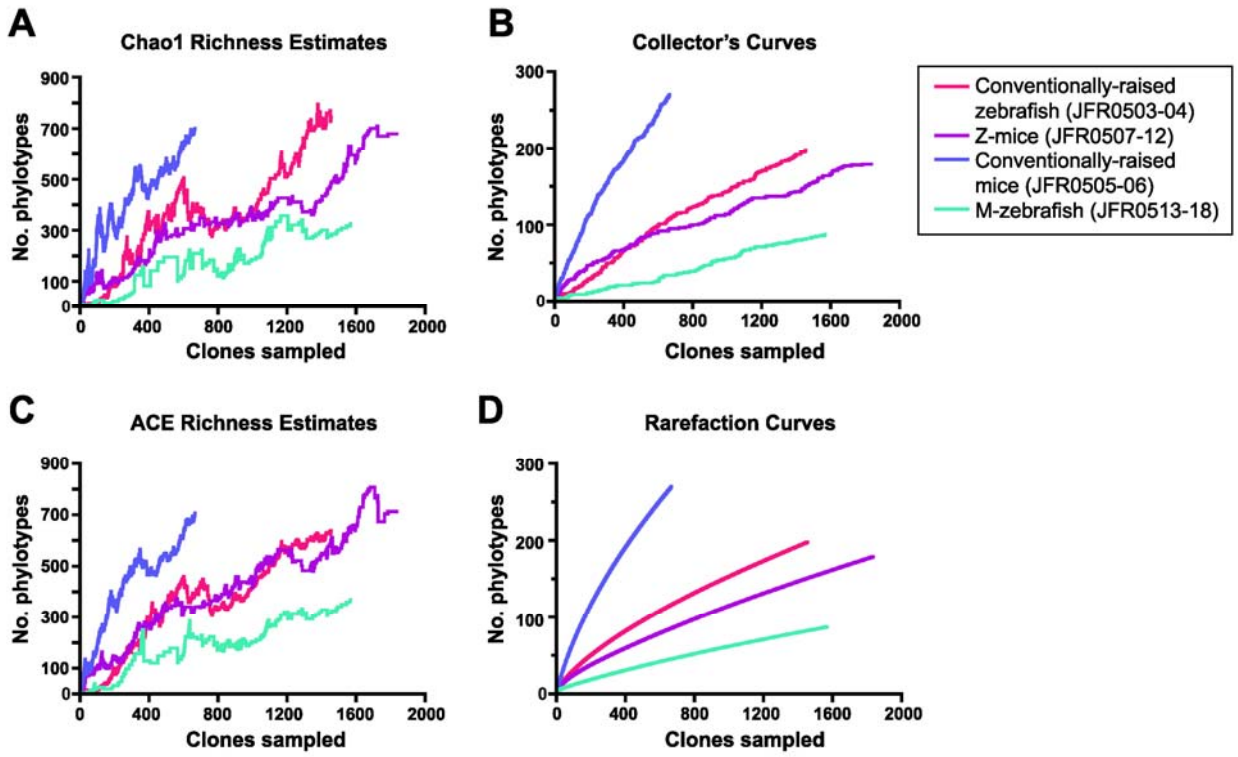

Figure S2. Sample-Based Assessments of Diversity and Coverage in Reciprocal Transplantation Experiments

The pooled libraries from the intestines of conventionally-raised zebrafish (CONV-R fish; libraries JFR0503-04), mice colonized with a zebrafish microbiota (Z-mice; libraries JFR0507-12), conventionally-raised mice (CONV-R mice; JFR0505-06), and zebrafish colonized with a normal mouse microbiota (M-zebrafish; JFR0513-18) were analyzed using DOTUR (Schloss and Handelsman, 2005). The phylotype richness for each treatment is expressed as full bias corrected Chao1 richness estimates (panel **A**) and abundance-based coverage estimates (ACE; panel **C**). The number of observed phylotypes (99%ID) and the number of sequences sampled are shown as Collector's curves (panel **B**) and Rarefaction curves (panel **D**). The addition of clones along the X-axis is non-random (ordered by library), producing the variability seen in panels **A** and **C**.

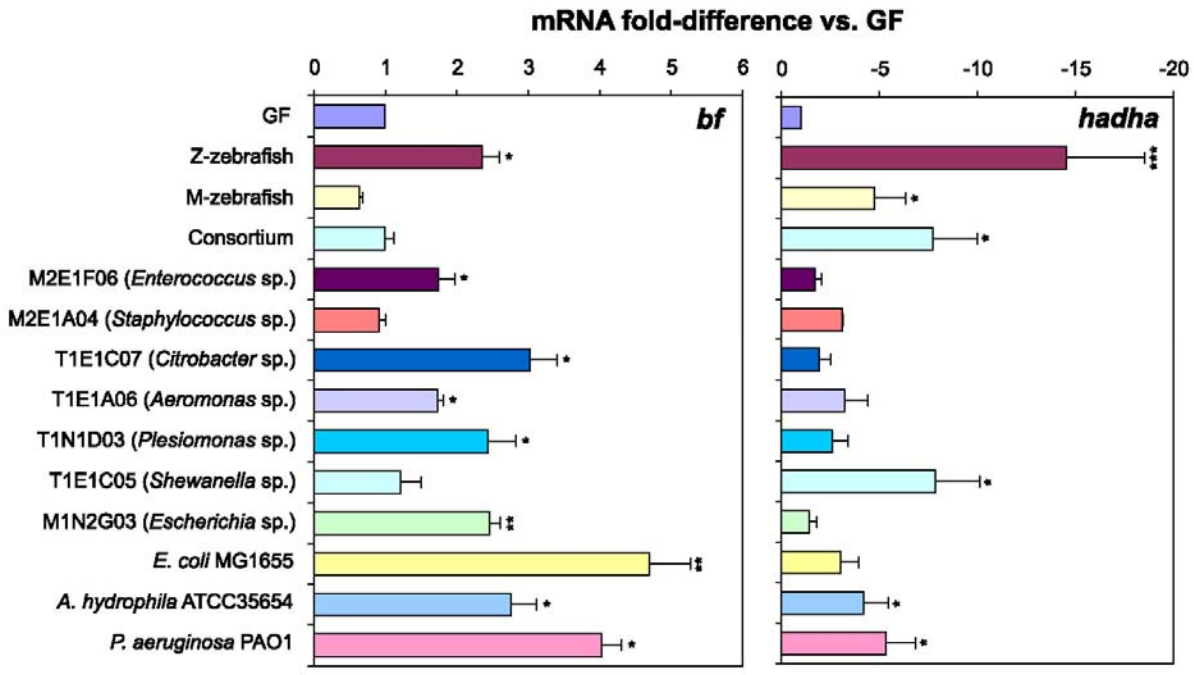

Figure S3. qRT-PCR Assays of the Responses of Germ-free Zebrafish to Colonization with Individual Culturable Members of the Zebrafish and Mouse Gut Microbiota

Expression levels of *complement factor b* (*bf*) and *hydroxyacylCoA dehydrogenase/3-ketoacylCoA thiolase/enoyl CoA hydratase* (*hadha*) were assessed using RNA extracted from the pooled digestive tracts of 6dpf zebrafish inoculated since 3dpf with a CONV-R zebrafish microbiota (Z-zebrafish), a CONV-R mouse microbiota (M-zebrafish), a consortium of 7 primary isolates (Consortium), a primary *Enterococcus* isolate (M2E1F06), a primary *Staphylococcus* isolate (M2E1A04), a primary *Citrobacter* isolate (T1E1C07), a primary *Aeromonas* isolate (T1E1A06), a primary *Plesiomonas* isolate (T1N1D03), a primary *Shewanella* isolate (T1E1C05), a primary *Escherichia* isolate (M1N2G03), an *Escherichia coli* type strain (MG1655), an *Aeromonas hydrophila* type strain (*A.hydrophila* ATCC35654), or a *Pseudomonas aeruginosa* type strain (PAO1). Data from biological duplicate pools (≥10 animals

per pool) were normalized to 18S rRNA levels and results are expressed as mean fold-change compared to GF controls ± SEM. ***, $P<0.0001$; **, $P<0.001$; *, $P<0.05$.

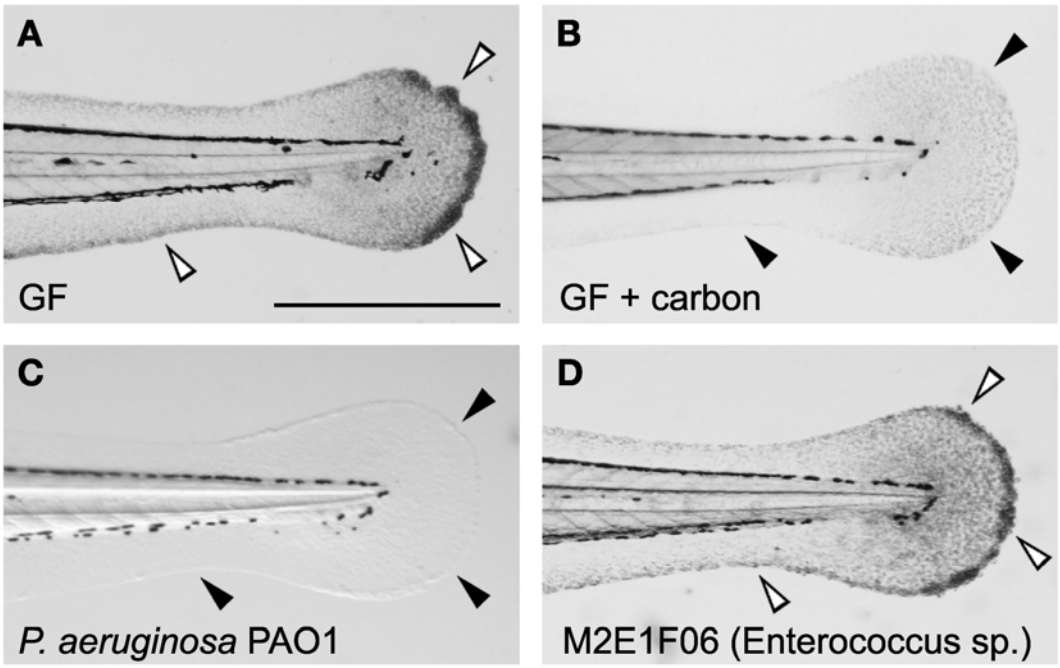

Figure S4. The Epidermal Degeneration Phenotype in Fed GF Zebrafish Is Ameliorated with Different Treatments

(**A**) Caudal region of a live 9dpf GF zebrafish, fed since 3dpf, displays loss of the transparency and integrity of the fin fold epidermis (white arrowheads; Rawls et al., 2004). (**B**) Age-matched fed GF zebrafish raised since 3dpf in the presence of activated carbon and ammonia-removing cation exchange resin (GF+carbon). The result is improved epidermal transparency and integrity (black arrowheads). GF zebrafish can survive under these conditions beyond 30dpf (data not shown). **(C)** 9dpf zebrafish colonized since 3dpf with *Pseudomonas aeruginosa* PAO1 (*P. aeruginosa* PAO1) do not develop the epidermal phenotype, as indicated by the healthy transparent fin fold epithelium (black arrowheads). (**D**) In contrast, 9dpf larvae colonized since 3dpf with a primary *Enterococcus* isolate (M2E1F06) display a phenotype similar to GF controls (white arrowheads). Scale bar: 500μm.

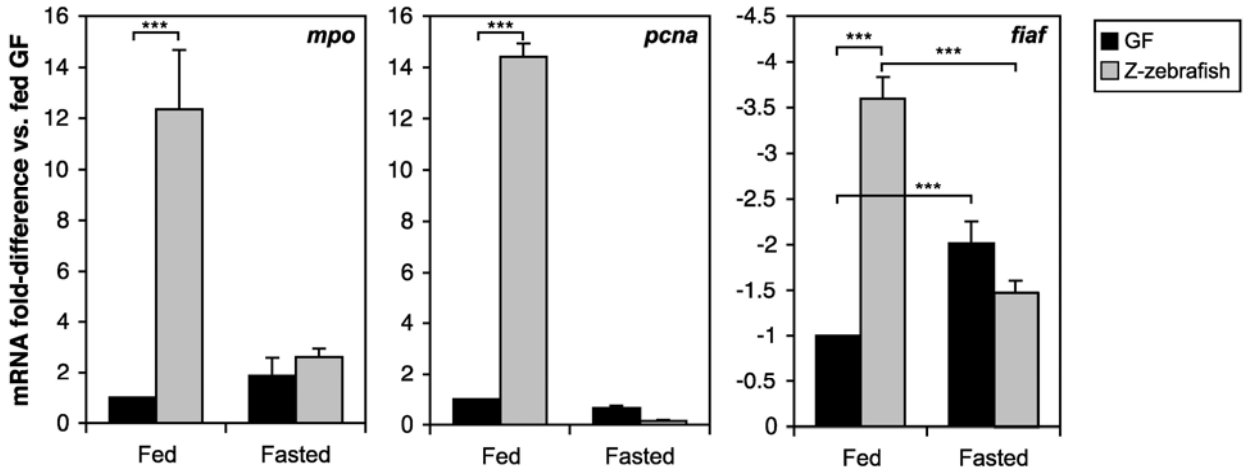

Figure S5. Zebrafish Host Responses to the Gut Microbiota Are Attenuated in the Absence of an Exogenous Nutrient Supply

6dpf zebrafish that were either germ-free (GF) or colonized since 3dpf with a CONV-R zebrafish microbiota (Z-zebrafish) and fed an autoclaved diet beginning at 3dpf (Fed) were compared with GF and Z-zebrafish siblings deprived of all food (Fasted). Expression levels of *myeloperoxidase* (*mpo*), *proliferating cell nuclear antigen* (*pcna*), and *fasting-induced adipose factor* (*fiaf*) were assessed by qRT-PCR using RNA extracted from the pooled digestive tracts of 6dpf zebrafish. Data from biological duplicate pools (≥10 animals per pool) were normalized to 18S rRNA levels and the results are expressed as mean fold-change compared to fed GF controls ± SEM. Note that nutrient (*fiaf*), innate immune (*mpo*) and proliferative responses (*pcna*) to colonization are markedly attenuated in fasted animals. Similar *fiaf* results were obtained in fed and fasted 6dpf zebrafish colonized with either *P. aeruginosa* PAO1 or *A. hydrophila* ATCC35654 since 3dpf (data not shown). Importantly, fasting did not produce a statistically significant reduction in gut microbial density in any of the colonization groups (data not shown). The sensitivity of 6dpf zebrafish to the presence of an exogenous nutrient supply was unanticipated: at this age, zebrafish have been consuming food for only 1-2 days; moreover, many 6dpf zebrafish have not

completed yolk resorption and, therefore, are presumably still utilizing this endogenous food source. ***, $P<0.0001$; **, $P<0.001$; *, $P<0.05$.

APPENDIX C

John F. Rawls, Michael A. Mahowald, Andrew L. Goodman, Chad M. Trent, and Jeffrey I. Gordon

In vivo imaging and genetic analysis link bacterial motility and symbiosis in the zebrafish gut

Proc Natl Acad Sci U S A. 2007 May 1;**104**(18):7622-7.

For supplemental movies please see enclosed CD.

In vivo imaging and genetic analysis link bacterial motility and symbiosis in the zebrafish gut

John F. Rawls*†‡, Michael A. Mahowald*, Andrew L. Goodman*, Chad M. Trent†, and Jeffrey I. Gordon*‡

*Center for Genome Sciences, Washington University School of Medicine, St. Louis, MO 63108; and †Department of Cell and Molecular Physiology, University of North Carolina, Chapel Hill, NC 27599

Contributed by Jeffrey I. Gordon, March 14, 2007 (sent for review January 26, 2007)

Complex microbial communities reside within the intestines of humans and other vertebrates. Remarkably little is known about how these microbial consortia are established in various locations within the gut, how members of these consortia behave within their dynamic ecosystems, or what microbial factors mediate mutually beneficial host–microbial interactions. Using a gnotobiotic zebrafish–*Pseudomonas aeruginosa* model, we show that the transparency of this vertebrate species, coupled with methods for raising these animals under germ-free conditions can be used to monitor microbial movement and localization within the intestine *in vivo* and in real time. Germ-free zebrafish colonized with isogenic *P. aeruginosa* strains containing deletions of genes related to motility and pathogenesis revealed that loss of flagellar function results in attenuation of evolutionarily conserved host innate immune responses but not conserved nutrient responses. These results demonstrate the utility of gnotobiotic zebrafish in defining the behavior and localization of bacteria within the living vertebrate gut, identifying bacterial genes that affect these processes, and assessing the impact of these genes on host–microbial interactions.

Danio rerio | establishment of a gut microbiota | flagellar motility | host–microbial symbiosis and mutualism | *Pseudomonas aeruginosa*

Starting at birth, we are colonized by communities of microorganisms that establish residency on our external and internal surfaces. These resident microbes outnumber our human cells by an order of magnitude, and their aggregate genomes (microbiome) specify important physiologic traits that are not encoded in our own genome (1). The vast majority of these microbes reside in our intestine: most of our 10–100 trillion gut-dwelling microbes belong to the domain Bacteria, although members of Archaea (Euryachaeota and Crenarchaeota) and Eukarya are also represented (2–6). Over the last 50 years, experiments comparing mice and rats raised in the absence of any microorganisms [germ-free (GF)] to those colonized with members of gut microbial communities have revealed that the microbiota plays an integral role in many aspects of intestinal and extraintestinal host biology, ranging from postnatal development of the gut's blood and lymphatic vascular systems (7, 8) to the proliferative activity of intestinal epithelial cells (9, 10), metabolism of ingested xenobiotics (1, 11), regulation of energy balance (12–14), maturation of the innate and adaptive immune systems (15–18), heart size (19), and behavior (e.g., locomotor activity) (14).

The notion that each of us is a supraorganism, composed of microbial and human parts, focuses attention on the question of how our microbial communities are assembled (20). Understanding the dynamic patterns of microbial entry into and movement within their gut habitats is critical for deciphering how different species establish and maintain a presence in the intestinal ecosystem, and how they interact with their host and other microbial community members. Fluorescence *in situ* hybridization and confocal and electron microscopic analyses have provided static rather than dynamic views of the positioning of microbial cells within the mammalian intestine, and *in vivo* bioluminescence analyses do not permit resolution of individual microbial cells.

The zebrafish (*Danio rerio*) possesses several key attributes that make it a distinctively powerful model organism for addressing these questions. First, the zebrafish digestive tract is structurally similar to that of mammals, with proximal-distal specification of functions and multiple self-renewing epithelial cell lineages (21, 22). Second, comparisons of GF zebrafish and those colonized with a microbiota harvested from the intestines of conventionally raised (CONV-R) zebrafish or mice have revealed a broad range of host processes that are impacted by the gut microbiota and that are conserved between mammals and fish (23–25). Moreover, individual bacterial representatives of the zebrafish and mouse gut microbiotas have been identified that can provoke evolutionarily conserved host responses in gnotobiotic zebrafish (23–25). Third, this vertebrate species and its gut are optically transparent from the time of fertilization through the onset of adulthood. This unusual feature provides an opportunity to make real-time *in vivo* observations of microbial–microbial and microbial–host interactions. Because zebrafish larvae can be grown in a 96-well plate format, their transparency could also be used to conduct genetic and chemical screens for host and/or microbial factors that mediate host–microbial interactions. Finally, with the development of methods for rearing zebrafish under GF conditions, reciprocal transplantations of gut communities from normal mouse and zebrafish donors into GF zebrafish and mouse recipients have revealed that differences in the normal gut communities of these vertebrates arise in part from distinct selective pressures imposed within their respective gut habitats. These experiments also revealed a striking degree of conservation of host responses to the different microbiotas (24).

We have used a simplified system, consisting of GF zebrafish colonized with the Gram-negative γ-proteobacterium *Pseudomonas aeruginosa*, to define the mechanisms by which members of the microbiota elicit these conserved host responses. *P. aeruginosa* is best known as an opportunistic pathogen. However, it has several characteristics that facilitate its use as a model mutualist in this system. Pseudomonads are common members of the fish gut microbiota (23–28) as well as the gut microbiota of some mammals (e.g., the African zebra and others; R. E. Ley and J.I.G, unpublished observations) [see

Author contributions: J.F.R., M.A.M., and J.I.G. designed research; J.F.R., M.A.M., and C.M.T. performed research; J.F.R., M.A.M., A.L.G., and J.I.G. analyzed data; and J.F.R., M.A.M., A.L.G., and J.I.G. wrote the paper.

The authors declare no conflict of interest.

Freely available online through the PNAS open access option.

Abbreviations: GF, germ-free; CONV-R, conventionally raised; dpf, days postfertilization; CONVD, conventionalized; GZM, gnotobiotic zebrafish medium; TEM, transmission electron microscopy; TTSS, Type III secretion system; qRT-PCR, quantitative RT-PCR.

‡To whom correspondence may be addressed. E-mail: jfrawls@med.unc.edu or jgordon@wustl.edu.

This article contains supporting information online at www.pnas.org/cgi/content/full/0702386104/DC1.

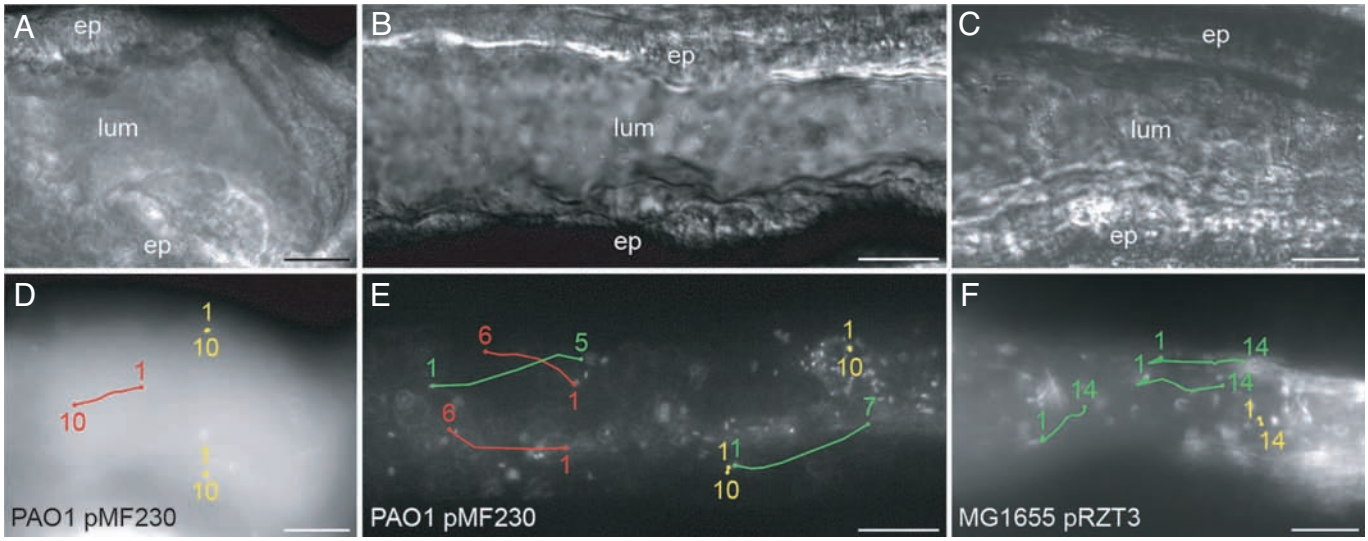

Fig. 1. Gut bacteria display diverse behaviors within the intestines of gnotobiotic zebrafish. (*A* and *D*) Whole-mount preparation of a live 3.5-dpf zebrafish colonized since 3 dpf with GFP-expressing *P. aeruginosa* PAO1 (PAO1 pMF230) demonstrates the transparency of the developing zebrafish intestine. Brightfield microscopy of the anterior intestine (segment 1, *A*) shows the intestinal lumen (lum) and the adjacent intestinal epithelium (ep). Fluorescence time-lapse microscopy of the same field (*D*) shows the movements of individual bacteria over the course of 10 frames, or 4 sec (*D* extracted from SI Movie 3). The locations of individual bacteria in the first (1) and the last (10) frames are numbered accordingly. (*B* and *E*) Brightfield (*B*) and fluorescence time-lapse (*E*) microscopy of the same field from a live 6-dpf zebrafish, colonized since 3 dpf with PAO1 pMF230, shows increasing bacterial density and behavioral complexity in the midintestine (junction of segments 1 and 2) over the course of 10 frames or 2.6 sec (*E* extracted from SI Movie 4). Note that the intestines shown in *D* and *E* both contain bacteria that are nonmotile in association with the host epithelium or luminal contents (yellow), whereas other bacteria exhibit high rates of motility in both ascending (distal to proximal; red tracks) and descending (green tracks) directions. Note that ascending and descending bacteria were tracked for only the first several frames because they quickly moved out of the focal plane; the first and last frames over which bacteria were tracked are numbered. (*C* and *F*) Brightfield (*C*) and fluorescence time-lapse (*F*) microscopy of a live 4.5-dpf zebrafish colonized since 3 dpf with DsRed-expressing *E. coli* MG1655 (MG1655 pRZT3) showing movement of luminal bacteria (green tracks) in the midintestine (segment 1). Over the course of 14 frames or 14 sec (*F* extracted from SI Movie 5), some bacteria appear adherent to the epithelium or luminal structures (yellow track), whereas most bacterial motion is synchronous and attributed to intestinal motility (green tracks). Anterior is to the left, and dorsal is to the top in all images. (Scale bars: 20 μm.)

supporting information (SI) *Materials and Methods* and Fig. 4 for a 16S rRNA sequence-based tree of zebrafish Pseudomonads and their relationship to *P. aeruginosa*]. Although Pseudomonads are rare members of the intestinal microbiota of healthy humans, their representation is increased in certain pathologic states, notably inflammatory bowel diseases (29–31). In an initial survey, 10 different bacterial species representative of the zebrafish or mouse gut microbiota were tested for their ability to elicit the innate immune and nutrient metabolic responses produced when a complete microbiota is introduced into GF zebrafish hosts. In this survey, *P. aeruginosa* was the most potent inducer of these responses (24) (see SI Fig. 5). Finally, in addition to the large body of knowledge that exists about *P. aeruginosa* biology, valuable genetic resources are available, including a finished genome sequence for strain PAO1 (32), deep draft genome assemblies for several other strains (PA14, C3719, 2192, PA7, and PACS2), and saturation-level sequenced transposon insertion libraries for strains PAO1 (33) and PA14 (34).

In the present study, we take advantage of the transparency of zebrafish and these genetic resources to demonstrate a linkage between motility/flagellar function and regulation of conserved innate immune responses.

Results

Real-Time *in Vivo* Imaging of Microbial Consortia and Individual Bacterial Species in the Transparent Intestine of Gnotobiotic Zebrafish. As noted above, the transparency of the zebrafish provides opportunities for exploring the movement as well as localization of microbes within their intestinal habitat through real-time microscopy of live whole-mount zebrafish. CONV-R zebrafish typically hatch from the GF environment within their protective chorions at 3 days postfertilization (dpf). This hatching event coincides with the anterior digestive tract achieving full patency (21, 35). Fluorescence *in situ* hybridization has revealed that the zebrafish digestive tract is colonized by bacteria as early as 4 dpf (25); however, the timing and route of initial colonization remained unclear.

Therefore, we first colonized GF zebrafish at 3 dpf with a normal zebrafish microbiota harvested from adult CONV-R zebrafish (a process called conventionalization) and then imaged their digestive tracts at different time points. *In vivo* bright-field microscopy of the gut microbiota in these conventionalized (CONVD) animals revealed a striking amount of microbial movement within their intestinal lumen (SI Movies 1 and 2), although the activity of individual microorganisms was difficult to monitor.

Upon exposure to *P. aeruginosa*, 3-dpf GF zebrafish are colonized at densities similar to the conventional zebrafish gut microbiota (10^4-10^5 cfu per gut at 6 dpf; SI Table 1) and elicit host responses that are conserved across vertebrate hosts (see below and ref. 24). To facilitate real-time *in vivo* microscopic observation of individual microbial cells, we introduced a plasmid that allows constitutive expression of the gene encoding GFP under the control of the *trc* promoter (pMF230) (36) into *P. aeruginosa* strain PAO1 to create PAO1 pMF230. GF 3-dpf zebrafish exposed to 10^4 cfu of *P. aeruginosa* PAO1 pMF230/ml gnotobiotic zebrafish medium (GZM) were initially colonized with a small cohort of bacteria that was readily seen as early as 3.5 dpf (Fig. 1 *A* and *D* and SI Movie 3). Because the anus does not achieve patency until ≈4 dpf (21, 35), our findings establish that the anterior digestive tract becomes colonized within just a few hours after its lumen first opens.

The size of this monocomponent community increased rapidly

MICROBIOLOGY

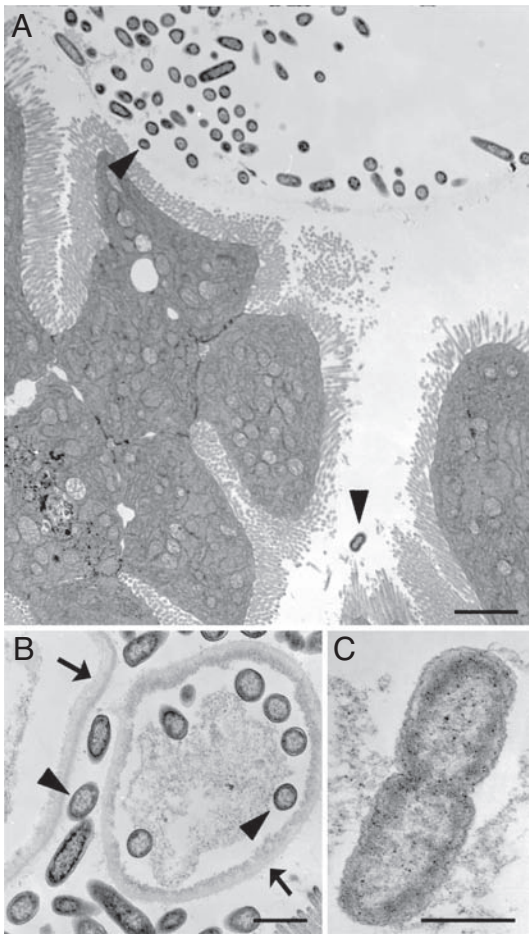

Fig. 2. TEM of gut bacteria in gnotobiotic zebrafish. Transverse sections are shown that include segments 1 and 2 of the intestine of a 6-dpf zebrafish colonized since 3 dpf with *P. aeruginosa* strain PAO1. (*A*) Bacteria are clustered together in the luminal space, and some remain close to the host epithelium (arrowhead in *A*). (*B* and *C*) Bacteria (arrowheads) are also observed in association with unidentified electron-dense laminated objects in the lumen (arrows in *B*) and undergoing fission (*C*). (Scale bars: *A*, 3 μm; *B*, 1 μm; *C*, 500 nm.)

over the course of the next 2.5 days. As in CONVD zebrafish, bacteria in 6-dpf *P. aeruginosa* monoassociated zebrafish were observed along the entire proximal-distal length of the intestine (e.g., SI Movie 4). Individual bacteria displayed a range of behaviors, from intimate association with the intestinal epithelium, to incorporation into large multicellular structures in the luminal space, to rapid movement of planktonic cells through the lumen (Fig. 1 *B* and *E* and SI Movie 4). In 6-dpf hosts, individual bacteria were observed moving at speeds as high as 24 μm/sec within the lumen (equivalent to $\approx$12 body lengths per sec). This movement is likely the result of flagella-mediated swimming motility (see below).

A central challenge for members of a gut microbiota is to avoid washout from its continuously perfused ecosystem. Static scanning electron microscopic studies in the gnotobiotic mouse intestine indicate this can be achieved by bacterial attachment to nutrient platforms consisting of partially digested food particles, exfoliated fragments of mucus, and shed epithelial cells (37, 38). From an engineering perspective, these platforms represent well settling particles, analogous to those that prevent microbial washout from human-made bioreactors (37).

Our gnotobiotic zebrafish provided a dynamic view of the interactions of bacteria with such luminal contents. Similar to the microbiota in CONV-R and CONVD zebrafish, PAO1 pMF230 was observed interacting with large slowly moving luminal structures (SI Movie 2 and data not shown) that were distributed along the length of the gut lumen; similar masses were observed in GF animals, indicating that their formation does not depend upon microbes. Individual bacterial cells could be seen intermittently contacting the surface of these masses (SI Movie 2).

To determine whether bacteria reside within these structures, we fixed *P. aeruginosa* PAO1 monoassociated 6-dpf zebrafish *en bloc* and processed them for transmission electron microscopy (TEM): this *en bloc* fixation was designed to minimize disruption of the *in vivo* spatial relationships among microbes, other gut contents, and host cells. Transverse TEM sections through the zebrafish intestine revealed that the luminal masses contained many intact bacteria mixed with other gut contents, including mucus-like material and large electron-dense lamina (Fig. 2*A* and *B*). Consistent with our real-time *in vivo* imaging results, bacterial cells were also observed outside these luminal aggregates in close juxtaposition to the host epithelium (Fig. 2*A*). TEM disclosed that in CONV-R, CONVD, and *P. aeruginosa*-monoassociated zebrafish, actively dividing and nondividing bacterial cells were closely associated with epithelial cells in the intact mucosa and in the luminal structures (Fig. 2*C* plus data not shown) (23).

Together, these findings show that *P. aeruginosa* appears to recapitulate the range of movements, as well as the locations occupied by members of the intestinal microbiota. To investigate whether the behavior of *P. aeruginosa* in this system was characteristic of other γ-Proteobacteria, we colonized 3-dpf GF zebrafish with *Escherichia coli* MG1655 carrying a plasmid that directs constitutive expression of red fluorescent protein (DsRed) under the control of the *lac* promoter (MG1655 pRZT3). Strain MG1655 pRZT3 displayed significantly less motility than strain PAO1 pMF230 in 6-dpf zebrafish digestive tracts (Fig. 1 *E* and *F* and SI Movies 4 and 5), even though its density of colonization was not significantly different from *P. aeruginosa* (SI Table 1). In contrast, *in vitro* assays revealed that *E. coli* MG1655 has higher rates of swimming motility than *P. aeruginosa* PAO1 in soft agar (SI Fig. 6), suggesting that the zebrafish gut environment influences motility in these bacterial species.

Characterization of *P. aeruginosa* as a Model Zebrafish Mutualist. *P. aeruginosa* strains generally express one of two flagellin proteins (type-a and -b flagellin) that differ by 35% in amino acid sequence (39). To determine whether the motility phenotype and other effects on the host were specific to type-b strains such as PAO1, we tested a well characterized *P. aeruginosa* strain that expresses type-a flagellin (strain PAK) (40). Both strains colonized the digestive tracts of GF zebrafish to similar densities (SI Table 1) and were highly motile *in vivo* (SI Movies 3 and 4 and data not shown). Moreover, both strains elicited evolutionarily conserved nutrient and innate immune responses: quantitative RT-PCR (qRT-PCR) assays conducted on RNA extracted from whole 6-dpf monoassociated zebrafish indicated they suppressed expression of *fiaf* [also known as *angptl4*; encodes a secreted inhibitor of lipoprotein lipase (12, 41)] and *carnitine palmitoyltransferase 1a* (*cpt1a*; involved in mitochondrial oxidation of fatty acids) and induced expression of *serum amyloid a* (*saa*; an acute-phase protein) and *myeloperoxidase* (*mpo*; a granulocyte-specific biomarker of the innate immune response to the normal gut microbiota) (23, 24) (Fig. 3 and SI Table 2).

Animal models of *P. aeruginosa* infection and disease have identified specific factors that this bacterium uses for virulence. A multicomponent Type III secretion system (TTSS) functions to translocate effector proteins into host cells. Strains PAO1 and PAK both secrete three effectors by the TTSS (ExoS, ExoT, and ExoY); these toxins target various host signaling pathways, leading to disruption of the actin cytoskeleton and cytotoxicity

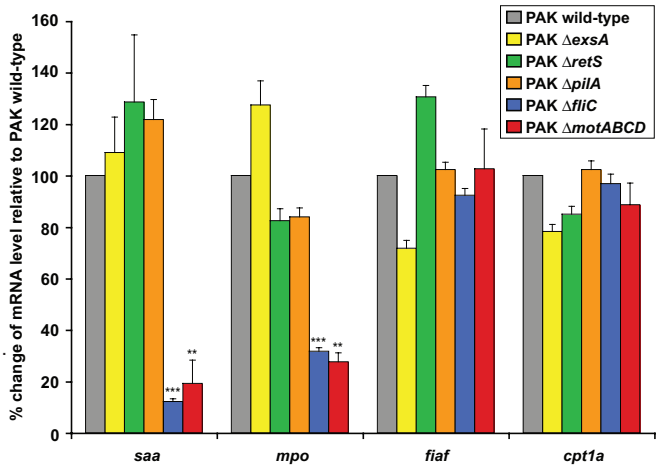

Fig. 3. The impact of *P. aeruginosa* flagellar mutants on host responses in gnotobiotic zebrafish. Expression levels of *serum amyloid a* (*saa*), *myeloperoxidase* (*mpo*), *fasting-induced adipose factor* (*fiaf*), and *carnitine palmitoyltransferase 1a* (*cpt1a*) were assessed by qRT-PCR by using RNA extracted from whole 6-dpf larvae colonized since 3 dpf with *P. aeruginosa* PAK wild-type strain, PAK *exsA* deletion mutant (PAK Δ*exsA*), PAK *retS* deletion mutant (PAK Δ*retS*), PAK *pilA* deletion mutant (PAK Δ*pilA*), PAK *fliC* deletion mutant (PAK Δ*fliC*), or PAK *motABCD* deletion mutant (PAK Δ*motABCD*). Data from biological duplicate pools (6–17 animals per pool) were normalized to 18S rRNA levels. Normalized mRNA levels in colonized fish were referenced against age-matched GF controls ($\Delta\Delta C_t$ method), and the results are expressed as mean percent change relative to the PAK wild-type strain ± SEM. ***, $P < 0.0001$; **, $P < 0.001$ compared with wild-type, based on a two-tailed Student's *t* test.

(42). The TTSS is required for colonization and virulence in a range of mouse models of infection (43–45).

To test whether these gene products play a role in *P. aeruginosa* colonization of the zebrafish gut, we exposed GF 3-dpf zebrafish to the PAK strain carrying a deletion for the TTSS master transcriptional regulator *exsA* (46). In many of the pathogenesis models of *P. aeruginosa* infection, this mutant exhibits decreased virulence and colonization (43, 47, 48). In contrast, the wild-type and *exsA* mutant strains achieved comparable densities of colonization within the intestines of 6-dpf zebrafish (SI Table 1), indicating that the TTSS and its secreted toxins are not essential for colonization. In addition, qRT-PCR analysis showed that the *exsA* mutant strain was capable of regulating expression of *fiaf*, *cpt1a*, *saa*, and *mpo* in a manner that was not significantly different from its wild-type parent strain (Fig. 3).

P. aeruginosa uses the RetS hybrid two-component system to coordinately activate TTSS expression and repress exopolysaccharide production (49). Similar to *exsA* mutants, deletion of *retS* leads to loss of the TTSS. In addition, these mutants overproduce exopolysaccharides implicated in biofilm formation (49). To ascertain whether overproduction of these exopolysaccharides influenced *P. aeruginosa*–zebrafish interactions, we introduced an isogenic PAK *retS* mutant strain into 3-dpf GF hosts. As with the TTSS mutant, neither colonization density nor the response of host innate immune and nutrient biomarker genes differed between the mutant and wild-type strains when measured at 6 dpf (Fig. 3 and SI Table 1).

P. aeruginosa utilizes several surface appendages for colonization and virulence, including a single polar flagellum and Type IV pili. To test the role of bacterial movement on host responses, we examined isogenic PAK strains with loss-of-function mutations in *fliC* and *pilA* (40, 50). The flagellar apparatus of *P. aeruginosa* is assembled through an intricate regulatory process, concluding with synthesis and assembly of FliC protein into the flagellar filament (40, 51). Transmembrane ion gradients provide energy for physical rotation of the filament by the flagellar motor (51). The motor consists of two structures: the rotor (the switch that determines direction of rotation) and the stator (the stationary component through which the rotor turns). Because FliC is the major structural component of the flagellar filament, the *fliC* mutant fails to assemble an intact flagellar filament (40, 51, 52). The *pilA* mutant, which is missing the major pilin structural subunit, does not exhibit pili-dependent twitching or swarming motility (53).

Both mutants achieved a normal density of colonization in the zebrafish gut (SI Table 1). However, the *fliC* strain did not show the highly motile phenotype characteristic of wild-type *P. aeruginosa* in this habitat or *in vitro* (SI Fig. 6 and data not shown), suggesting that swimming motility is a primary method of locomotion *in vivo*. qRT-PCR assays revealed that, like wild-type *P. aeruginosa*, the *fliC* and *pilA* mutants were able to suppress expression of the nutrient metabolic biomarkers *fiaf* and *cpt1a* in 6-dpf larvae (Fig. 3). Unlike the wild-type or three other mutant strains, *fliC*-deficient bacteria failed to elicit a significant increase in expression of innate immune response biomarkers *saa* or *mpo* (reference controls, GF 6-dpf animals; Fig. 3).

The attenuated host immune responses to *fliC* mutants could be caused by absence of FliC protein, the absence of an intact flagellar filament, and/or the absence of flagellar function. To help distinguish among these possibilities, we colonized 3-dpf GF zebrafish with a *P. aeruginosa* PAK strain that carries deletions of the *motAB* and *motCD* genes (Δ*motABCD*), encoding the bacterium's two flagellar stators. PAK *motABCD* mutants assemble an intact flagellar filament that contains the FliC protein, but the assembled filament is nonmotile (SI Fig. 6) because of a failure of filament rotation (54, 55). As with the *fliC* mutant, we found that the *motABCD* mutant was able to colonize 6-dpf zebrafish at densities comparable to the isogenic wild-type strain (SI Table 1) and to recapitulate its elicited nutrient responses: thus, flagellar motility is not required for these host reactions to colonization (Fig. 3). Also similar to *fliC* mutants, innate immune responses to *motABCD* mutants in 6-dpf zebrafish larvae were significantly attenuated (Fig. 3). Therefore, the ability of *P. aeruginosa* to evoke these conserved innate immune responses to a complete gut microbiota is due in part to flagellar function, rather than exclusively to the presence of an intact flagellar filament and its component proteins such as FliC.

Discussion

For *P. aeruginosa* and other bacteria, flagella perform several nonexclusive functions that can impact bacterial colonization and host responses in the digestive tract. First, flagella mediate swimming motility that can facilitate interactions with and invasion of host cells (56), as well as chemotaxis toward preferred habitats and nutrient sources (57) [e.g., studies of *V. cholerae* mutants indicate bacterial motility and chemotaxis are important virulence determinants in the (mouse) intestine (58)]. Second, flagella can act as adhesins that bind bacteria to host epithelial cells independent of their role in motility (59, 60). Third, flagella can serve as a secretion apparatus for virulence factors (61, 62), a role that may be played by *P. aeruginosa* flagella (63). Finally, flagellin can serve as a major immunostimulatory antigen recognized by Toll-like receptor 5 (TLR5) homologs in both fish and mammals (64–66). Activation of mammalian TLR5 triggers NF-κB-dependent proinflammatory signaling pathways that stimulate production of acute-phase proteins and neutrophil chemoattractants (67, 68). *P. aeruginosa* flagella can also bind the glycolipid asialoGM1, leading to TLR2-dependent activation of similar signaling pathways (69). Recent studies have revealed that flagellin from other bacterial species can also be detected by TLR5-independent mechanisms (70).

Our observations suggest that flagellar function, including the swimming motility observed by real-time *in vivo* microscopy, is an important component of host–bacterial interaction in this system. We hypothesize that flagella-dependent swimming mo-

tility promotes physical interaction between *P. aeruginosa* and the host epithelium, where the presence of surface-attached antigens (including the flagellum itself) and other bacterial products can be monitored by the host. Although it remains possible that flagella-dependent immune responses are ultimately stimulated by FliC acting as an antigen, the attenuated immune response to the flagellated but nonmotile *motABCD* mutant shows that flagella motor function is required for this process to occur. These observations set the stage for future experiments that further dissect how dynamic interactions between *P. aeruginosa* and the gut epithelium mediate the observed flagellar-motility-dependent host response in zebrafish.

Our results demonstrate the utility of using gnotobiotic zebrafish for defining and monitoring microbial behavior and localization within the living vertebrate gut and for identifying bacterial genes that affect host–microbial interactions. As such, this genetically pliable host provides an opportunity to explore how habitat influences the establishment of a microbiota, and how microbial dynamics *in vivo* affect host biology. Although *P. aeruginosa* is often used as a model opportunistic pathogen, our study indicates that it can also serve as a model mutualist, capable of colonizing the gut of gnotobiotic zebrafish and eliciting nutrient metabolic and innate immune responses that have been conserved during the ≈400 million years since fish and mammals diverged from their last common ancestor. The combined advantages of *P. aeruginosa* (genome sequence, saturation-level insertion libraries, and genetic tools) and gnotobiotic zebrafish (conservation of metabolic and immune responses to a microbiota with mammals, amenability to high-throughput genetic and chemical screens and the ability to directly observe the gut and its microbial inhabitants in a living vertebrate) offer an opportunity to systematically decipher the foundations of host–microbial mutualism in the gut and perhaps to apply the findings to our own species.

Materials and Methods

Animal Husbandry. All experiments using zebrafish were performed by using protocols approved by the Animal Studies Committees of Washington University and the University of North Carolina at Chapel Hill.

Zebrafish gametes were expressed manually from CONV-R adults (C32 inbred strain), fertilized *in vitro*, and embryos derived as GF according to established protocols (23). GF zebrafish were reared under a 14-h light cycle in sterile vented tissue culture flasks (Becton Dickinson, Sparks, MD) at an average density of 1.3 individuals per milliliter of GZM (GZM components are defined in ref. 23). Animals were maintained at 28.5°C in an air incubator. Fish were fed daily beginning at 3 dpf with a sterilized solution containing 0.1 mg of ZM000 fish food (ZM Ltd., Winchester, United Kingdom) per milliliter of GZM. A 90% water change was performed before each daily feeding, starting at 3 dpf. GF zebrafish were monitored routinely for sterility by using culture-based methods (23).

Colonization and *in Vivo* Imaging. At the time of hatching at 3 dpf, we exposed GF zebrafish reared in sterile vented tissue culture flasks to (*i*) an unfractionated gut microbiota harvested directly from CONV-R adult C32 donors, (*ii*) *P. aeruginosa* PA01 containing pMF230 [harbors GFP under the control of a constitutive *trc* promoter (36); supplied by Michael Franklin, Montana State University, Bozeman, MT], (*iii*) *E. coli* MG1655 containing pRZT3 (DsRed under the control of a constitutive *lac* promoter; a gift from Wilbert Bitter, Vrije University Medical Centre, Vrije, The Netherlands), (*iv*) wild-type *P. aeruginosa* PAK or the isogenic Δ*fliC* strain carrying pSMC21 [a derivative of pSMC2 (71), harboring GFP under the control of a constitutive *lac* promoter; provided by Matthew Wolfgang, University of North Carolina, Chapel Hill], or (*v*) isogenic wild-type or mutant *P. aeruginosa* PAK strains without plasmids (supplied by Matthew Wolfgang and Reuben Ramphal, University of Florida, Gainesville, FL; plus Stephen Lory, Harvard University, Boston, MA). Bacterial strains were grown overnight at 37°C in Luria–Bertani broth before inoculation. Microbes were introduced at a density of 10^4 cfu/ml GZM. A complete list of bacterial strains and plasmids used can be found in SI Table 1.

Monoassociated and age-matched CONVD zebrafish were imaged at various times after exposure to bacteria by using the following protocol. Animals were anesthetized in 0.2 mg/ml Tricaine (Sigma, St. Louis, MO), placed on a 40 × 22-mm glass coverslip, and imbedded in low-melting-point 1% NuSieve GTG agarose (FMC Bioproducts, Philadelphia, PA) containing 0.2 mg/ml Tricaine anesthetic. After the agarose quickly solidified, animals were viewed by using an Axiovert 200M inverted fluorescence microscope and Axiovision 4.1 software (Zeiss, Thornwood, NY).

We are grateful to Edward Flynn for zebrafish husbandry; to Jaime Dant and Howard Wynder for help with TEM; to Adam Schreck for video editing; and to Fredrik Bäckhed, Eric Martens, Justin Sonnenburg, and Matthew Wolfgang for helpful suggestions. This work was supported in part by the Ellison Medical Foundation, the W. M. Keck Foundation, and National Institutes of Health Grants DK30292, DK62675, and DK73695.

1. Gill SR, Pop M, Deboy RT, Eckburg PB, Turnbaugh PJ, Samuel BS, Gordon JI, Relman DA, Fraser-Liggett CM, Nelson KE (2006) *Science* 312:1355–1359.
2. Miller TL, Wolin MJ (1986) *Syst Appl Microbiol* 7:223–229.
3. Rieu-Lesme F, Delbes C, Sollelis L (2005) *Curr Microbiol* 51:317–321.
4. Eckburg PB, Bik EM, Bernstein CN, Purdom E, Dethlefsen L, Sargent M, Gill SR, Nelson KE, Relman DA (2005) *Science* 308:1635–1638.
5. Fricke WF, Seedorf H, Henne A, Kruer M, Liesegang H, Hedderich R, Gottschalk G, Thauer RK (2006) *J Bacteriol* 188:642–658.
6. Ley RE, Turnbaugh PJ, Klein S, Gordon JI (2006) *Nature* 444:1022–1023.
7. Stappenbeck TS, Hooper LV, Gordon JI (2002) *Proc Natl Acad Sci USA* 99:15451–15455.
8. Bäckhed F, Crawford PA, O'Donnell D, Gordon JI (2007) *Proc Natl Acad Sci USA* 104:606–611.
9. Lesher S, Walburg HE, Jr, Sacher GA, Jr (1964) *Nature* 202:884–886.
10. Khoury KA, Floch MH, Hersh T (1969) *J Exp Med* 130:659–670.
11. Dumas ME, Barton RH, Toye A, Cloarec O, Blancher C, Rothwell A, Fearnside J, Tatoud R, Blanc V, Lindon JC, *et al.* (2006) *Proc Natl Acad Sci USA* 103:12511–12516.
12. Bäckhed F, Ding H, Wang T, Hooper LV, Koh GY, Nagy A, Semenkovich CF, Gordon JI (2004) *Proc Natl Acad Sci USA* 101:15718–15723.
13. Turnbaugh PJ, Ley RE, Mahowald MA, Magrini V, Mardis ER, Gordon JI (2006) *Nature* 444:1027–1131.
14. Bäckhed F, Manchester JK, Semenkovich CF, Gordon JI (2007) *Proc Natl Acad Sci USA* 104:979–984.
15. Hooper LV, Stappenbeck TS, Hong CV, Gordon JI (2003) *Nat Immunol* 4:269–273.
16. Macpherson AJ, Uhr T (2004) *Science* 303:1662–1665.
17. Mazmanian SK, Liu CH, Tzianabos AO, Kasper DL (2005) *Cell* 122:107–118.
18. Cash HL, Whitham CV, Behrendt CL, Hooper LV (2006) *Science* 313:1126–1130.
19. Gordon HA, Wostmann BS, Bruckner-Kardoss E (1963) *Proc Soc Exp Biol Med* 114:301–304.
20. Ley RE, Peterson DA, Gordon JI (2006) *Cell* 124:837–848.
21. Ng AN, de Jong-Curtain TA, Mawdsley DJ, White SJ, Shin J, Appel B, Dong PD, Stainier DY, Heath JK (2005) *Dev Biol* 286:114–135.
22. Wallace KN, Akhter S, Smith EM, Lorent K, Pack M (2005) *Mech Dev* 122:157–173.
23. Rawls JF, Samuel BS, Gordon JI (2004) *Proc Natl Acad Sci USA* 101:4596–4601.
24. Rawls JF, Mahowald MA, Ley RE, Gordon JI (2006) *Cell* 127:423–433.
25. Bates JM, Mittge E, Kuhlman J, Baden KN, Cheesman SE, Guillemin K (2006) *Dev Biol* 297:374–386.
26. Cahill MM (1990) *Microb Ecol* 19:21–41.
27. Huber I, Spanggaard B, Appel KF, Rossen L, Nielsen T, Gram L (2004) *J Appl Microbiol* 96:117–132.
28. Romero J, Navarrete P (2006) *Microb Ecol.*
29. Graham DY, Yoshimura HH, Estes MK (1983) *J Lab Clin Med* 101:940–954.
30. Wei B, Huang T, Dalwadi H, Sutton CL, Bruckner D, Braun J (2002) *Infect Immun* 70:6567–6575.

31. Spivak J, Landers CJ, Vasiliauskas EA, Abreu MT, Dubinsky MC, Papadakis KA, Ippoliti A, Targan SR, Fleshner PR (2006) *Inflamm Bowel Dis* 12:1122–1130.
32. Stover CK, Pham XQ, Erwin AL, Mizoguchi SD, Warrener P, Hickey MJ, Brinkman FS, Hufnagle WO, Kowalik DJ, Lagrou M, *et al.* (2000) *Nature* 406:959–964.
33. Jacobs MA, Alwood A, Thaipisuttikul I, Spencer D, Haugen E, Ernst S, Will O, Kaul R, Raymond C, Levy R, *et al.* (2003) *Proc Natl Acad Sci USA* 100:14339–14344.
34. Liberati NT, Urbach JM, Miyata S, Lee DG, Drenkard E, Wu G, Villanueva J, Wei T, Ausubel FM (2006) *Proc Natl Acad Sci USA* 103:2833–2838.
35. Wallace KN, Pack M (2003) *Dev Biol* 255:12–29.
36. Nivens DE, Ohman DE, Williams J, Franklin MJ (2001) *J Bacteriol* 183:1047–1057.
37. Sonnenburg JL, Angenent LT, Gordon JI (2004) *Nat Immunol* 5:569–573.
38. Sonnenburg JL, Xu J, Leip DD, Chen CH, Westover BP, Weatherford J, Buhler JD, Gordon JI (2005) *Science* 307:1955–1959.
39. Spangenberg C, Heuer T, Burger C, Tummler B (1996) *FEBS Lett* 396:213–217.
40. Dasgupta N, Wolfgang MC, Goodman AL, Arora SK, Jyot J, Lory S, Ramphal R (2003) *Mol Microbiol* 50:809–824.
41. Sukonina V, Lookene A, Olivecrona T, Olivecrona G (2006) *Proc Natl Acad Sci USA* 103:17450–17455.
42. Barbieri JT, Sun J (2004) *Rev Physiol Biochem Pharmacol* 152:79–92.
43. Holder IA, Neely AN, Frank DW (2001) *Burns* 27:129–130.
44. Lee VT, Smith RS, Tummler B, Lory S (2005) *Infect Immun* 73:1695–1705.
45. Vance RE, Rietsch A, Mekalanos JJ (2005) *Infect Immun* 73:1706–1713.
46. Wolfgang MC, Lee VT, Gilmore ME, Lory S (2003) *Dev Cell* 4:253–263.
47. Smith RS, Wolfgang MC, Lory S (2004) *Infect Immun* 72:1677–1684.
48. Zolfaghar I, Evans DJ, Ronaghi R, Fleiszig SM (2006) *Infect Immun* 74:3880–3889.
49. Goodman AL, Kulasekara B, Rietsch A, Boyd D, Smith RS, Lory S (2004) *Dev Cell* 7:745–754.
50. Kagami Y, Ratliff M, Surber M, Martinez A, Nunn DN (1998) *Mol Microbiol* 27:221–233.
51. Macnab RM (2003) *Annu Rev Microbiol* 57:77–100.
52. Soscia C, Hachani A, Bernadac A, Filloux A, Bleves S (2007) *J Bacteriol.*
53. Strom MS, Lory S (1993) *Annu Rev Microbiol* 47:565–596.
54. Arora SK, Neely AN, Blair B, Lory S, Ramphal R (2005) *Infect Immun* 73:4395–4398.
55. Toutain CM, Zegans ME, O'Toole GA (2005) *J Bacteriol* 187:771–777.
56. O'Neil HS, Marquis H (2006) *Infect Immun* 74:6675–6681.
57. Ottemann KM, Lowenthal AC (2002) *Infect Immun* 70:1984–1990.
58. Butler SM, Camilli A (2004) *Proc Natl Acad Sci USA* 101:5018–5023.
59. Arora SK, Ritchings BW, Almira EC, Lory S, Ramphal R (1998) *Infect Immun* 66:1000–1007.
60. Giron JA, Torres AG, Freer E, Kaper JB (2002) *Mol Microbiol* 44:361–379.
61. Young GM, Schmiel DH, Miller VL (1999) *Proc Natl Acad Sci USA* 96:6456–6461.
62. Konkel ME, Klena JD, Rivera-Amill V, Monteville MR, Biswas D, Raphael B, Mickelson J (2004) *J Bacteriol* 186:3296–3303.
63. Fleiszig SM, Arora SK, Van R, Ramphal R (2001) *Infect Immun* 69:4931–4937.
64. Hayashi F, Smith KD, Ozinsky A, Hawn TR, Yi EC, Goodlett DR, Eng JK, Akira S, Underhill DM, Aderem A (2001) *Nature* 410:1099–1103.
65. Gewirtz AT, Navas TA, Lyons S, Godowski PJ, Madara JL (2001) *J Immunol* 167:1882–1885.
66. Tsujita T, Tsukada H, Nakao M, Oshiumi H, Matsumoto M, Seya T (2004) *J Biol Chem* 279:48588–48597.
67. Schleimer RP, Sha Q, Vandermeer J, Lane AP, Kim J (2004) *Clin Exp All Rev* 4:176–182.
68. Prince A (2006) *Am J Respir Cell Mol Biol* 34:548–551.
69. Adamo R, Sokol S, Soong G, Gomez MI, Prince A (2004) *Am J Respir Cell Mol Biol* 30:627–634.
70. Neish AS (2007) *Am J Physiol* 292:G462–G466.
71. Bloemberg GV, O'Toole GA, Lugtenberg BJ, Kolter R (1997) *Appl Environ Microbiol* 63:4543–4551.

APPENDIX D

Mahowald MA,* Rey FE,* Seedorf H, Turnbaugh PJ, Fulton RS, Wollam A, Shah N, Wang C, Magrini V, Wilson RK, Cantarel BL, Coutinho PM, Henrissat B, Crock LW, Russell A, Verberkmoes NC, Hettich RL, Gordon JI

Characterizing a model human gut microbiota composed of members of its two dominant bacterial phyla.

Proc Natl Acad Sci U S A. 2009 Apr 7;106(14):5859-64

For supplemental information please see enclosed CD.

Characterizing a model human gut microbiota composed of members of its two dominant bacterial phyla

Michael A. Mahowald[a,1], Federico E. Rey[a,1], Henning Seedorf[a], Peter J. Turnbaugh[a], Robert S. Fulton[b], Aye Wollam[b], Neha Shah[b], Chunyan Wang[b], Vincent Magrini[b], Richard K. Wilson[b], Brandi L. Cantarel[c,d], Pedro M. Coutinho[c], Bernard Henrissat[c,d], Lara W. Crock[a], Alison Russell[e], Nathan C. Verberkmoes[e], Robert L. Hettich[e], and Jeffrey I. Gordon[a,2]

[a]Center for Genome Sciences and [b]Genome Sequencing Center, Washington University School of Medicine, St. Louis, MO 63108; [c]Universités Aix-Marseille I and II, Marseille, France and [d]Centre National de la Recherche Scientifique, Unité Mixte de Recherche 6098, Marseille, France; and [e]ORNL-UTK Genome Science and Technology Graduate School, Oak Ridge National Laboratory, Oak Ridge, TN 37830

Contributed by Jeffrey I. Gordon, February 12, 2009 (sent for review January 22, 2009)

The adult human distal gut microbial community is typically dominated by 2 bacterial phyla (divisions), the Firmicutes and the Bacteroidetes. Little is known about the factors that govern the interactions between their members. Here, we examine the niches of representatives of both phyla in vivo. Finished genome sequences were generated from *Eubacterium rectale* and *E. eligens*, which belong to Clostridium Cluster XIVa, one of the most common gut Firmicute clades. Comparison of these and 25 other gut Firmicutes and Bacteroidetes indicated that the Firmicutes possess smaller genomes and a disproportionately smaller number of glycan-degrading enzymes. Germ-free mice were then colonized with *E. rectale* and/or a prominent human gut Bacteroidetes, *Bacteroides thetaiotaomicron*, followed by whole-genome transcriptional profiling, high-resolution proteomic analysis, and biochemical assays of microbial–microbial and microbial–host interactions. *B. thetaiotaomicron* adapts to *E. rectale* by up-regulating expression of a variety of polysaccharide utilization loci encoding numerous glycoside hydrolases, and by signaling the host to produce mucosal glycans that it, but not *E. rectale*, can access. *E. rectale* adapts to *B. thetaiotaomicron* by decreasing production of its glycan-degrading enzymes, increasing expression of selected amino acid and sugar transporters, and facilitating glycolysis by reducing levels of NADH, in part via generation of butyrate from acetate, which in turn is used by the gut epithelium. This simplified model of the human gut microbiota illustrates niche specialization and functional redundancy within members of its major bacterial phyla, and the importance of host glycans as a nutrient foundation that ensures ecosystem stability.

human gut Firmicutes and Bacteroidetes | carbohydrate metabolism | gnotobiotic mice | gut microbiome | nutrient sharing

The adult human gut houses a bacterial community containing trillions of members comprising thousands of species-level phylogenetic types (phylotypes). Culture-independent surveys of this community have revealed remarkable interpersonal variations in these strain- and species-level phylotypes. Two bacterial phyla, the Firmicutes and the Bacteroidetes, commonly dominate this ecosystem (1), as they do in the guts of at least 60 mammalian species (2).

Comparative analysis of 5 previously sequenced human gut Bacteroidetes revealed that each genome contains a large repertoire of genes involved in acquisition and metabolism of polysaccharides. This repertoire includes (*i*) up to hundreds of glycoside hydrolases (GHs) and polysaccharide lyases (PLs); (*ii*) myriad paralogs of SusC and SusD, outer membrane proteins involved in recognition and import of specific carbohydrate structures (3); and (*iii*) a large array of environmental sensors and regulators (4). These genes are assembled in similarly organized, selectively regulated polysaccharide utilization loci (PULs) that encode functions necessary to detect, bind, degrade and import carbohydrate species encountered in the gut habitat–either from the diet or from host glycans associated with mucus and the surfaces of epithelial cells (5–7). Studies of gnotobiotic mice colonized only with human gut-derived *Bacteroides thetaiotaomicron* have demonstrated that this organism can vary its pattern of expression of PULs as a function of diet, e.g., during the transition from mother's milk to a polysaccharide-rich chow consumed when mice are weaned (5), or when adult mice are switched from a diet rich in plant polysaccharides to a diet devoid of these glycans and replete with simple sugars (under the latter conditions, the organism forages on host glycans) (6, 7).

Our previous functional genomic studies of the responses of *B. thetaiotaomicron* to cocolonization of the guts of gnotobiotic mice with *Bifidobacterium longum*, an Actinobacterium found in the intestines of adults and infants, or with *Lactobacillus casei*, a Firmicute present in a number of fermented diary products, have shown that *B. thetaiotaomicron* adapts to the presence of these other microbes by modifying expression of its PULs in ways that expand the breadth of its carbohydrate foraging activities (8).

These observations support the notion that gut microbes may live at the intersection of 2 forms of selective pressure: bottom-up selection, where fierce competition between members of a community that approaches a population density of 10^{11} to 10^{12} organisms per milliliter of colonic contents drives phylotypes to assume distinct functional roles (niches); and top-down selection, where the host selects for functional redundancy to ensure against the failure of bioreactor functions that could prove highly deleterious (9, 10).

The gene content, genomic arrangement and functional properties of PULs in sequenced gut Bacteroidetes illustrate the specialization and functional redundancy within members of this phylum. They also emphasize how the combined metabolic activities of members of the microbiota undoubtedly result in

Author contributions: M.A.M., F.E.R., and J.I.G. designed research; M.A.M., F.E.R., H.S., R.S.F., A.W., N.S., C.W., V.M., R.K.W., B.L.C., L.C., A.R., and N.C.V. performed research; M.A.M., F.E.R., H.S., P.T., R.S.F., A.W., B.L.C., P.M.C., B.H., N.C.V., R.H., and J.I.G. analyzed data; and M.A.M., F.E.R., R.H., and J.I.G. wrote the paper.

The authors declare no conflict of interest.

Freely available online through the PNAS open access option.

Data deposition: The data reported in this paper have been deposited in the Gene Expression Omnibus (GEO) database, www.ncbi.nlm.nih.gov/geo (accession nos. GSE14686, 14709, 14737). The sequence reported in this paper has been deposited in the GenBank database [accession nos. CP001107 (ATCC 33656, *Eubacterium rectale*) and CP001104–CP001106 (ATCC 27750, *E. eligens*)].

[1]M.A.M. and F.E.R. contributed equally to this work.

[2]To whom correspondence should be addressed. E-mail: jgordon@wustl.edu.

This article contains supporting information online at www.pnas.org/cgi/content/full/0901529106/DCSupplemental.

interactions that are both very dynamic and overwhelmingly complex (at least to the human observer), involving multiple potential pathways for the processing of substrates (including the order of substrate processing), varying patterns of physical partitioning of microbes relative to substrates within the ecosystem, plus various schemes for utilization of products of bacterial metabolism. Such a system likely provides multiple options for processing of a given metabolite, and for the types of bacteria that can be involved in these activities.

All of this means that the task of defining the interactions of members of the human gut microbiota is daunting, as is the task of identifying general principles that govern the operation of this system. In the present study, we have taken a reductionist approach to begin to define interactions between members of the Firmicutes and the Bacteroidetes that are commonly represented in the human gut microbiota. In the human colon, Clostridium cluster XIVa is 1 of 2 abundantly represented clusters of Firmicutes. Therefore, we have generated the initial 2 complete genome sequences for members of the genus *Eubacterium* in Clostridium cluster XIVa (the human gut-derived *E. rectale* strain ATCC 33656 and *E. eligens* strain ATCC 27750) and compared them with the draft sequences of 25 other sequenced human gut bacteria belonging to the Firmicutes and the Bacteroidetes. The interactions between *E. rectale* and *B. thetaiotaomicron* were then characterized by performing whole-genome transcriptional profiling of each species after colonization of gnotobiotic mice with each organism alone, or in combination under 3 dietary conditions. Transcriptional data were verified by mass spectrometry of cecal proteins, plus biochemical assays of carbohydrate metabolism. Last, we examined colonization and interactions between these microbes from a host perspective; to do so, we performed whole-genome transcriptional analysis of colonic RNA prepared from mice that were germ-free or colonized with one or both species. Our results illustrate how members of the dominant gut bacterial phyla are able to adapt their substrate utilization in response to one another and to host dietary changes, and how host physiology can be affected by changes in microbiota composition.

Results and Discussion

Comparative Genomic Studies of Human Gut-Associated Firmicutes and Bacteroidetes. We produced finished genome sequences for *Eubacterium rectale*, which contains a single 3,449,685-bp chromosome encoding 3,627 predicted proteins, and *Eubacterium eligens*, which contains a 2,144,190-bp chromosome specifying 2,071 predicted proteins, plus 2 plasmids (Table S1). We also analyzed 25 recently sequenced gut genomes, including (*i*) 9 sequenced human gut-derived Bacteroidetes [includes the finished genomes of *B. thetaiotaomicron*, *B. fragilis*, *B. vulgatus*, *and Parabacteroides distasonis*, plus deep draft assemblies of the *B. caccae*, *B. ovatus*, *B. uniformis, B. stercoris* and *P. merdae* genomes generated as part of the human gut microbiome initiative (HGMI) (http://genome.wustl.edu/hgm/HGM_frontpage.cgi)], and (*ii*) 16 other human gut Firmicutes where deep draft assemblies were available through the HGMI (see Fig. S1 for a phylogenetic tree). We classified the predicted proteins in these 2 genomes using Gene Ontology (GO) terms generated via Interproscan, and according to the scheme incorporated into the Carbohydrate Active Enzymes (CAZy) database [www.cazy.org (11)], and then applied a binomial test to identify functional categories of genes that are either over- or under-represented between the Firmicutes and Bacteroidetes phyla. This analysis, described in *SI Results*, Figs. S2 and S3, and Table S2 and Table S3, emphasized among other things that the Firmicutes, including *E. rectale* and *E. eligens*, have significantly fewer polysaccharide-degrading enzymes and more ABC transporters and PTS systems than the Bacteroidetes (12). We subsequently chose *E. rectale* and *B. thetaiotaomicron* as representatives of these 2 phyla for further characterization of their niches in vivo, because of their prominence in culture-independent surveys of the distal human gut microbiota (13, 14), the pattern of representation of carbohydrate active enzymes in their glycobiomes and *E. rectale's* ability to generate butyrate as a major end product of fermentation (15, 16). These choices set the stage for an "arranged marriage" between a Firmicute and a Bacteroidetes, hosted by formerly germ-free mice.

Functional Genomic Analyses of the Minimal Human Gut Microbiome.

Creating a "minimal human gut microbiota" in gnotobiotic mice. Young adult male germ-free mice belonging to the NMRI inbred strain were colonized with *B. thetaiotaomicron* or *E. rectale* alone (monoassociations) or cocolonized with both species (biassociation). Ten to fourteen days after inoculation by gavage, both species colonized the ceca of recipient mice, fed a standard chow diet rich in complex plant polysaccharides, to high levels (n = 4–5 mice per treatment group in each of 3 independent experiments; Fig. S4*A*). Moreover, cecal levels of colonization for both organisms were not significantly different between mono- and biassociated animals (Fig. S4*A*).

B. thetaiotaomicron's response to E. rectale. A custom, multispecies, human gut microbiome Affymetrix GeneChip was designed (*SI Methods*), and used to compare the transcriptional profile of each bacterial species when it was the sole inhabitant of the cecum, and when it coexisted together with the other species. A significant number of *B. thetaiotaomicron* genes located in PULs exhibited differences in their expression upon *E. rectale* colonization [55 of 106; $P < 10^{-15}$ (cumulative hypergeometric test); see *SI Methods* for the statistical criteria for defining significantly different levels of gene expression]. Of these 55 genes, 51 (93%) were up-regulated (Fig. S4*B*; see Table S4A for a complete list of differentially regulated *B. thetaiotaomicron* genes).

As noted in the *Introduction*, 2 previous studies from our lab examined changes in *B. thetaiotaomicron's* transcriptome in the ceca of monoassociated gnotobiotic mice when they were switched from a diet rich in plant polysaccharides to a glucose-sucrose chow (6), or in suckling mice consuming mother's milk as they transitioned to a standard chow diet (5). In both situations, in the absence of dietary plant polysaccharides, *B. thetaiotaomicron* adaptively forages on host glycans. The genes up-regulated in *B. thetaiotaomicron* upon cocolonization with *E. rectale* have a significant overlap with those noted in these 2 previous datasets ($P < 10^{-14}$, cumulative hypergeometric test; Fig. S4*C*). In addition, they include several of the genes up-regulated during growth on minimal medium containing porcine mucosal glycans as the sole carbon source (7). For example, in cocolonized mice and in vitro, *B. thetaiotaomicron* up-regulates several genes (BT3787-BT3792; BT3774-BT3777) (Fig. S4*D*) used in degrading α-mannosidic linkages, a component of host N-glycans and the diet. (Note that *E. rectale* is unable to grow in defined medium containing α-mannan or mannose as the sole carbon sources; Table S3). *B. thetaiotaomicron* also up-regulates expression of its starch utilization system (Sus) PUL in the presence of *E. rectale* (BT3698–3704) (Fig. S4*D*). This well-characterized PUL is essential for degradation of starch molecules containing ≥6 glucose units (17).

Thus, it appears that *B. thetaiotaomicron* adapts to the presence of *E. rectale* by up-regulating expression of a variety of PULs so that it can broaden its niche and degrade an increased variety of glycan substrates, including those derived from the host that *E. rectale* is unable to access. There are a number of reasons why the capacity to access host glycans likely represents an important trait underpinning microbiota function and stability: (*i*) glycans in the mucus gel are abundant and are a consistently represented source of nutrients; (*ii*) mucus could serve as a microhabitat for Bacteroidetes spp. to embed in (and adhere to via SusD paralogs), thereby avoiding washout from the

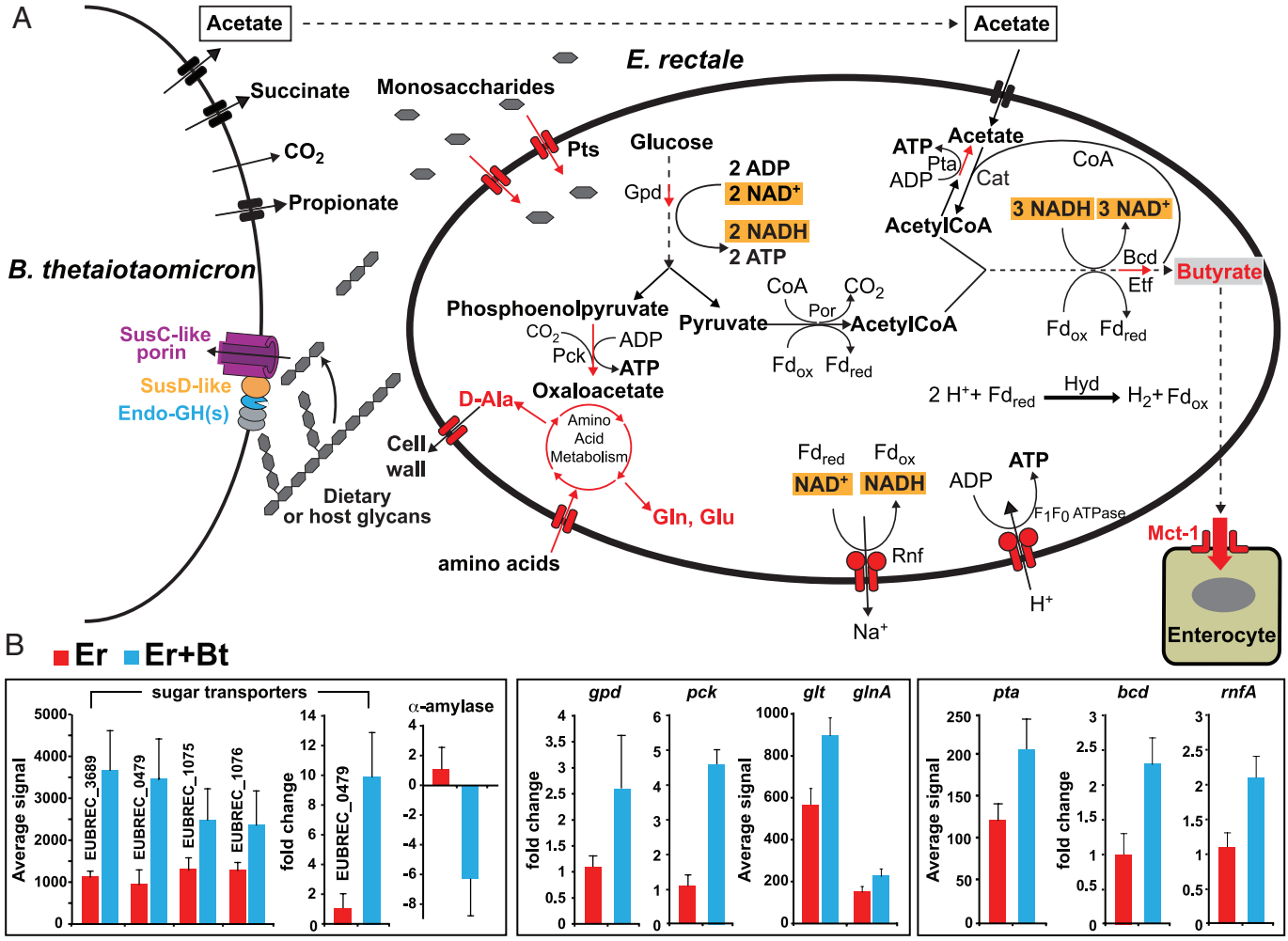

Fig. 1. Summary of metabolic responses of *E. rectale* to *B. thetaiotaomicron*. (*A*) Overview of metabolic pathways. (*B*) GeneChip probeset intensities and qRT-PCR validation assays are shown for a subset of genes. Mean values for triplicate qRT-PCR determinations (n = 4 mice per group) ± SD are plotted. Pts, phosphotransferase systems; Gpd, glycerol 3-phosphate dehydrogenase; Pck, phosphoenolpyruvate carboxykinase; Por, pyruvate:ferredoxin oxidoreductase; Hyd, hydrogenase; Rnf, NADH: ferredoxin oxidoreductase complex; Fd_{red}, reduced ferredoxin; Fd_{ox} oxidized ferredoxin; Pta, phosphate acetyltransferase; Bcd, butyryl-CoA dehydrogenase; Etf electron transport flavoproteins; Cat, butyryl CoA: acetate CoA transferase; Glt, glutamate synthetase; GlnA, glutamine synthetase Gln, glutamine; Glu, glutamate; Mct1, monocarboxylate transporter 1.

ecosystem; and (*iii*) the products of polysaccharide digestion/fermentation generated by Bacteroidetes spp. could be shared with other members of the microbiota that are also embedded in mucus (7).

***E. rectale*'s response to *B. thetaiotaomicron*.** *E. rectale's* response to *B. thetaiotaomicron* in the mouse cecum stands in marked contrast to *B. thetaiotaomicron*'s response to *E. rectale.* Carbohydrate metabolism genes, particularly GHs, are significantly overrepresented among the *E. rectale* genes that are downregulated in the presence of *B. thetaiotaomicron* compared with monoassociation; i.e., 12 of *E. rectale's* predicted 51 GHs have significantly reduced expression while only 2 are up-regulated (Fig. S4 *E* and *F*; see Table S4B for a complete list of *E. rectale* genes regulated by the presence of *B. thetaiotaomicron*). The 2 up-regulated GH genes (EUBREC_1072, a 6-P-β-glucosidase and EUBREC_3687, a cellobiose phosphorylase) are predicted to break down cellobiose. Three simple sugar transport systems with predicted specificity for cellobiose, galactoside, and arabinose/lactose (EUBREC_3689, EUBREC_0479, and EUBREC_1075–6, respectively) are among the most strongly up-regulated genes (Fig. S4*G* and Table S4B). Phosphoenolpyruvate carboxykinase (Pck EUBREC_2002) is also induced with cocolonization (Table S4B, GeneChip data were verified by qRT-PCR assays in 2 independent experiments involving 3–4 mice per treatment group; Fig. 1*B*). This enzyme catalyzes an energy conserving reaction that produces oxaloacetate from phosphoenolpyruvate. In a subsequent transaminase reaction, oxaloacetate can be converted to aspartate, linking this branching of the glycolytic pathway with amino acid biosynthesis (Fig. 1*A*).

Additional data support the notion that *E. rectale* is better able to access nutrients in the presence of *B. thetaiotaomicron.* For example, a number of peptide and amino acid transporters in *E. rectale* are up-regulated, as are the central carbon and nitrogen regulatory genes CodY (EUBREC_1812), glutamate synthase (EUBREC_1829) and glutamine synthetase (EUBREC_2543) (Fig. 1*B* and Fig. S4*H*; note that these genes are also up-regulated during growth in tryptone glucose medium; Table S4C).

Changes in *E. rectale's* fermentative pathways. *E. rectale* possesses genes (EUBEC733–737; EUBEC1017) for the production of butyrate that show high similarity to genes from other Clostridia. This pathway involves condensation of 2 molecules of acetylCoA to form butyrate and is accompanied by oxidation of NADH to NAD^+ (Fig. 1). Transcriptional and high-resolution proteomic analyses (see below) disclosed that the enzymes involved in

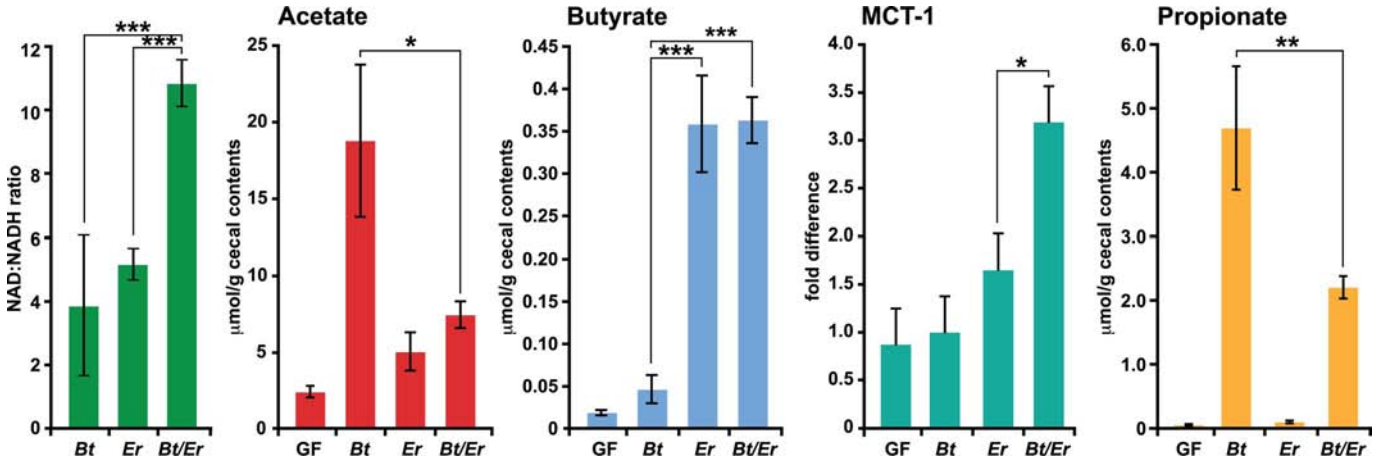

Fig. 2. Cocolonization affects the efficiency of fermentation. Cecal contents from 4 mice in each treatment group were assayed for NAD^+, NADH acetate, butyrate and proprionate levels. Expression of Mct-1 mRNA, a monocarboxylate transporter whose preferred substrate is butyrate was defined by qRT-PCR in the proximal colon. Cecal propionate concentrations. Mean values ± SEM are plotted; $n = 4–5$ mice per group; *, $P < 0.05$, **, $P < 0.001$ compared with cocolonization (Student's *t* test).

production of butyrate are among the most highly expressed in cecal contents recovered from mono- and biassociated mice containing *E. rectale* (Table S4B and Table S6A).

In vitro studies have shown that in the presence of carbohydrates, *E. rectale* consumes large amounts of acetate for butyrate production (18). Several observations indicate that *E. rectale* utilizes *B. thetaiotaomicron*-derived acetate to generate increased amounts of butyrate in the ceca of our gnotobiotic mice. First, *E. rectale* up-regulates a phosphate acetyltransferase (EUBREC_1443; EC 2.3.1.8)—1 of 2 enzymes involved in the interconversion of acetyl-CoA and acetate (Fig. 1*B*). Second, cecal acetate levels are significantly lower in cocolonized mice compared with *B. thetaiotaomicron* monoassociated animals (Fig. 2). Third, although cecal butyrate levels are similar in *E. rectale* mono- and biassociated animals (Fig. 2), expression of mouse *Mct-1*, encoding a monocarboxylate transporter whose inducer and preferred substrate is butyrate (19), is significantly higher in the distal gut of mice containing both *E. rectale* and *B. thetaiotaomicron* versus *E. rectale* alone ($P < 0.05$; Fig. 2). The cecal concentrations of butyrate we observed are similar to those known to up-regulate Mct-1 in colonic epithelial cell lines (19). Higher levels of acetate (i.e., those encountered in *B. thetaiotaomicron* monoassociated mice) were insufficient to induce any change in Mct-1 expression compared with germ-free controls (Fig. 2).

The last step in *E. rectale*'s butyrate production pathway is catalyzed by the butyrylCoA dehydrogenase/electron transfer flavoprotein (Bcd/Etf) complex (EUBREC_0735–0737; EC 1.3.99.2), and offers a recently discovered additional pathway for energy conservation, via a bifurcation of electrons from NADH to crotonylCoA and ferredoxin (20). Reduced ferredoxin, in turn, can be reoxidized via hydrogenases, or via the membrane-bound oxidoreductase, Rnf, which generates sodium-motive force (Fig. 1*A*). The up-regulation and high level of expression of these key metabolic genes when *E. rectale* encounters *B. thetaiotomicron* (Fig. 1*B*; Table S4B and Table S6A) indicates that *E. rectale* not only employs this pathway to generate energy, but to also accommodate the increased demand for NAD+ in the glycolytic pathway. Consistent with these observations, we found that the NAD^+/NADH ratio in cecal contents was significantly increased with cocolonization (Fig. 2).

The pathway for acetate metabolism observed in this simplified model human gut community composed of *B. thetaiotaomicron* and *E. rectale* differs markedly from what is seen in mice that harbor *B. thetaiotaomicron* and the principal human gut methanogenic archaeon, *Methanobrevibacter smithii*. When *B. thetaiotaomicron* encounters *M. smithii* in the ceca of gnotobiotic mice, there is increased production of acetate by *B. thetaiotaomicron*, no diversion to butyrate and no induction of Mct-1 (21), increased serum acetate levels, and increased adiposity compared with *B. thetaiotaomicron* mono-associated controls. In contrast, serum acetate levels and host adiposity (as measured by fat pad to body weight ratios) are not significantly different between *B. thetaiotaomicron* monoassociated and *B. thetaiotaomicron-E. rectale* cocolonized animals ($n = 4–5$ animals/group; $n = 3$ independent experiments; data not shown).

Colonic transcriptional changes evoked by *E. rectale-B. thetaiotaomicron* cocolonization. We subsequently used Affymetrix Mouse 430 2 GeneChips to compare patterns of gene expression in the proximal colons of mice that were either germ-free, monoassociated with *E.rectale* or *B. thetaiotaomicron*, or cocolonized with both organisms ($n = 4$ mice per group; total of 16 GeneChip datasets). In contrast to the small number of genes whose expression was significantly changed (≥1.5-fold, FDR <1%) after colonization with either bacterium alone relative to germ-free controls (Table S7 A and B), cocolonization produced significant alterations in the expression of 508 host genes (Table S7C). Expression of many of these genes also changed with monoassociation with either organism, and in the same direction as seen after cocolonization, but in most cases the changes evoked by *B. thetaiotaomicron* or *E. rectale* alone did not achieve statistical significance. Unsupervised hierarchical clustering of average expression intensity values derived from each of the 4 sets of GeneChips/group, revealed that the *E.rectale* monoassociation and *E.rectale-B.thetaiotaomicron* biassociation profiles clustered separate from the germ-free and *B. thetaiotaomicron* monoassociation datasets (Fig. S5).

Ingenuity Pathway Analysis (www.ingenuity.com) disclosed that the list of 508 host genes affected by cocolonization was significantly enriched in functions related to cellular growth and proliferation (112 genes; Table S8A), and cell death (130 genes) (Table S8B). A number of components of the canonical wnt/β catenin pathway, which is known to be critically involved in controlling self-renewal of the colonic epithelium, were present in this list (*Akt3*, *Axin2*, *Csnk1D*, *Dkk3*, *FrzB*, *Fzd2*, *Gja1*, *Mdm2*, *Ppp2r5e*, *Sfrp2*, *Tgfb3*, *Tgfbr1*, and *Tgfbr2*). Many of the changes observed in biassociated mice are likely to be related to the

increased influx of butyrate, generated by *E. rectale*, into colonic cells (Fig. 1*A*). Butyrate, a histone deacetylase inhibitor that evokes pronounced transcriptional changes in different types of cultured epithelial cell lines (22–25), is the preferred energy substrate for colonic enterocytes (26). While transcriptional changes caused by butyrate differ depending upon the cell lineage, state of cellular differentiation, and cellular energy status (23, 24, 27, 28), in vitro and in vivo studies have shown that it affects expression of genes involved in proliferation, differentiation and apoptosis (25, 28).

As mentioned above, as part of its adaptation to the presence of *E. rectale*, *B. thetaiotaomicron* up-regulates a number of genes involved in the harvest of host glycans. Included among these *B. thetaiotaomicron* genes are components of a fucose utilization operon linked to production of a bacterial signal that induces synthesis of intestinal mucosal fucosylated glycans, and microbial catabolism of fucose from O-glycans (29). GeneChip profiling of colonic gene expression disclosed that cocolonization results in increased expression of *Fut2* (α-1,2 fucosyltransferase), *Fut4* (α-1,3-fucosyltransferase), plus 10 other genes involved in the synthesis of mucosal glycans (glycosphingolipids and O-glycans) (Table S8C). Thus, by increasing host production of glycans, *B. thetaiotaomicron* can benefit itself, and through its metabolic products, *E. rectale*.

***E. rectale's* Colonization Levels and Production of Butyrate Are Affected by Host Diet.** In a final series of experiments, we assessed how *E. rectale* and *B. thetaiotaomicron* were affected by changes in host diet. Groups of age- and gender-matched cocolonized mice were fed 1 of 3 diets that varied primarily in their carbohydrate and fat content: (*i*) the standard *l*ow-*f*at, *p*lant *p*olysaccharide-rich diet used for the experiments described above (abbreviated "LF/PP" for low-fat/plant polysaccharide), (*ii*) a high-fat, "high-sugar" Western-type diet (abbreviated HF/HS) that contained sucrose, maltodextrin, and corn starch, plus complex polysaccharides (primarily cellulose) that were not digestible by *B. thetaiotaomicron* or *E. rectale*, and (*iii*) a control diet that was similar to (*ii*) except that the fat content was 4-fold lower ("LF/HS" for low-fat, high-sugar; $n = 5$ mice per group). Whereas *B. thetaiotaomicron's* colonization levels were similar in all 3 diets, colonization of *E. rectale* was significantly reduced (5-fold) in mice fed either the LF/HS or HF/HS diets ($P < 0.01$, heteroscedastic t test).

Whole-genome transcriptional profiling of both bacterial species showed that relative to the standard polysaccharide-rich chow diet (LF/PP), both the Western style HF/HS diet and its LF/HS control produced a significant up-regulation of *B. thetaiotaomicron* PULs involved in harvesting and degrading host polysaccharides, and a downregulation of several PULs involved in the degradation of dietary plant polysaccharides (Fig. S6*A*). *E. rectale*'s response to the HF/HS and LF/HS diets was to down-regulate several of its GHs and a number of its sugar transporters (Fig. S6*B*). Moreover, levels of butyrate were 5-fold lower in cocolonized mice fed these compared with the standard chow (LF/PS) diet [0.496 ± 0.0051 μmol per gram of wet weight cecal contents; (LF/PP) vs. 0.095 ± 0.002 (HF/HS) vs. 0.080 ± 0.008 (LF/HS) ($P < 0.05$ ANOVA)].

These dietary manipulations lend further support to the view that *B. thetaiotaomicron* with its large repertoire of PUL-associated GHs functions in this model 2-member human microbiota to process complex dietary plant polysaccharides and to distribute to the products of digestion to *E. rectale*, which, in turn, synthesizes butyrate. The reduced colonization response of *E. rectale* to the HF/HS and LF/HS diets can be explained by a number of factors: (*i*) this Firmicute does not have predicted GHs and PLs that can process host glycans (Fig. S3); (*ii*) it cannot use most of the sugars we tested that are derived from mucosal polysaccharides (Table S3); and (iii) the host possesses enzymes in its glycobiome that can directly process the simple sugars present in these 2 diets. Indeed, human subjects that are fed diets deficient in complex polysaccharides harbor lower levels of butyrate-producing gut bacteria, including members of the *E. rectale*-containing clade (30). Our simplified gnotobiotic model of the microbiota underscores the functional implications of diet-associated changes in the representation of this clade, not only as they relate to the operations of the microbiota itself but also potentially as they relate to butyrate-mediated changes in gut epithelial homeostasis.

Proteomic Studies of This Simplified 2-Component Model of the Human Gut Microbiome. Model communities such as the one described above, constructed in gnotobiotic mice, where microbiome gene content is precisely known and transcriptional data are obtained under conditions where potentially confounding host variables such as diet and host genotype can be constrained, provide a way to test the efficacy of high-resolution mass spectrometric methods for characterizing gut microbial community proteomes. Therefore, we assayed the proteins present in luminal contents, collected from the ceca of 8 gnotobiotic mice fed the standard polysaccharide-rich LF/PP diet (germ-free, monoassociated, and cocolonized; $n = 2$ mice per treatment group representing 2 independent biological experiments; see *SI Methods* for additional details).

The measured proteomes had high reproducibility in terms of total number of proteins observed and spectra matching to each species. Table S5 and *SI Results* provide a summary of our analyses, including the percentage of mRNAs called "Present" in the GeneChip datasets for which there was an identified protein product. The most abundant identified products from both microbes included ribosomal proteins, elongation factors, chaperones, and proteins involved in energy metabolism (for a full list of identified proteins, see Table S6; note that Table S4 A and B, which list differentially expressed genes in monoassociation versus bias-sociation experiments, also indicate whether protein products from their transcripts were identified in these mass spectrometry datasets). Many conserved hypothetical and pure hypothetical proteins were identified, as were proteins encoded by 10 genes in *B. thetaiotaomicron* whose presence had not been predicted in our initial annotation of the finished genome (Table S6A). Together, the results provide validation of experimental and computational procedures used for proteomic assays of a model gut microbiota, and illustrate some of the benefits in obtaining this type of information.

Prospectus. These studies of a model 2-member human gut microbiota created in gnotobiotic mice support a view of the Bacteroidetes, whose genomes contain a disproportionately large number of glycan-degrading enzymes compared with sequenced Firmicutes, as responding to increasing microbial diversity in the distal intestine by modulating expression of their vast array of polysaccharide utilization loci. *B. thetaiotaomicron* adapts to the presence of *E. rectale* by up-regulating a variety of loci specific for host-derived mucin glycans that *E. rectale* is unable to use. *E. rectale*, which like other Firmicutes has a more specialized capacity for glycan degradation, broadly downregulates its available GHs in the presence of *B. thetaiotaomicron*, even though it does not grow efficiently in the absence of carbohydrates. It also becomes more selective in its harvest of sugars and its transcriptional profile suggests improved access to other nutrients (e.g., there is a generalized up-regulation of amino acid biosynthetic genes and a set of nutrient transporters that can harvest peptides). Thus, this simplified, model microbial community illustrates some of the basic ecologic principles that likely shape the operations of the human gut microbiota: nutrient interchange and the observed reciprocal effects on metabolism of these 2 organisms provide examples of classic syntrophy while "character displacement", where cooccurrence drives (niche) divergence, also operates.

We have previously used gnotobiotic mice to show that the

efficiency of fermentation of dietary polysaccharides to short chain fatty acids by *B. thetaiotaomicron* increases in the presence of *M. smithii* (21). Cocolonization increases the density of colonization of the distal gut by both organisms, increases production of formate and acetate by *B. thetaiotaomicron* and allows *M. smithii* to use H_2 and formate to produce methane, thereby preventing the build-up of these fermentation end-products (and NADH) in the gut bioreactor, and improving the efficiency of carbohydrate metabolism (21). Removal of H_2 by this methanogenic archaeon allows *B. thetaiotaomicron* to regenerate NAD^+, which can then be used for glycolysis. This situation constitutes a mutualism, in which both members show a clear benefit. The present study, characterizing the cocolonization with *B. thetaiotaomicron* and *E. rectale*, describes a more nuanced interaction where both species colonize to similar levels if carbohydrate substrates are readily available. Moreover, certain aspects of bacterial-host mutualism become more apparent with cocolonization, including increased microbial production and host transport of butyrate, and increased host production and microbial consumption of mucosal glycans.

It seems likely that as the complexity of the gut community increases, interactions between *B. thetaiotaomicron* and *E. rectale* will either by subsumed or magnified by other "similar" phylogenetic types (as defined by their 16S rRNA sequence and/or by their glycobiomes). Synthesizing model human gut microbiotas of increasing complexity in gnotobiotic mice using sequenced members should be very useful for further testing this idea, as well as a variety of ecologic concepts and principles that may operate to influence the assembly and dynamic operations of our gut microbial communities.

Materials and Methods

Genome Comparisons. All nucleotide sequences from all contigs of completed genome assemblies containing both capillary sequencing and pyrosequencer data, produced as part of the HGMI, were downloaded from the Washington University Genome Sequencing Center's website (http://genome.wustl.edu/pub/organism/Microbes/Human_Gut_Microbiome) on September 27, 2007. The finished genome sequences of *B. thetaiotaomicron* VPI-5482, *Bacteroides vulgatus* ATCC 8482, and *B. fragilis* NCTC9343 were obtained from GenBank.

For comparison purposes, protein-coding genes were identified in all genomes using YACOP (32). Each proteome was assigned InterPro numbers and GO terms using InterProScan release 16.1. Statistical comparisons between genomes were carried out as described in ref. 4, using perl scripts that are available upon request from the authors.

GeneChip Analysis. Previously described methods were used to isolate RNA from a 100- to 300-mg aliquot of frozen cecal contents, synthesize cDNA, and to biotinylate and hybridize the cDNAs to a custom bacterial GeneChip (21). The only modification was that in RNA isolation protocol, 0.1 mm zirconia/silica beads (Biospec Products) were used for lysis of bacterial cells in a bead beater (Biospec; 4-min run at highest speed). Genes in a given bacterial species that were differentially expressed in mono- versus biassociation experiments were identified using CyberT (default parameters) after probe masking and scaling with the MAS5 algorithm (Affymetrix; for details about the methods used to create the mask, see the *Methods* section of *SI Text*).

RNA was purified from proximal colon using Mini RNeasy kit (Qiagen) with on-column DNase digestion. Biotinylated cRNA targets were prepared from each sample ($n = 4$ per treatment group). cRNA was hybridized to Affymetrix Mouse Genome Mo430 2 GeneChips, and the resulting datasets analyzed using Probe Logarithmic Error Intensity Estimate method (PLIER + 16). Fold-changes and *p*-values were calculated using Cyber-t. Significance was defined by maintaining a FDR $<1\%$ using Benjamini–Hochberg correction (33).

Other Methods. Details about bacterial culture, genome sequencing and finishing, animal husbandry, quantitative PCR assays of the level of colonization of the ceca of gnotobiotic mice, GeneChip design and masking, plus proteomic and metabolite assays of cecal contents are provided in *SI Methods*.

ACKNOWLEDGMENTS. We thank Maria Karlsson and David O'Donnell for help with gnotobiotic husbandry; Jan Crowley, Janaki Guruge, Jill Manchester, and Sabrina Wagoner for technical assistance; Ruth Ley for valuable comments during the course of this work; and Manesh Shaw for proteomics data-mining and computational aspects related to mass spectrometry. This work was supported by National Science Foundation Grant 0333284 and National Institutes of Health Grants DK30292, DK70977, DK52574, GM07200, and T32-AI07172 and by the Laboratory Directed Research Program of Oak Ridge National Laboratory.

1. Turnbaugh PJ, et al. (2009) A core gut microbiome in obese and lean twins. *Nature* 457:480–484.
2. Ley RE, et al. (2008) Evolution of mammals and their gut microbes. *Science* 320:1647–1651.
3. Shipman JA, Berleman JE, Salyers AA (2000) Characterization of four outer membrane proteins involved in binding starch to the cell surface of Bacteroides thetaiotaomicron. *J Bacteriol* 182:5365–5372.
4. Xu J, et al. (2007) Evolution of symbiotic bacteria in the distal human intestine. *PLoS Biol* 5:e156.
5. Bjursell MK, Martens EC, Gordon JI (2006) Functional genomic and metabolic studies of the adaptations of a prominent adult human gut symbiont, Bacteroides thetaiotaomicron, to the suckling period *J Biol Chem* 281:36269–36279.
6. Sonnenburg JL, et al. (2005) Glycan foraging in vivo by an intestine-adapted bacterial symbiont. *Science* 307:1955–1959.
7. Martens EC, Chiang HC, Gordon JI (2008) Mucosal glycan foraging enhances the fitness and transmission of a saccharolytic human gut symbiont. *Cell Host Microbe* 4:447–457.
8. Sonnenburg JL, Chen CT, Gordon JI (2006) Genomic and metabolic studies of the impact of probiotics on a model gut symbiont and host. *PLoS Biol* 4:e413.
9. Lozupone CA, et al. (2008) The convergence of carbohydrate active gene repertoires in human gut microbes. *Proc Natl Acad Sci USA* 105:15076–15081.
10. Ley RE, Peterson DA, Gordon JI (2006) Ecological and evolutionary forces shaping microbial diversity in the human intestine. *Cell* 124:837–848.
11. Cantarel BL, et al. (2009) The Carbohydrate-Active EnZymes database (CAZy): An expert resource for Glycogenomics. *Nucleic Acids Res* 37:D233–238.
12. Brigham CJ, Malamy MH (2005) Characterization of the RokA and HexA broad-substrate-specificity hexokinases from Bacteroides fragilis and their role in hexose and N-acetylglucosamine utilization. *J Bacteriol* 187:890–901.
13. Eckburg PB, et al. (2005) Diversity of the human intestinal microbial flora. *Science* 308:1635–1638.
14. Ley RE, Turnbaugh PJ, Klein S, Gordon JI (2006) Microbial ecology: Human gut microbes associated with obesity. *Nature* 444:1022–1023.
15. Barcenilla A, et al. (2000) Phylogenetic relationships of butyrate-producing bacteria from the human gut. *Appl Environ Microbiol* 66:1654–1661.
16. Duncan SH, et al. (2008) Human colonic microbiota associated with diet, obesity and weight loss. *Int J Obes (London)* 32:1720–1724.
17. Koropatkin NM, Martens EC, Gordon JI, Smith TJ (2008) Starch catabolism by a prominent human gut symbiont is directed by the recognition of amylose helices. *Structure* 16:1105–1115.
18. Duncan SH, Flint HJ (2008) Proposal of a neotype strain (A1–86) for Eubacterium rectale. *Int J Syst Evol Microbiol* 58:1735–1736.
19. Cuff MA, Lambert DW, Shirazi-Beechey SP (2002) Substrate-induced regulation of the human colonic monocarboxylate transporter, MCT1. *J Physiol* 539:361–371.
20. Li F, et al. (2008) Coupled ferredoxin and crotonyl coenzyme A (CoA) reduction with NADH catalyzed by the butyryl-CoA dehydrogenase/Etf complex from Clostridium kluyveri. *J Bacteriol* 190:843–850.
21. Samuel BS, Gordon JI (2006) A humanized gnotobiotic mouse model of host-archaeal-bacterial mutualism. *Proc Natl Acad Sci USA* 103:10011–10016.
22. Candido EP, Reeves R, Davie JR (1978) Sodium butyrate inhibits histone deacetylation in cultured cells. *Cell* 14:105–113.
23. Tabuchi Y, et al. (2006) Genetic networks responsive to sodium butyrate in colonic epithelial cells. *FEBS Lett* 580:3035–3041.
24. Joseph J, et al. (2004) Expression profiling of sodium butyrate (NaB)-treated cells: Identification of regulation of genes related to cytokine signaling and cancer metastasis by NaB. *Oncogene* 23:6304–6315.
25. Lecona E, et al. (2008) Upregulation of annexin A1 expression by butyrate in human colon adenocarcinoma cells: Role of p53, NF-Y, and p38 mitogen-activated protein kinase. *Mol Cell Biol* 28:4665–4674.
26. Roediger WE (1982) Utilization of nutrients by isolated epithelial cells of the rat colon. *Gastroenterol* 83:424–429.
27. Comalada M, et al. (2006) The effects of short-chain fatty acids on colon epithelial proliferation and survival depend on the cellular phenotype. *J Cancer Res Clin Oncol* 132:487–497.
28. Daly K, Shirazi-Beechey SP (2006) Microarray analysis of butyrate regulated genes in colonic epithelial cells. *DNA Cell Biol* 25:49–62.
29. Hooper LV, Xu J, Falk PG, Midtvedt T, Gordon JI (1999) A molecular sensor that allows a gut commensal to control its nutrient foundation in a competitive ecosystem. *Proc Natl Acad Sci USA* 96:9833–9838.
30. Duncan SH, et al. GE (2007) Reduced dietary intake of carbohydrates by obese subjects results in decreased concentrations of butyrate and butyrate-producing bacteria in feces. *Appl Environ Microbiol* 73:1073–1078.
31. Hubbell SP (2006) Neutral theory and the evolution of ecological equivalence. *Ecology* 87:1387–1398.
32. McHardy AC, Goesmann A, Puhler A, Meyer F (2004) Development of joint application strategies for two microbial gene finders. *Bioinformatics* 20:1622–1631.
33. Benjamini Y, Hochberg Y (1995) Controlling the False Discovery Rate: A Practical and Powerful Approach to Multiple Testing. *J R Stat Soc Methodol* 57:289–300.